ANALYTE SENSING WITH LUMINESCENT QUANTUM DOTS

Ray Mulrooney

A thesis submitted in partial fulfilment of the requirements for the degree of

Doctor of Philosophy

Based on work conducted in the School of Pharmacy & Life Sciences

The Robert Gordon University, Aberdeen

From Sept 2005 – Sept 2008

under the guidance of

Dr John F. Callan

Declaration

This thesis is the sole work of the author and has not been submitted for any previous application for a higher degree.

Ray Mulrooney

Acknowledgments

I would like to express my gratitude to everyone who helped me in so many ways during my time here in Aberdeen. I would especially like to convey my thanks and appreciation to my supervisor Dr John F. Callan who introduced me to the fascinating world of quantum dots and guided me through the PhD.

I would also like to thank and acknowledge various people who have helped me along the way with analyses and technical expertise.

Mr Russell Gray (Aberdeen University) for running NMR samples prior to the purchase of our instrument. Mr Ross Blackley (St. Andrew's University) for the TEM measurements. EPSRC National Mass Spectrometry Service Centre Swansea University for accurate mass measurements. Dr Raymond Reid, Mrs Maureen Byres and Mrs Moira Middleton at RGU for their technical support.

I enjoyed being part of a laboratory group and benefited greatly from the experience and knowledge of the post-doctoral researchers, Dr Narinder Singh and Dr Sukanta Kamila who were always enthusiastic and insightful about the world of chemistry research. Also, thanks to Dr Navneet Kaur, Ruth Behan, John Dunn, Carol Byrne and Martha Mackay who were part of the research group at various stages.

A particular word of thanks goes to all the folks who I've met along the way who made the time here all the more enjoyable. A special thanks to Dr Graeme Kay, Dr Colin Thompson, Dr Alberto di Salvo, Dr Bridgeen McCaughan, Dr Benjamart Warasiha, Dr Tim Cushnie, Dr Ciprian Dospinescu, Karen Skene, Clare Hoskins, Pramod Gadad, Olga Labovitiadi, Noelle O'Driscoll and Barbara Buchan.

A special mention goes to my family and friends back home in Dublin, and without all their love and support this would have been a much more difficult undertaking.

Finally, I would like to thank the Research Development Initiative (RDI) for their financial support during my time at The Robert Gordon University in Aberdeen.

Table of Contents

Abstract

Semiconducting nanocrystals otherwise known as Quantum Dots (QDs) have attracted considerable attention over the last number of years due to their unique optical properties and potential applications. Their narrow size-tunable emission spectra, broad absorption spectra, resistance to photobleaching and long fluorescent lifetimes make them ideal for sensing ions and small molecules.

This thesis explores the potential of QDs to function as the emissive unit in fluorescent probes. Primarily, the focus of the work is to develop QD-based sensors that operate through an electron transfer mechanism.

Chapter 3 discusses the synthesis and characterisation of CdSe and CdSe/ZnS QDs. Three different sized QDs were prepared each with distinct emission wavelengths. The sizes of these nanoparticles were determined by three methods, transmission electron microscopy (TEM), dynamic light scattering (DLS) and by a UV-vis method.

Surface functionalisation of these synthesised QDs (chapter 4) with mercaptosuccinic acid rendered them water soluble and were shown to display selectivity for Cu^{2+} over a number of biologically relevant metal ions. The negatively charged surface of the QDs and the position of copper in the Irving-William series were believed to be responsible for this interaction. Positively charged CdSe/ZnS QDs were also prepared and were shown to detect ATP and to a much lesser extent GTP over the other nucleotides screened. The greater net negative charge of the ATP and GTP when compared to their mono and diphosphate analogues was the likely cause of this discrimination.

In chapter 5 the relatively unexplored field of anion sensing with QDs was examined using charge neutral urea and thiourea receptors. Based on a design by Gunnlaugsson *et al*, a CdSe/ZnS QD with a thiourea receptor anchored to its surface displayed similar PET-mediated

fluorescence quenching as an organic dye sensor containing the same receptor. A ferrocenyl urea receptor was also anchored to a QD surface and shown to "switch off" the QD's fluorescence emission. On addition of fluoride ions the emission was restored, most likely due to a modulation of the ferrocene's redox activity.

In chapter 6 the assembly of Schiff base receptors on the surface of preformed CdSe/ZnS QDs were shown to arrange in such a way to enable the simultaneous detection of Cu^{2+} and Fe^{3+}. The intriguing aspect of this study was that the receptors themselves displayed no selectivity for any metal ion until they were assembled on the QDs. Recognition was also confirmed by a distinct colour change visible to the naked eye.

CHAPTER ONE

INTRODUCTION

1.1 Introduction

1.1.1 Fluorescence

Since the 16th century the phenomenon of photoluminescence has intrigued scientists and has grown to encompass many diverse areas from biology to material sciences. One technique that is central to many studies within various disciplines is fluorescence. Fluorescence can be distinguished from other types of photoluminescence as the excited electron returns immediately to the ground state. Fluorescence lifetimes are of the order of 10^{-8} seconds[1], which may seem quite short but when compared to other processes like molecular vibrations (10^{-14} s) and transitions between electronic states (10^{-15} s) they are relatively long. In organic molecules certain molecular structures known as chromophores interact with UV-vis light and absorb photons. An energy diagram or 'Jablonski' diagram can be used to illustrate the various possible quantised energy values available to the electrons in a chromophore. As illustrated in figure 1.1 the ground state is represented by S_0. These electronic states are divided into vibrational levels which are spaced by energies much less than the difference between the electronic states. After absorption the excited electron will reside in the excited electronic state S_1 or S_2 or indeed a higher state S_n. It then relaxes back to its lowest vibrational level in the first excited state by dissipating the excess vibrational energy through thermal collisions and other processes. This is followed by a return to the ground state by emitting a photon with energy $\Delta E = \hbar\upsilon$, corresponding to the energy difference between S_0 and S_1. Alternatively, phonon interaction can lead to transitions from the singlet state to the triplet state (intersystem crossing) which is spin forbidden and as a result the rates of relaxation from the triplet state to the ground state is about 2 orders of magnitude less than the rate of relaxation from the singlet state. This longer lifetime emission is known as phosphorescence.

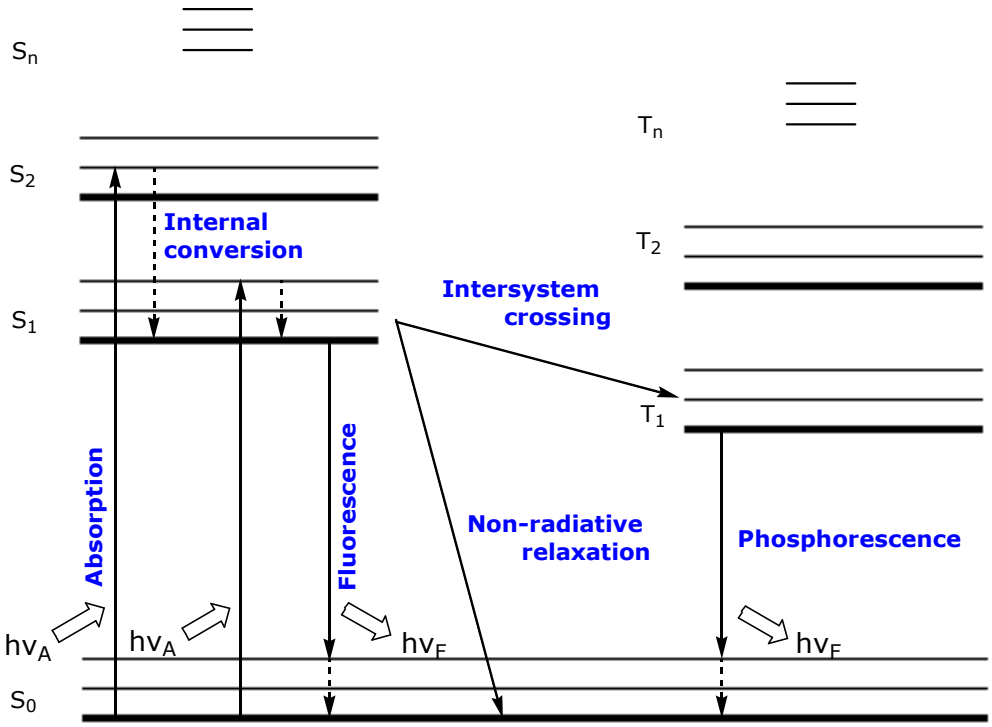

Figure 1.1 *Jablonski diagram depicting absorption and emission processes from the ground state to the first and second excited electronic states. The electronic states are split into vibrational states populated according to Boltzmann distribution. The relaxation back to the ground state is due to fluorescence, intersystem crossing to a triplet state and the resultant phosphorescence or non-radiative relaxation from internal conversion or energy transfer and quenching from neighbouring molecules*[1].

Today, molecular sensing continues to be dominated by organic dye-based fluorescent sensors with lanthanide complexes also contributing. However, in the past decade or so a new class of fluorescent compounds have emerged with impressive photophysical properties that make them a viable alternative to organic dyes. These fluorescent semiconducting nanoparticles are known as quantum dots.

1.2 Semiconducting quantum dots

1.2.1 Background

From the early 1980's a family of fluorescent materials with nanometre-sized dimensions became of great interest to chemists and the science community in general. These semiconducting nanocrystals, otherwise known as Quantum Dots (QDs) were first discovered in the late 1970's by Ekimov and his colleague, Efros[2-5] and for almost three decades they have been investigated with ever growing interest. Their current and potential applications are immense with interest spanning many disciplines and diverse sectors such as life sciences (chemical & biological sensing)[6-9], biological tagging & labelling[9-11], high quality LEDs & lighting[12-14] and also the military[15], using state of the art security and marking products for covert night-time operations.

QDs are typically 1 – 10 nm in diameter, containing as few as 100 to 100,000 atoms in each particle with their sizes confined in all three dimensions[6]. The most common QDs consist of elements from group IIb, IIIa or IVa, combined with a chalcogenic element (e.g. S, Se or Te). Examples of these are cadmium selenide (CdSe)[16-18], cadmium sulfide (CdS)[16, 17], cadmium telluride (CdTe)[16, 17] or lead sulfide (PbS)[19, 20]. Other not so common QDs are comprised of elements from group III – V such as gallium nitride (GaN)[21, 22], or indium arsenide (lnAs)[23, 24]. Their attractive photophysical properties are due to a phenomenon known as quantum confinement[25]. In bulk semiconductors energy levels are in close proximity with little difference in energy between them and are thus referred to as being continuous. There is a region known as the bandgap where electrons are forbidden. This gap separates the valence band, where almost all the electrons occupy, from the conduction band. In bulk semiconductors the valence band is almost completely full with a very small percentage of electrons occupying the conduction band. To cross this gap, energy must be supplied to the electrons filling the valence band. Most electrons in bulk semiconductors don't possess enough energy to make the transition unless heat or electrical charge stimulates them.

Due to the fact that the bulk semiconductor has continuous energy levels with many atoms present the bandgap is therefore fixed. In

addition, when electrons promoted to the conduction band fall back to the valence band they do so from one edge of the bandgap to the other, i.e. from the bottom of the conduction band to the top of the valence band. With the bandgap fixed this leads to emissions of fixed wavelengths.

Quantum Dots differ from bulk semiconductors by allowing the tuning of the emission frequencies by altering the bandgap. The physical dimensions of QDs can approach the exciton-Bohr radius (the spatial separation of the electron from the hole). Bohr approximation can be used to determine this distance[26]:

$r = \varepsilon h^2 / \pi m_r e^2$ (Equation 1.1)

where r is the radius of the sphere (extent of separation of electron-hole pair), ε is the dielectric constant of the particle, h is Planck's constant, m_r is the reduced mass of the electron-hole pair and e is the charge on the electron. This "hole" that is created is essentially the absence of an electron and can be thought of as a particle in its own right with effective mass.

In bulk, the semiconductor particle is much greater than its exciton-Bohr radius permitting the exciton to extend to its natural confines (figure 1.2). With QDs the physical dimensions are of the order of the exciton-Bohr radius and often less. They are a prime example of a "particle in a box"[27]. This theory illustrates the dependence on the size of the box in calculating the particle's energies. When the particle approaches the size of the Exciton-Bohr radius they cease to behave like the bulk semiconductor in that the energy levels cannot be considered as continuous - they are now said to be discrete. This phenomenon is referred to as quantum confinement.

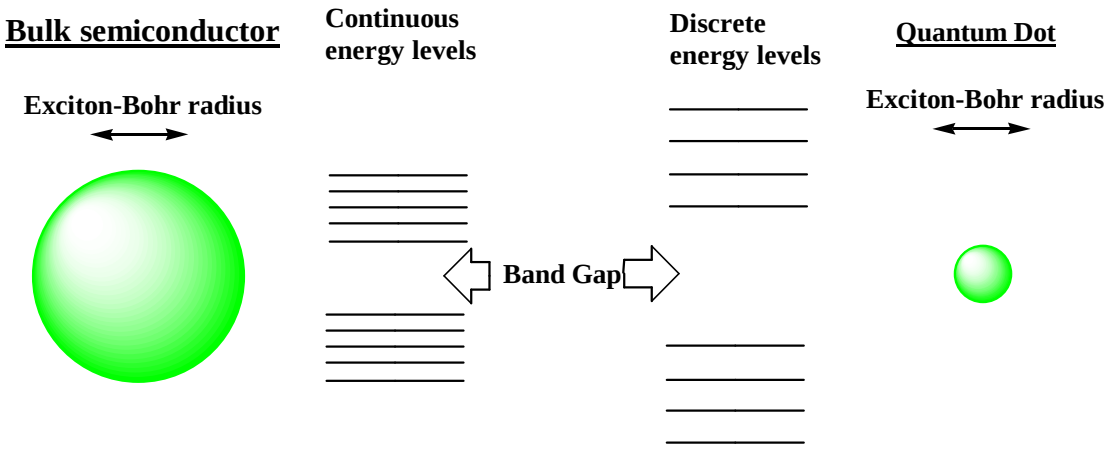

Figure 1.2 *Schematic representation of the tunable bandgap of Quantum Dots compared to the fixed bandgap of the bulk semiconductor*[28]*.*

Figure 1.3 illustrates the discrete energy levels in the valence and conduction bands of QDs due to the limited number of atoms present. When the particle is excited with energy greater than the band gap energy (E_g), an electron is promoted from the valence band to the conduction band, leaving a positively charged "hole" behind. The promoted electron and the hole generated are attracted together by Coulombic forces, forming short lived electron hole pairs (excitons).The electron and the hole recombine rapidly emitting photons corresponding to the band gap energy. Some of the energy may be released in a non-radiative way and as a result the emission energy is lower than the excitation, a phenomenon known as Stoke's shift. In figure 1.3 some other possible emissions are shown (i.e. E_{em1}, E_{em2}, E_{em3}, E_{em4}) corresponding to trap states located in the band gap which are lower in energy to the band gap emission (E_{em0}). By controlling the growth of these nanoparticles the bandgap size and thus the emission wavelength can be tailored[6, 29, 30].

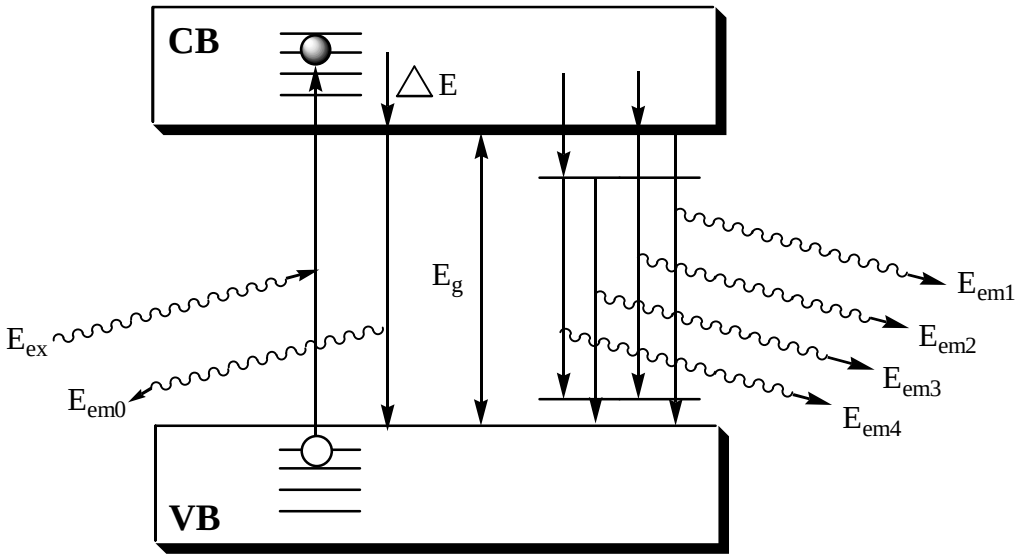

Figure 1.3 *Schematic representation of the excitation and emission of QDs. VB = valence band, CB = conduction band, ΔE = Stokes shift, E_g = band gap energy, E_{ex} = excitation energy, E_{em0-4} = various emission energies*[1]*.*

1.2.2 Chemical synthesis of QDs

Colloidal synthesis has been the favoured technique by chemists for the preparation of QDs for chemical and biological studies[6, 7, 30, 31]. The origins of this approach are steeped in similar preparative strategies to that employed in the colloidal synthesis of gold nanoparticles. Early development in QD work was hampered somewhat by issues of size disparity and polydispersity and due to this variation in the particle dimensions (particle size dimension (PSD) > 15%), they generated poor quantum yields with their size-dependent properties poorly resolved. Seminal work carried out by Murray and colleagues addressed these issues by using organometallic precursors suspended in organic media[16]. Organometallic monomers injected into the hot solvent cause a release of the atomic species that constitute the QD leading to an oversaturation of these monomers which favours crystal growth. The mono-dispersity improved immensely with this approach (PSD < 5%) and produced QDs with nearly defect free crystalline structures. Despite these advances in improving the synthetic strategies the quantum yields remained quite low

(~10%). The reason for this was attributed to poor passivation of the QD surface.

Murray *et al*'s early work utilised trioctylphosphine oxide (TOPO) and trioctylphosphine (TOP) as surfactants to help improve the surface quality and passivation. These have since been augmented with certain carboxylic acids and amines (e.g. stearic acid, hexadecylamine)[32, 33]. The role of the surfactant is quite interesting in that it influences the growth dynamics of the nanocrystals. A polar head group will affect the binding efficiency while the non-polar alkyl chain controls the diffusion characteristics[34]. The solvent also plays a major role in the growth of the nanocrystal. Its obvious function is to solubilise and disperse the various components involved in the growth phase but it is also required to control the speed of the reaction. As the crystal is growing, solvent molecules detach from the surface and are replaced by monomers in a dynamic process[34]. TOPO has been used quite successfully as both a solvent and surfactant due to its high boiling point and ability to coordinate metals and chalcogens readily.

1.2.2.1 Core synthesis

In the case of cadmium based QDs, a typical core QD synthesis is carried out under an inert atmosphere in a three-necked flask[6]. One neck is connected to a Schlenk line while the other two necks are stoppered with rubber septa and are used for temperature monitoring and reactant addition. The requirement for airless procedures is due to the reactivity of the precursors with oxygen and moisture. However, the QDs themselves are stable to air and therefore relatively easy to work with post-synthesis. When all the reactants have been charged to the reaction vessel they are heated to 130 – 180 °C under vacuum for 10 – 20 mins to remove any volatile impurities. The temperature is then raised to ~300 °C and at this temperature the Cd metal ions will bind to the surfactants, usually long alkyl chain phosphonic acids (e.g. TOPO) or oleic acid. As this is occurring, the colour of the solution changes from dark red to colourless. For this type of core synthesis only a chalcogen complex is introduced with nucleation occurring shortly after its injection. For group II/VI nanocrystals, the chalcogens are incorporated into the reaction as

complexes of TOP or tributylphosphine (TBP). The cadmium source in the early syntheses of QDs was dimethyl cadmium Me_2Cd but this has since been replaced by CdO due to the pyrophoric, toxic and unstable nature of Me_2Cd.

Several synthetic approaches have emerged since these pioneering efforts and have involved the use of various precursors, stabilizers and solvents. As mentioned above, the change to using CdO instead of Me_2Cd proposed by Peng *et al* has made synthesis of QDs much more user friendly[17]. Another significant contribution was the replacement of the coordinating solvent TOPO with the non-coordinating 1-octadecene (ODE), a cheaper and more environmentally friendly alternative. This also has a practical advantage in that it's a liquid at room temperature, unlike TOPO. In addition, ODE has the ability to fine tune the reactivity of Cd and doesn't have the added function of being a stabilizing ligand. This stabilization is performed by fatty acids (e.g. oleic acid). Recently it has been reported that the use of certain alkylamines can function as stablizing ligands and reactions can be performed at much lower temperatures (~150 °C)[35].

Coating of the core QDs is an important step to help increase quantum efficiency by passivating non-radiative recombination sites on the QD surface. ZnS is a common shell coating material due to the wide band gap it exhibits[36]. This inorganic capping renders these QDs more robust than organically passivated ones. Furthermore, there is an approximate ~10% increase in photoluminescence quantum yields relative to the bare core QDs.

1.2.2.2 Core-shell synthesis

A synthethic procedure for synthesis of CdSe/ZnS core-shell QDs involving the use of Me_2Cd has been developed by Dabbousi *et al*[37]. This procedure describes the pyrolytic decomposition of the organometallic precursors Me_2Cd and TOPSe as outlined earlier. After injecting into the coordinating solvent TOPO at a temperature of 340-360 °C the nanocrystals were then grown at a reduced temperature of 300 °C. The core QDs were then isolated as a powder by size-selective precipitation with MeOH and redispersed in hexane. The ZnS capping was performed by

heating TOPO to 190 °C under vacuum for 3 hours and then cooling to 60 °C, after which TOP was added. The newly formed CdSe core QDs in hexane were syringed into the reaction and the hexane removed under vacuum. The zinc and sulfur precursors were derived from diethylzinc ($ZnEt_2$) and hexamethyldisilathiane ($(TMS)_2S$) with the amount required to grow a ZnS shell determined by estimating the size of the core from TEM measurements, and, assuming a spherical core, a molar ratio was calculated[37]. The precursors were then dissolved in TOP under inert conditions and loaded into syringes. The reaction flask containing the core QDs dispersed in TOPO and TOP was heated under a N_2 atmosphere. When a temperature of ~150 °C was attained the precursors were added dropwise over a period of about 10 mins with vigorous stirring. After completion, the reaction was cooled to 90 °C and stirred for several hours. An aliqout of butanol was added to prevent the TOPO from solidifying. The QDs were then precipitated using methanol and were readily dispersible in chloroform, hexane, THF, toluene and pyridine.

1.2.3 Aqueous phase synthesis of QDs

Synthesis of colloidal QDs using high boiling solvents like TOPO and 1-octadecene has been the preferred and more practised route. However, another strategy exists that avoids the use of high temperatures and air-free apparatus. The medium for this route is water and provides for a less toxic and cheaper alternative. CdTe QDs synthesised by this aqueous method have enjoyed the most attention mainly due to their high quantum yields (40 – 60%). However, CdS and CdSe QDs synthesised by aqueous methods do not result in high quantum yields and the reason for this is explained in figure 1.4. The difference in the valence bands of the CdSe and CdTe QDs is about 0.5 eV. This is significant as hole trapping by a thiol is energetically favourable if the thiol's redox energy is higher than the top of the valence band of the QD and thus results in fluorescence quenching. The probability of this occurring with CdSe QDs is high and is even more pronounced for CdS QDs with the difference between the valence bands of CdS and CdTe being about 1.0 eV[38]. Despite these low QYs, interest in this synthetic approach remains high, with direct aqueous

synthesis of CdS, CdSe and CdTe performed using various short chain thiols as stabilising ligands.

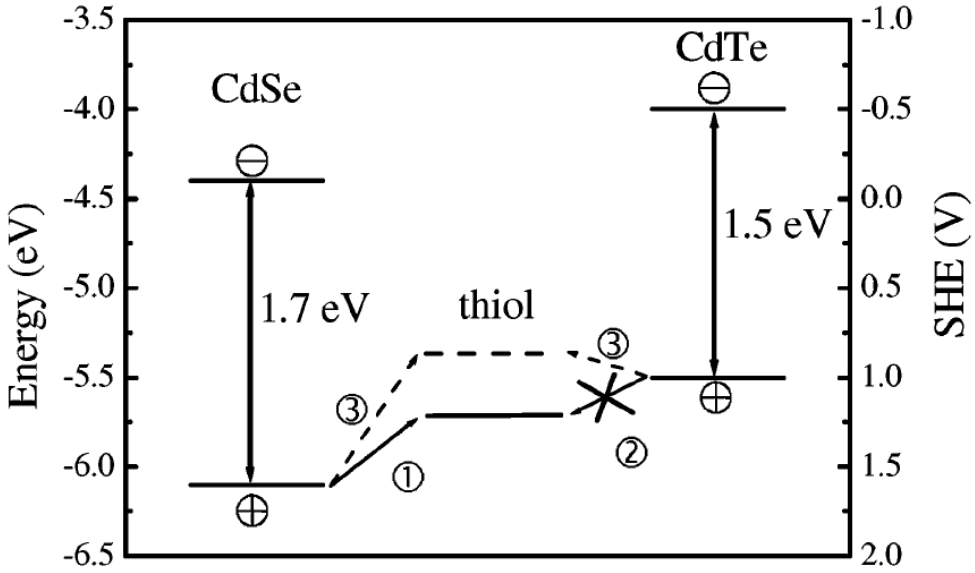

Figure 1.4 *Positions of CdSe and CdTe bulk band edges with respect to a standard hydrogen electrode reference. Hole trapping can occur from CdSe (1) but not from CdTe (2). Path (3) is the assumed position for the standard potential of a thiol that quenches the fluorescence of both the CdSe and CdTe processes*[38]*.*

A typical aqueous synthesis of CdTe QDs involves dissolving $Cd(ClO_4)_2.6H_2O$ in water in a three-necked flask and adding an appropriate amount of thiol stabilizer (e.g. 2-mercaptoethanol, 1-thioglycerol, thioglycolic acid)[39]. The solution is then stirred and the pH adjusted using 1M NaOH to between 11.2 and 11.8. The flask is then evacuated by bubbling N_2 through the solution for 30 mins. Whilst stirring, H_2Te gas, (generated by the reaction of Al_2Te_3 and 0.5 M H_2SO_4) is bubbled through the solution with N_2 for about 20 mins. The CdTe precursors are formed at this stage and depending on the thiol ligands used they can be yellow, orange or dark red in colour. These precursors are then converted into QDs after refluxing at 100 °C exposed to the open air. After 5 – 10 mins the smallest crystallites are formed and the reflux can be continued up to 2-3 days (using the thiols listed above) to generate QDs of ~5 nm.

1.3 Growth mechanism of QDs

1.3.1 Nucleation

The growth process of colloidal QDs can be divided into two parts. The first stage is referred to as nucleation where the nanoparticles are spontaneously formed through the coming together of the dispersed monomers in solution. The second stage is the actual growth process.

Nucleation can be viewed as an overcoming of a barrier whereby a thermodynamically stable state is attained after the assembly of a core of monomers that do not decay back to the free atoms or ions[34, 40]. Two phases are encountered at this point, the crystalline and solution phase. As the names would suggest, the crystalline phase is when the atoms are bound to the crystal while the solution phase refers to the freely dispersed atoms in solution. The difference in the free energy between the two phases governs the nucleation in solution at constant temperature and pressure. The driving force for this nucleation is the gain in chemical potential, i.e. the energy released by the formation of bonds in the growing crystal and the increase in total surface energy, which accounts for the incomplete saturation of surface bonds. The change in the free energy ΔG, on formation of the spherical nucleus with n atoms is governed by the equation[34].

$$\Delta G = n(\mu_c - \mu_s) + 4\pi r^2\sigma \qquad \textit{equation 1.2}^{34}$$

where: μ_c is the chemical potential of the crystalline phase
μ_s is the chemical potential of the solution phase
r is the radius of the nucleus
σ is the surface tension (or more correctly for solids, surface energy. However, this terminology has been borrowed from the field of liquid droplet formation).

Equation 1.2 is for a simplified case where the surface tension σ is constant for any size/morphology of the crystal. For a more detailed approach the defined crystalline surface would need to be accounted for. The role of faceting (i.e. the arrangement of atoms and dangling bonds on

the surface) and also the density of atoms will affect the total surface energy. For ease of discussion this effect is ignored and an isotropic crystal without facets is assumed. In equation 1.2 the first term is expressed by the radius r of the nanocrystals and the density (d_m) of atoms in the crystal.

$$\Delta G = \frac{4\pi d_m}{3} \cdot r^3(\mu_c - \mu_s) + 4\pi r^2\sigma$$

equation 1.3[34]

When the chemical potential of the atoms in solution is less than that in the crystal, the minimum free energy is when all the atoms are freely dispersed and therefore no stable crystals develop. When the chemical potential of the atoms in solution is greater than that in the bound crystal, the first term in equation 1.3 becomes negative and ΔG reaches a maximum at the critical size r_c.

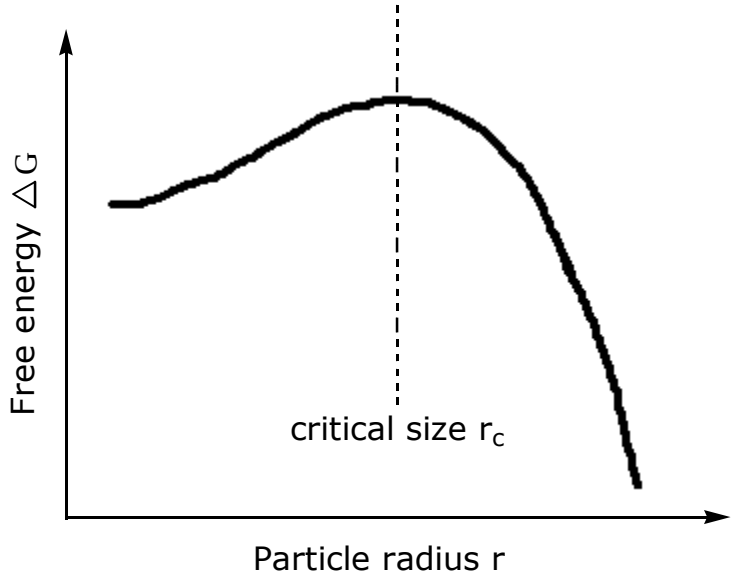

Figure 1.5 *Potential landscape for nucleation. From equation 1.3, when r is small, r^2 of the surface energy term can outcompete the r^3 contribution of the chemical potential resulting in a barrier at critical size r_c*[34]*.*

At this point a nucleation barrier exists. With small nuclei the surface energy term controls the free energy while the larger crystals are controlled by gain in the chemical potential.

1.3.2 Growth

Two steps are involved in the growth process. The first involves the transportation of the monomers to the nanoparticle surface and the second stage is their reaction on the surface. The growth rate ($\dot{r}$) is controlled by the rate of deposition of monomers on the nanocrystal surface and can be written as:

$$\frac{dr}{dt} = \frac{\dot{n}}{4\pi r^2 d_m} \qquad \text{equation 1.4}^{34}$$

where: d_m is the density of monomers in the nanocrystal

$\dot{n} = dn/dt$ (no. of n monomers in the nanocrystal solved for $\dot{r}$).

To initiate the growth process an excess of monomers is injected into the reaction. Due to the high concentration of monomer the rate of incorporation $\dot{n}$ only depends on the reaction rate for the conversion of monomer to crystal. The surface area of the nanocrystal dictates this rate. When the concentration of monomers has reduced, the growth rate then depends on the rate at which the monomers reach the nanoparticle surface.

When the radius of the crystal reaches the point where it is in equilibrium with the monomer concentration a zero growth rate is observed. In the course of a reaction the concentration of monomers decreases and the smaller crystals enter a size focussing stage after which the critical size r_c increases and a broadening process occurs. The critical size ultimately becomes greater than the radius of the smallest nanocrystals and enters the Ostwald ripening stage, characterised by a significant broadening of the size distribution[41]. This is accompanied by a reduction in the concentration of the nanocrystals. The smaller crystals

"melt" back into the solution freeing the monomers and these are incorporated into the larger crystals.

The nucleation stage has a major impact on the final size distribution. This stage should ideally be finished well before it enters the diffusion controlled growth stage. If the nucleation event occurs over too long an interval then this causes a broadening of the size distribution as illustrated in the emission spectra in figure 1.6.

The fluorescence spectrum is a good indicator of the quality of the nanocrystals in terms of size distribution[42]. A full width half maximum (FWHM) of about 30 nm shows good size distribution. Synthetically, a high temperature reaction and an excess of monomers ensures a short nucleation period and reduces the chance of entering a broadening regime. Some synthesis routes cause a rapid depletion in the supply of monomers resulting in a broadening of the fluorescence band. This can be overcome by a fresh injection of monomers during the growth phase. However, to produce a perfect size distribution at the synthesis stage is quite difficult but can be achieved in a somewhat laborious way by repeated precipitations with a polar solvent during the work-up.

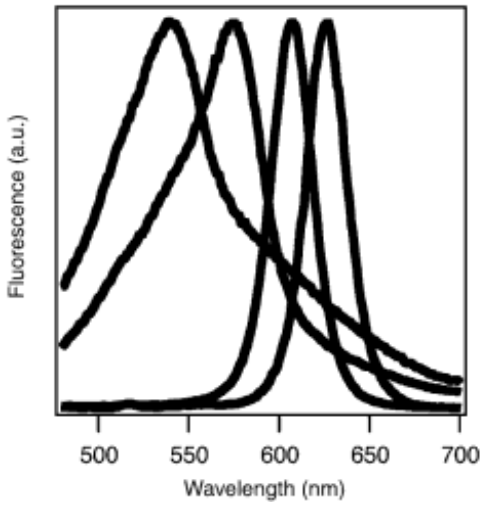

Figure 1.6 *The effect of size focussing during the synthesis of CdSe QDs. Aliquots were taken every 20 secs and the fluorescence spectrum recorded. The first sample taken (λ_{max} = 530 nm) shows broad fluorescence with wide size distribution whereas the spectrum with λ_{max} = 640 nm is the final sample taken and shows a very narrow spectrum with narrow size distribution*[34]*.*

1.4 Photophysical properties

One of the most striking and beneficial features of QDs is their size-dependent emission spectra. By altering the size and composition of the nanocrystals they can be tuned to emit from the near ultra-violet region of the spectrum up to the near infra-red. As the particle size reduces the band gap increases (see figure 1.2 in section 1.2.1) and this results in shorter emission wavelengths. CdS QDs can be tuned to emit from 400 nm to 500 nm while with CdSe QDs the tunability limits are from about 500 – 700 nm range[43]. Other composites like Pb-based QDs have been employed to extend this range into the near infra-red which essentially means that a range of 400 – 2000 nm can be spanned by using different materials[6, 44].

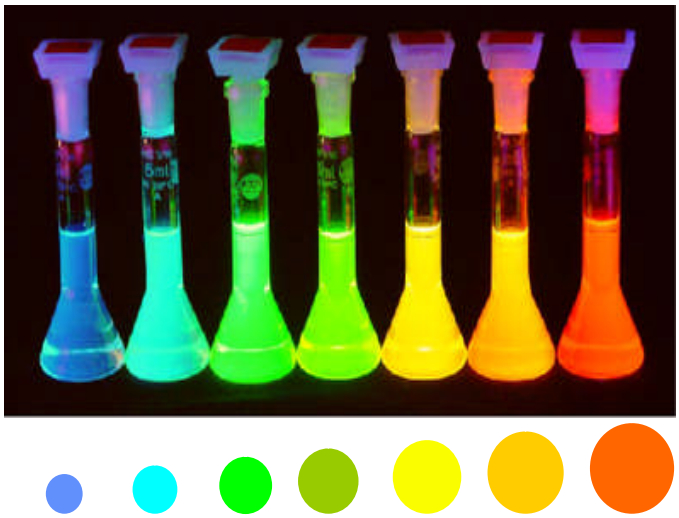

Figure 1.7 *Different sized CdSe/ZnS QDs extending from 490 nm to 620 nm excited under UV light. The blue QDs dimensions are ~ 2 nm while the orange QDs measurements are ~ 6 nm*[28].

This feature is highly attractive for biological applications as it allows the user to choose an emission wavelength suited to their needs for a particular experiment. Another desirable property of QDs is their broad absorption spectra that extend back into the UV region with increasing extinction coefficients. The molar extinction coefficients for the bandgap of these QDs[43] can be 10 – 50 times greater than commercially available

organic dyes. The broad absorption of QDs corresponds to the overlapping of a series of peaks that increase in size as the wavelengths get shorter. Each peak represents an energy transition between discrete electron-hole pairs (excitons), again attributable to the discrete nature of the QD's energy levels. QDs will not absorb at wavelengths longer than that of the 1st exciton peak.

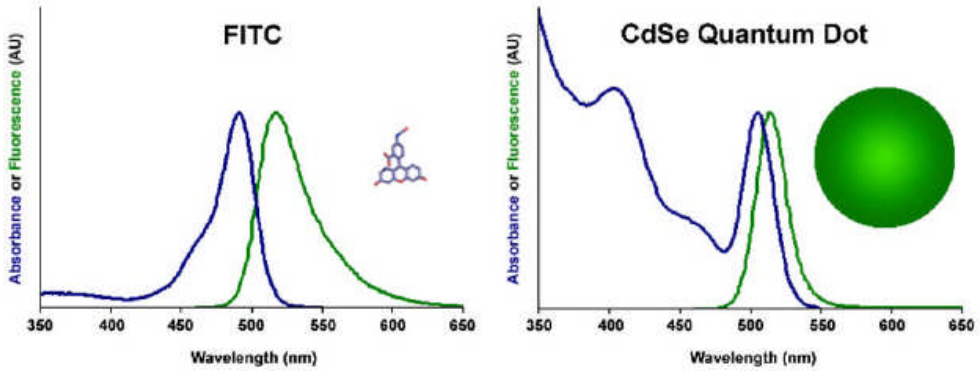

Figure 1.8 *Absorbance (blue spectra) and fluorescence (green spectra) of fluorescein isothiocyanate (FITC) on the left and CdSe QD on the right with the identical emission wavelengths*[6]*.*

Figure 1.8 illustrates the advantageous optical properties of QDs when compared to a typical fluorescein organic dye[6]. It is evident that the emission of the QD is more symmetrical and narrow than the organic dye with a full width half maximum (FWHM) of typically 25 - 35 nm with the absorption spectrum extending back into the UV region meaning any wavelength less than the emission can be selected for excitation. This feature makes them ideal for multiplexing applications where several fluorophores may be excited simultaneously.

1.5 Biological applications of QDs

To simultaneously discriminate multicolour QDs under long-term excitation offers great promise for fluorescent labelling applications and to those interested in biomedical research in general[10, 45]. Organic dyes are limited in this respect due to their narrow absorption spectra and difficulty in exciting multiple dyes with a single excitation source. In one particular experiment (figure 1.9a) a mouse was injected with cancer cells tagged

with both green fluorescent protein (GFP) and orange emitting QDs[46]. In the cell culture images of figure 1.9, both sets of tagged cancer cells are as bright as each other, however when injected into a mouse only QD emission was observed. This demonstrates that the QD emission can be shifted away from endogenous autofluorescence by selecting an appropriate excitation wavelength. This was not possible with GFP due to its small Stoke's shift and emission in the same region as the background fluorescence.

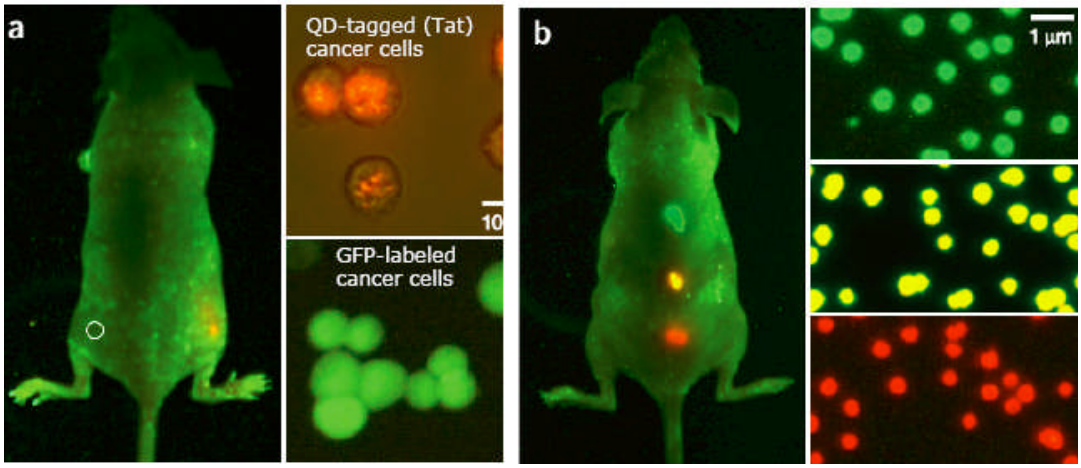

Figure 1.9 *(a) Image of a mouse tagged with green fluorescent protein (GFP) transfected cells and also QD-tagged cells. Approximately 1,000 of both QD (orange glow on right flank of mouse) and GFP (circled on left flank of mouse) cells injected into the mouse. (b) mouse injected with multicolour QD-encoded microbeads. Visible are the emission from green, yellow and red QDs excited simultaneously with UV light*[46]*.*

Figure 1.9b illustrates another desirable feature of QDs where *in vivo* they appear brighter than organic dyes. The lifetime limited emission of single QDs are 5 – 10 times lower than that of single organic dyes, however fluorescent imaging operates under absorption-limited conditions and hence the rate of absorption is the limiting factor for emission. The large molar extinction coefficients of QDs mean their absorption rates can be 10 – 50 times faster than organic dyes under the same excitation photon flux. This increase in the rate of light emission means the QDs will appear 10 – 20 times brighter than a typical organic dye[46]

With *in vivo* studies it is desirable to continuously monitor fluorescence over a period of time and this is a problem for organic fluorophores which have poor photobleaching thresholds. QDs do not suffer from these limitations and this makes them ideal for biosensing applications.

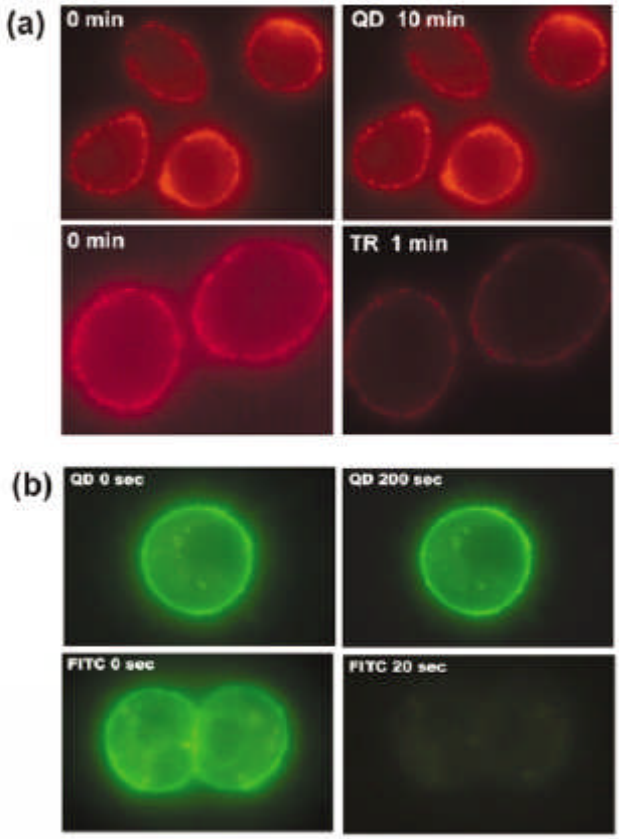

Figure 1.10 *(a) Human breast tumour cells labelled with Texas Red (TR) organic dye and also a red emitting QD. (b) Same cells labelled with fluorescein isothiocyanate (FITC) dye and also a green emitting QD*[30]*.*

Figure 1.10 illustrates the superior imaging with QDs over an extended period of time. In (a) the QD labelled breast tumour cell's fluorescence remains as intense 10 mins after its initial excitation. With the Texas Red labelled cells the emission has already diminished significantly only after 1 min. The same situation was observed with fluorescein isothiocyanate (FITC) with the emission from these labelled cells quenched after 20 seconds while the QDs remain luminescent after 200 seconds[30].

Although QDs have been shown to possess more desirable properties than organic dyes, there are still challenges to overcome in order to replace organic dyes as the signalling unit of choice in biological environments. The physical dimensions of QDs are at least an order of magnitude greater than organic dyes which may have repercussions for biological sensing applications and the extent of this has to be evaluated[30]. Coating of the QDs with higher bandgap material like zinc sulfide has the benefit of increasing their quantum efficiencies by passivating any surface defects however this protective shell makes the physical dimensions of the nanoparticle significantly bigger. Issues over toxicity is a concern in biological *in vivo* experiments due to the use of cadmium, however most reports describe no toxicity in live animals including embryos under standard conditions[47, 48]. Nevertheless, the use of bare cadmium-based QDs (e.g. CdSe) is becoming more uncommon due to the fact that CdSe can be oxidised in the air or by UV light, releasing Cd^{2+} which is toxic to cells[48]. The use of core-shell QDs (e.g. CdSe/ZnS) negates some of these worries as the outer shell, in this case ZnS is a lot less toxic than cadmium and so can be utilised in biological studies without any major concerns.

1.6 Mechanisms involved in sensor design

There are several mechanisms involved in the design of fluorescent sensors. These mechanisms are responsible for communicating the binding of analyte by the receptor to the signalling unit, the fluorophore. There are four main mechanisms involved in fluorescent sensor design: Photoinduced electron transfer (PET), Förster Resonance Energy Transfer (FRET), Internal Charge Transfer (ICT) and excimer/exciplex. Only the first two have been utilised in QD sensors and so only these will be discussed here. The reader is directed to several review articles for discussion of other mechanisms if required[49-51].

1.6.1 Photoinduced Electron Transfer (PET)

Photoinduced electron transfer (PET) plays a central role in biochemical processes like photosynthesis, both in plants and bacteria[52, 53]. This mechanism relies on the separation of charge at membrane bound pigment protein complexes known as reaction centres, producing redox species. These reaction centres are present in all green plants and also in bacteria and algae[53]. In the example of photosynthesis, the pigment chlorophyll absorbs sunlight which causes the promotion of an electron to a higher energy level within this pigment. This energy is used to reduce a chain of electron acceptors that have lowered redox potentials thus producing chemical energy. This PET principle has led researchers to incorporate the mechanism into sensing systems due to its elegance and modular design.

The field has flourished over the last few decades since it was first reported by Weller in 1968[54] and then expanded on by de Silva[49, 55, 56] and others[57, 58]. From the initial reports of PET sensing with cations and protons the area has moved on to the sensing and recognition of other targets like glucose[59, 60] and anions[61-63]. Several detailed reviews and books have been dedicated to the area of PET sensing[53, 64-66].

PET sensors are modular in format, comprising three distinct and separate components. A fluorophore, traditionally organic in nature is joined to a receptor via a spacer.

Figure 1.11 *Schematic representation of the PET sensor modular format describing the three distinct and separate parts: fluorophore – spacer – receptor[56].*

The fluorophore is the signalling component of the sensor, relaying information from the probe via fluorescence. When integrated into a sensor, the fluorophore can engage in reversible redox reactions when exposed to certain conditions. There are a huge number of fluorophores

available to the user and selection is based on the desired excitation and emission wavelengths and redox potentials[67].

The receptor is the recognition unit of the sensor and will bind the desired analyte by chelation or by some other means (e.g. hydrogen bonding). It is important to choose a receptor that will show good selectivity and sensitivity for a particular analyte whilst ensuring it is available to partake in redox processes with the fluorophore[68].

The spacer is the final component and plays an important role in keeping the two integral parts of the sensor apart (i.e. fluorophore and receptor). This spacer unit is crucial for preserving the modular format of the sensor, essentially electronically decoupling the emitting unit from the receptor allowing the two entities to retain their individual photophysical characteristics. The transfer of electrons occurs along the σ framework of the spacer or through space. Methylene or ethylene spacers are usually chosen for this role as they promote faster, efficient PET[69].

Figure 1.12 illustrates the PET process in the absence of target analyte. In its simplest form an aliphatic amine serves as the electron donor and the receptor for the ion being sensed, the spacer a short alkyl chain (e.g. methyl or ethyl) and the fluorophore an organic dye (e.g. anthracene, fluorescein). In the absence of a target analyte, the free amine participates in PET and quenches fluorescence by transferring an electron from the nitrogen atom to the excited fluorophore[68]. Figure 1.12 also shows the frontier orbital energy diagram of a PET sensor in this unbound state. Excitation causes an electron of the fluorophore to be promoted from the highest occupied molecular orbital (HOMO) to the lowest unoccupied molecular orbital (LUMO). The excited state energy is dissipated in the most energetically favourable route and in this unbound case the HOMO of the receptor is higher in energy than the HOMO of the fluorophore and as a result the electron is transferred to the HOMO of the fluorophore from the HOMO of the receptor and no fluorescence is emitted. Regeneration of the ground state is achieved through a secondary process known as back electron transfer[49].

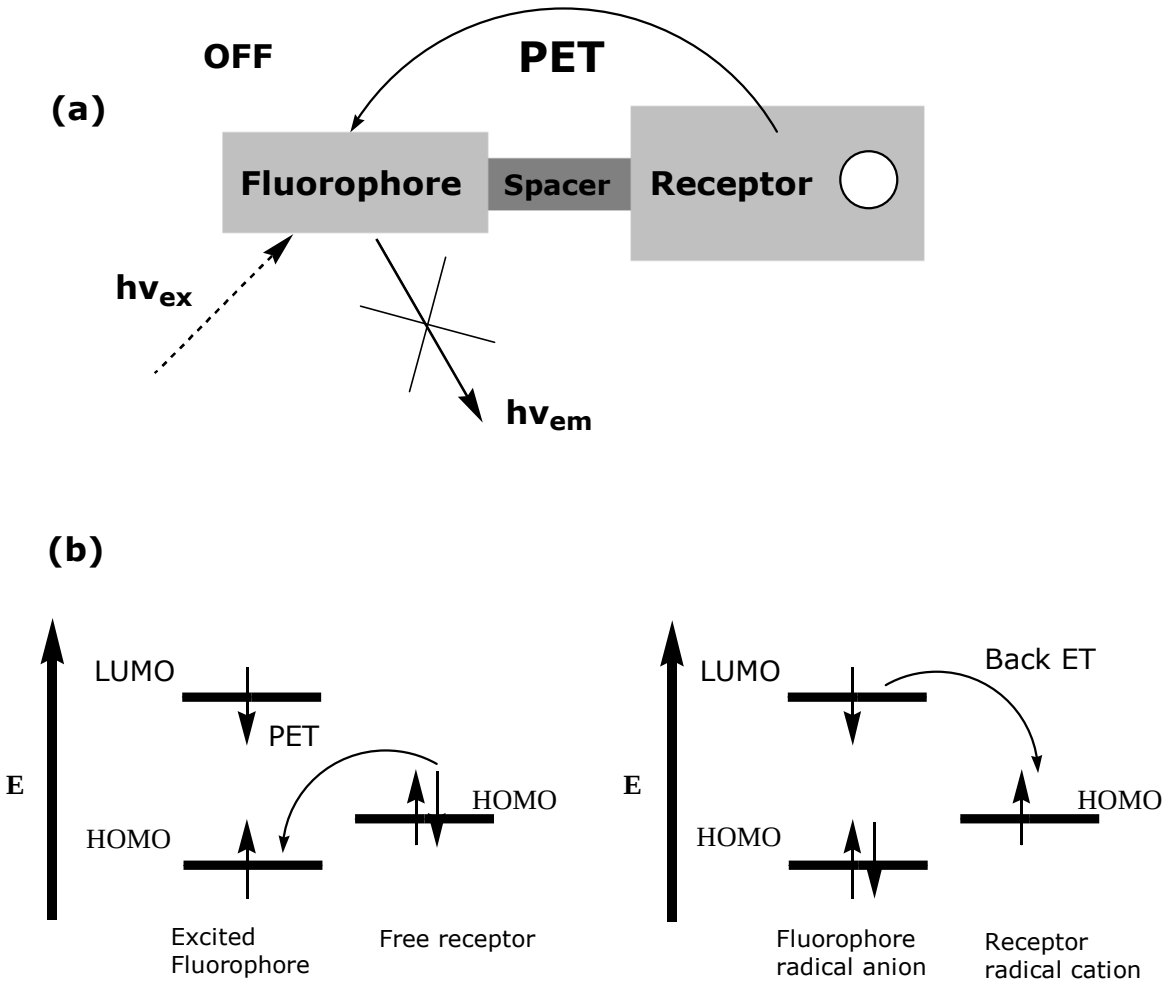

Figure 1.12 *(a) Schematic representation of the "off" state when no target is bound. (b) Frontier orbital theory explaining the "off" state in PET based sensors*[56]*.*

The "on" state is depicted in figure 1.13 illustrating how the PET process is cancelled on binding of a target analyte. In this bound state, the oxidation potential of the receptor is raised and this removes the thermodynamic condition for PET to occur. The frontier orbital diagram shows that due to the receptor becoming more stabilised upon analyte binding its HOMO is reduced in energy such that it is energetically lower than the HOMO of the fluorophore. As a result these electrons cannot engage in PET and no longer perform as quenchers and so the fluorescence is recovered. This emission signals the capture of the guest molecule by the receptor.

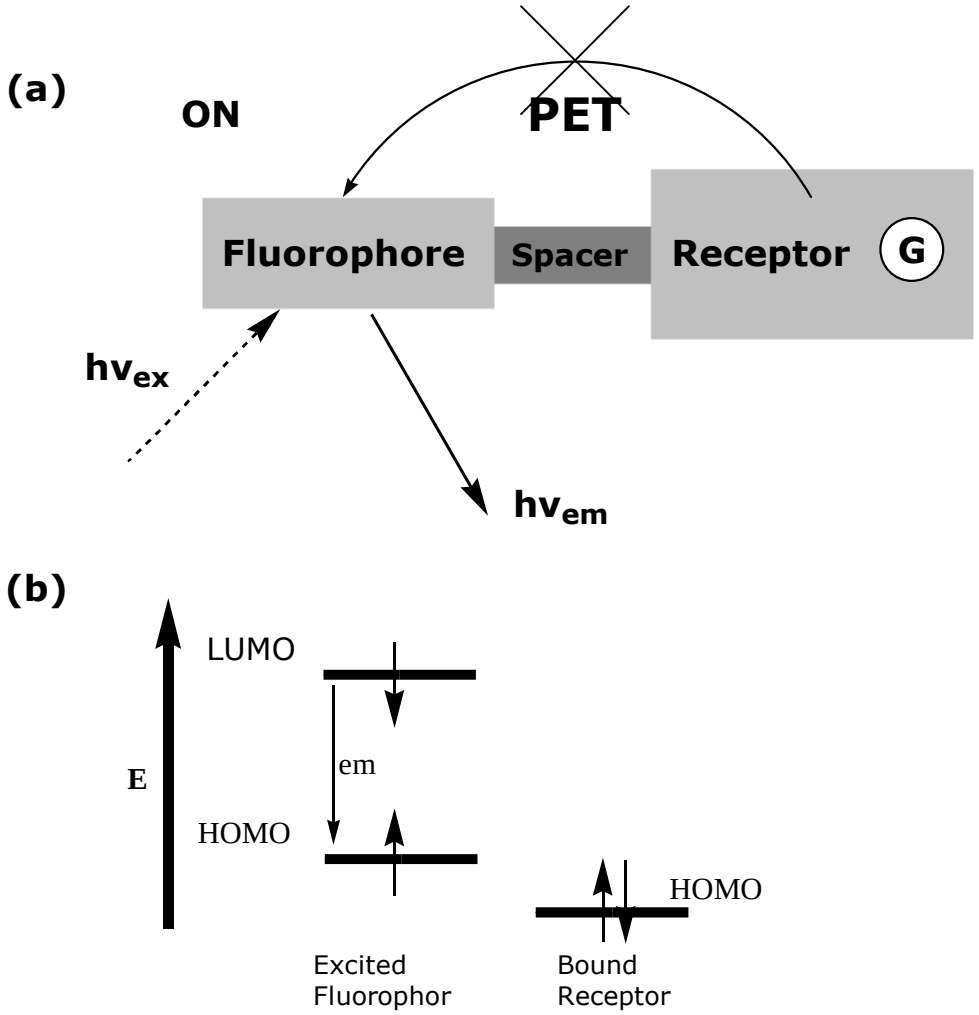

Figure 1.13 *(a) Schematic representation of the "on" state when a target is bound. (b) Frontier orbital theory explaining the "on" state in PET based sensors*[56]*.*

1.6.2 Förster Resonance Energy Transfer (FRET)

The first mechanism discussed in this section was the PET mechanism due to its relevance in the work presented in the following chapters. However, the Förster Resonance Energy Transfer (FRET) has also been extensively studied in QD based sensing systems reported in the literature[31, 70-75, 75-77]. Due to their broad absorption spectra QDs are ideal energy acceptors. FRET can be defined as a non-radiative energy transfer from a donor molecule to an acceptor molecule. Apart from an efficient quenching process it has also been employed extensively as a

molecular ruler for distances 1 – 10 nm[78]. The primary condition for FRET to occur is that the donor and acceptor molecules must be in close proximity, typically 10 – 100 Å [79]. The efficiency of this process is governed by the equation.

$$E = (1 + (r/R_0)^6)^{-1} \qquad \textit{equation 1.1}^{79}$$

Where E = efficiency of FRET, r = distance between donor and acceptor and R_0 = Förster radius, the distance at which the FRET efficiency = 50%.

$$R_0 = \sqrt[6]{0.211k^2n^{-4}QY_DJ} \qquad \textit{equation 1.2}^{79}$$

Where k^2 = orientation factor, n = index of refraction, QY_D = quantum yield of the donor, J = spectral overlap

The absorption spectrum of the acceptor molecule must overlap the emission spectrum of the donor and the transition dipoles must be orientated almost parallel for efficient FRET to occur. Specific examples of FRET based QDs are presented in the next section.

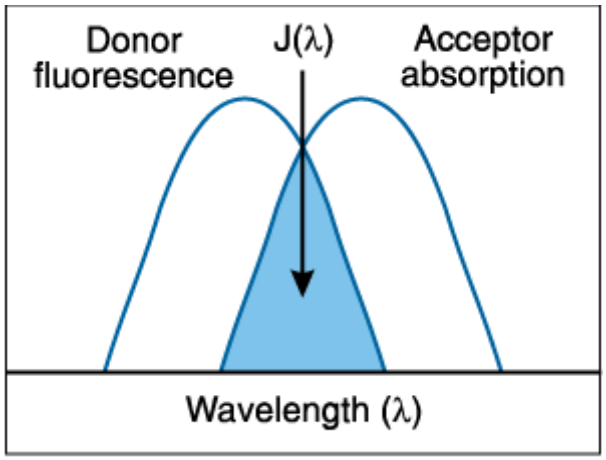

Figure 1.14 *Schematic representation of the overlap (J) required for efficient FRET*[78]*.*

1.7 QD sensors based on energy transfer

1.7.1 Background

The concept of energy transfer between QDs was first demonstrated by Kagan *et al* who reported that when rows of closely packed CdSe QDs comprised of large sized nanoparticles (620 nm) and lower wavelength emitters (555 nm) were assembled in thin films, a simultaneous decrease in the steady-state emission of the small QDs with an increase in emission from the larger QDs was noted[70]. This energy transfer was confirmed by Förster theory after it was observed that the lifetime of the smaller QDs shortened while the larger QDs lifetimes were lengthened. From these experiments the viability of CdSe QDs as FRET donors and acceptors was established paving the way for further studies.

1.7.2 QDs as FRET donors

The FRET mechanism is central to many QD sensor designs with most sensing strategies relying on energy transfer from the QD to a dye acceptor[31, 70-75] with only a small number operating in the reverse[75-77]. FRET can occur from QDs to an organic acceptor molecule as described by Willard *et al*[71]. CdSe/ZnS QDs were rendered water soluble and then conjugated to thiolated biotinilated bovine serum albumin. The acceptor molecule, prepared separately was the organic dye tetramethylrhodamine (TMR) appended with streptavidin (figure 1.15). This modified dye was titrated into the QD solution buffered in phosphate buffered saline (PBS) and it was observed that when **1** was excited at 400 nm its emission energy was used to excite the organic dye resulting in an enhancement of the TMR fluorescence and a quenching of the QD emission.

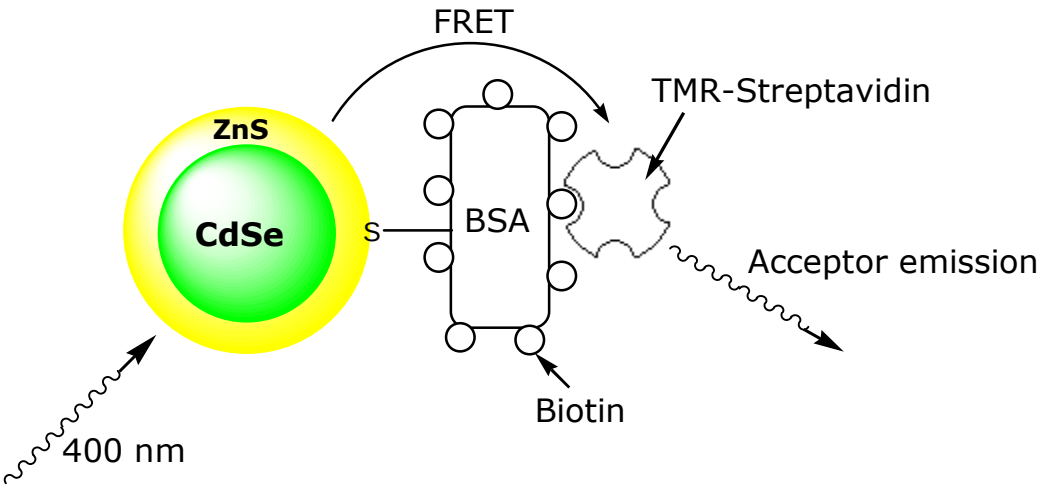

(1)

Figure 1.15 *Schematic representation of the FRET binding assay. Only one protein complex is shown for clarity*[71].

Mattoussi and co-workers have also demonstrated FRET from QDs to acceptor molecules in aqueous environments[73]. CdSe/ZnS QDs were made water soluble by modifying them with dihydrolipoic acid, a reduced form of lipoic acid containing a bidentate thiol pendant group. A maltose binding protein (MBP) with site specific labeled dye acceptors was anchored to the QD surface. This was achieved by either electrostatic attraction between the negatively charged DHLA surface ligands on the QD to the basic leucine zipper on the MBP or by a metal-affinity interaction between the QD and the C-terminal of the oligohistidine on the MBP (figure 1.16). The number of MBP groups and size of QDs were varied for the studies in order to evaluate the optimum FRET efficiency. Increasing the number of MBP groups on the QD surface had the effect of increasing the dye emission while decreasing the QD's output. This was confirmed by time-resolved fluorescence experiments showing the QD lifetime diminishing as more MBP was added. Furthermore, it was observed that altering the size of QD had the effect of changing the spectral overlap between the QD and MBP and hence the efficiency of energy transfer. It is evident from these studies that there must be an energy transfer mechanism in place, between the QD donor and dye acceptor molecule.

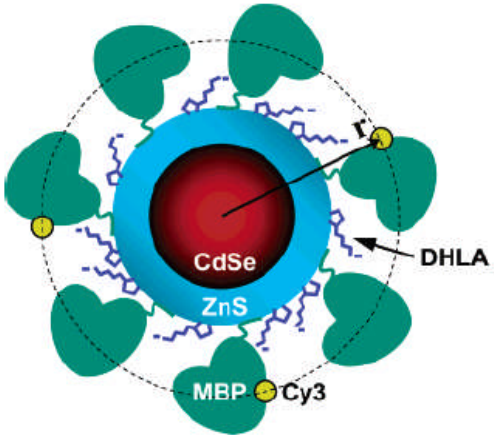

(2)

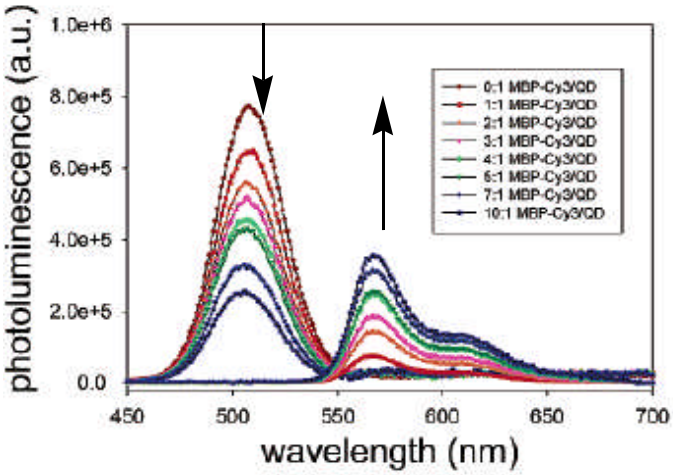

Figure 1.16 *(A) Mattoussi's schematic representation of the QD-MBP assembly* ***2****. The ligand DHLA is used to attract the MBP to the QD surface. The cyanine dye (Cy3) is attached to the MBP. (B) The QD-conjugate emission spectra with increasing amounts of dye to QD ratio*[73]*.*

The addition of MBP to CdSe/ZnS QDs has also been used to detect the explosive trinitrotoluene (TNT)[74] and also the disaccharide maltose[72]. MBP was bound to a beta-cyclodextrin analogue of maltose and then covalently linked to an organic dye quencher (QSY-9). This was then assembled on to CdSe/ZnS QDs by metal-affinity interactions via the oligohistidine C-terminal of MBP, as described in the previous example. With the quencher attached, efficient FRET was observed from the QD to the dye. On addition of maltose the beta-cyclodextrin dye complex was

ejected from the MBP binding pocket by competitive displacement and the QD emission was restored. The probe was tested for exclusive selectivity toward maltose by screening a variety of sugars and the results confirmed that the binding was specific for the α1-4 glucosidic linkages, found only in maltose.

A similar strategy was employed for the detection of trinitrotoluene (TNT) in aqueous solution[74].

(A)

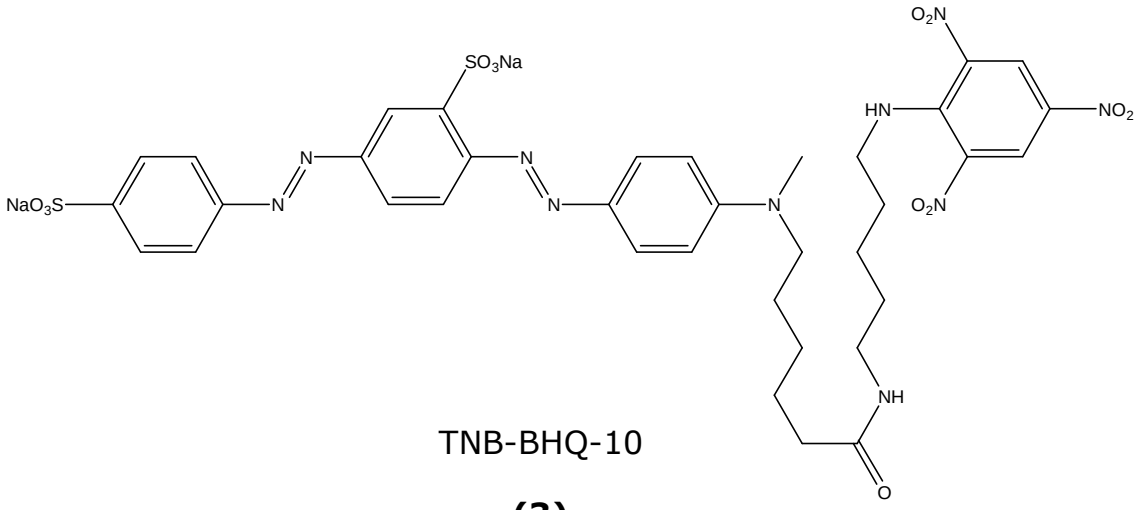

TNB-BHQ-10

(3)

(B)

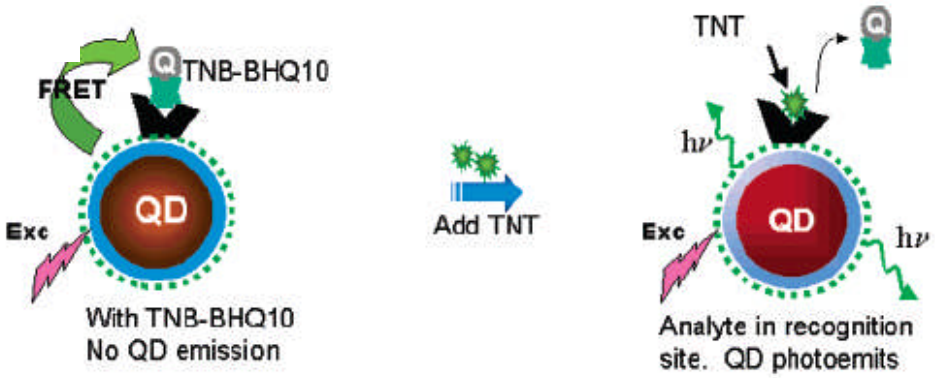

Figure 1.17 *(A) Structure of dye-labelled TNT analogue (TNB-BHQ-10)* ***(3)****. (B) Schematic of the TNT assay. The dye labelled TNT analogue TNB-BHQ-10 bound by the scFvs on the QD surface results in a complete quench due to FRET from the QD. Addition of TNT displaces the dye and fluorescence is recovered*[74]*.*

Anti-TNT specific antibody fragments (single-chain Fv fragments, scFvs) were appended to the surface of CdSe/ZnS QDs through an oligohistidine sequence. These scFvs fragments were preferred to the full antibody due to size considerations and so with a more compact QD conjugate, the distances were reduced, ensuring more efficient FRET. The dye labelled analogue of TNT (TNB-BHQ-10) **3** binds with the recognition site of the antibody fragment and participates in a FRET induced quenching of the QD photoluminescence. Spectral overlap of the QD donor and dye acceptor and the number of quenchers on the surface of the QD dictated the efficiency of the energy transfer. Addition of TNT resulted in the displacement of the analogue quencher and a significant recovery of the QD emission. Selectivity for TNT was confirmed after the probe was tested against a number of other explosives.

Zhou *et al* demonstrated FRET from a CdSe/ZnS QD to a double stranded DNA molecule labelled with an Alexa 594 dye[80]. The QDs were first made water soluble through a ligand exchange with 3-mercaptopropionic acid and then using a C_6-thiol linker[81] they were conjugated to DNA. This direct attachment to the QD surface reduced the distance between donor and acceptor and hence improved the FRET efficiency. Zhou's example demonstrated that even at low donor to acceptor ratios, a high level of FRET (~88%) can be achieved. However, other reports where dye-labelled DNA has been attached to QD-protein conjugates as donor acceptor pairs have shown these to be quite inefficient in terms of energy transfer and required a high number of acceptor molecules on the QD surface to participate in FRET[72, 73, 76].

Chen *et al* devised a ratiometric sensor for K^+ using two different sized QDs[82]. FRET occurring between a small QD (donor) emitting at 545 nm and a large QD (acceptor) emitting at 635 nm facilitated the sensing of potassium at the μM level. 15-crown-5 ether receptors were bound to the QD surface through the dithiol of an appended dihydrolipoic acid to give **4**. In the absence of K^+ emission is present for both sized QDs with the solutions of sufficient dilution to prevent any energy transfer between the QDs. Upon addition of $KClO_4$, the crown ether binds the K^+ cation and forms a QD (small) : K^+ : QD (large) complex. This results in a decrease in the emission of the small QDs with a concomitant increase in the output of

the large QDs due to FRET. In figure 1.18 these changes are illustrated with increasing concentration of K^+ denoted by a $\rightarrow$ n. Also presented is a titration with Na^+ in the presence of K^+ represented by the orange spectra. Upon addition of Na^+ to the solution the emissions returned to almost their original intensities. From the Hofmeister series it is observed that the hydrophobicity of K^+ in water is greater than Na^+[83]. This implies that if an excess of each cation is added and almost all the crown ethers have bound a cation, the K^+ may encourage aggregation more easily than Na^+ due to Van der Waals forces in aqueous media. This aggregation results in the formation of these sandwich complexes and facilitates the energy transfer. One drawback from this approach is the possibility of the formation of QD (545 nm): K^+:QD (545 nm) and QD (635 nm): K: QD (635 nm). However this outcome is statistically less probable (25%) compared to 50% for the mixed sized complex.

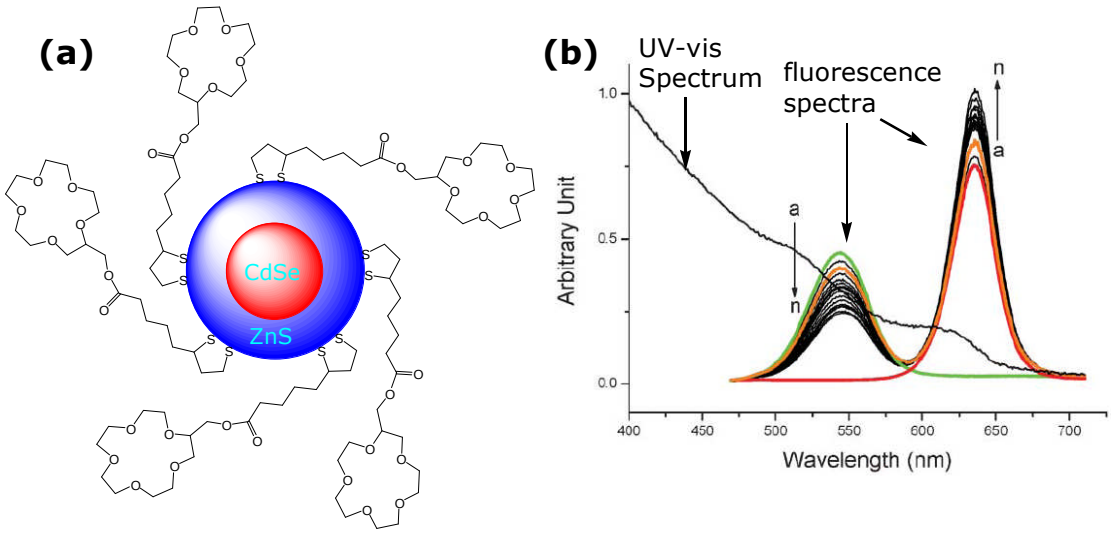

Figure 1.18 *(a) CdSe/ZnS QDs capped with 15-crown-5 ether receptors* ***(4)****. (b) fluorescence titration of* ***4*** *with K^+ (black spectra). Also shown is the UV-vis spectrum of the modified QDs prior to K^+ addition*[82]*.*

A QD sensor sensitive to changes in pH was designed by Raymo and colleagues[84]. A [1,3]-oxazine **5** covalently linked to lipoic acid was adsorbed onto CdSe/ZnS QDs and at low pH showed an absorption band centred at 398 nm. Addition of hydroxide ions (TBAOH) to the solution

resulted in the disappearance of this band with the appearance of a new band centred at 539 nm attributed to the transformation of **5** into the hemiaminal **6**. This resulted in a decrease of the fluorescence intensity (~80 %) for the QD-conjugate due to energy transfer from the QD to the ligand. The absorption spectra in figure 1.19 shows a substantial overlap in the emission of the QDs with the absorption band of the hemiaminal ensuring a favourable path for energy transfer to occur. The fluorescence was almost completely restored on addition of trifluoroacetic acid (figure 1.19(ii)), demonstrating the reversibility of the system.

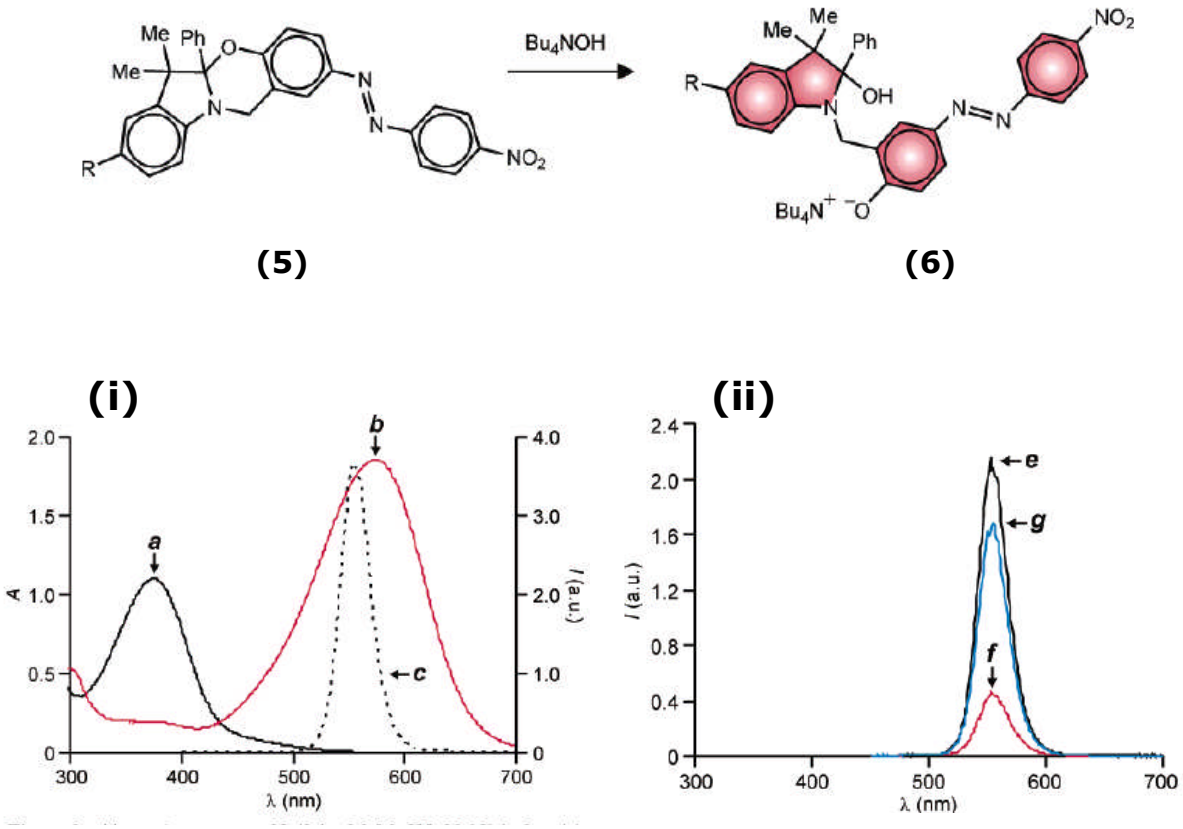

Figure 1.19 *Conversion of [1,3] oxazine **5** into hemiaminal **6** on addition of TBAOH. (i) absorption spectra of **5** before (a) and after (b) addition of TBAOH. The emission of the CdSe/ZnS QDs are included (c) illustrating the spectral overlap on conversion to the hemiaminal. (ii) Emission spectra of CdSe/ZnS QDs appended with **5** via a DHLA linker (e) (R = DHLA) and after equimolar additions of TBAOH (f) and then TFA (g)*[84].

1.8 Electron transfer with QDs

1.8.1 Background

The luminescence output of QDs are very much influenced by the surface states generated on the nanoparticle surface. These states can be affected by the physical and chemical interaction of certain species with the surface which causes modulation of the core's electron-hole recombination efficiency[85]. From the late 1980's, QDs have been used as a signalling unit to report the presence of small molecules and ions. In pioneering work, Spanhel *et al* observed that on adding Cd^{2+} to basic aqueous solution of unpassivated CdS QDs, the fluorescence was significantly enhanced[86]. This was attributed to the formation of $Cd(OH)_2$ on the surface. This shell essentially passivated the surface eliminating the non-radiative recombination of excitons. A similar effect was observed for the detection of metal ions such as Zn^{2+} and Mn^{2+}. A passivation of the surface trap states by the formation of metal species on the surface caused an enhancement of the luminescence.

1.8.2 Sensors based on PET and other mechanisms

The photoinduced electron transfer mechanism has been central to the design of many sensors incorporating organic dyes as the signalling unit. This mechanism has also been observed to influence the emission of QDs. Addition of p-phenylenediamine (PPD) (E_{ox} = 0.26 eV) to a colloidal solution of CdSe QDs (E_{ox} = 1.2 eV) has been shown to result in a quench of QD fluorescence[87]. This was attributed to the reduction of a hole in the valence band of the CdSe QDs thus disrupting the radiative recombination of the charge carriers. However, addition of n-butylamine (E_{ox} = 1.9 eV) resulted in an enhancement in the emission due to passivation of the surface traps.

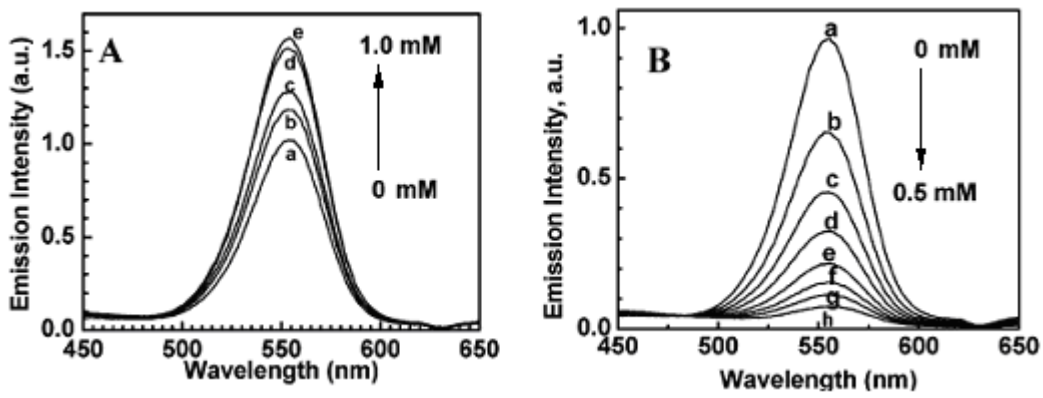

Figure 1.20 *(a) Illustrating the fluorescent enhancement on titration of CdSe QDs with n-butylamine. (b) Quenching effect on addition of PPD to the QD solution*[87]*.*

In another study Chen and Rosenzweig appended the amino acid L-cysteine to the surface of CdS QDs **7**[88]. They reported the first QD-ligand conjugate for the determination of ion concentration in aqueous solution. They found that upon addition of Zn^{2+}, an enhancement was observed due to activation of surface states. In a concurrent study, the authors exchanged thioglycerol onto the QD surface and the resulting conjugate **8** showed selectivity for Cu^{2+} ions. The binding of Cu^{2+} produced a quench in the fluorescence intensity attributed to the formation of Cu_xS (x = 1,2) or the presence of Cu^{2+} on the QD surface as reported by Isarov *et al* [89]. L-cysteine modified CdS QDs were also prepared by Chen and Zhu[90]. They found their QD probe to be selective to Ag^{+}, an ion not tested by Chen and Rosenzweig. An enhancement was observed upon addition of Ag^{2+} attributed to the formation of a silver complex with the L-cysteine. The creation of new radiative centres at the CdS/Ag-cysteine complex microheterojunctions essentially blocked non-radiative electron-hole recombination defect sites on the surface and increased the luminescence output of the QDs.

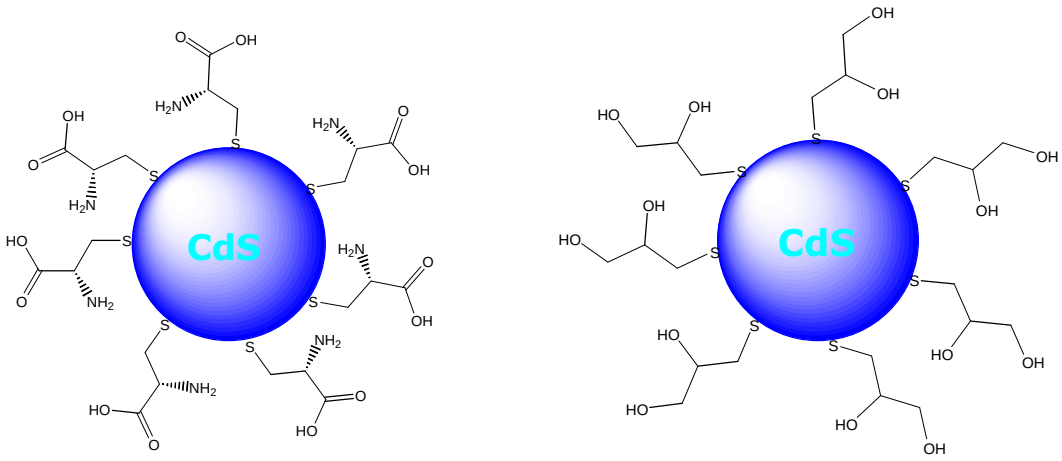

(7) **(8)**

Figure 1.21 *Schematic representation of (a) CdS QDs modified with L-cysteine **7** and (b) CdS QDs modified with thioglycerol **8**[88].*

A probe selective for both Ag^{+} and Cu^{2+} was proposed by Gattas-Asfura and Leblanc[91] when they assembled short peptides on the surface of CdS QDs. They found that the peptide sequence Gly-His-Leu-Leu-Cys showed the best selectivity of the peptides tested. The Leu-Leu unit was incorporated into the peptide chain to provide a hydrophobic sheath keeping the metal ions and basic histidine from the surface of the QD. The Gly-His component was chosen due to its proven selectivity for Cu^{2+} [88]. The QD-conjugate displayed excellent selectivity for Cu^{2+} and Ag^{+} even in the presence of a number of cations (i.e. K^{+}, Mg^{2+}, Ca^{2+}, Co^{2+}, Ni^{2+}, Fe^{3+}, Zn^{2+} and Cd^{2+}). This selectivity manifested itself optically in a complete quench of the fluorescence, most likely caused by an electron transfer mechanism from the redox active Cu^{2+} to the excited QD.

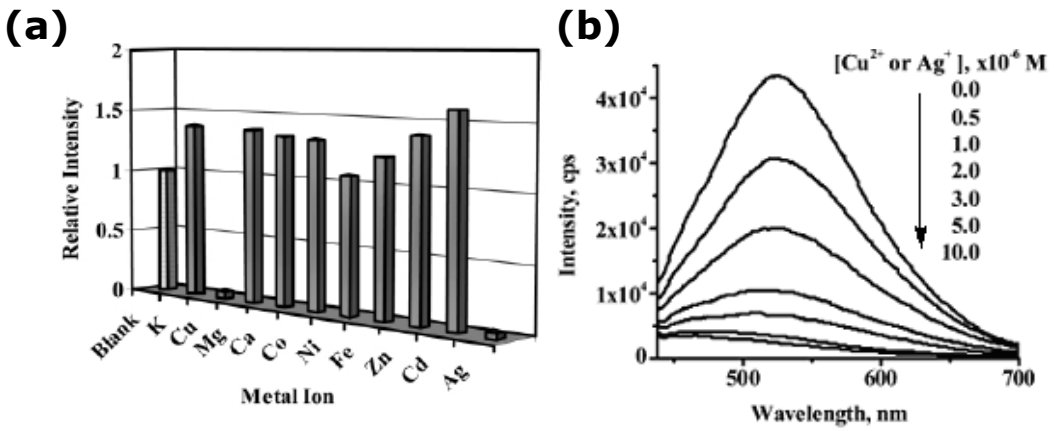

Figure 1.22 *(a) Bar chart illustrating the effect of various metal ions on the PL of Gly-His-Leu-Leu-Cys coated CdS QDs. (b) Effect of* Cu^{2+} *and* Ag^{2+} *on the PL of QD-conjugate shown spectrally*[91]*.*

Another probe with selectivity for Cu^{2+} has been described by Xie *et al* [92]who used core-shell CdSe/ZnS QDs functionalised with the protein Bovine Serum Albumin (BSA). An almost complete quench was observed for Cu^{2+} with a detection limit of 10 nM. Of the other ions screened Fe^{3+} also produced a moderate quench, however this was attributed to an inner filter effect which was cancelled by the addition of fluoride ions forming the colourless FeF_6^{3-} complex. The quench from Cu^{2+} was believed to be caused by the displacement of Cd^{2+} ions from the surface by Cu^{2+} ions. The driving force for this displacement was the increased solubility of CdSe in the aqueous solution compared to CuSe. Other QD systems have displayed similar quenching effects with Cu^{2+} by using mercaptopropionic acid[93]and mercaptoethanol[94] ligands grafted to their surface.

Section 1.3.2 discussed how a modified MBP bound to the surface of CdSe/ZnS QDs could detect maltose and TNT by displacement of a dye-quencher in favour of the target hence disrupting the energy transfer process. Unfortunately, this type of sensing strategy can be susceptible to interferences from dilution and diffusion[95]. Sandros *et al* [95]reported a chimeric MBP-metallothionein protein with surface cysteine residues appended to (tetraamine)(5-maleimido-phenanthroline)ruthenium (II) for the detection of maltose. This modified protein was assembled on to a CdSe QD via adsorption through the thiol group. The ruthenium donor in

the resulting assembly is close enough to engage in electron transfer with the QD, leading to a 5-fold decrease in its emission. Upon binding maltose a conformational change was induced thus increasing the distance between the ruthenium donor and QD. This led to a decrease in effective electron transfer between the two components with a 1.4 fold increase in the QD luminescence.

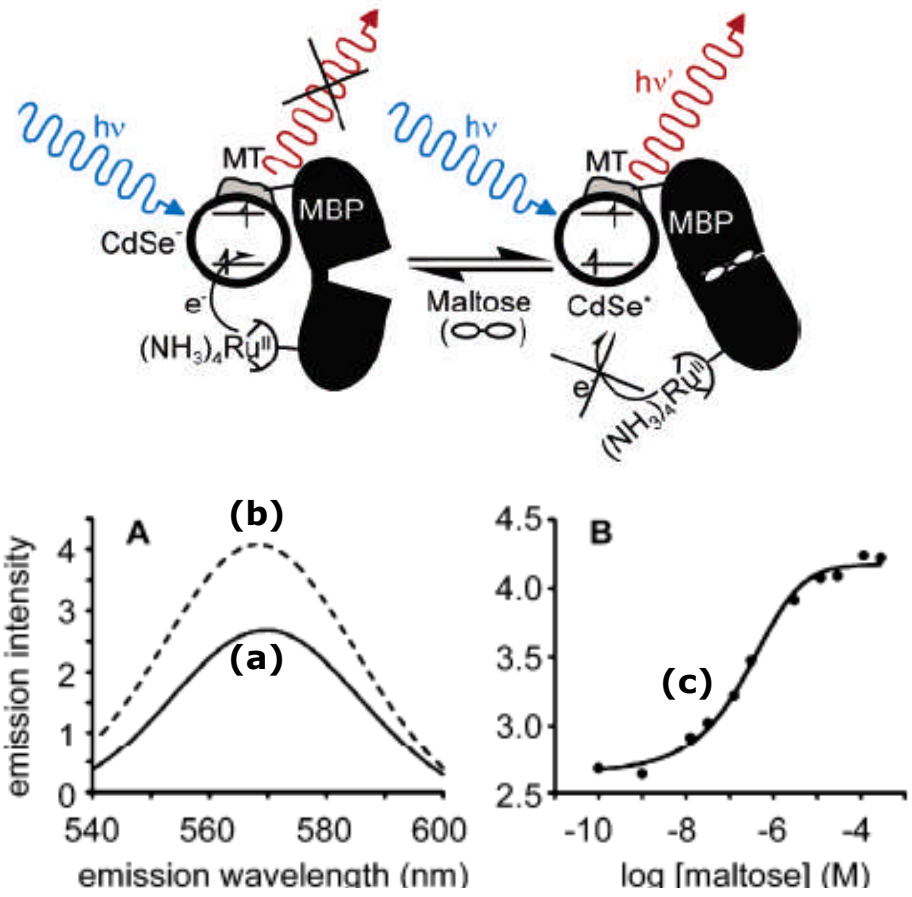

Figure 1.23 *(A) Schematic representation of Sandros et al's maltose probe. The conformational change upon binding maltose results in a cancellation of the electron transfer process between the* Ru^{2+} *and the QD resulting in a restoration of fluorescence. (a) the fluorescence spectra of the sensor (5 nM conc) without (solid line) and (b) with 1 mM maltose (broken line), (c) plot of emission intensity v log [maltose] (M)*[95].

In a similar fashion Yildiz *et al*[96] designed a sensor that was sensitive to the distant dependent nature of PET. In this instance CdSe/ZnS QDs were coated with the negatively charged mercaptoacetic acid ligand and exposed to **9**. This quencher comprised of a bipyridinium

dication conjugated to a biotin ligand. The positively charged bipyridinium component adsorbed onto the anionic QD surface and engaged in PET with the QD upon excitation[97, 98] resulting in a 2.5 fold decrease in luminescence intensity. The addition of streptavidin, which is known only to bind biotin, increased the distance between the cationic species and the QD resulting in a 1.4-fold increase in emission. The emission was restored to only 30% of its original intensity, presumably due to some residual bipyridinium complex remaining attracted to the negatively charged QDs.

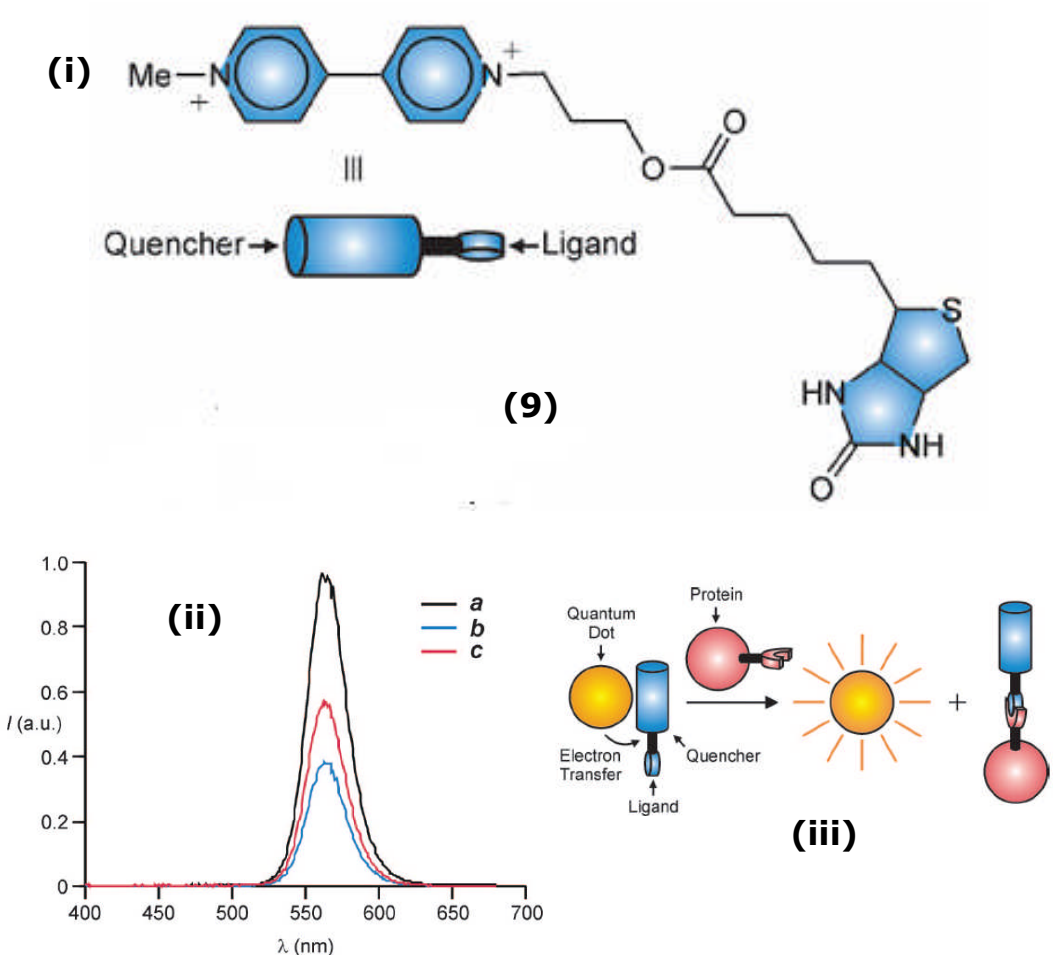

Figure 1.24 *(i) Chemical structure of the cationic bipyridinium conjugated to a biotin ligand (**9**). This species performs as the quencher on the surface of the QD engaging in PET. (ii) fluorescence spectrum of (a) the natural fluorescence of the host QD, (b) the fluorescence spectrum in the presence of the quencher and (c) the fluorescence spectrum after addition of the streptavidin, (iii) schematic diagram illustrating the supramolecular association of protein and ligand preventing electron transfer and switching "on" the QD's emission*[96]*.*

In a concurrent study Raymo's group looked at using the same quencher molecule without the biotin ligand attached. Again, this was adsorbed onto the surface of CdSe/ZnS QDs coated with negatively charged mercaptoacetic acid ligands.

(i)

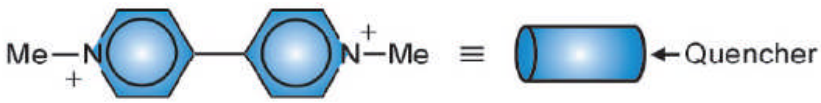

(10)

(ii)

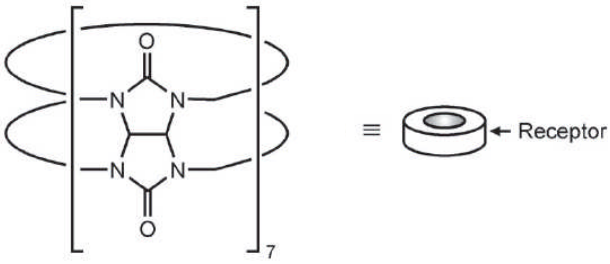

(11)

(iii)

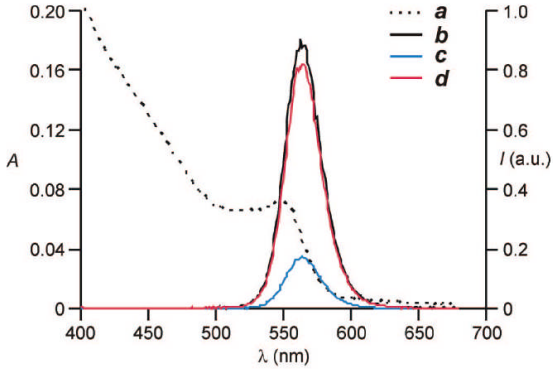

(iv)

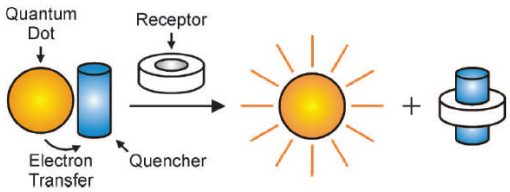

Figure 1.25 *(i) Chemical structure of the bipyridinium dication* ***10****. (ii) structure of the receptor, cucurbituril* ***11****. (iii) absorbance (a) and fluorescence (b) spectra of the host in the presence of* ***10*** *and (c) fluorescence spectrum of host +* ***10*** *to which* ***11*** *was added (d). (iv) schematic representation of interaction between QD host,* ***10*** *and* ***11****[96].*

A substantial quenching of the fluorescence was observed through electron transfer from the QD to the bipyridinium dications. However, this was reversed on addition of cucurbituril which disturbed the electrostatic attraction between the quencher and QD. Cucurbituril is a known binder of bipyridinium dications with high association constants in aqueous systems[99, 100]. In figure 1.25 the fluorescence spectrum illustrates the effect of the quencher on the luminescence intensity of the QD (line c). There was a substantial decrease followed by an 80% recovery on addition of cucurbituril. This recovery was substantially greater than the previous example which described an increase of just 30%. The shortfall was probably due to the difference in binding approaches by biotin and **11**. For **9**, binding with the streptavidin only occurs at the biotin end while the macrocycle **11** can effectively encapsulate the dication reducing its electrostatic attraction to the QD surface and decreasing its quenching ability.

Cordes *et al* designed a two component system for the detection of glucose based on a boronic acid substituted viologen as the quencher/receptor and CdSe/ZnS QDs (em = 604 nm) as the emitting unit[101]. In this study two sets of QDs were used and rendered water soluble by functionalising the surface with amine or carboxyl groups. At pH 7.4, the carboxyl groups exist in anionic form while the amine groups are usually as the free base. Not surprisingly the carboxyl capped QDs demonstrated more efficient quenching on the introduction of the viologen quencher due to superior electrostatic attraction. This quenching was achieved through excited-state electron transfer from the QD to the viologen, reducing the methyl viologen (MV) from MV^{2+} to $MV^{\cdot+}$.

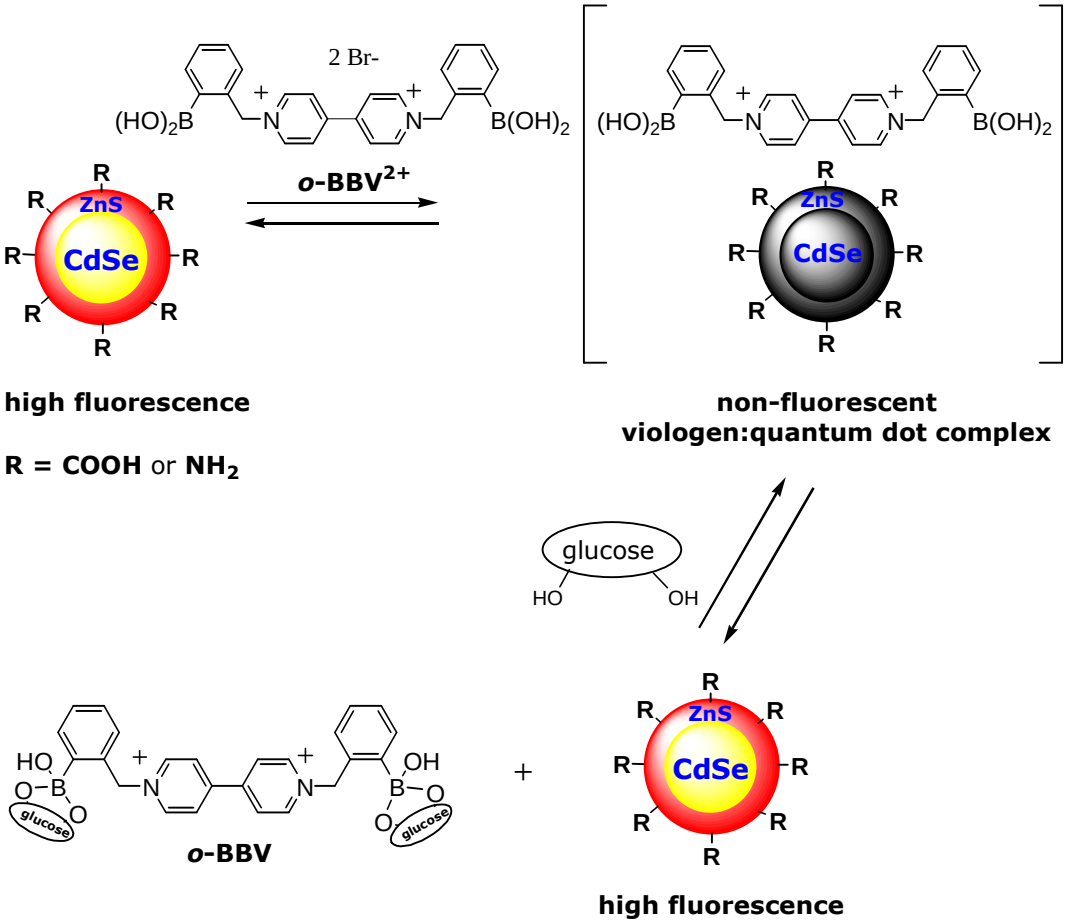

Figure 1.26 *Mechanism for glucose sensing with CdSe/ZnS QDs*[101].

The effectiveness of this sensor was displayed upon the introduction of the monosaccharide, glucose. In the absense of glucose, the boronic acids on the viologen exist in a trigonal neutral form at pH 7.4. When they bind glucose they form the glucose boronate ester, reverting into their anionic tetrahedral form. This intreraction resulted in a restoration of the QD fluorescence due to the decrease in the positive charge on the viologen and concomitant loss in electrostatic attraction between the QD and quencher. The fluorescent response to glucose was modest in the physiological range with a quencher / QD ratio of 1000:1 giving the optimum results. The authors didn't report any selectivity for other physiological relevant monosaccharides.

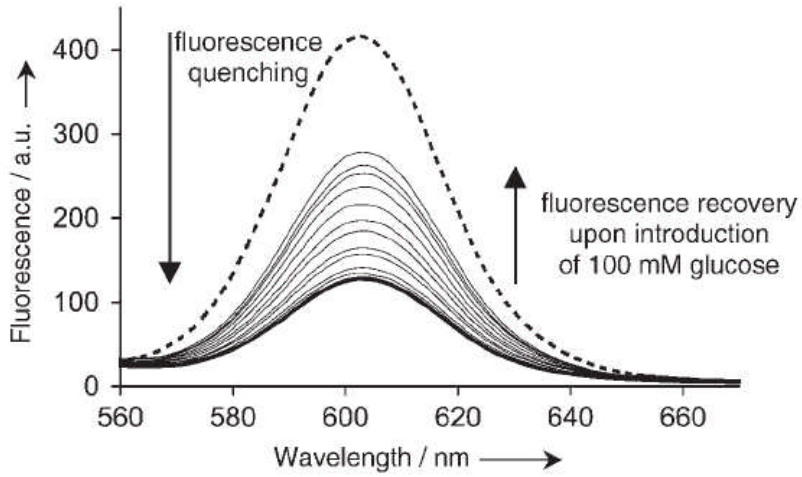

Figure 1.27 *Fluorescence response of amine-capped QDs upon addition of quencher and the subsequent recovery on addition of glucose (final glucose concentration = 100 nm)*[101].

A simple strategy for selective Cd^{2+} determination has been proposed by Banerjee *et al*[102]. CdS:Mn/ZnS core-shell QDs were surface modified with 1,10-diaza-18-crown-6, **12** via a CS_2 linker. The receptor **12** was directly attached to the QD surface through the linker molecule forming a zero-length coupling with the secondary amine group on the receptor (figure 1.28). A competitive ligand exchange with thioglycolic acid showed no loss of the receptor from the surface illustrating the robustness of the attachment. From photoluminescence studies it was shown that the emission from the **13** was markedly less than the parent QDs. It was proposed that PET from the secondary amine to the QD through the CS_2 linker was the likely mechanism for the quench. The authors validated this theory through a ligand detachment study to see if a restoration in the emission would be observed. Using dithiothreitol (DTT), a commonly used cleaver of disulfide bonds, they added this to the QD solution. An initial minor recovery of the PL was noted but this was not significantly intense to attribute it to detachment. It was deduced that reattachment of the ligand must be occurring after the initial detachment so it was decided to repeat the experiment, again using DTT but also adding a trapping agent, methyl acrylate in order to capture the free carbodithioate and prevent it from reattaching to the QD surface. This had

the desired effect and a significant restoration of the QD emission was observed thus proving electron transfer from the amine lone pairs on **12**.

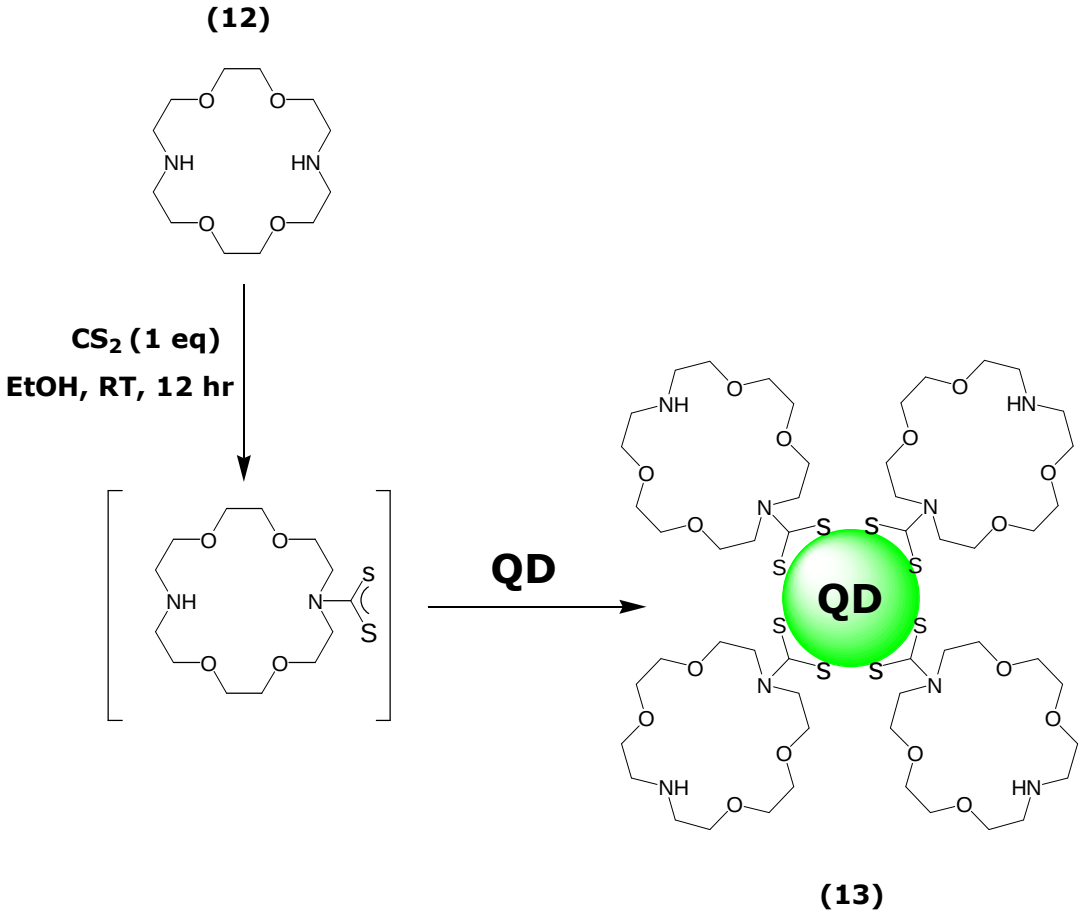

Figure 1.28 *Reaction scheme for the synthesis of Banerjee et al's cadmium sensor*[102]*.*

A number of metal ions were screened for selectivity and of those tested only Cd^{2+} exhibited a significant response. Similar selectivity was observed for an organic dye probe containing the same receptor **12**[103]. An almost complete restoration of the original parent QD PL was observed for the probe highlighting its excellent sensitivity toward Cd^{2+}. It was noted that a small effect was produced with Zn^{2+} resulting in a minor recovery in the PL of the probe. This lower affinity of **12** for Zn^{2+} has been observed before by others[103, 104].

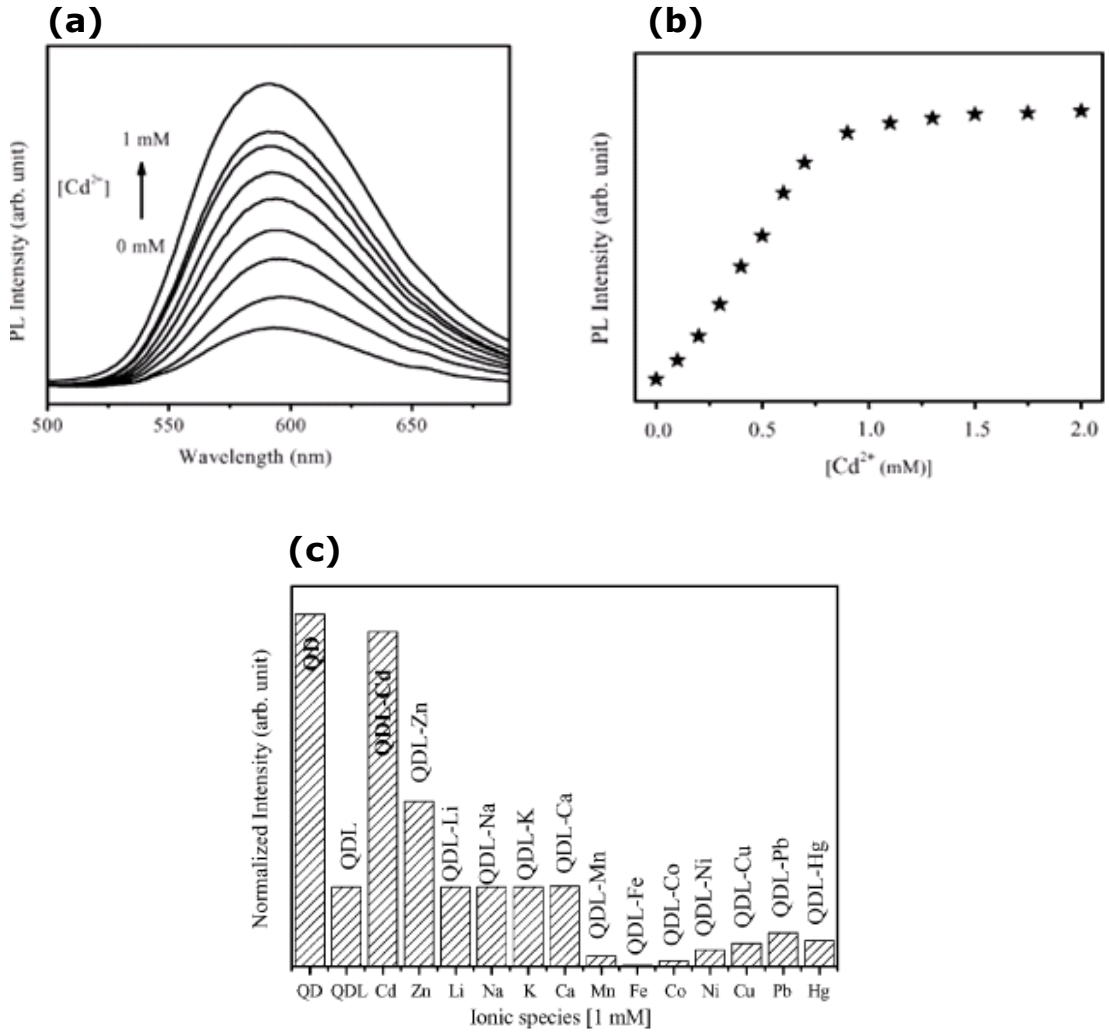

Figure 1.29 *(a) Restoration of the PL of* ***13*** *on addition of* Cd^{2+}*. (b) Plot of PL intensity of* ***13*** *v* Cd^{2+} *concentration. (c) Bar chart illustrating the selectivity of* ***13*** *for common metal ions*[102]*.*

Although this method provides an "off-on" sensor for metal ions, targeting cations such as Cd^{2+} and Zn^{2+} can prove problematic due to their presence in the nanoparticle. Addition of these ions as analytes may re-passivate the QD surface damaged by ligand exchange and lead to a "false positive" increase in emission intensity. Therefore in this thesis only analytes not present in the QD core and shell will be investigated.

These examples show that significant progress has been made in the development of QD based sensors in the past few years. When the work conducted in this thesis began in 2005 examples of electron transfer controlled QD sensors were limited and often used elaborate mechanisms

in their operation. This thesis aims to develop more simplistic sensors incorporating the PET mechanism.

CHAPTER TWO

EXPERIMENTAL

2.1 General method

2.1.1 Reagents and materials

Amberlite resin, aminoethanethiol, aniline, cadmium oxide, CdSe/ZnS QDs (Evident technologies), *N,N*-dimethylcysteamine, diphenylphosphoryl azide, dimethylzinc, ferrocene carboxaldehyde, hexamethyldisilathiane, hydroxylamine hydrochloride, iodomethane, lithium aluminium hydride, 2-mercaptoaniline, mercaptosuccinic acid, 1-octadecene, oleic acid, 2- phenyl isothiocyanate, salicylaldehyde, selenium powder, sodium borohydride, sodium hydroxide, tetrabutylammonium hydroxide, thioctic acid, trioctylphosphine, triethylamine, trioctylphosphine (TOP).

2.1.2 UV-vis and fluorescence measurements

Absorption spectra were recorded on an Agilent UV-vis spectrometer using 10 mm quartz cuvettes. Fluorescence measurements were recorded on a Perkin Elmer LS55 Luminescence spectrometer using 10 mm quartz cuvettes. Spectrophotometric grade solvents were used for analyses. Excitation wavelength, unless otherwise stated, was set at 370 nm. Similarly, unless otherwise stated, excitation slit size was set at 10 nm and emission slit size was 10 nm. Scan speed was set at 500. All spectroscopic experiments were repeated in triplicate.

2.1.3 NMR analysis

NMR spectra were recorded on a Bruker Ultrashield 400 MHz spectrometer. ^{1}H NMR samples were prepared by dissolving 5 mg of sample in 1 mL of deuterated solvent. ^{13}C NMR samples were prepared by dissolving 10 mg of sample in 1 mL of deuterated sample and were recorded at 100 MHz. Chemical shifts are reported in parts per million (ppm), downfield of trimethylsilane.

2.1.4 Mass spectrometry

Low resolution mass spectrometry (LRMS) experiments were performed on an Agilent LCMS spectrometer. The ionisation method was electrospray (ESI). Accurate mass measurements for novel compounds

were provided courtesy of the Engineering and Physical Sciences Research Council (EPSRC) National MS service in Swansea.

2.1.5 Infrared analysis

Infrared spectra recorded as Nujol mulls were measured on a Nicolet Avatar 370 DTGS I.R. instrument.

2.1.6 Dynamic light scattering and zeta potential

Zeta potential measurements were recorded in aqueous solution at 25°C on a Malvern NanoZS zetasizer calibrated against polystyrene latex. Dynamic light scattering (DLS) measurements were recorded on the same instrument. Particle size distributions were recorded at 25°C using a He-Ne laser at 633 nm. The average size quoted was the average of 20 independent experiments and the standard deviation was taken as the error. Spectrophotometric grade solvents were used for DLS studies.

2.1.7 Transmission Electron Microscopy

Transmission Electron Micrographs were recorded with a JEOL-JEM 2011 electron microscope operating at 200 kV at the Electron Microscopy Unit in the Department of Chemistry, St. Andrew's University.

2.2 Experimental Procedures

2.2.1 Organic synthesis

2.2.1.1 Synthesis of dihydrolipoic acid (16)

Following a literature procedure by Uyeda *et al*,[105] lipoic acid (1.44 g, 7.0 mmoles, 1 eq) was dissolved in MeOH / 0.25 N $NaHCO_3$ (1:1, 50 mL). The mixture was stirred on ice, keeping the temperature below 5 °C. Sodium borohydride (0.6 g, 16.0 mmoles, 2.3 eq) was added portionwise. This was stirred for about 30 mins after which toluene (50 mL) was added to the reaction mixture. The solution's pH was adjusted to 1 with the aid of 38% HCl. The toluene layer was separated from the aqueous layer, dried over sodium sulfate and the solvent evaporated under reduced

pressure. Yield = 1.32 g, 90.7 %. ^{1}H NMR (MeOD) δ(ppm) 1.46 – 1.752 (m, 7H, 3 x C*H*$_2$, CH$_2$ (*H*$_a$)), 1.91 (m, 1H, CH$_2$(*H*$_b$)), 2.32 (t, *J* = 7.2 *Hz*, 2H, C*H*$_2$C=O), 2.68 (m, 2H, ring, C*H*$_2$), 2.92 (m, 1H, C*H*), 4.99 (br.s, 2H, S*H*). ^{13}C NMR (100 MHz, MeOD) δ(ppm) 177.60 (*C*=O), 44.23 (*C*H), 40.14 (*C*H$_2$), 39.60 (*C*H$_2$), 34.91 (*C*H$_2$), 27.68 (*C*H$_2$), 25.90 (*C*H$_2$), 22.86 (*C*H$_2$). -ve ESMS expected for $C_8H_{16}O_2S_2$: *m/z* 208.1. Found: *m/z* 207.1 (M – H$^+$) (30%).

2.2.1.2 Synthesis of *N,N,N*-trimethyl-2-sulfanylethanaminium iodide (26).

Following a procedure by Bernardes *et al*,[106] *N,N*-dimethylcysteamine (1.0 g, 9.52 mmol, 1 eq) was dissolved in anhydrous acetonitrile (10 mL) and allowed to stir. Iodomethane (5.4 g, 38 mmol, 4 eq) was pipetted into this solution and the reaction proceeded overnight at room temperature. A precipitate developed overnight which was collected by filtration and washed several times with acetonitrile. The product was isolated as a white powder and was dried *in vacuo*. Yield = 2.3 g, 49.7 %. ^{1}H NMR (D$_2$O) δ(ppm) 3.62 (m, 2H, HSC*H*$_2$), 3.08 (s, 9H, 3 x C*H*$_3$), 3.06 (m, 2H, NC*H*$_2$). ^{13}C NMR (D$_2$O) δ(ppm) 66.2 (N*C*H$_2$), 53.0 (*C*H$_3$), 29.7 (SH*C*H$_2$). +ve ESMS expected for $C_5H_{14}NS$: *m/z* 120.1. Found: *m/z* 119.2 (disulfide, *m*/2) (58%).

2.2.1.3 Preparation of *N,N,N*-trimethyl-2-sulfanylethanaminium chloride (27).

Compound **26** (1.0 g) was dissolved in deionised water (100 mL). Amberlite resin (30 mL) was charged into a separating funnel and 2M HCl (~200 mL) was introduced. When all the HCl had drained from the resin, deionised water was flushed through until the pH had neutralised. The solution containing **26** was then poured onto the resin and this was allowed to drip through into a conical flask. Three passes through the resin were carried out and the final solution freeze-dried to yield the product. Yield = 0.51g (82%)

2.2.1.4 Synthesis of 1-(2-mercapto-ethyl)-3-phenyl-thiourea (38).

Following a literature procedure by Heinelt *et al*[107], 2-aminoethanethiol (2.0 g, 26 mmol, 1 eq) was dissolved in anhydrous chloroform (25 mL). Into this solution was added phenyl isothiocyanate (3.13 mL, 26.3 mmol, 1.eq). The contents were stirred at room temperature for 18 hr. The solvent was evaporated under reduced pressure yielding a yellow residue. This was triturated with diethyl ether (20 mL) and a white precipitate developed. Ethanol (50 mL) was added to the precipitate and the contents stirred for 30 mins. The product was filtered under reduced pressure and washed with ethanol (50 mL) and dried *in vacuo.* The crude product was purified by dissolving in a hot solution of methanol / ethyl acetate and precipitating with cold hexane. Yield = 2.49 g, 45.2 %. ^{1}H NMR ($CDCl_3$) δ(ppm) 7.66 (br.s, 1H, PhN*H*), 7.38 (dd, J = 7.8 Hz, 2H, aryl), 7.25 (dd, J= 7.4 Hz, 1H, aryl), 7.17 (d, J = 8.4 Hz, 2H, aryl), 6.42 (br.s, 1H, -CH_2N*H*), 3.88 (q, J = 6.0 Hz, 2H, -NHC*H_2*-), 2.91 (t, J=6.2 Hz, 2H, HSC*H_2*). ^{13}C NMR ($CDCl_3$) δ(ppm) 180.91 (1C, -C=S), 135.85 (CH), 130.28 (CH), 127.61 (C), 125.41 (CH), 43.85 (CH_2), 37.14 (CH_2). +ve ESMS expected for $C_9H_{12}N_2S_2$: *m/z* 213.0 (M + H^+). Found: *m/z* 445.1 (Disulfide + Na^+) (100%), 213.0 (10%), 211.1 (70%). Melting point = 150° C.

2.2.1.5 Synthesis of Ferrocenylcarboxaldehyde oxime (46).

Following a literature procedure by Baramee *et al*[109], ferrocene carboxaldehyde (3.00 g, 14 mmol, 1 eq) was dissolved in ethanol (130 mL). To this solution, sodium hydroxide (3.30 g, 82.5 mmol, 5.9 eq) and hydroxylamine hydrochloride (1.95 g, 28 mmol, 2 eq) was charged and the reaction was refluxed for 3 hr. After cooling, water (150 mL) was added and the product was extracted with dichloromethane (3 x 150 mL). The organic layers were combined, dried over sodium sulfate and the solvent was removed *in vacuo* to give ferrocenylcarboxaldehyde oxime as an orange solid (2.99 g, 92.8 %). ^{1}H NMR (400 MHz, $CDCl_3$) δ(ppm) 7.91 (s, 1H, C*H*=N), 7.79 (br.s, 1H, O*H*), 4.56 (m, 2H, C_p), 4.28 (m, 2H, C_p), 4.15 (s, 5H, C_p). ^{13}C NMR (100 MHz, $CDCl_3$) δ(ppm) 150.0 (*C*H=N), 70.0

(C_p), 69.3 (C_p), 67.6 (C_p). +ve ESMS expected for $C_{11}H_{11}NOFe$: *m/z* 229.0. Found: *m/z* 230.0 (M + H^+) (100%).

2.2.1.6 Synthesis of Ferrocenylmethylamine (47).

Following a literature procedure by Baramee *et al*[109], compound **46** (2.34 g, 10.2 mmol, 1 eq) dissolved in dry THF (50 mL) was added dropwise to Lithium aluminium hydride (LAH) (2.06 g, 54.2 mmol, 5.3 eq) in dry THF (50 mL). The reaction was refluxed under nitrogen for 6 hr. After cooling, water (100 mL) was slowly added (extreme caution was observed for LAH quenching) and the product was extracted with diethyl ether (3 x 150 mL). The combined organic layers were dried over sodium sulfate and concentrated under vacuum to give an orange oil (1.97 g, 90.0 %). ^{1}H NMR (400 MHz, $CDCl_3$) δ(ppm) 4.14 (m, 2H, C_p), 4.12 (m, 5H, C_p), 4.09 (m, 2H, C_p), 3.53 (s, 2H, CH_2). ^{13}C NMR (100 MHz, $CDCl_3$) δ(ppm) 90.9 (*C*H=N), 68.3 (C_p), 67.6 , (C_p) 67.1 (C_p), 41.3 (C_p). +ve ESMS expected for $C_{11}H_{13}NFe$: *m/z* 215.1. Found: *m/z* 216.1 (M + H^+) (48%).

2.2.1.7 Synthesis of 5-(1,2-dithiolan-3-yl)pentanoyl azide (49).

Based on a procedure by Fidesser *et al*[110], an ice cold solution of thioctic acid (3.80 g, 18.5 mmol, 1 eq) and triethylamine (1.87 g, 18.5 mmol, 1 eq) was dissolved in dry DMF and allowed to stir under N_2. A solution of diphenylphosphoryl azide (5.10 g, 18.5 mmol, 1 eq) in dry DMF (15 mL) was added dropwise over a period of 2 hrs. After removal of the ice bath, stirring was continued for 3 hrs at room temperature. The reaction contents were then poured into a mixture of ether and ice. When the ice had thawed, the upper layer was collected and washed with a saturated solution of $NaHCO_3$. This was then washed with H_2O, dried over Na_2SO_4 and then solvent evaporated under reduced pressure (bath temperature not exceeding 30 °C) to afford the product. Yield = 2.93 g (68.6 %). ^{1}H NMR (400 MHz, $CDCl_3$) δ(ppm) 1.45 (m, 2H, CHC*H*$_2$), 1.65 (m, 4H, 2 x CH_2), 1.88 (m, 1H, ring C*H*$_2$), 2.33 (t, *J* = 7.2 *Hz*, 2H, C*H*$_2$C=O), 2.44 (m, 1H, ring C*H*$_2$), 3.12 (m, 2H, S-C*H*$_2$), 3.54 (m, 1H, S-C*H*). ^{13}C NMR (100 MHz, $CDCl_3$) δ(ppm) 24.41 (*C*H$_2$), 28.58 (*C*H$_2$), 34.56 (*C*H$_2$C=O), 36.60 (CH*C*H$_2$), 38.52 (S-*C*H$_2$), 40.22 (CH-*C*H$_2$), 56.23 (*C*H),

180.40 (*C*=O). I.R. (Nujol) 2138 cm^{-1} (N_3). ESMS expected for $C_8H_{13}N_3OS_2$: *m/z* 231.1. +ve ESMS found: *m/z* 276.0 (M + 2Na –H). –ve ESMS found: *m/z* 265.2 (M + Cl^-), 309.0 (M + Br^-).

2.2.1.8 Synthesis of 1-ferrocenyl-3-[4-(1,2-dithiolan-3-yl)butyl]urea (51).

Based on a procedure described by Fidesser *et al*[110], a solution of **49** (1.95 g, 8 mmol, 1 eq) in dry toluene (100 mL) was refluxed for 15 mins under N_2 after which **47** (1.64 g, 8 mmol, 1 eq) in dry toluene (10 mL) was pipetted into the stirring solution. Refluxing was continued for 2 hrs. The solvent was then removed under reduced pressure (bath temp < 40 °C). The crude product was purified by flash chromatography (DCM / MeOH, 98:2) and evaporated to give a dark orange oil. Yield = 3.2 g (95.7 %). ^{1}H NMR (400 MHz, $CDCl_3$) δ(ppm) 1.47 (m, 4H, 2 x CH_2), 1.65 (m, 2H, CH_2), 1.88 (m, 1H, ring CH_2(H_a)), 2.39 (m, 1H, ring CH_2(H_b), 3.07 (m, 2H, CH_2-NH), 3.14 (m, 2H, S-CH_2), 3.53 (m, 1H, C*H*), 4.03 (s, 2 H, CH_2-C_p), 4.03 (m, 2H, C_p), 4.14 (s, 5H, C_p), 4.18 (m, 2H, C_p). ^{13}C NMR (100 MHz, $CDCl_3$) δ(ppm) 157.84 (*C*=O), 85.73 (NH-*C*H_2), 68.55 (C_p), 68.09 (C_p), 67.92 (C_p), 56.51 (*C*H), 40.27 (*C*H*C*H_2), 39.89 (S-*C*H_2), 38.48 (CHCH_2), 34.55 (*C*H_2C=O), 30.32 (*C*H_2), 26.55 (*C*H_2). HRMS, calculated for $C_{19}H_{26}ON_2S_2Fe$: 419.0909 [M + H^+]. Found: 419.0907 [M + H^+].

2.2.1.9 Synthesis of 1-ferrocenyl-3-(5,7-disulfanylheptyl)urea (52).

Based on a procedure by Chittiboyina *et al*,[111] A solution of $NaBH_4$ (0.53 g, 14 mmol, 1.9 eq) in 15 mL of H_2O was added dropwise to an ice-cold solution of **51** (3.12 g, 7.5 mmol, 1 eq). The mixture was allowed to stir for an additional 1 hr. After completion of the reaction, 1N HCl (37.5 mL) was added and the solvent removed under reduced pressure (bath temp < 40 °C). The residue was diluted with H_20 (100 mL) and extracted with DCM (2 x 200 mL). The combined organic layers were washed with brine, dried over Na_2SO_4 and concentrated under reduced pressure to afford the product. Yield = 3.0 g (95.2 %). ^{1}H NMR (400 MHz, $CDCl_3$) δ(ppm) 1.26 (d, 1H, *J* = 8 Hz, CH-S*H*), 1.33 (m, 1H, *J* = 8 Hz, CH_2-S*H*), 1.65 (m, 2H, CH-CH_2), 1.47 (m, 4H, 2 x CH_2), 1.88 (m, 1H, ring CH_2(H_a)),

2.43 (m, 1H, ring CH_2(H_b), 3.08 (m, 2H, CH_2-NH), 3.14 (m, 2H, S-CH_2), 3.53 (m, 1H, CH), 4.05 (s, 2 H, CH_2-C_p), 4.09 (m, 2H, C_p), 4.13 (s, 5H, C_p), 4.15 (m, 2H, C_p). ^{13}C NMR (100 MHz, $CDCl_3$) δ(ppm) 158.05 (*C*=O), 85.80 (NH-*C*H_2), 68.79 (C_p), 68.04 (C_p), 67.92 (C_p), 56.52 (*C*H), 40.33 (CH*C*H_2), 40.27 (S-*C*H_2), 39.84 (CH*C*H_2), 38.49 (*C*H_2C=O), 29.98 (*C*H_2), 26.56 (*C*H_2). ESMS expected for $C_{19}H_{28}ON_2S_2Fe$: *m/z* 420.1. –ve ESMS found *m/z* 419.1 (M - H^+) (base peak), 455.0 (M + Cl^-).

2.2.1.10 Synthesis of 1-[4-(1,2-dithiolan-3-yl)butyl]-3-phenylurea (54).

Based on a procedure described by Fidesser *et al*[110], a solution of **49** (1.5 g, 6.49 mmol, 1 eq) in dry toluene (80 mL) was refluxed for 15 mins under nitrogen, after which aniline (0.604 g, 6.49 mmol, 1 eq) was pipetted into the stirring solution. Refluxing was continued for 2 hr. The solvent was then removed under reduced pressure (bath temp < 40 °C). Yield = 0.765 g (39.8 %) ^{1}H NMR (400 MHz, $CDCl_3$) δ(ppm) 1.37 (m, 4H, 2 x CH_2), 1.55 (m, 2H, CH_2), 1.79 (m, 1H, ring CH_2(H_a)), 2.32 (m, 1H, ring CH_2(H_b), 3.01 (m, 2H, CH_2-NH), 3.06 (m, 2H, S-CH_2), 3.42 (m, 1H, CH), 5.54 (bs, 1H, CH_2-N*H*), 6.95 (m, 1H, Ar), 7.19 (m, 5H, Ar), 7.38 (s, 1H, Ar-N*H*). ^{13}C NMR (100 MHz, $CDCl_3$) δ(ppm) 156.17 (*C*=O), 138.61 (*C*H), 129.53 (*C*H), 129.08 (*C*H), 123.77 (*C*H), 121.05 (*C*H), 120.19 (*C*H), 56.51 (*C*H), 40.26 (*C*H_2), 40.05 (*C*H_2), 38.47 (*C*H_2), 34.51 (*C*H_2), 29.86 (*C*H_2), 26.54 (*C*H_2). ESMS expected for $C_{14}H_{20}N_2OS_2$: *m/z* 296.1. +ve ESMS found: *m/z* 335.1 (M + K^+) (100%), 297.1 (M + H^+) (75%), 319.1 (M + Na^+) (20%).

2.2.1.11 Synthesis of 1-(5,7-disulfanylheptyl)-3-phenylurea (55).

Based on a procedure by Chittiboyima *et al*,[111] A solution of $NaBH_4$ (0.065 g, 1.7 mmol, 2 eq) in 2 mL of H_2O was added dropwise to an ice-cold solution of **54** (0.25 g, 0.85 mmol, 1 eq). The mixture was allowed to stir for an additional 1 hr. After completion of the reaction, 1N HCl (4 mL) was added and the solvent was removed under reduced pressure (bath temp < 40 °C). The residue was diluted with H_20 (20 mL) and extracted with DCM (2 x 25 mL). The combined organic layers were washed with

brine, dried over Na_2SO_4 and concentrated under reduced pressure to afford the product. Yield = 0.19 g (75.0 %). ^{1}H NMR (400 MHz, $CDCl_3$) δ(ppm) 1.19 (m, 1H, S*H*), 1.28 (m, 1H, S*H*), 1.37 (m, 4H, 2 x CH_2), 1.55 (m, 2H, CH_2), 1.79 (m, 1H, ring CH_2(H_a)), 2.32 (m, 1H, ring CH_2(H_b), 3.01 (m, 2H, CH_2-NH), 3.06 (m, 2H, S-CH_2), 3.42 (m, 1H, C*H*), 5.54 (bs, 1H, CH_2-N*H*), 6.95 (m, 1H, Ar), 7.19 (m, 5H, Ar), 7.38 (s, 1H, Ar-N*H*). ^{13}C NMR (100 MHz, $CDCl_3$) δ(ppm) 155.72 (*C*=O), 138.20 (*C*H), 128.55 (*C*H), 127.71 (*C*H), 121.84 (*C*H), 119.28 (*C*H), 118.80 (*C*H), 41.74 (*C*H), 38.93 (*C*H_2), 38.43 (*C*H_2), 37.68 (*C*H_2), 28.88 (*C*H_2), 23.34 (*C*H_2), 21.34 (*C*H_2). HRMS, calculated for $C_{14}H_{22}ON_2S_2$: 299.1246 [M + H^+]. Found: 299.1248.

2.2.1.12 Synthesis of 2-[(2-mercapto-phenylimino)-methyl]-phenol (61).

From a literature procedure described by Tisato *et al*[112], salicylaldehyde (2.04 g, 16 mmol, 1 eq) and 2-mercaptoaniline (2.10 g, 16 mmol, 1 eq) were mixed in ethanol (30 mL). The solution immediately became yellow and after 30 mins a white powder precipitated from solution. This was filtered and washed with ethanol and finally diethyl ether to give the product. Yield = 1.85 g (48.2 %). ^{1}H NMR (400 MHz, $CDCl_3$) δ(ppm) 4.53 (s, 1H, S*H*), 6.76 (m, 2H, Ar), 6.93, (m, 2H, Ar), 7.02 (m, 2H, Ar), 7.21 (m, 1H, Ar), 7.25 (s, 1H, C*H*=N) 8.79 (br.s 1H, O*H*). ^{13}C NMR (100 MHz, $CDCl_3$) δ(ppm) 157.12 (*C*H=N), 145.17 (*C*-OH), 130.75 (*C*H), 128.98 (*C*H), 128.48 (*C*H), 127.41 (*C*H), 125.77 (*C*H), 122.44 (*C*H), 122.38 (*C*H), 120.19 (*C*H), 119.73 (*C*H), 117.95 (*C*H), 111.60 (*C*-SH). ESMS expected for $C_{13}H_{11}NOS$: *m/z* 229.1 [M + H^+]. +ve ESMS found: *m/z* 230.1 [M + H^+].

2.2.1.13 Synthesis of 2,2'-(1E, 1'E)-(2,2'-disulfanediylbis(2,1-phenylene)bis(azan-1-yl-1-ylidene)bis(methan-1-yl-1-ylidene)diphenol (66).

From a literature based on a procedure by Wang *et al*[113], salicylaldehyde (1.75g, 14 mmol, 1 eq) and 2-mercaptoaniline (1.79 g, 14 mmol, 1 eq) were mixed in ethanol (30 mL). The mixture was stirred and aerated over night at room temperature. A yellow precipitate resulted which was filtered, washed with ethanol and finally diethyl ether to give

the product which was dried *in vacuo*. Yield = 1.75 g (27.4 %). ^{1}H NMR (400 MHz, $CDCl_3$) δ(ppm) 4.62 (s, 2H, O*H*), 7.68 (m, 1H, Ar), 6.93, (m, 2H, Ar), 7.02 (m, 2H, Ar), 7.21 (m, 1H, Ar), 8.79 (s, 1H, C*H*=N). ^{13}C NMR (100 MHz, $CDCl_3$) δ(ppm) 162.84 (*C*H=N), 161.17 (*C*-OH), 145.19 (*C*H), 133.71 (*C*H), 132.62 (*C*H), 131.63 (*C*H), 127.75 (*C*H), 127.41 (*C*H), 127.66 (CH), 119.73 (*C*H), 119.24 (*C*H), 117.93 (*C*H), 117.49 (*C*-SH). ESMS expected for $C_{26}H_{20}N_2O_2S_2$: *m/z* 456.1. -ve ESMS found: *m/z* 535.1 [M + acetic acid - H^+].

2.2.2 QD synthesis

2.2.2.1 Synthesis of CdSe QDs

CdSe QDs were prepared modifying slightly a procedure developed by Peng *et al*.[17] A stock selenium solution was prepared by dissolving selenium powder (0.15 g, 1.9 mmol, 1 eq.) and trioctylphosphine (TOP), (0.6 g, 1.6 mmol, 1 eq) in 1-octadecene (12.5 mL), a high boiling, non-coordinating solvent. The solution was heated to 150 °C and maintained at this temperature for 10 mins. Preparation of the cadmium solution involved dissolving cadmium oxide (0.65 g, 0.5 mmol, 1 eq) and oleic acid (1.4 g, 5 mmol, 10 eq) in 1-octadecene (25 mL). This solution was heated to 265 °C and a portion of the TOPSe (5 mL) solution was added. The temperature was maintained for 10 seconds and a portion of the reaction was quenched by pouring on to crushed ice. This was repeated for a reaction time of 30 seconds and also 2 minutes. After the ice had melted, the QDs were separated from the aqueous solution as the upper intensely coloured layer (10 mL).

2.2.2.2 Synthesis of CdSe/ZnS QDs

CdSe/ZnS QDs were prepared following a literature procedure by Asokan *et al*[114]. Cadmium oxide (0.05 g, 0.4 mmol) and oleic acid (2 mL) were charged to 1-octadecene (ODE) (25 mL) in a three-necked flask. This mixture was degassed and heated under nitrogen to 250 °C. The mixture became colourless at about 150 °C. The selenium precursor was prepared by mixing selenium (0.016 g, 0.2 mmol) and trioctylphosphine (TOP) under nitrogen. After sonication the solution became transparent.

The zinc sulfide precursor was prepared by combining hexamethyldisilathiane (0.2 mL), TOP (0.75 mL) and dimethylzinc (0.3 mL) in ODE (5 mL). When the cadmium solution had reached 250 °C, the heat was turned off and the selenium solution was quickly injected in via syringe. After the desired time had elapsed, the ZnS solution was injected into the core QD solution. The reaction was then stirred for 2hrs at 100 °C and dispersed in hexane. (25 mL)

2.2.3 Ligand exchange of hydrophilic ligands

2.2.3.1 Ligand exchange of CdSe and CdSe/ZnS QDs with mercaptosuccinic acid to form 21 and 22.

Based on a procedure by Chen *et al*[115], CdSe QDs (12 mL) in octadecene were charged to a solution of **14** (0.16 g, 1.04 mmol) in anhydrous methanol (120 mL). The mixture was pH adjusted to 10 with the aid of tetrabutylammonium hydroxide and refluxed for 5 hrs under N_2. It was then concentrated to about one third of its original volume under reduced pressure and treated with diethyl ether (100 mL) to precipitate the QDs. The supernatant was carefully decanted off and the remaining solution was centrifuged for 5 mins at 12,500 rpm. The resulting pellet was vacuum dried overnight. Yield = 0.31 g.

A similar procedure was followed for the exchange with the CdSe/ZnS QDs to yield **22** (0.20 g).

2.2.3.2 Ligand exchange of CdSe/ZnS QDs with 27 to form 28

A similar procedure to that used in 2.2.3.1 was followed using 0.60 g, 3.85 mmol of **27** in anhydrous methanol to yield 0.18 g of **28**.

2.2.3.3 Ligand exchange of CdSe/ZnS QDs with 16 to form 29

A similar procedure to that used in 2.2.3.1 was followed using 0.11 g, 0.70 mmol of **16** in anhydrous methanol to yield 0.06 g of **29**.

2.2.4 Ligand exchange of hydrophobic ligands

2.2.4.1 Ligand exchange of CdSe/ZnS QDs with 38 to form 39.

The procedure developed by Tomasulo *et al* [31]was used for ligand exchange with hydrophobic ligands. A solution of CdSe/ZnS core shell QDs (0.5 mL, 0.027 μmol) and **38** (0.03g, 150 μmol) in chloroform (20 mL) was heated under reflux for 24 hr. After cooling to ambient temperature, the solvent was removed *in vacuo*. The residue was suspended in acetonitrile (8 mL) and centrifuged at 12,500 rpm for 5 min. The centrifugation step was repeated three more times to afford the modified CdSe/ZnS core shell QDs as a yellow powder (0.02 g).

2.2.4.2 Ligand exchange of CdSe/ZnS QDs with 52 to form 53.

Following a procedure by Tomasulo *et al* [31], a solution of CdSe/ZnS core shell QDs (0.5 mL, 0.027 μmol) and **52** (0.05g, 119 μmol) in dry chloroform (5 mL) was heated at reflux under N_2 for 3 hr. TBAOH (0.25 mL) was added to the solution. The reaction proceeded for another 3 hrs after which a further addition of the ligand **52** (0.01g, 0.6 μmol) in dry chloroform was transferred to the reaction. The reaction was removed from the heat and allowed to stir overnight at RT under N_2. The solvent was removed *in vacuo* and the residue was suspended in acetonitrile (8 mL) and then centrifuged at 12,500 rpm for 5 min. The centrifugation step was repeated three more times to afford the modified CdSe/ZnS core shell QDs as an orange powder (0.02 g).

2.2.4.3 Ligand exchange of CdSe/ZnS QDs with 55 to form 56.

Following a procedure by Tomasulo *et al* [31], a solution of CdSe/ZnS core shell QDs (2 mL, 0.108 μmol), **55** (0.19g, 638 μmol) and TBAOH (0.5 mL) was refluxed in dry chloroform (15 mL) for 24 hr under N_2. After cooling to ambient temperature, the solvent was removed *in vacuo*. The residue was suspended in acetonitrile (8 mL) and centrifuged at 12,500 rpm for 5 min. The centrifugation step was repeated three more times to afford the modified CdSe/ZnS core shell QDs as an orange powder (0.07 g).

2.2.4.4 Ligand exchange of CdSe/ZnS QDs with 61 to form 67.

Following a procedure by Tomasulo *et al* [31], a solution of CdSe/ZnS core shell QDs (0.5 mL, 0.027 μmol), **61** (2.3 g, 0.01 mol) and TBAOH (0.25 mL) in dry chloroform was heated at reflux for 24 h. Upon completion of reaction, the solvent was removed under reduced pressure. The crude mass was suspended in acetonitrile (5 ml) and centrifuged at 12,500 rpm for 5 min. The supernatant solution was decanted off and the solid was again suspended in fresh acetonitrile. This step was repeated a further three times and the product was vacuum dried to obtain pure **67** as an orange coloured powder (0.02 g).

2.3 Quantum yield

Quantum yields were determined by preparing a sample of the probe and the reference standards (rhodamine 6G or fluorescein) both with an optical density of 0.08 A.U. at the excitation wavelength to be selected. The fluorescence spectrum for both the probe and reference were recorded and the integrated area under the curves was calculated.
The quantum yield was then obtained using equation 2.1:

$\Phi_{QD} = \Phi_R(\text{spectral area}_{QD} / \text{spectral area}_R)(\eta_{QD}^2 / \eta_R^2)$ *equation 2.1*[116]

Where Φ = quantum yield, η = refractive index of solvent, R = reference.

CHAPTER THREE

SYNTHESIS OF CdSe AND CdSe/ZnS QDs

3.1 History

The history of quantum dots is a relatively short one but even from the middle ages there was evidence of such nanotechnology. Stained glass windows in some European churches were impregnated with gold nanoparticles and actually acted as air purifiers. The glaziers were oblivious to this at the time but when the sunlight hit the gold nanoparticles they resonated to the wavelength of the sunlight's electromagnetic field and became charged and this created their own electromagnetic field. Any pollutants in the air were then broken down in this field.

Fast forward a few centuries to the late 1970's and in the Ioffe Institute in St. Petersburg where Ekimov and his colleague Efros first observed the birth of semiconducting nanocrystals (NCs) or quantum dots (QDs)[3-5]. Since then two popular approaches for synthesising QDs have been developed. Physicists have gravitated towards molecular beam epitaxy (MBE) due to exact measurements and characterisation they perform on single QDs[117]. The second approach, the colloidal route is the most favoured by chemists due to the advantages of continuous size control and chemical accessibility, enabling functionalisation of their surface.

3.2 CdSe core and CdSe/ZnS core-shell synthesis

3.2.1 CdSe QD synthesis

The colloidal synthesis of CdSe QDs dates back only 21 years, from the initial efforts of Dimitrijevic and Kamat[118] followed by the now favoured method developed by Murray, Norris and Bawendi[16]. This revolutionary approach involved injecting the precursors dimethylcadmium and elemental selenium into a hot (300 °C) matrix of coordinating ligands trioctylphosphine (TOP) and trioctylphosphine oxide (TOPO).

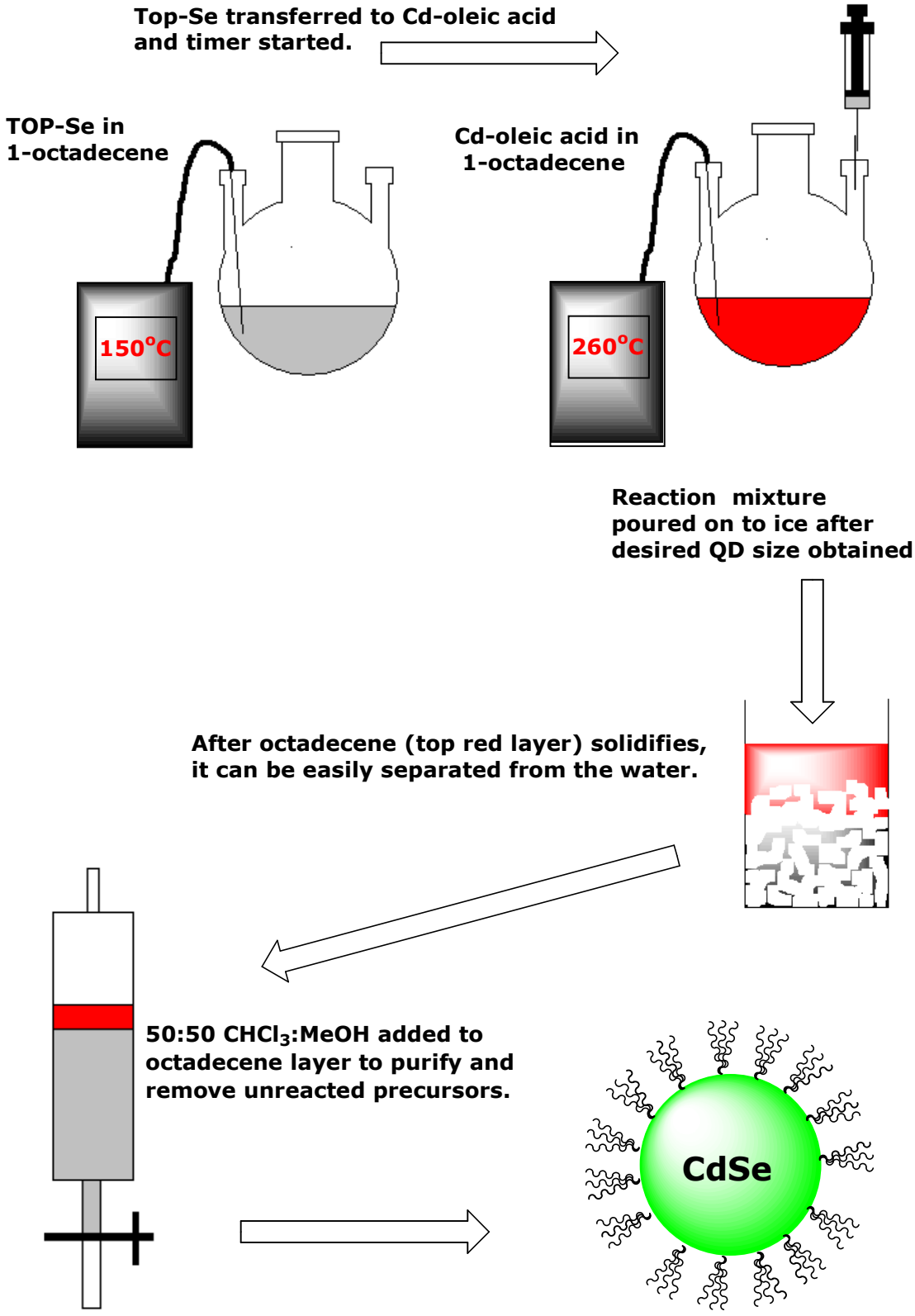

Figure 3.1 *Schematic diagram illustrating the preparation of CdSe core nanocrystals*[18].

By varying the crystal growth time different size QDs were obtained. It still remains the preferred mode of fabrication although other methods have emerged which have produced comparable results. Peng and others[17, 18, 119] report a similar procedure to Bawendi, replacing the very toxic dimethylcadmium precursor with cadmium oxide and using an alternative capping ligand in oleic acid while also retaining TOP. A somewhat lower temperature was required (270 °C), producing very monodisperse nanocrystals with quantum yields of ~10 - 15%. In this thesis several procedures have been employed to synthesise QDs but the method of choice has been the less toxic route, using CdO as the cadmium source. From this route CdSe QDs ranging from ~2 nm to ~7 nm can be synthesised (see table 3.1). The reaction involved preparing a selenium solution, which contained elemental selenium, trioctylphosphine as a capping ligand and octadecene, a high boiling, non-coordinating solvent (figure 3.1). A second solution containing cadmium oxide and oleic acid was also prepared in octadecene. When the selenium solution heated to 150 °C had become clear, an aliquot was injected into the cadmium solution. The timer was started at this point and depending on the desired size of QD, the solution was then poured into ice after a specific time interval thus quenching the reaction. Removal of unreacted materials was achieved by extractions with a 50/50 chloroform/methanol solution. The QDs suspended in the octadecene layer were freely dispersible in a range of solvents, e.g. toluene, chloroform, hexane and tetrahydrofuran.

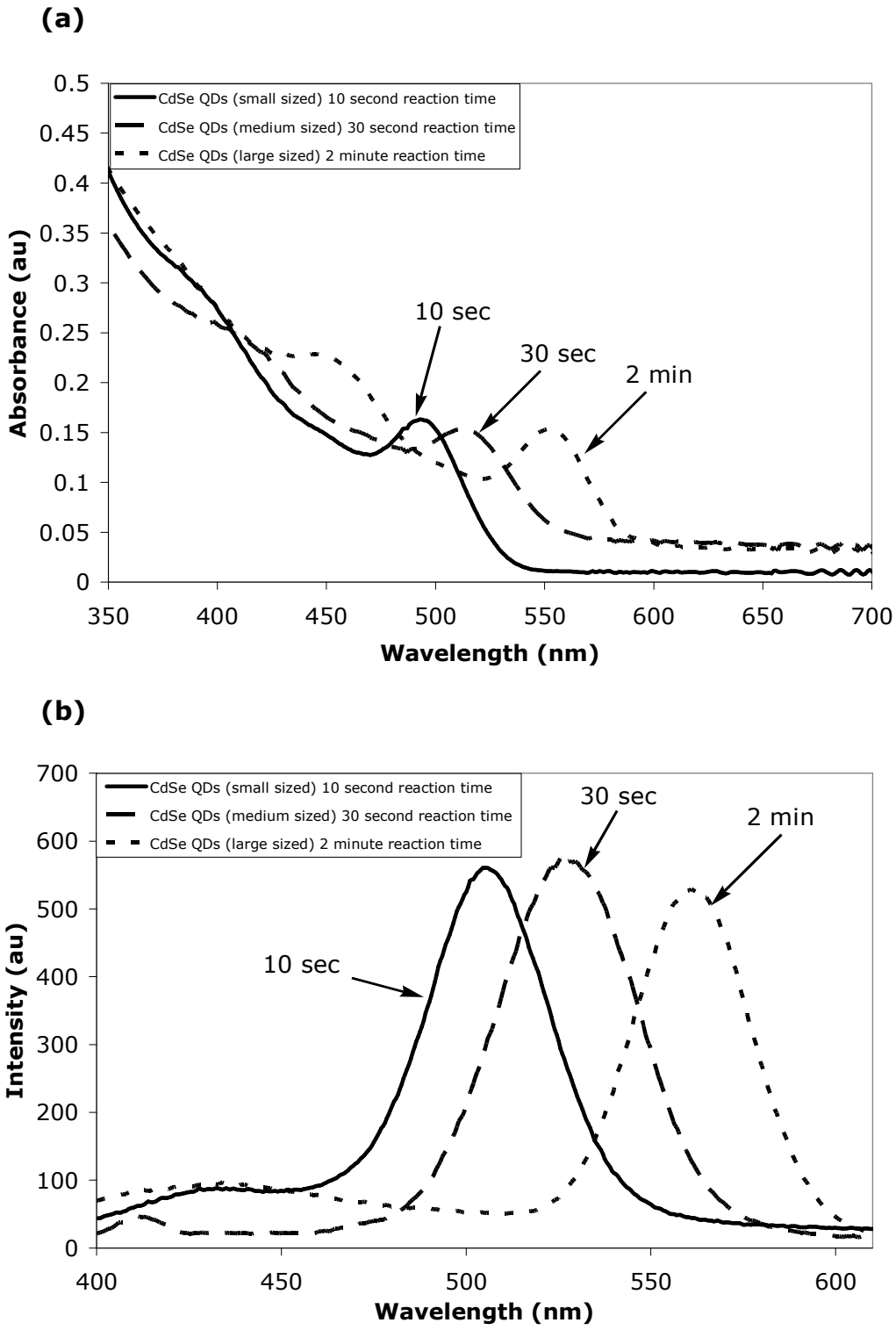

Figure 3.2 *(a) Absorption and (b) photoluminescence spectra of various sizes of CdSe QDs dispersed in chloroform. Excitation wavelength for the three QDs was set at 370 nm.*

Figure 3.2 reveals the spectral data (absorption and emission) for various sizes of CdSe QDs produced. In figure 3.2a one of the unique

properties of quantum dots is observed. As the QDs increase in size, as a result of longer reaction time, the absorption onset or what is termed the 1st exciton peak moves to a longer wavelength. The shortest wavelength absorption band (full line) is the absorbance profile of the smallest CdSe QDs synthesised. These QDs were quenched after 10 seconds with the 1st exciton peak appearing at λ_{max} = 495 nm. The second spectrum (broken line) shows the absorbance spectrum for the medium sized CdSe QDs, quenched at 30 seconds with the 1st exciton peak at λ_{max} = 514 nm. The largest CdSe QDs (dotted line) prepared from a reaction time of 2 minutes had a 1st exciton peak at λ_{max} = 553 nm. Thus, as expected, increasing the crystal growth phase by increasing reaction time led to an increase in the absorption onset of the QD.

The emission profiles in figure 3.2b show another unique property of QDs. The spectra are relatively narrow and Gaussian in shape with a full width half maximum (FWHM) of ~50 nm. This sets them apart from organic dyes which have a tendency to red-tail[10]. The excitation wavelength used for all three QDs was 370 nm. From the emission profiles it is evident that as the reaction time increases, so too does the emission wavelength of the resulting QDs. A 10 second reaction time led to an emission band centred at λ_{max} = 505 nm while 30 second and 120 second reactions led to emission bands with λ_{max} = 528 nm and λ_{max} = 560 nm respectively. Thus, as the reaction time is increased, the crystal diameter increases and the resulting emission wavelength is longer or lower in energy. This can be explained by a decrease in the band gap energy with increasing particle size (see figure 1.2 in chapter 1). Due to the fact that QD electronic energy levels are discrete rather than continuous, the addition of just a few atoms decreases the boundaries of the band gap and the electron has a shorter energy drop to the ground state and hence less energy is emitted (i.e. longer wavelength).

One of the more striking features of QDs is the vibrant range of colours that they emit depending on their size. Controlling their growth can result in QDs with emission colours ranging from violet through to red. The emission λ_{max} of the three batches of CdSe QDs shown in figure 3.2b are quite close together and as a result so too is their emission colours as shown in figure 3.3. The quantum yields of the small, medium

and large QDs calculated using a rhodamine 6G reference were 6.5%, 9.0% and 4.2% respectively (table 3.1).

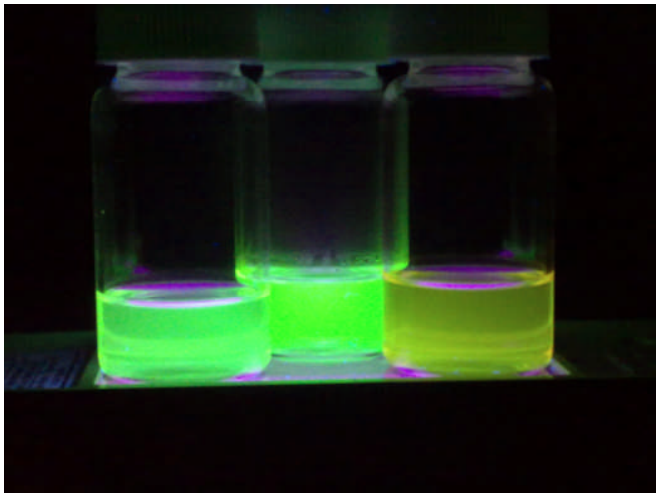

Figure 3.3 *Various sizes of CdSe QDs dispersed in toluene, irradiated under UV Light. Small QDs (Blue / green), medium QDs (Green), large QDs (green / yellow).*

3.2.2 CdSe/ZnS QD synthesis

Core QDs usually require surface capping to produce materials with higher quantum efficiencies. Surface passivation involves coating the core QD with a substance that has a larger band gap such as ZnS. CdSe QDs have a band gap energy of 1.73 eV at room temperature[120]. Overcoating them with ZnS, which has a band gap energy of 3.6 eV[120], increases their luminescence quantum yield while retaining the spectral characteristics of the core. The thickness of the ZnS shell is of importance in achieving optimum photoluminescence (PL) QY. Optical phonon Raman studies have been conducted on several samples of CdSe/ZnS QDs with varying thickness of ZnS shell and the results have shown that at ~2 monolayers (ML) the surface of the CdSe core is almost defect free but is not too thick to prohibit effective electron transfer between the QD and the appended ligands[121].

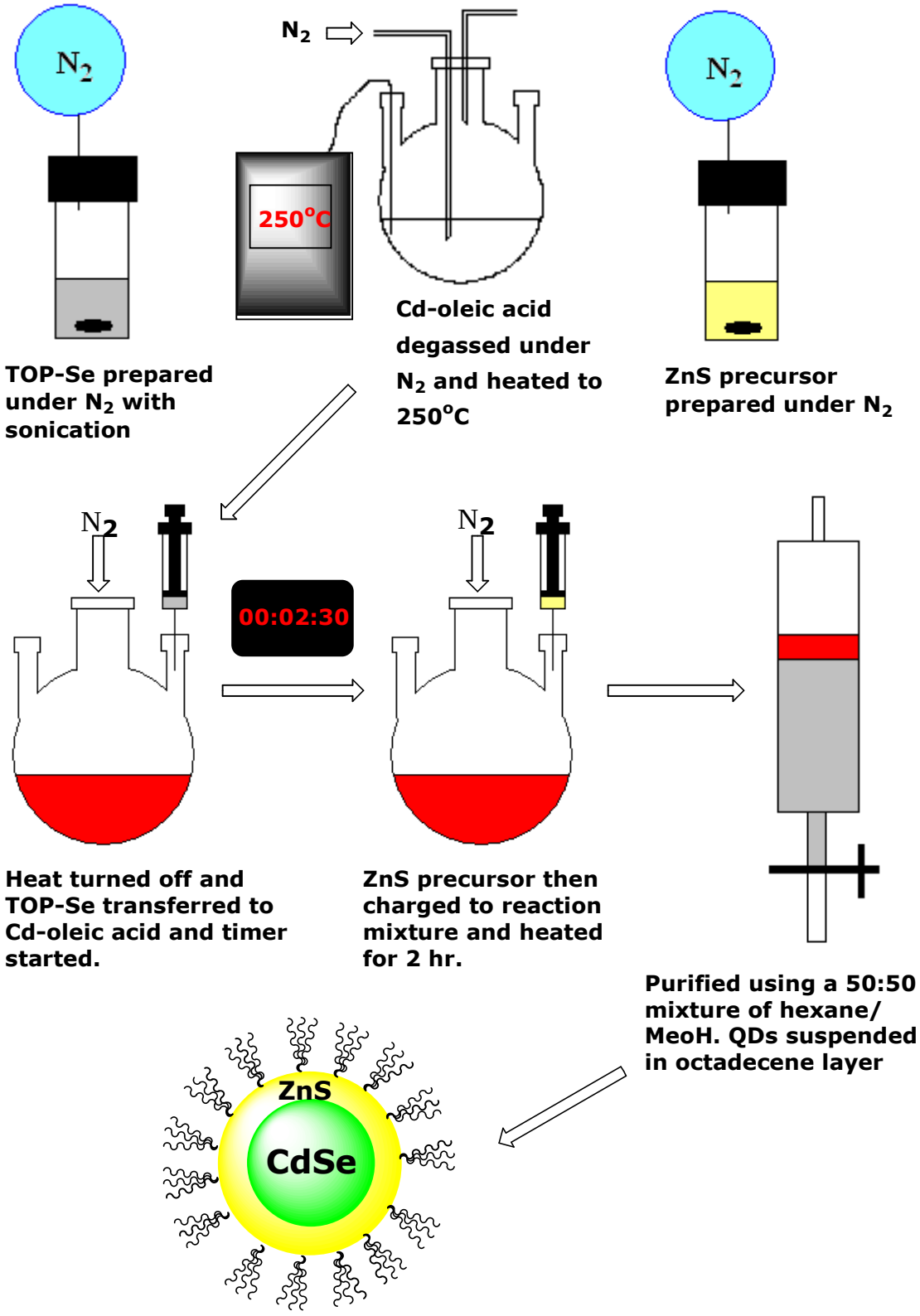

Figure 3.4 *Schematic representation for the preparation of CdSe/ZnS core-shell nanocrystals*[114].

The issue of toxicity is another concern when dealing with cadmium based compounds and the use of bare CdSe QDs as labels or bio-markers has been restricted. Oxidation in air and from exposure to UV light leads to release of cadmium from the QD surface[122]. This cytotoxicity can be overcome by surface coating and the capping with a ZnS shell has somewhat addressed this worry.

A typical procedure for the synthesis of CdSe/ZnS QDs involved preparing the core QDs as described previously. The ZnS precursor was prepared by combining hexamethyldisilathiane and dimethylzinc in octadecene, under N_2. After the desired QD core had been synthesised, the ZnS solution was injected, the temperature lowered to 100 °C and maintained at this temperature over several hours. The QDs were then purified by repeated extractions with hexane / methanol (50/50)[114]. A schematic diagram illustrating the CdSe/ZnS synthesis is shown in figure 3.4.

Figure 3.5 illustrates the absorption spectra of synthesised CdSe/ZnS QDs. As with the CdSe QDs the position of the 1st exciton peak moved to a longer wavelength with increasing reaction time. The shortest reaction time (5 seconds) resulted in QDs with the shortest wavelength 1st exciton peak at 389 nm which is close to the minimum possible for CdSe QDs[123]. A quench at 30 seconds reaction time resulted in the formation of medium sized QDs with the 1st exciton peak at λ_{max} = 527 nm, while quenching at 2.5 mins yielded larger nanoparticles, with the 1st exciton peak at λ_{max} = 575 nm.

The emission spectra obtained after excitation at 370 nm again were Gaussian in shape with the exception of the small QDs which exhibit significant red tailing. This may be due to a lengthy nucleation stage resulting in a large size distribution[34]. The emission maximum of these QDs was observed at 470 nm with a FWHM of 58 nm. The medium sized QDs displayed an emission maximum at 547 nm and FWHM of 49 nm while the largest nanoparticles had an emission maximum of 584 nm and a FWHM of 42 nm.

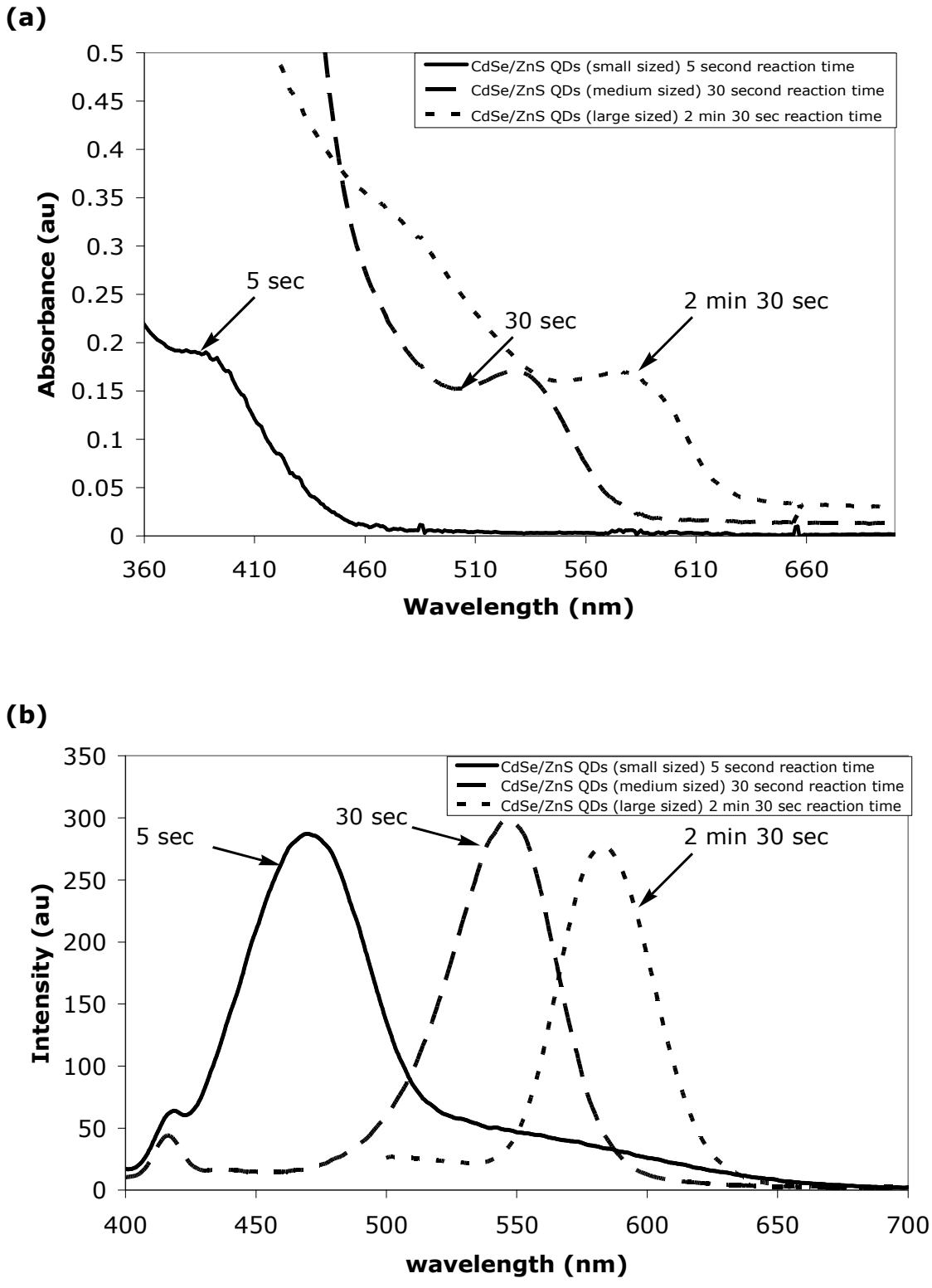

Figure 3.5 *(a) Absorption and (b) photoluminescence spectra of various sizes of CdSe/ZnS QDs dispersed in chloroform. Excitation wavelength for the three QDs was set at 370 nm.*

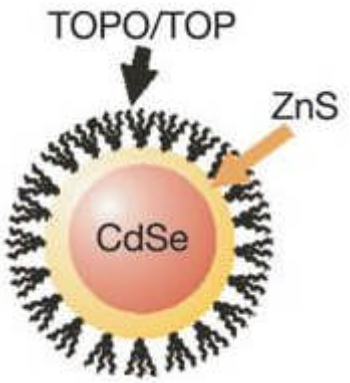

Figure 3.6 *Schematic representation of CdSe/ZnS core-shell QDs.*

Again, as with CdSe core QDs it is evident from the data presented above that the emission wavelength can be tailored by controlling the crystal growth reaction time. As all these QDs can be excited with a single wavelength, possibilities for multiplexing are significantly greater than for organic dyes.

Figure 3.7 shows a photograph of the small, medium and large batches of CdSe/ZnS QDs. Although not very clear from the photo, the smallest QDs are emitting a light blue fluorescence when excited with 340 nm light. The medium sized batch of QDs emitted green fluorescence while the largest batch emitted orange fluorescence. The quantum yield of the three batches of QDs were approximately 11%, slightly greater than the CdSe core QDs (see table 3.1). However the magnitude of the increase was not as great as anticipated. For comparison, a batch of CdSe/ZnS QDs purchased from Evident Technologies, USA was also analysed. The quantum yield of these 540 nm emitting QDs was determined as 38.1% using rhodamine 6G as reference. It is clear that the Evident QDs are significantly brighter than any of the three batches of CdSe/ZnS QDs synthesised here. The reasons for this could be due to an ineffective quenching of the reaction by not cooling the core QDs quickly enough. Another possibility could be that the optimum shell thickness may not have been achieved. In addition, the purification and size selection strategies available to Evident are presumably more rigorous and advanced. As these Evident QDs were of better quality than the QDs prepared here, they were used in the probes developed in chapters four, five and six.

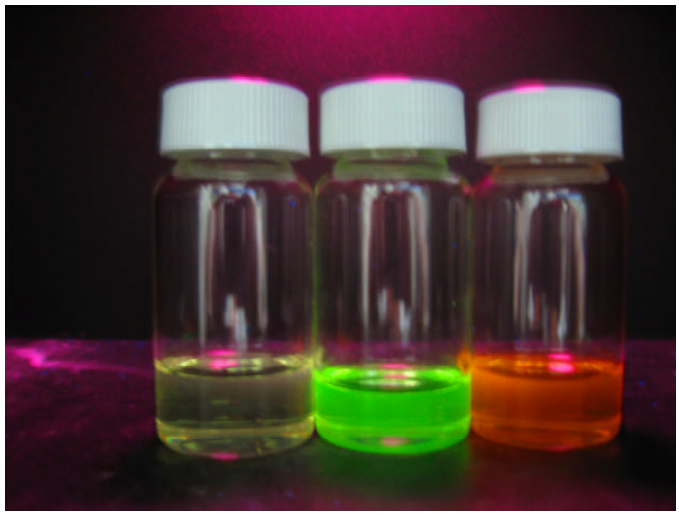

Figure 3.7 *Various sizes of CdSe/ZnS QDs dispersed in toluene, irradiated under UV Light. Small QDs (blue), medium QDs (Green), large QDs (orange).*

3.3 Size determination

3.3.1. Size determination by transmission electron microscopy (TEM)

One method for determining the size of QDs is transmission electron microscopy (TEM). It is the most important tool for the measurement of QD size but can be laborious and tedious due to the time and expense associated with it. TEM involves passing a beam of electrons through a very thin specimen of sample. The electrons interact with the sample and form an image which is picked up by a fluorescent screen, charge-coupled device (CCD) camera or photographic film. TEM images of all six batches of prepared QDs as well as the Evident QDs were obtained from the EPSRC National Service at St Andrew's University. The images for the CdSe QDs are shown in figure 3.8 while those for the prepared CdSe/ZnS QDs are shown in figure 3.9. The Evident CdSe/ZnS QDs are shown separately in figure 3.10. The average particle size for each of the prepared QDs and also the Evident batch were obtained by taking an average value from ten independent measurements and calculated using the available software. Due to the sparse number of small CdSe QDs

present in the sample used for the measurements an accurate dimension proved difficult to obtain. During the TEM measurement of this batch it was noted that the solvent had encroached over the aperture on the grid in an obtrusive way and thus making it difficult to obtain a clear image. A set of 10 nm scale images were the only viable captures and measurements were obtained from these.

Tables 3.1 and 3.2 summarises the sizes obtained for each batch of QD. For the CdSe QDs, the average particle size increases from 4.5 nm for the small batch, to 4.7 nm for the medium batch and 5.0 nm for the large batch. Similarly, a gradual increase in size was also observed for the CdSe/ZnS QDs with a value of 4.6 nm observed for the small QDs, a value of 5.5 nm for the medium QDs and a value of 6.9 nm for the large QDs. In contrast, the CdSe/ZnS QDs obtained from Evident Technologies displayed a particle diameter of 3.8 nm. The medium batch of prepared CdSe/ZnS QDs had an almost identical emission wavelength and therefore would be expected to be of a similar size. There may be several reasons for this difference in size. For one, there may be small aggregates present in the prepared QDs that increase the average particle diameter. The well defined synthesis and purification technology established at Evident may result in more specific size distribution of the prepared nanocrystals. The size of the ZnS shell may also be a factor which would increase the particle size. However, this can be discounted as all batches of the CdSe core QDs also had TEM diameters greater than the Evident CdSe/ZnS QDs.

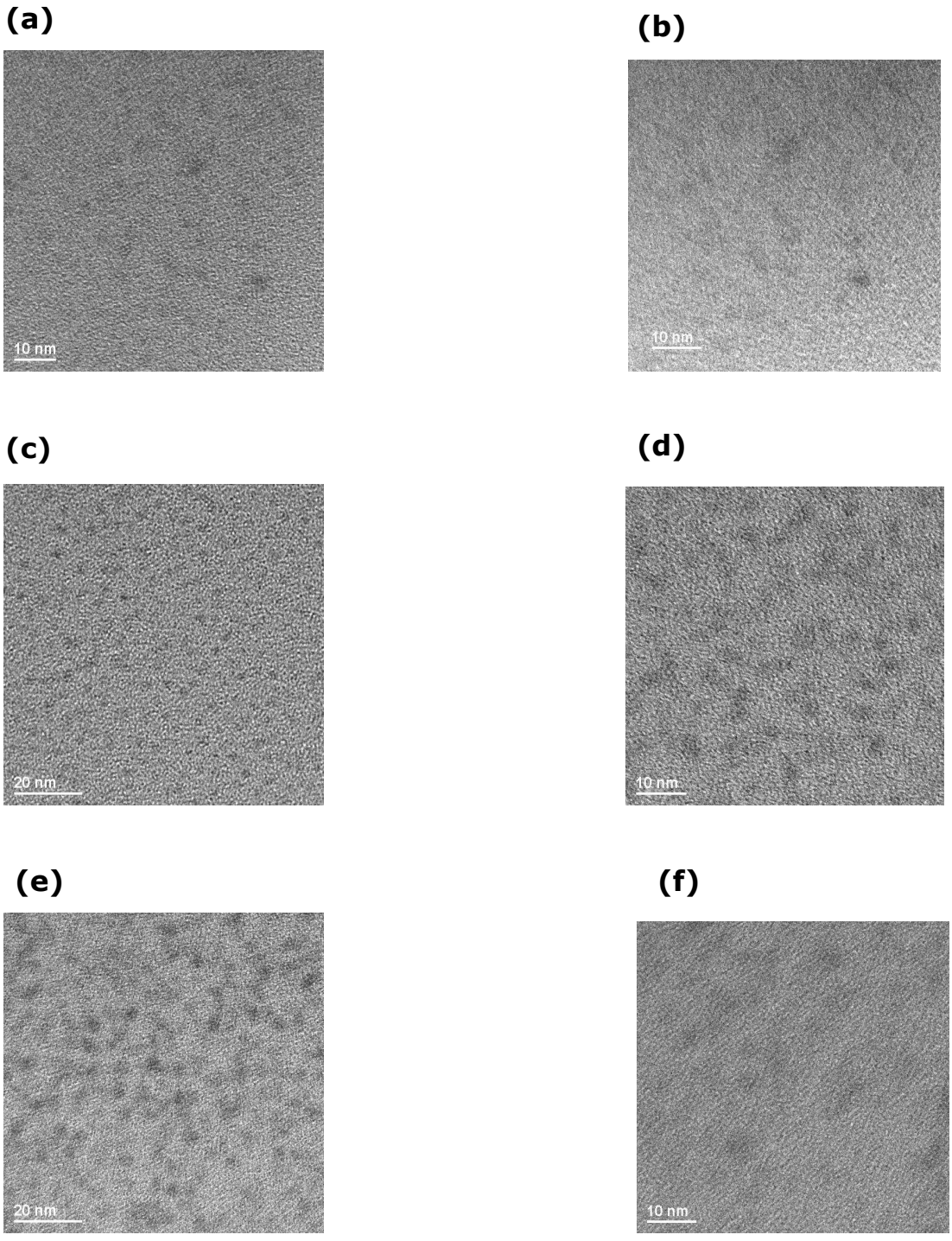

Figure 3.8 *TEM images of (a, b) small, (c, d) medium and (e, f) large diameter batches of CdSe QDs. 10 nm and 20 nm magnification shown for medium and large batches.*

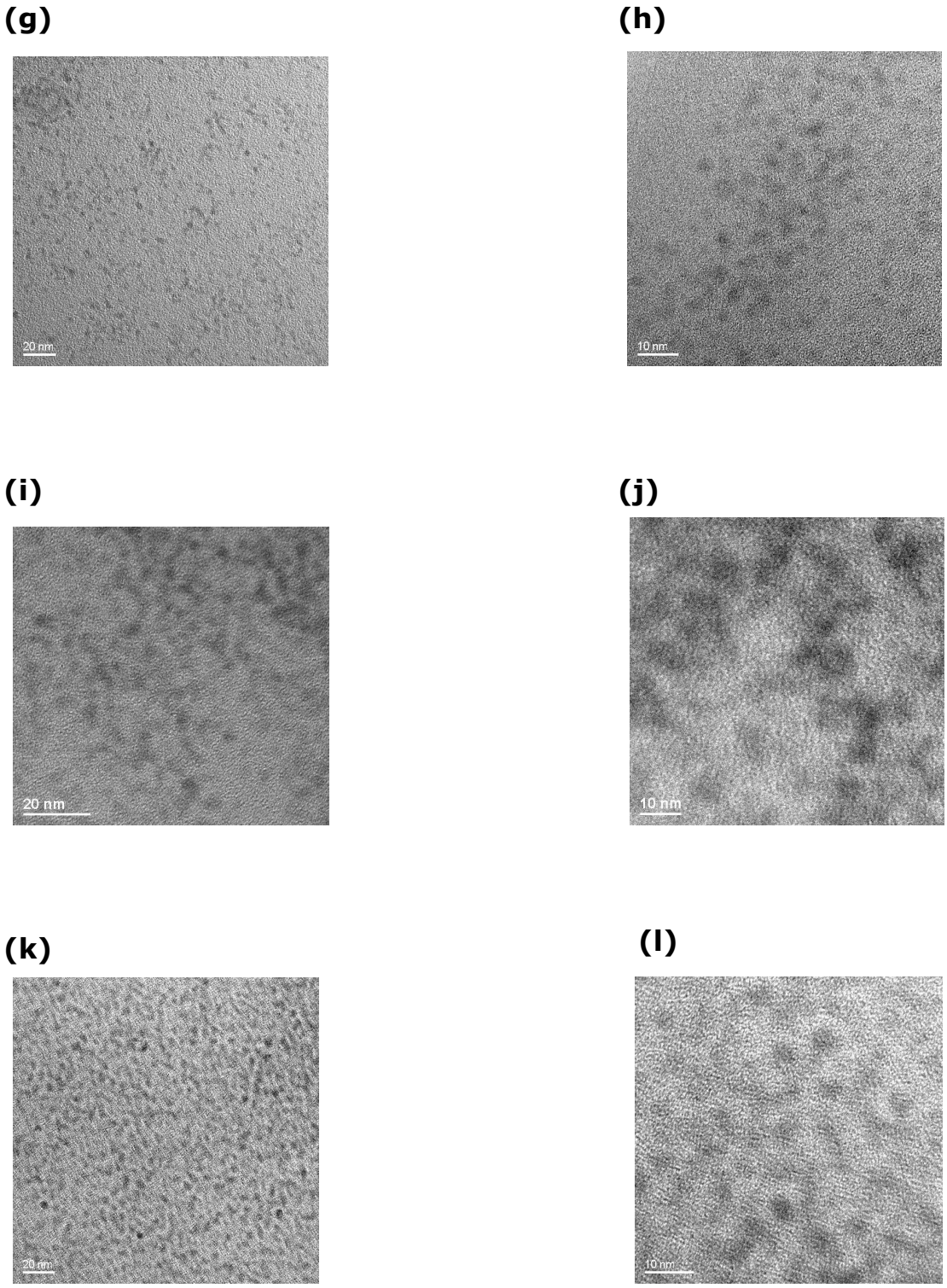

Figure 3.9 *TEM images of (g, h) small, (i, j) medium and (k, l) large diameter batches of CdSe/ZnS QDs. 10 nm and 20 nm magnification shown for small, medium and large batches.*

(m) **(n)**

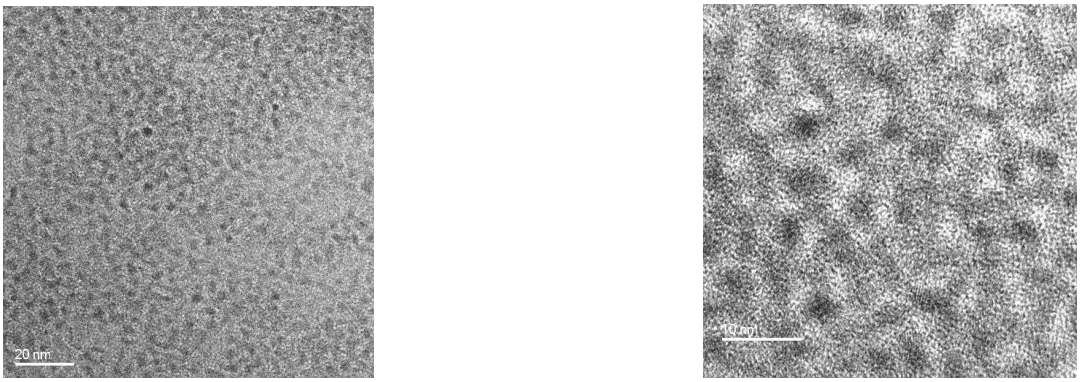

Figure 3.10 *TEM images (m, n) of Evident CdSe/ZnS QDs. 10nm and 20 nm magnification provided.*

3.3.2 Size determination by dynamic light scattering (DLS)

Another technique to determine the size of nanoparticles is dynamic light scattering (DLS), also called photon correlation spectroscopy (PCS). Due to Brownian motion, particles are in constant movement in solution and when a coherent light source, like a laser of known frequency is directed at these particles, the light is scattered at a different frequency. This change in frequency is referred to as a Doppler shift or broadening[124]. For measurement purposes, this shift in light frequency is associated with particle size. Figures 3.11 and 3.12 show the DLS spectra for the CdSe and CdSe/ZnS QDs respectively, with the Evident CdSe/ZnS QDs shown in figure 3.13. As for the TEM results, the results of the average particle diameter by DLS are presented in tables 3.1 and 3.2. Again, there was an increase in the average particle diameter on progressing from the small to the medium to the large batches of QDs for both the CdSe and CdSe/ZnS QDs.

(a)

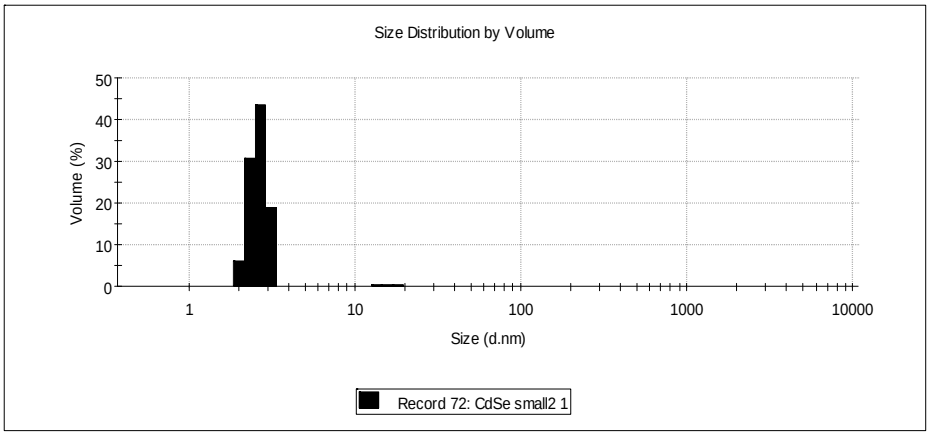

(b)

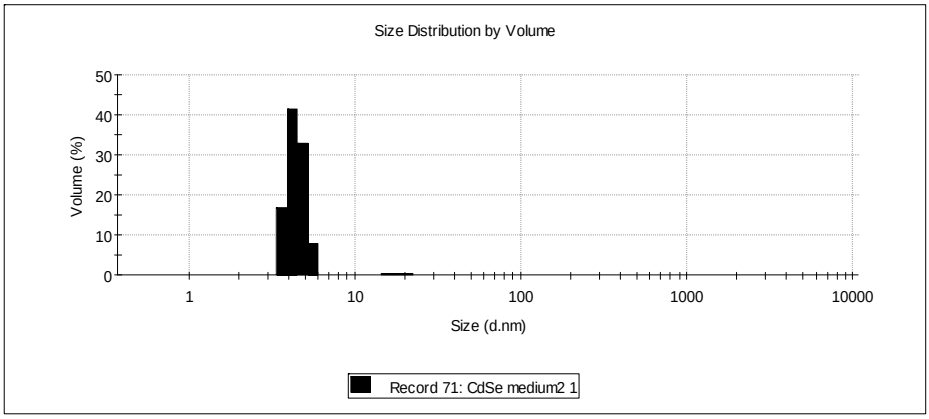

(c)

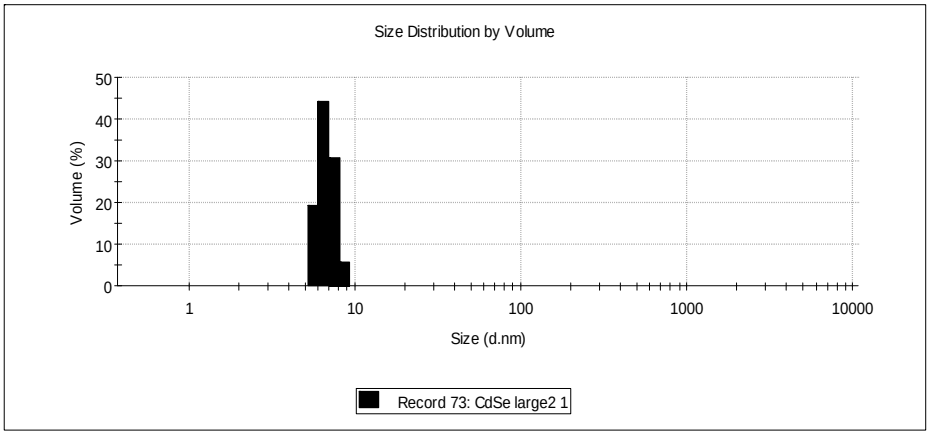

Figure 3.11 *Dynamic light scattering (DLS) histogram plot of CdSe QDs dispersed in toluene (a) small, (b) medium and (c) large.*

(d)

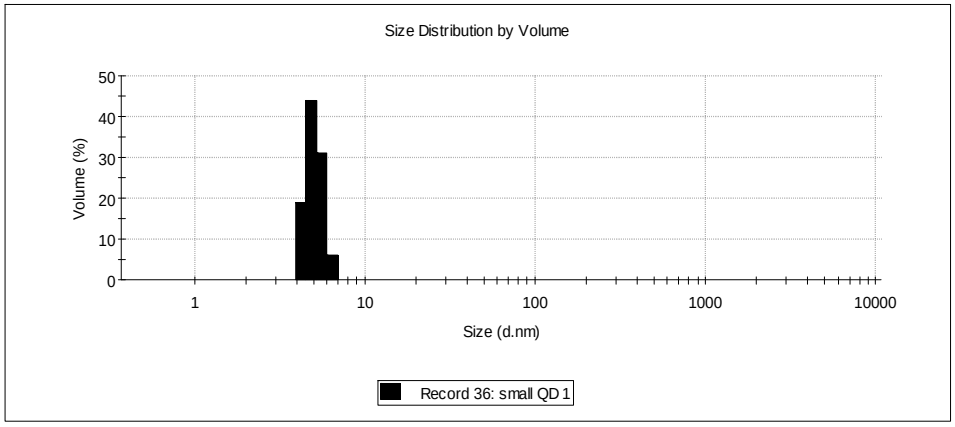

(e)

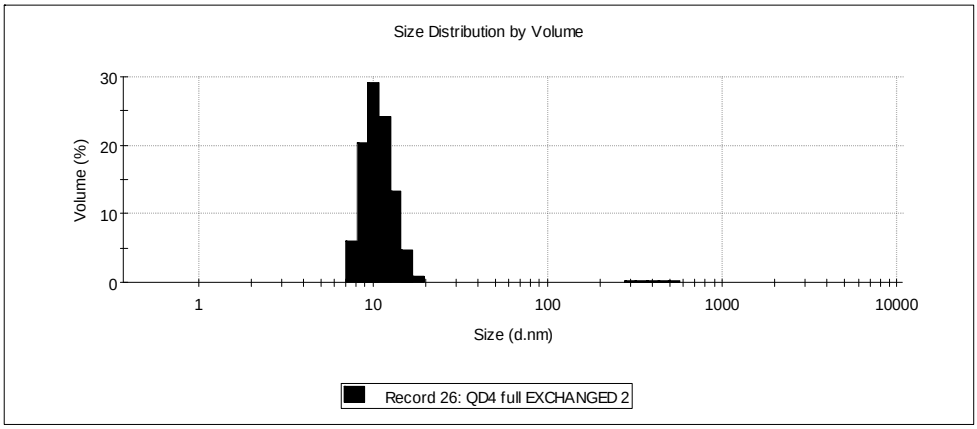

(f)

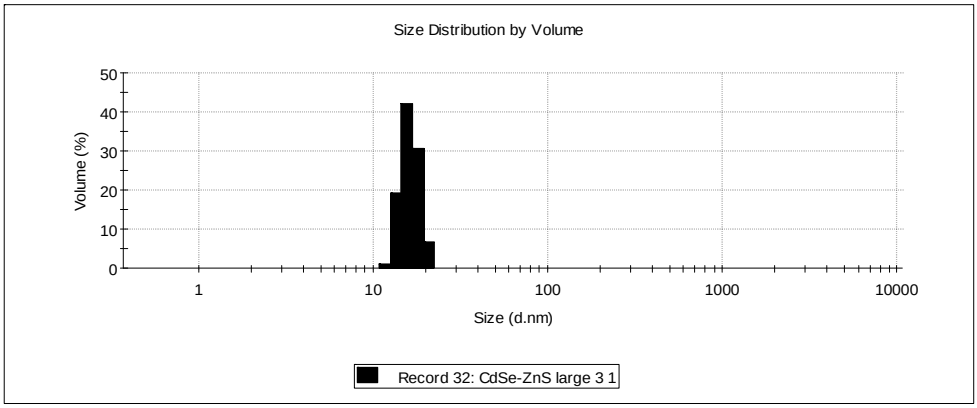

Figure 3.12 *Dynamic light scattering (DLS) histogram plot of CdSe/ZnS QDs dispersed in toluene (d) = small, (e) = medium and (f) = large.*

A surprisingly small particle diameter of 2.62 nm was obtained for the small batch (i.e. quenched at 10 seconds) of CdSe QDs which was significantly smaller than the TEM result of 4.5 nm for the same batch. Given that DLS gives a measure of the hydrodynamic diameter which includes the surface ligands and hydration shell of the nanoparticle, the values obtained for DLS are normally greater than that of TEM. This suggests that the larger than expected particle diameters obtained by TEM for the prepared batches of QDs are most likely due to aggregation. However, the DLS instrument may also be at its operational limit at such a small size as 2.62 nm. For the large CdSe QDs and for all the CdSe/ZnS QDs the particle diameter obtained by DLS was larger than that obtained for TEM, as would be expected. The hydrodynamic diameter remains the most quoted value in the literature for QD particle diameter characterisation as it is the most realistic when considering biological applications[125-127].

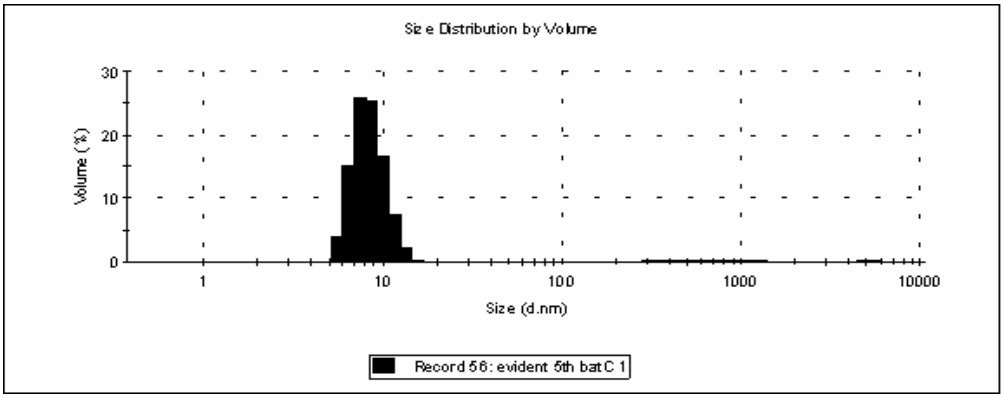

Figure 3.13 *Dynamic light scattering (DLS) histogram plot of Evident CdSe/ZnS QDs dispersed in toluene.*

3.3.3 Size determination by UV-vis absorption spectroscopy

The determination of QD size is an important factor in their characterisation and applications. Peng [43]developed a formula which was derived from TEM measurements and made it possible to measure the size of QDs from the 1st exciton peak in the absorption spectrum. It has its limitations though, due to the fact that only the core size is accounted for and surface ligands or stabilizing layers are not considered. From the UV

data the QD particle diameter, the concentration of the solution and the extinction coefficient may be determined. By inputting the wavelength at the 1st exciton peak into equation 3.1 (when the optical density is kept between 0.15 and 0.25) the size of the QD core may be calculated. This method gives a good approximation for the size of the QDs and is easily obtained. The equations shown are for CdSe core QDs only due to their relevance in this thesis. Similar equations for the determination of CdS and CdTe QDs can also be found in the same publication[43].

$$D = (1.6122 \times 10^{-9})\lambda^4 - (2.6575 \times 10^{-6})\lambda^3 + (1.6242 \times 10^{-3})\lambda^2 - (0.4277)\lambda + (41.57) \qquad \textit{(equation 3.1)}$$

(where D = crystal size, λ = wavelength at 1st exciton peak).

From equation 3.1 crystal size (D), may be determined. Once the crystal diameter is known it is possible to determine the extinction coefficient from two different approaches. The first is from the transition energy of the 1st exciton peak in eV using the equation:

$$\varepsilon = 1600\ \Delta E\ (D)^3 \qquad \textit{(equation 3.2)}$$

(where ε = extinction coefficient, ΔE = transition energy)

A second approach developed by Peng doesn't consider the transition energy ΔE and from experimental values equation 3.3 was derived.

$$\varepsilon = 5857\ (D)^{2.65} \qquad \textit{(equation 3.3)}$$

The determination of the extinction coefficient of QDs is essential in the estimation of the actual concentration of the nanoparticles in any given solution. In applications such as bio-medical labelling[10, 45] and also in the study of the nucleation and growth processes of QDs[119, 128, 129] this information can be critical. Through gravimetric methods, the concentration of organic and inorganic compounds can be determined,

however this is quite difficult with nanoparticles due to the variation in the number of ligands populating the surface of the QDs. As a result, the use of the absorption spectrum is a convenient and practical way to measure the nanoparticle concentration. Once the extinction coefficient is known, the concentration of the solution can be determined using the Beer-Lambert Law.

Using equation 3.1, values were obtained for each batch of QDs and are presented in tables 3.1 and 3.2. Again, a gradual increase in particle size was obtained for the small, medium and large batches of prepared QDs. A particularly small diameter was obtained for the small CdSe/ZnS QDs which had a core size of just 1.46 nm. This is nearing the lower limits of CdSe QD dimensions and it was feared that Peng's calculation would not be viable at these size ranges. However, a recent publication by Xia and Zhu has reported CdSe QDs ranging in size from 1 – 2 nm[123]. These so-called magic sized clusters were measured using Peng's equation.

From the absorption onset, the extinction coefficient may also be obtained by equation 3.3. As shown in table 3.1, the extinction coefficients for the three sizes of CdSe QDs increases as the size of the nanoparticle becomes larger. When compared to organic dyes like rhodamine 6G and fluorescein, the molar extinction coefficients for the band-gap absorption of QDs are comparable to the dyes when excited at their λ_{max} and can be of the order of 10 – 100 times greater, depending on the excitation wavelength used. Using equation 3.3 the calculated values for the core QDs were 5.32×10^4 M^{-1}/cm^{-1}, 6.57×10^4 M^{-1}/cm^{-1} and 1.18×10^5 M^{-1}/cm^{-1} for the small, medium and large batches respectively. These values compare quite well with their organic dye counterparts excited at their λ_{max} (e.g. Rhodamine 6G = 1.16×10^5 M^{-1}/cm^{-1}). A similar trend was observed for the three prepared batches of CdSe/ZnS QDs as shown in table 3.2.

3.4 Summary

Table 3.1 *Characterisation data for various sizes of CdSe QDs.*

QD sample	λmax abs (nm)	λmax em (nm)	Extinction Coefficient (M^{-1}/cm^{-1})	θ (UV) (nm)	θ (DLS) (nm)	θ (TEM) (nm)	FWHM (nm)	QY (Φ) (%)
CdSe (small)	495	505	5.32×10^4	2.30	2.62	4.5	43	6.5
CdSe (med)	514	528	6.57×10^4	2.49	4.43	4.7	46	9.0
CdSe (large)	553	560	1.18×10^5	3.10	6.77	5.0	39	4.2

Table 3.2 *Characterisation data for various sizes of CdSe/ZnS QDs (Evident and the three synthesised batches).*

QD sample	λmax abs (nm)	λmax em (nm)	Extinction Coefficient (M^{-1}/cm^{-1})	θ (UV) (nm)	θ (DLS) (nm)	θ (TEM) (nm)	FWHM (nm)	QY (Φ) (%)
CdSe/ZnS Evident	525	540	7.2×10^4	2.4	8.54	3.4	36	38.0
CdSe/ZnS (small)	389	470	1.58×10^4	1.46	5.07	4.6	58	10.9
CdSe/ZnS (med)	527	547	7.78×10^4	2.65	10.86	5.5	49	11.3
CdSe/ZnS (large)	575	584	1.83×10^5	3.66	16.36	6.9	42	10.4

3.5 Conclusions

Three batches of CdSe and CdSe/ZnS QDs were successfully prepared with varying sizes and distinct absorption and emission profiles. The particle size was controlled by adjusting the reaction time during the crystal growth phase. A gradual increase in particle size was observed for the CdSe and CdSe/ZnS QDs within each series using TEM, DLS and

absorption onset methods, however, there was significant variation between the absolute values obtained using each method. The availability of QDs with three distinct emission wavelengths that can all be excited with the same excitation wavelengths offers the opportunity of multiplex sensing. By attaching analyte specific receptors to their surface, probes capable of simultaneously identifying numerous targets using a single excitation source would be produced, a feature not possible with organic dyes. However, it is clear the quality of the QDs prepared here are not as good as those available from Evident Technologies and more development is required to improve the synthetic procedure. As a result, for the future chapters, CdSe/ZnS QDs used were obtained from Evident.

CHAPTER FOUR

WATER SOLUBLE QDs

4.1 Background

Optically sensing biologically relevant analytes in aqueous environments using organic dye based sensors has been hampered somewhat by the solubility issues of organic compounds in aqueous media. Quantum Dots have emerged as viable alternatives to organic dyes in biomedical applications due to their versatility in surface derivatisation, in addition to their superior optical properties. Various strategies have been employed to impart water solubility to these inherently hydrophobic nanoparticles.

4.1.1 Ligand exchange

Exchange of the native hydrophobic ligands for hydrophilic ligands is the most common approach to obtain water soluble QDs. These hydrophilic ligands usually possess dual functionality; a thiol group for anchorage to the QD surface and a hydrophilic group to impart the desired water solubility. Some examples of such ligands are mercaptosuccinic acid[130], 2-aminoethanethiol[131], mercaptopropionic acid[45], dihydrolipoic acid[132] and cysteine based peptides[133]. Mono thiols have routinely been used for anchoring ligands on to gold surfaces forming strong interactions. The homolytic bond strength of the Au-S bond is 44 kcal/mol and analysis with gold nanoparticles has revealed a short Au-S inter atomic distance (r_{Au-S} = 2.31 Å) indicating a strong surface interaction[134, 135]. This phenomenon of surface attachment demonstrated with gold nanoparticles has been observed with QDs and the use of mono-thiols have been extensively used as the mode of imparting functionality on to the QD surface. Recently, dithiols have become a more popular approach due to their more robust attachment[121, 136-138]. Oxygen and nitrogen terminated ligands have also been employed in surface attachment though not as often[139-141]. There are drawbacks however to ligand exchange as a means of derivatisation due to the altered chemical and physical states of the QD surface atoms. After exchange, the quantum efficiencies of the nanoparticles can decrease dramatically, and may fall from as much as ~50 % for CdSe/ZnS core-shell QDs to <2 %. There is also the issue of precipitation of the QDs from aqueous solution which can occur over time

with desorption of the grafted hydrophilic ligands from the QD surface due to thiol oxidation.

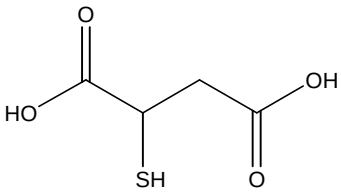

(14)

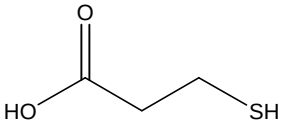

(15)

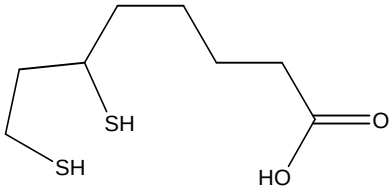

(16)

Figure 4.1 *Examples of hydrophilic compounds routinely used in ligand exchange reactions to impart water solubility on QDs. Mercaptosuccinic acid* ***14****, mercaptopropionic acid* ***15*** *and dihydrolipoic acid* ***16****.*

4.1.2 Micelles

Another means of imparting water solubility to QDs is though hydrophobic interaction of the parent ligands with phospholipids such as 1,2-dipalmitoyl-sn-glycero-3-phosphocholine (**17**) or 1,2-dipalmitoyl-*sn*-glycero-3-phosphoethanolamine-*N*-[methoxy(polyethylene glycol)] (**18**). These amphiphilic compounds use their hydrophobic hydrocarbon chains to interdigitate with the hydrocarbon chains of TOPO and leave their hydrophilic head groups protruding into the solution to impart water solubility.

Wang *et al* has also reported a procedure using octylamine-modified poly (acrylic acid) to prepare amphiphilic polymers[142]. Solubility in water is achieved through the carboxylate groups that orientate out towards the solvent with the aliphatic portion adhering to the QD surface. Hydrophobic interactions force the aliphatic portion of the octylamine to interdigitate with the native TOP/TOPO groups thus encapsulating the QD. The solubility is subject to the number of acrylic acid groups on the polymer with between 40 – 45 % considered optimum. Above this figure, the QD luminescence is more intense, however the water solubility diminishes.

(a)

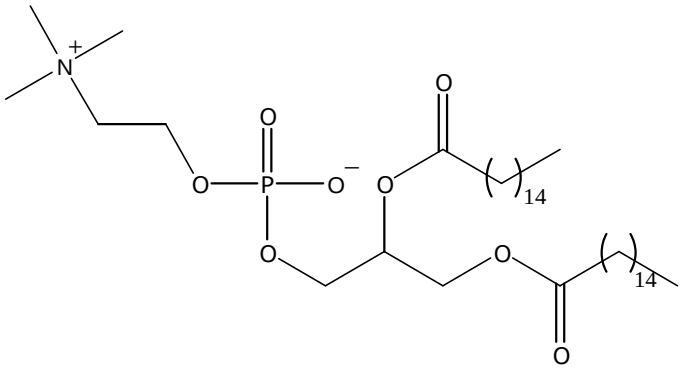

(17)

(b)

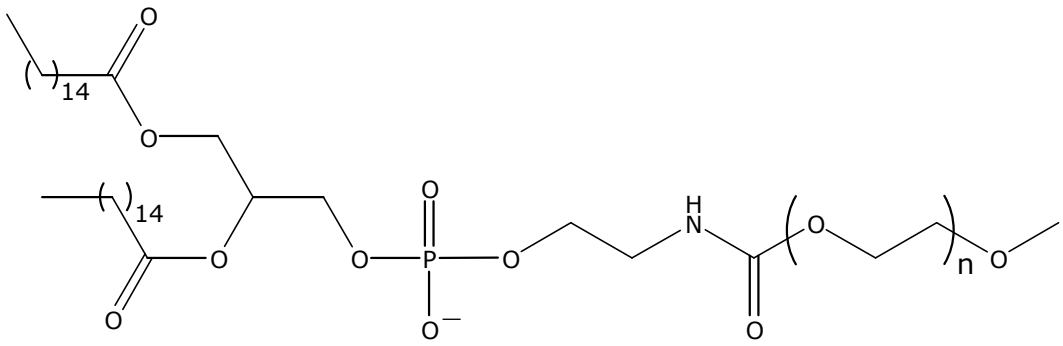

(18)

Figure 4.2 *(a) 1,2- dipalmitoyl-sn-glycero-3-phosphocholine* ***17****. (b) 1,2-dipalmitoyl-sn-glycero-3-phosphoethanolamine-N-[methoxy(polyethylene glycol)* ***18****.*

Another issue affecting the QDs after modification is the reduction in quantum efficiency of about 10 – 20 %. This is most likely due to a couple of factors. Firstly, the isolation of the QDs after transfer from the organic phase into the aqueous phase results in the loss of TOPO and other capping ligands from the surface of the QDs thus reducing the passivation of surface defects resulting in diminished luminescence. Secondly, a dipole effect can exist from the action of water molecules on the surface of the QD and also from the polymer[142]. The quantum

efficiencies of these modified QDs are comparable to the values obtained via another technique of water solubilisation called silanization.

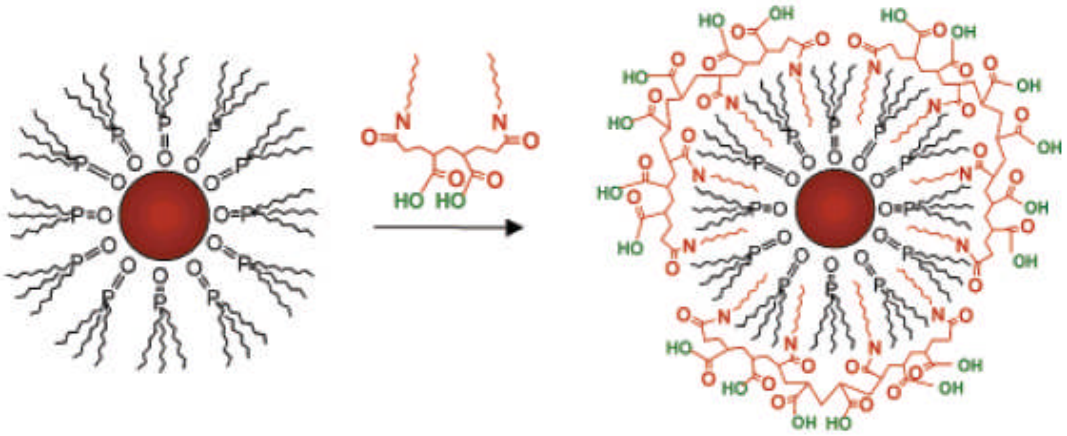

(19)

Figure 4.3 *Formation of polymer-QD complex (**19**) showing an idealized micellar polymer shell (40% octylamine-modified PAA) encapsulating the QD*[143]*.*

4.1.3 Silanization

This alternative technique aligns itself with ligand exchange in terms of quantum efficiencies. The process of silanization involves coating the QD with an organosilicone compound functionalised with amines and dithiols[144]. The dithiol has two roles with one adsorbing to the surface of the QD and the second providing surface functionality. The free thiol can form thioester linkages in the same way as the free amine can form a peptide linkage. Silanization does, however, have a detrimental effect on quantum yields due to the difficulty in controlling the silica shell growth and the surface states that are generated leading to trap emission. A method of silica encapsulation has been reported by Ying and co-workers which involves a process called reverse micro-emulsion[145]. By carefully controlling the silica layer growth and using alternative starting silanes, for example an amino terminated silane rather than a thiol the quantum yields can be increased.

Silica encapsulation is a solid strategy for providing water solubility although its use is restricted to very small scale quantities as dilute conditions are required. From this approach, like the micellar routes

mentioned, larger particle sizes are produced (from tens of nanometres to several micrometres). The subsequent size increase after encapsulation can hamper their suitability for biological applications. The increase in dimensions brought about by this modification could cause intracellular delivery of water soluble QDs to be affected.

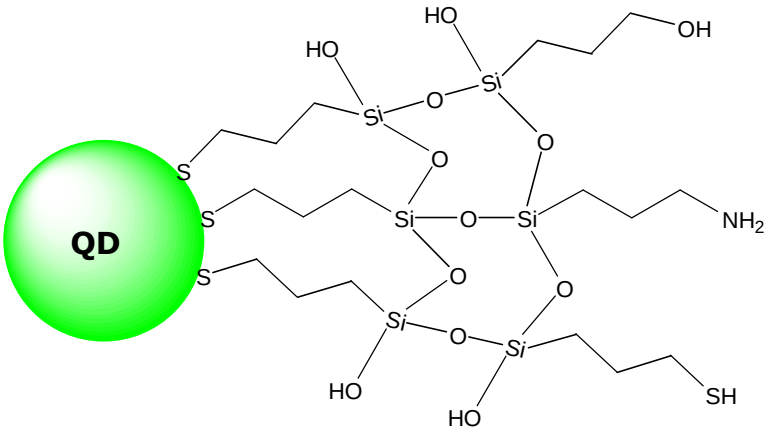

(20)

Figure 4.4 *Quantum dot particle encapsulated in a silica shell*[143].

4.1.4 Polydentate Ligands

Ligand exchange of hydrophilic thiols onto the QD surface is a convenient way to impart water solubility around the emissive inorganic QD core. However, after the displacement of the hydrophobic capping ligands the core can become somewhat exposed and in aqueous environments the quantum yields are greatly diminished[10, 146]. In addition, the desorption of thiols from the surface over time can cause aggregation and precipitation of the QDs in solution. Coating the surface of the nanoparticle with polymers or amphiphilic macromolecular constructs protects it from the aqueous environment, however, it does increase the dimensions of the QDs which can hamper biological applications. Callan and Raymo recently reported the preparation of CdSe/ZnS QDs coated with a polydentate thiol comprising a poly(methacrylate) backbone with reduced DHLA ligands attached to each residue and have shown them to be stable at pH 5 – 9 in aqueous environments for several days possessing good luminescence yields (35 – 41 %) and relatively small

hydrodynamic diameters (15 – 29 nm)[138]. From cellular imaging studies, these modified QDs were shown to enter the cytosol or nucleus of human umbilical vein endothelial cells (HUVEC), depending on the ligand used. Furthermore, no cellular toxicity was detected in assays thus opening up possibilities for use as intracellular probes.

Ligand exchange is by far the most common method for surface functionalisation of QDs used in sensing applications and characterisation tends to be more straightforward as particle size is not significantly affected. Using thiol terminated ligands allows for convenient proof of principle determination of new receptor types. Therefore, ligand exchange using thiol terminated ligands will be the method used in this thesis.

4.2 Luminescent detection of Cu^{2+} ions in aqueous solution

4.2.1 Introduction

Copper is an essential element in all plant and animal life and plays a vital role in biological electron transport in cells[145]. Blue copper proteins like azurin and plastocyanin are involved in this electron transport and are referred to as blue copper proteins due to the absorption band centred at 600 nm arising from the metal to ligand charge transfer (LMCT)[147]. Copper is also found in the copper centres of cytochrome c oxidase and superoxide dismutase enzymes[148]. Its anti-bacterial and anti-microbial effects have been exploited for use in hospital surfaces and fittings. There are however detrimental effects associated with copper in terms of its consumption. There have been reports in India of cirrhosis of the liver from cooking acidic food in copper pots[149], therefore the detection of Cu^{2+} is of considerable importance.

4.2.2 Design of water soluble QD probe for Cu^{2+}

Sub-micromolar recognition of copper ions in aqueous systems is an area of great interest in the field of biology and environmental science and historically this has been achieved through organic dye based sensors. QD based sensors have recently been employed in the detection of Cu^{2+} ions in aqueous solution[88, 150, 151]. In addition to those examples outlined in section 1.8, Zhu and co-workers have designed a Cu^{2+}

sensitive CdTe/CdSe Type-II core shell QD functionalised with mercaptopropionic acid (MPA)[152]. This type-II core shell QD emits in the near infra-red (NIR) and has shown potential as fluorescent NIR probes in biological imaging and NIR Cu^{2+} sensing. However, the lack of a protective coating over the two cadmium based shells may limit it in terms of toxicity for *in vivo* applications. Sanz-Medel and colleagues have modified CdSe QDs with 2-mercaptoethane sulfonic acid and also with mercaptoacetic acid and both have displayed selectivity towards Cu^{2+} ions in aqueous solutions[150]. The sulfonate functionalised QDs were found to be more sensitive to Cu^{2+} and further analysis was carried out using this probe in the determination of trace copper levels in fountain and tap water.

In the work presented here, CdSe and CdSe/ZnS QDs were surface functionalised with mercaptosuccinic acid (MSA), rendering them water soluble. MSA has two important functions when grafted on to the QD. At physiological pH the negatively charged MSA not only ensures water solubility but also serves to electrostatically attract positively charged substrates close to the QD surface. MSA has been used before as a capping ligand for QDs[130] but its resulting conjugate was not tested for selectivity against cations. It is known that Cu^{2+} can quench the excited state energy of fluorophores by electron / energy transfer[153]. In addition, this design strategy is helped by the position of Cu^{2+} in the Irving-William series, meaning it is expected to bind more strongly than any other divalent 1st row transition metal ion to ligands, irrespective of the nature or number of ligands involved[50]. In this capacity the MSA will serve as a receptor and thus a QD-receptor conjugate with an "On-Off" response could be realised. The effect the ZnS shell has on the quenching efficiency of Cu^{2+} will also be investigated by performing titrations of CdSe and CdSe/ZnS functionalised QDs with $CuCl_2$. The ZnS shell would be expected to insulate the emissive QD core and therefore influence the ability of redox active substrates to interact with it. From table 3.1 the core size of Evident CdSe/ZnS QDs was determined as 2.4 nm by UV methods while TEM gave a value for the core-shell diameter to be 3.4 nm. Given that the average contribution of one hemi-layer of ZnS has been reported as 0.31 nm, this would suggest that the Evident CdSe/ZnS QDs have approximately three layers of ZnS coating the core. This is sufficiently thin

to allow electron transfer processes between the core QD and the appended receptors / analytes[121].

4.2.3 Synthesis of QD conjugates 21 and 22

CdSe QDs (λ_{max} em = 525 nm) prepared in section 2.2.2 and CdSe/ZnS QDs (Evident technologies) (λ_{max} em = 535 nm) were both subjected to ligand exchange reactions with MSA as discussed in section 2.2.3. Briefly, the QD solution was pipetted into a stirring solution of MSA in anhydrous methanol and adjusted to pH 10 with the aid of TBAOH.

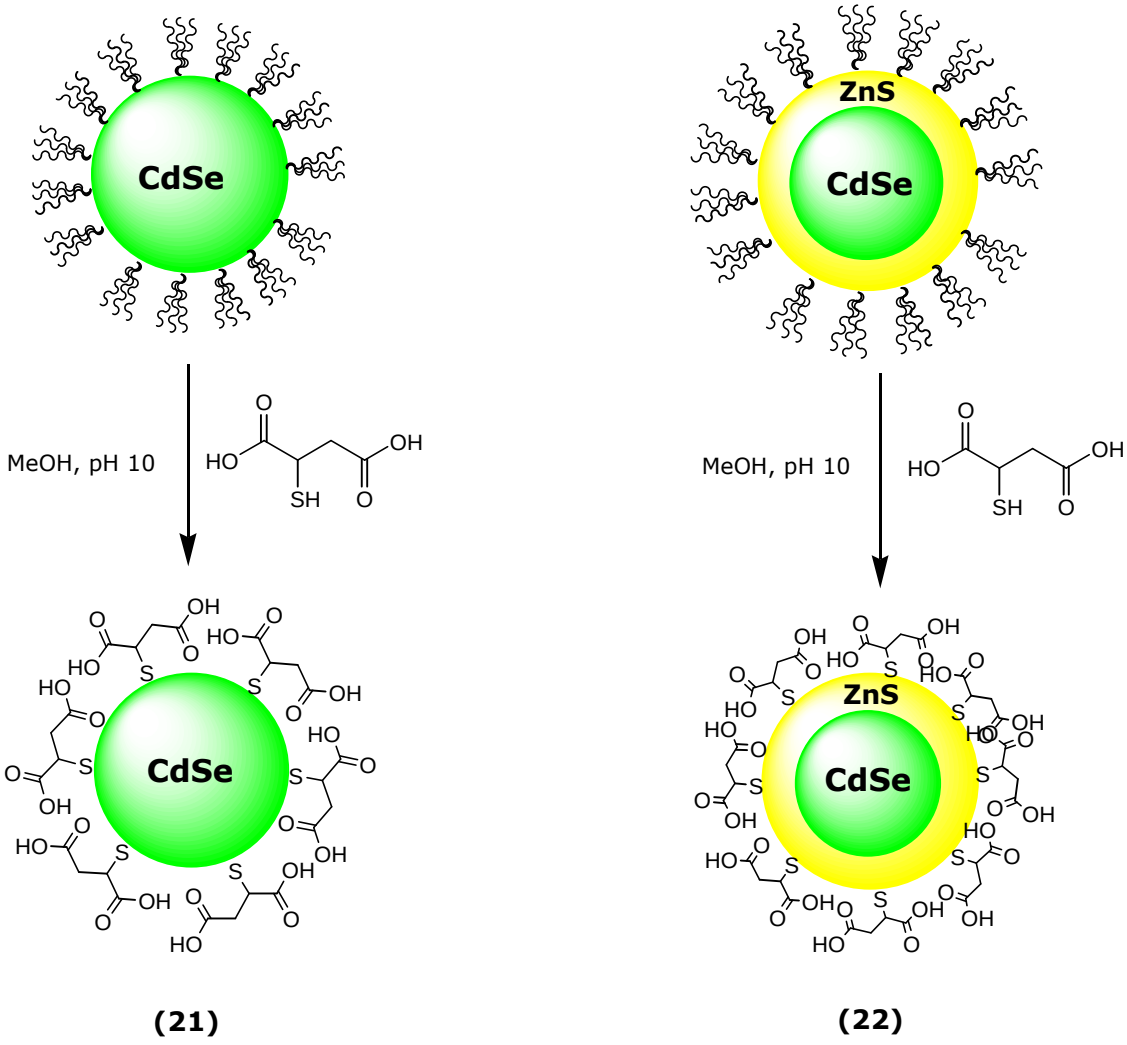

(21) **(22)**

Scheme 4.1 *Exchange reaction of MSA ligand with TOP/ TOPO groups on QD surface. Reaction conducted in dry MeOH at pH 10.*

The reaction was refluxed for 5 hrs under N_2, after which the solvent was evaporated to one third of the original volume. Diethyl ether was used to precipitate the QDs and the supernatant was carefully decanted off. The suspended solid was centrifuged for 5 mins at 13,500 rpm. The resulting solid was vacuum dried overnight. After exchange the modified QDs were fully dispersible in water.

^{1}H NMR was used to confirm ligand exchange of the QDs with MSA. An example is shown for the CdSe/ZnS QDs in figure 4.5, with the stacked ^{1}H NMR spectra for MSA, CdSe/ZnS QDs and **22** shown in descending order. The MSA was characterised by two distinct resonances, one for the methine proton centred at 3.60 ppm and a symmetric multiplet for the diastereotropic methylene protons centred at 2.85 ppm. The acidic carboxyl protons are observed at about 12 ppm and are not shown in the expanded figure 4.5. However, the thiol proton was not observed most likely due to deuterium exchange with the D_2O solvent. The parent QDs were characterised by the resonances centred at 5.75 and 4.85 ppm representing the olefinic protons of 1-octadecene, a non-co-ordinating solvent used in the synthesis of the QD, while the resonance at 1.95 ppm represents the methylene protons adjacent to the olefinic group of 1-octadecene. The remaining methylene protons of octadecene were represented by the large resonance centred at 1.20 ppm while the methyl protons were observed at 0.80 ppm. The methyl protons from TOPO overlap with those of 1-octadecene. However, the methylene protons adjacent to the P=O bond are observed as small broad resonances at 1.50 and 1.25 ppm, the latter appearing as a shoulder on the main methylene peak observed for octadecene.

The spectrum for the QD-MSA conjugate reveals that the ligand exchange and subsequent work-up results in the complete removal of octadecene from the solution. In contrast, some TOPO groups remain with the resonances at 1.50 and 1.25 ppm now more evident than in the spectrum of the QD alone. Successful exchange was confirmed by the upfield shift of the methine proton b, from 3.60 ppm in free MSA to 3.05 ppm in the QD-MSA conjugate. The smaller upfield shift observed for methylene protons c and c’ to 2.55 ppm is most likely due to these being

further from the sulfur atom and consequently are less influenced by the QD surface.

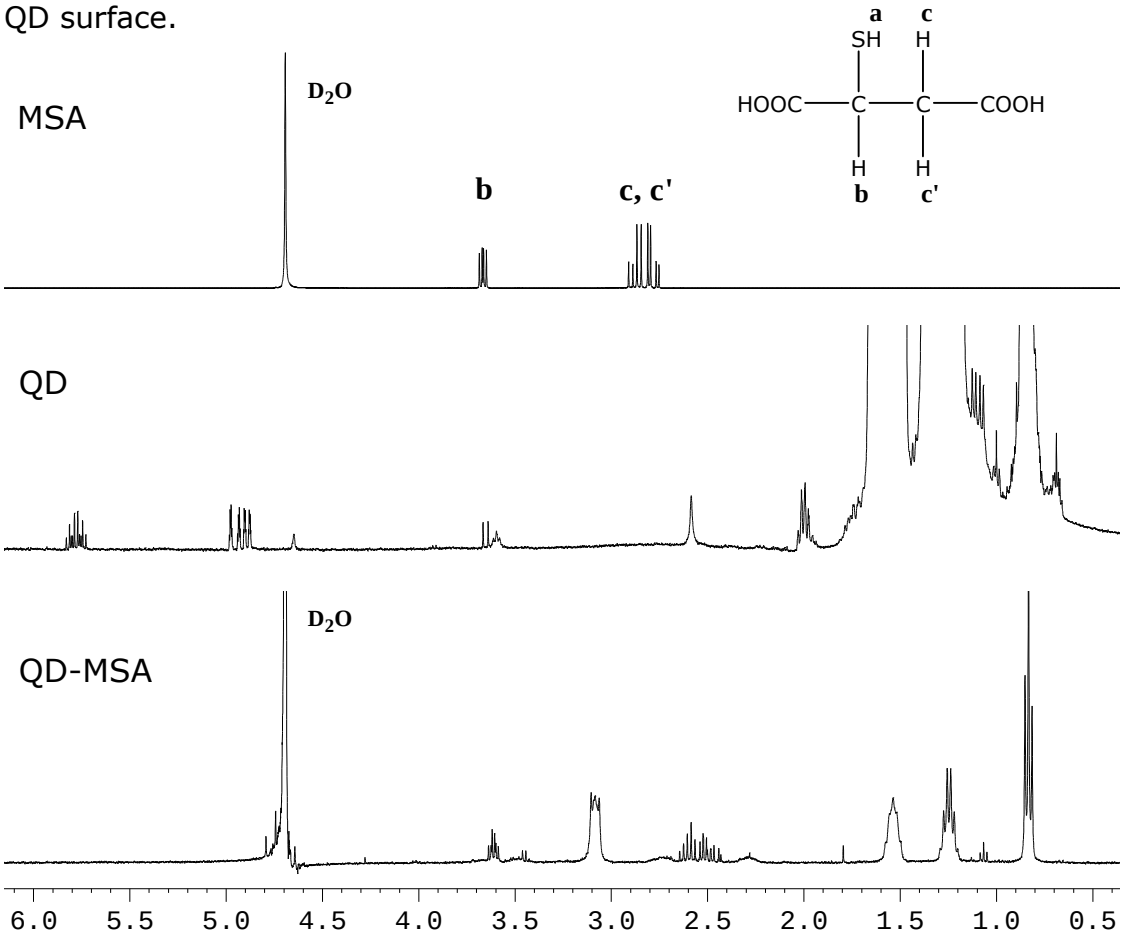

Figure 4.5 *Stacked ^1H NMR spectra of top: mercaptosuccinic acid (MSA) recorded in D_2O, middle: CdSe–ZnS QDs recorded in $CDCl_3$ and bottom: QD-MSA conjugate recorded in D_2O.*

4.2.4 Photophysical properties of 21 and 22

The absorption spectrum for the parent CdSe QDs recorded in toluene and **21** recorded in 100% H_2O are shown in figure 4.6a. A significant red shift of the 1st exciton peak was observed after the exchange with MSA. This red shift from 505 nm to 515 nm may be a result of aggregation of QDs leading to this apparent increase in the 1st excitonic peak. A particle diameter of 2.4 nm was calculated using equation 3.1. When excited at 370 nm, emission was observed for **21** at 525 nm with a FWHM of 52 nm. Again, the profile and emission λ_{max} are similar to the parent QDs with the spectrum of **21**, if anything less broad than the parent QDs. This is most likely due to the extra precipitation

steps involved in the reaction work-up after the exchange reaction. Also observed is a slight blue shift in the emission spectrum which is possibly due to a size selection process upon re-precipitation with the larger sizes being excluded.

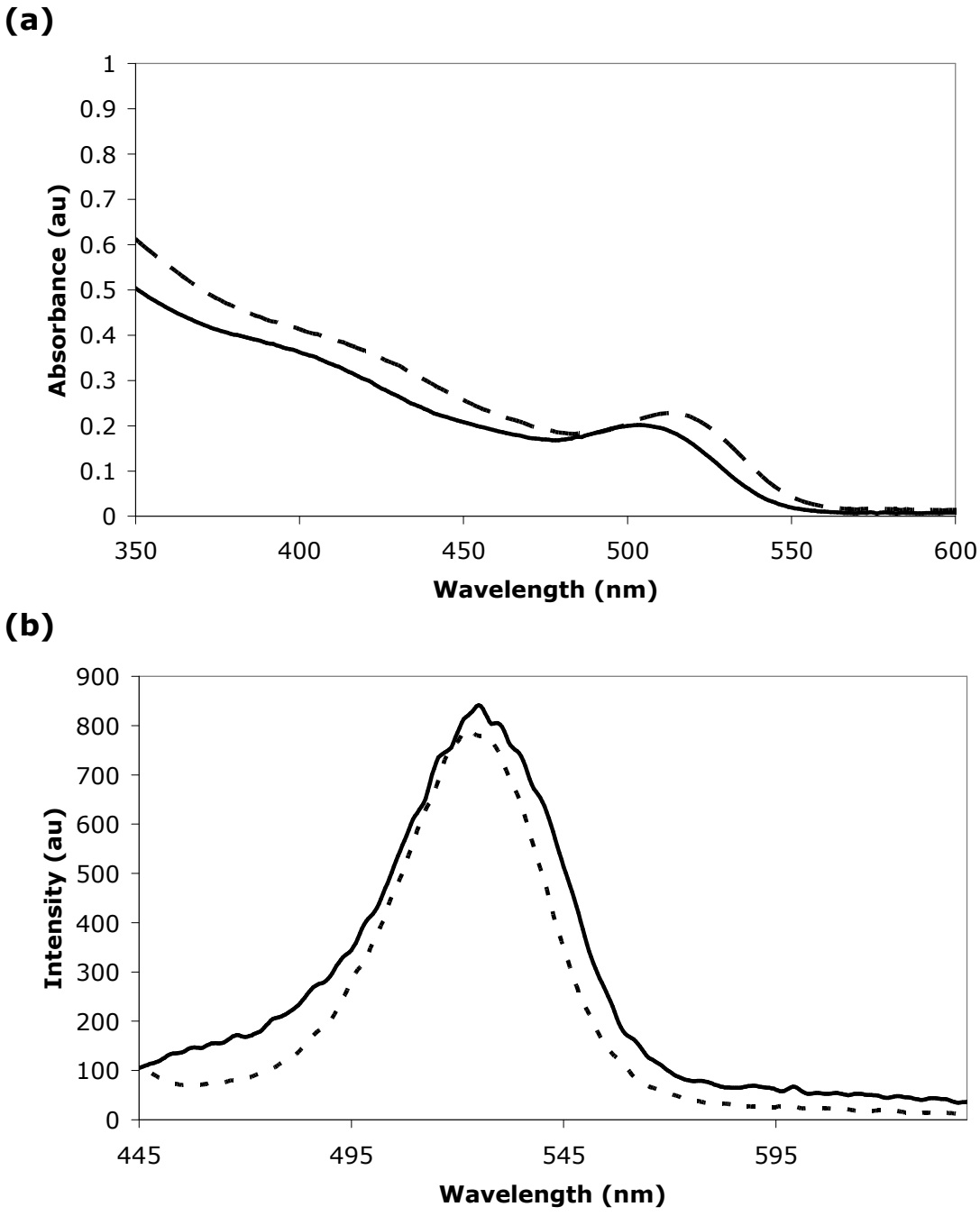

Figure 4.6 *(a) absorbance and (b) emission spectra for parent CdSe QDs (**–**) and **21** (--).*

The absorption spectra for the parent CdSe/ZnS QDs and **22** are presented in Figure 4.7a and a significant blue shift was observed after ligand exchange. The 1st exciton peak in the parent QDs at 514 nm was blue shifted to 525 nm for **22**.

(a)

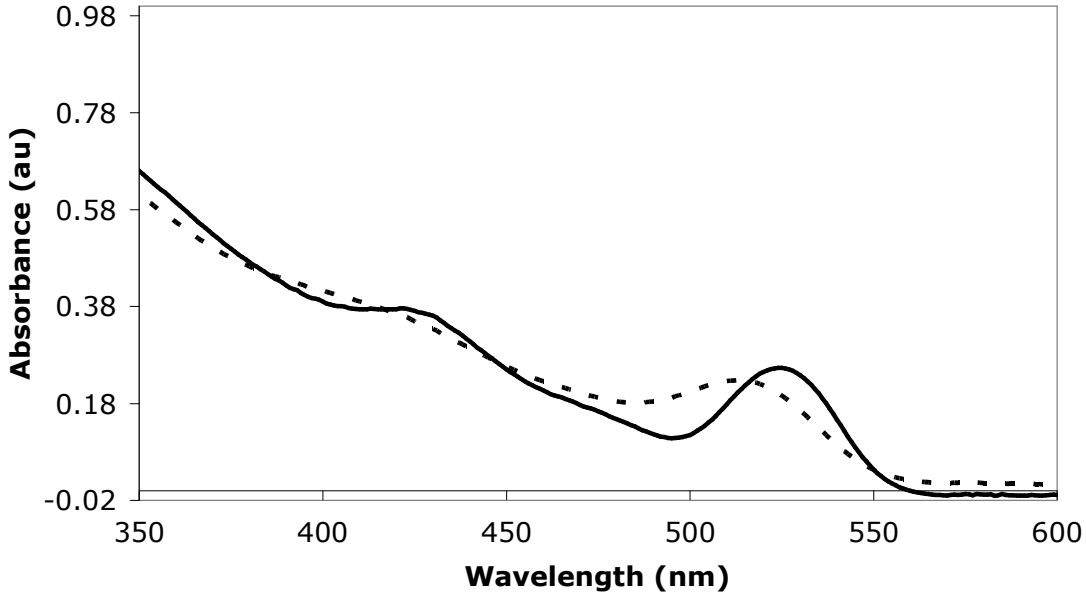

(b)

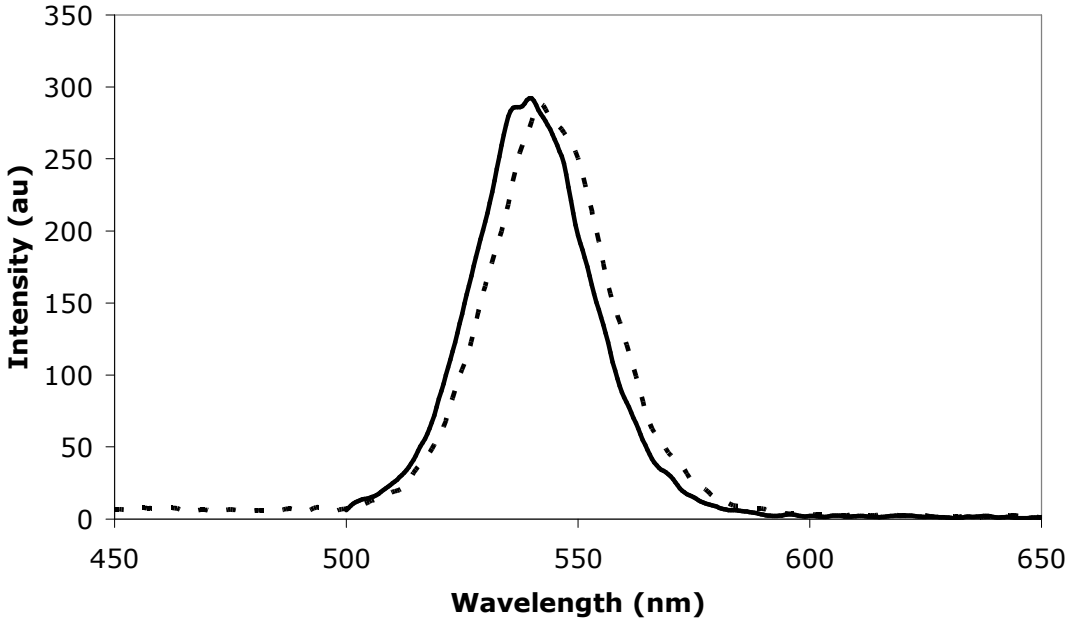

Figure 4.7 *(a) absorbance and (b) emission spectra for parent CdSe/ZnS QDs (–) and* ***22*** *(--).*

This blue shift may be due to partial disruption of the ZnS shell through photo-oxidation and removal of surface atoms resulting in a slightly reduced diameter[122]. The diameter of the nanocrystals obtained from the first exciton peak was 2.6 nm, using equation 3.1.

The emission spectra for **22** (figure 4.7b) when excited at 370 nm was also relatively unchanged when compared to the parent CdSe/ZnS QDs with λ_{max} values of 541 nm and 539 nm respectively. The small red shift into the emission may be due to leakage of the exciton into the ZnS shell which has been observed before[37]. The quantum yield for **21** was 1% (± 1%) while **22** returned a value of 2% (± 1%). These low quantum yield values are common for water soluble QDs passivated with monothiols. The appearance of the emission peak for **22** relative to **21** is significantly narrower and is due to better passivation of the core with the higher band gap ZnS.

4.2.5 Selectivity studies of 21 and 22

The selectivity of the MSA functionalised QDs were tested against a range of physiologically and environmentally relevant cations in 100% H_2O solution, buffered to pH 7.4 using HEPES. Specifically, a 1 x 10^{-5} M solution of Na^+, K^+, Mg^{2+}, Ca^{2+}, Fe^{2+}, Mn^{2+} and Cu^{2+}, as their chloride salts in H_2O were prepared in the presence of **21** or **22** (2.5 x 10^{-7} M). A bar chart illustrating the results is presented in figure 4.8. For **21**, Cu^{2+} was observed to produce a 90% quench of the original fluorescent intensity while Fe^{2+} also resulted in a quench, although of a much smaller magnitude (48%), with the other ions tested producing only minor effects.

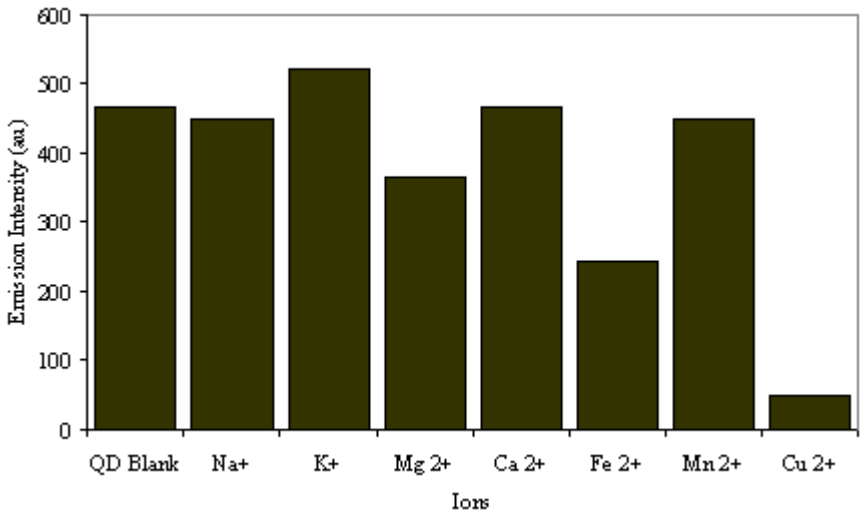

Figure 4.8 *Selectivity data for **21**. Ion concentration was 1 x 10^{-5} M, λ_{ex} = 370 nm. [**21**]= 2.5 x 10^{-7} M.*

The effect produced by Cu^{2+} was expected, due to its previously mentioned position in the Irving-William series[154]. It would therefore be expected to bind strongly to the carboxylate ligands of MSA and quench **21**'s fluorescence by electron transfer.

The selectivity studies for **22** yielded similar results as for **21** (see figure 4.9). Again, Fe^{2+} and Cu^{2+} were the main quenchers but surprisingly, a significant enhancement was observed for K^{+}, the reason for which is unclear. As Cu^{2+} produced the most significant quench for both **21** and **22**, sensitivity titrations were undertaken to determine the range over which the probe may be useful and to determine the effect if any, the ZnS shell has on the quenching efficiency.

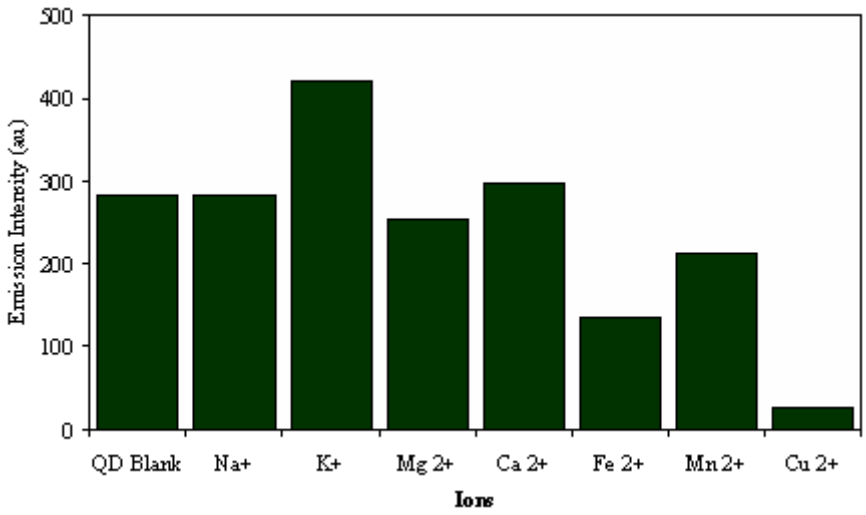

Figure 4.9 *Selectivity data for **22**. Ion concentration was 1 x 10^{-5} M, λ_{ex} = 370 nm. [**22**] = 1.2 x 10^{-8}M.*

4.2.6 Sensitivity of 21 and 22 to Cu^{2+}

The emission spectra for **21** and **22** in the presence of increasing amounts of Cu^{2+} are shown in Figure 4.10. For **21** there is a distinct red shift in the emission wavelength (~ 10 nm) at higher concentrations of Cu^{2+} while for **22** the effect is much less significant (~ 4 nm). This red-shift is indicative of surface effects between Cu^{2+} and the QD. This type of interaction has been seen in other systems (the formation of Ag_2Se upon addition of Ag^+ ions to CdSe QDs[155] and the formation of HgTe on addition of Hg^+ ions to CdTe QDs[156]) and in the present case is explained by the much lower solubility product of CuSe (-log K_{SP} = 60)[157] compared to CdSe (-log K_{SP} = 35)[88].

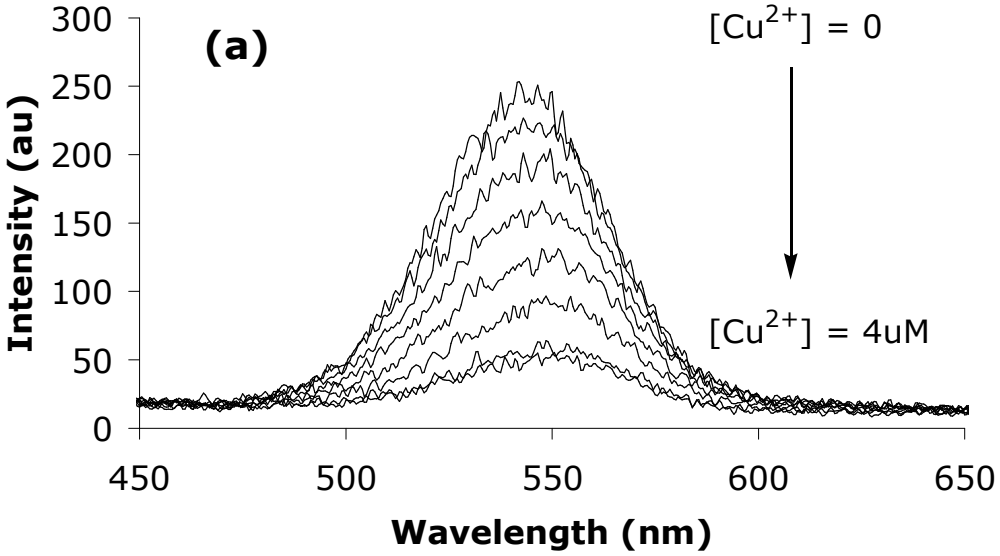

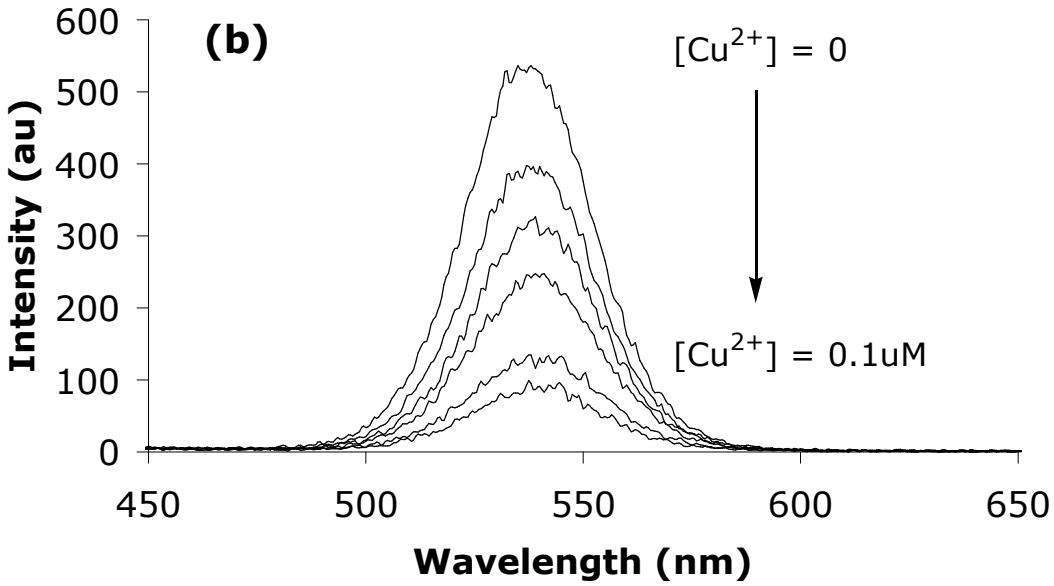

Figure 4.10 *Emission Spectra for (a)* ***21*** *and (b)* ***22****. Concentrations of* Cu^{2+} *shown in the emission plots for CdSe were 0, 0.019, 0.13, 0.59, 1.10, 1.78, 3.31 and 3.99* μ*m and for CdSe/ZnS were 0, 6.00, 14.00, 24.00, 64.00 and 104 nM with decreasing fluorescence intensity. [****21****]=* 2.5×10^{-7} *M, [****22****] =* 1.2×10^{-8}*M.*

A much smaller red shift (~4 nm) was observed for the CdSe/ZnS QDs after addition of 104 nM Cu^{2+}. It is unlikely that this is due to the formation of CuSe due to the presence of the ZnS shell but could be due

to the formation of small amounts of CuS or Cu_2S[157]. Again this is supported by the lower solubility product of CuS (-log K_{SP} = 35) compared to ZnS (-log K_{SP} = 20)[158]. This indicates that at higher concentrations of Cu^{2+}, the formation of CuSe and CuS / Cu_2S may contribute to the fluorescence quenching of **21** and **22** respectively. However, at lower concentrations of Cu^{2+} where the emission maximum remains constant, the most probable cause for the quenching is electron transfer from the excited QD to Cu^{2+}. UV-vis analysis was not carried out on the modified QDs in the presence of Cu^{2+} due to the limited amount of **21** and **22** available for these studies.

To determine the sensitivity of the two QD-receptor conjugates toward Cu^{2+}, and to investigate the effect the ZnS shell may have on the quenching efficiency, a plot of relative fluorescence intensity against –log [Cu^{2+}] is shown in Figure 4.11.

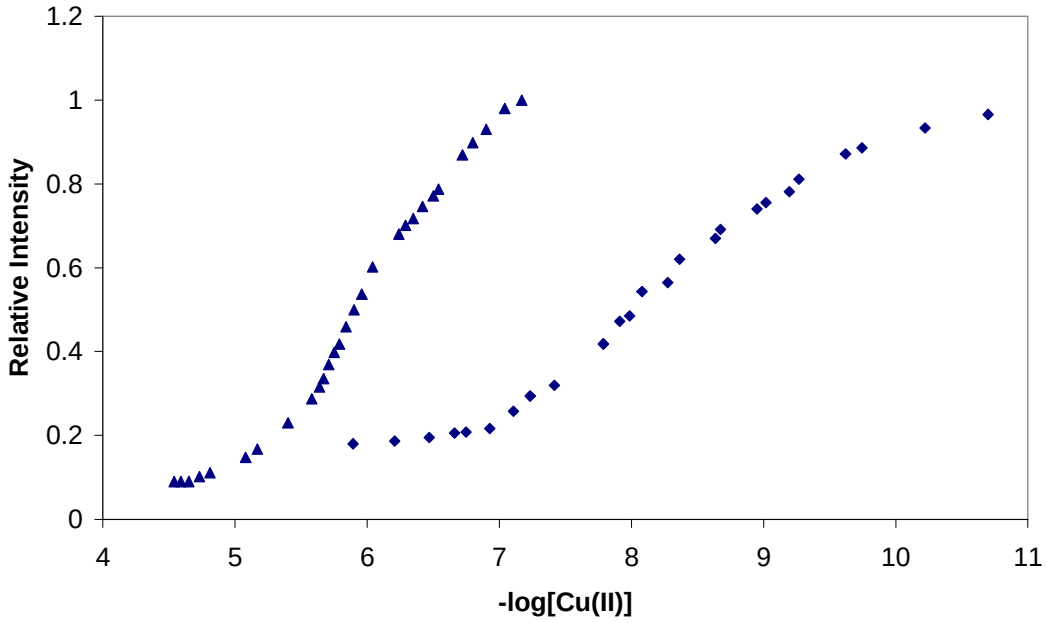

Figure 4.11 *Plot of relative intensity against –log [Cu^{2+}] for **21** (triangles) and **22** (diamonds). [**21**] = 2.3 x 10^{-7} M, [**22**] 1.3 x 10^{-8} M.*

From figure 4.11 it is evident that **21** and **22** display different binding responses to the presence of Cu^{2+}. For **21**, the fluorescence "switched off" over about two log units which suggests a 1:1 binding between Cu^{2+} and the QD conjugate[108]. In contrast, **22** displayed a

greater range of quenching, "switching off" over about four log units. Furthermore, **22** appears to be much more sensitive to Cu^{2+} addition with the quenching process occurring over a significantly less concentrated range. However, due to the slightly higher quantum yield of **22**, this solution had to be about 17 times more dilute than **21** in order to obtain the same starting fluorescence intensity. Therefore, it was expected that less Cu^{2+} would be required to bind to cause a quench in the intensity of **22** compared to **21**. However, it was also observed from figure 4.11 that a more complete quench was observed for **21** with a residual fluorescence of 10% remaining after Cu^{2+} addition compared to 20% for **22**, a feature again attributed to an insulating effect by the ZnS shell. Although the binding stoichiometry could not be confirmed due to the inability to calculate the number of surface ligands on **21** or **22**, the quenching for **21** occurred over approximately 2 log units and so a 1:1 binding was assumed. A derivation of the Henderson-Hasslebalch equation can be made to fit a 1:1 binding model and hence obtain a binding constant (β) value.

The Henderson-Hasselbalch equation calculates the pK_a values for the dissociation of weak acids[159]. The equation derived to calculate pK_a values from changes in emission intensity is shown in equation 4.1.

$$\text{Log}[(I_{Fmax} - I_F) / I_F - I_{Fmin}] = -pH + pK_a \qquad \text{equation 4.1}$$

$$y = mx + c$$

When y is plotted against x, dividing the y-axis intercept by the modulus of the gradient gives an accurate value for the pK_a of the probe. For **21**, equation 4.12 can be rearranged by replacing –pH with $\log[Cu^{2+}]$ and replacing pKa with log β[160, 161]. The binding constants –Log β, obtained from such a plot gave a value of 5.89 for **21**.

4.3 Conclusions

CdSe QDs synthesised by a literature procedure and CdSe/ZnS QDs purchased from Evident technologies were functionalised with MSA, rendering them water soluble. On functionalisation, the QDs displayed well defined spectral characteristics however as expected quantum yields were

low ~ 1 % for both core and core-shell QDs. Both sets of QDs showed selectivity for Cu^{2+} with a moderate interference by Fe^{2+} which was attributed to an inner filter effect. The quenching of the fluorescence on the introduction of Cu^{2+} was most likely due to a combination of electron transfer from the QD and surface effects from the formation of CuSe for **21** and CuS or Cu_2S for **22**. A binding constant of 5.89 was determined for **21** from the 1:1 association of **21** and Cu^{2+}.

4.4 Luminescent detection of ATP using positively charged CdSe/ZnS Quantum Dots.

4.4.1 Background

Virtually all life-forms use adenosine triphosphate (ATP). It is a near universal molecule of energy transfer and within cells it serves as the main energy currency. It is produced as the energy source in the processes of photosynthesis and cellular respiration and consumed by enzymes and cellular processes like biosynthetic reactions and cell division[162].

Its structure consists of the purine base, adenine attached to a ribose sugar and three phosphate groups. ATP has multiple ionizable groups with different acid dissociation constants[162]. It is ionized in neutral solution and exists mostly as ATP^{4-} and to a lesser extent as ATP^{3-}. It has been shown that ATP can chelate metals with great affinity due to its negatively charged phosphate groups when in neutral solution and in cells it exists as a complex with Mg^{2+}.[163]

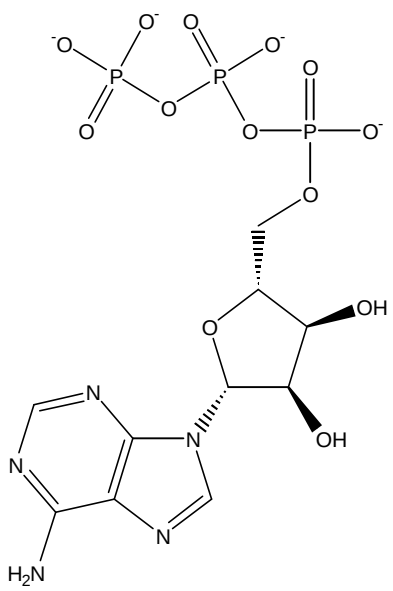

(23)

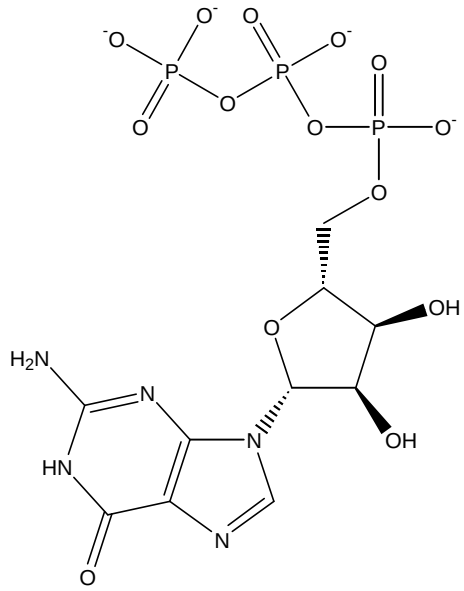

(24)

Figure 4.12 *Structures of ATP* ***(23)*** *and GTP* ***(24)*** *both in the ionised form.*

Kanekiyo *et al* developed a novel fluorescent probe for the detection of ATP based on the aggregation of pyrene-appended boronic acids on a polycation[164]. Due to the formation of reversible boronate esters with the diol groups on the ATP, electrostatic attraction between the negatively charged ATP and the polycation surface resulted in a hydrophobic interaction between the pyrene units causing excimer emission (figure 4.13). Selectivity studies revealed significant spectral changes for ATP and adenosine diphosphate (ADP) with a minor response from adenosine monophosphate (AMP). The selectivity for ATP and ADP over AMP was attributed to the decrease net charge of AMP relative to ATP and ADP which decreased its extent of attraction to the polycation surface. Non-charged species like adenosine and fructose were used as controls and resulted in no response.

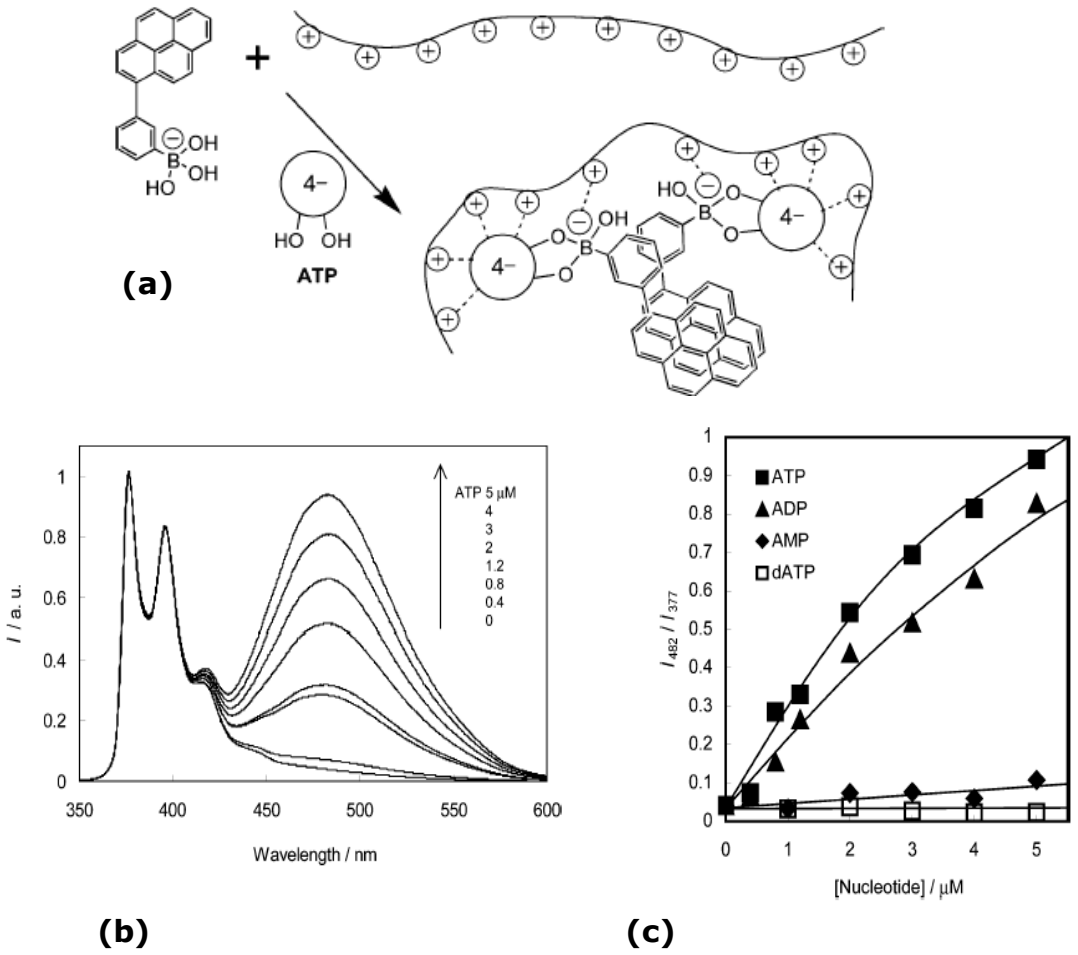

Figure 4.13 *(a) ATP-mediated aggregation of pyrene-appended boronic acid on polycationic surface. (b) Fluorescence spectra illustrating the excimer emission upon addition of various concentrations of ATP. (c) Dependence of the intensity ratio at 482 nm to 377 nm (I_{482}/I_{377}) on nucleotide concentration*[164]*.*

Inspired by these results and noting how ATP and ADP were attracted to the polycationic surface while AMP and other non-charged species showed no affinity for these quarternised amines, it was envisaged that a comparable response would be observed by a QD appended with similar positively charged ligands.

Therefore, a QD probe was designed where a charged quaternary ammonium group was used not only as a receptor but also to ensure aqueous solubility and was co-ordinated to the surface of a CdSe/ZnS QD

via a thiol group, to give conjugate **28**. The oxidisability of guanine and adenine is well known as they have the lowest oxidation potentials among the nucleic acid bases[165]. CdSe QDs can be oxidised and reduced at relatively moderate potentials and can thus participate in electron transfer processes in a similar manner to organic dyes[166]. Therefore, the present design attempts to discriminate between nucleotides based on differences in their surface charge, which in turn modulates their attraction to the surface of the QD. Electron transfer efficiency is known to be distance dependant[167] and so only those nucleotides that are attracted close to the surface of the QD can participate in effective electron transfer.

4.4.2 Synthesis of receptor 27 and QD conjugate 28

The synthetic scheme adopted for the synthesis of the charged receptor ligand and its attachment to the surface of the QD is shown in scheme 4.2. The receptor was synthesized in one step by the direct N-alkylation of 2-dimethylamino-ethanethiol with iodomethane (see section 2.2.1.2).

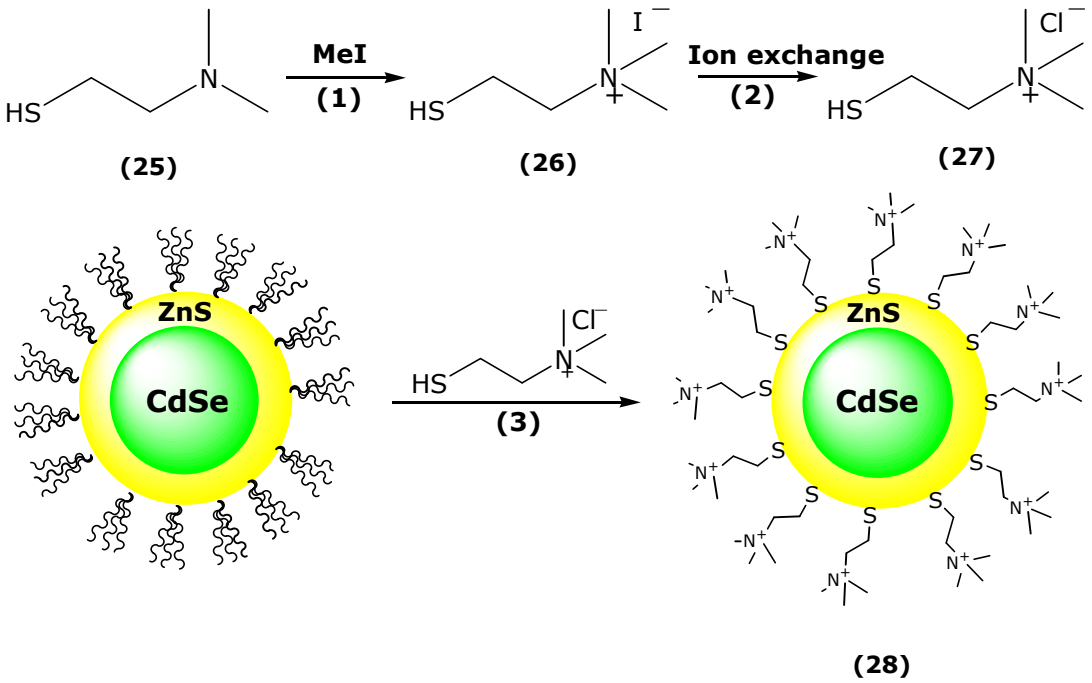

Scheme 4.2 *Synthesis of* ***28*** *(1) iodomethane, dry DCM, 18 hr, 25°C. (2) amberlite ion exchange resin. (3) CdSe / ZnS QDs, MeOH, pH 10.0, 5 hr.*

An aqueous solution of the receptor was then passed through amberlite ion exchange resin to substitute the iodide for chloride to prevent potential quenching by the heavy atom effect. The new ligand was then exchanged for the TOPO groups of the native CdSe/ZnS QDs by refluxing in dry methanol for 5 hrs. The nanoparticle chosen was again a 2.4 nm CdSe/ZnS QD purchased from Evident Technologies. The QD-receptor conjugate was purified by reiterative dissolution in methanol and precipitation from diethyl ether.

The ^{1}H NMR spectra of the free ligand **27**, the free QD and the QD-ligand conjugate **28** are shown in figure 4.15. The S-CH_2- and N-$(CH_3)_3$ protons of the receptor were observed together at 3.08 ppm while the -CH_2-N- protons were observed at 3.60 ppm (figure 4.15). The spectrum of the free QD shows the methyl and methylene protons of trioctylphosphine oxide (TOPO) resonating at 0.8 and 1.1 – 1.7 ppm respectively (figure 4.15). After the ligand exchange reaction, these signals disappear almost completely as shown in the spectrum of **28**. This confirms an almost complete exchange of the TOPO ligands for **27**. As expected however, the signals from the receptor remain but are relatively unaffected in terms of chemical shift when compared to the free ligand. This contrasts with the MSA-functionalised QDs where a shift in the receptor proton signals were observed upon surface exchange. A similar effect was also observed in section 5.1 and appears to be a common feature associated with cysteamine derivatised QDs. The zeta potential of an aqueous solution of the **28** was + 56 mV / mol, which was similar in magnitude but opposite in sign to a solution of QDs whose surface TOPO groups were exchanged for dihydrolipoic acid (**29**) which had a zeta potential of - 61 mV / mol.

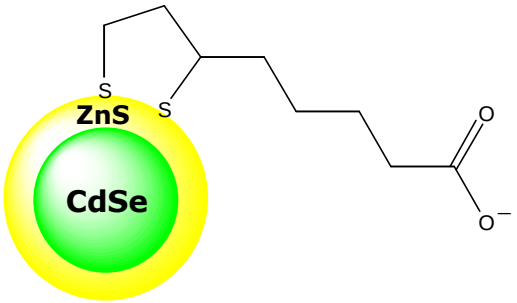

(29)

Figure 4.14 *TOPO groups of CdSe/ZnS QDs exchanged with dihydrolipoic acid (DHLA)*[121]*.*

Colloidal particles when dispersed in solution will be electrically charged due to their ionic characteristics. Zeta potential is a measure of how much particles repel or attract each other in solution. It is normally used to predict the stability of formulations and optimisation of emulsions and suspensions[168]. It can also be used to confirm the charge on the surface of QDs and predict if they will attract species near the surface.

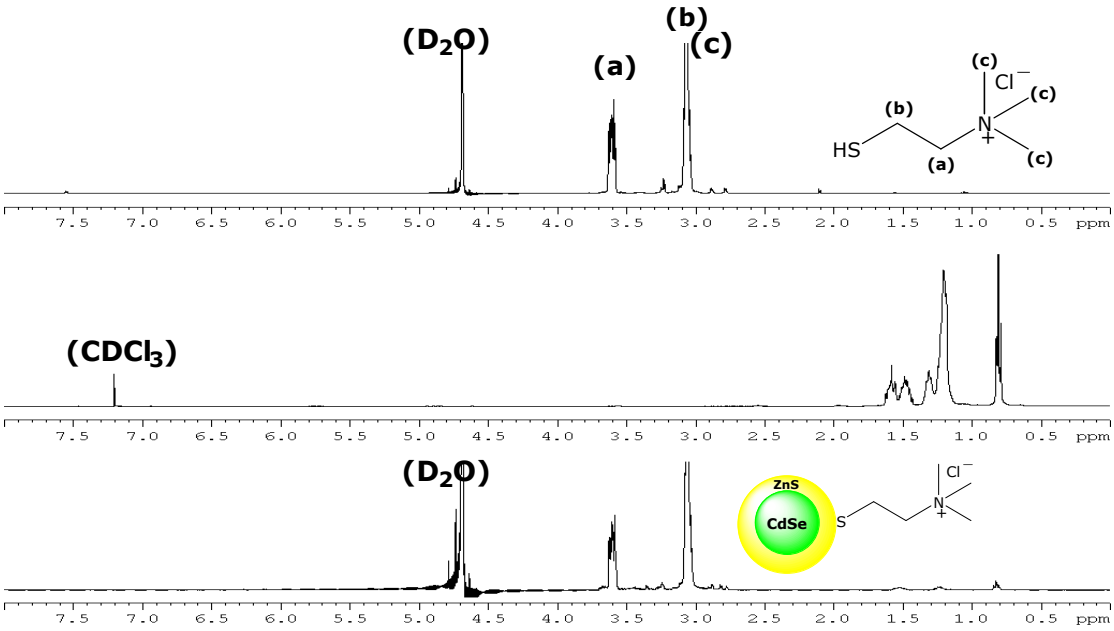

Figure 4.15 *Stacked ^1H NMR spectra of top:* ***27****, recorded in D_2O, middle: CdSe/ZnS QDs recorded in $CDCl_3$ and bottom:* ***28*** *recorded in D_2O.*

The absorption spectra for the parent CdSe/ZnS QDs and **28** are shown in figure 4.16. From the spectra it is evident that the 1st exciton peak of **28** was not as well defined compared to the parent QDs, however its position remains relatively unchanged as expected. This lack of definition in the UV spectrum is common for water soluble QDs where the surface states become altered and leads to broadening of the peak[144].

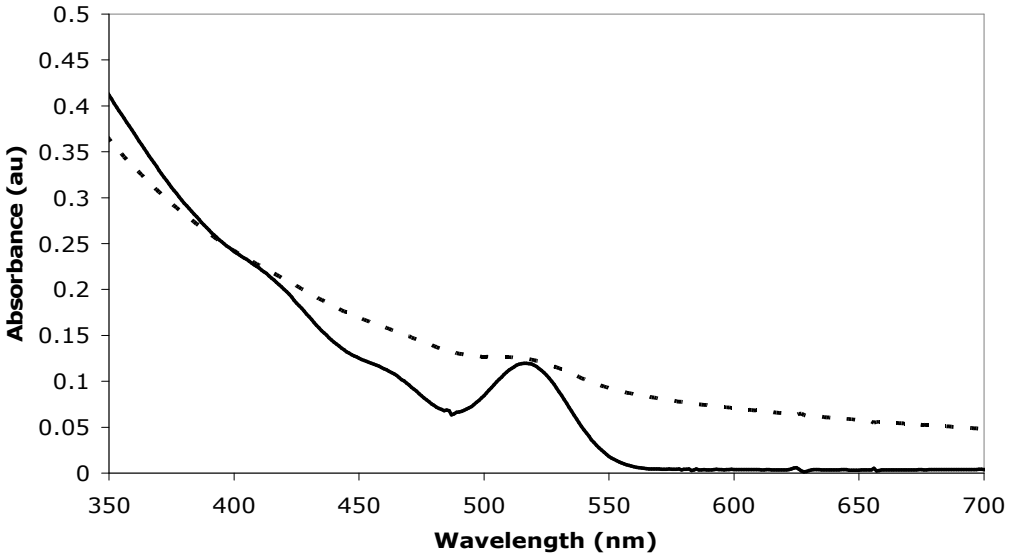

Figure 4.16 *Absorbance spectrum of parent CdSe/ZnS QDs (—) and* ***28*** *(---). Parent CdSe/ZnS QDs dispersed in $CHCl_3$ [2.0 x 10^{-6} M].* ***28*** *dispersed in H_2O [8.0 x 10^{-5} M].*

The fluorescence spectra for the parent QDs and **28** are shown in figure 4.17. The parent CdSe/ZnS-TOPO QDs emit at 531 nm while the exchanged QDs **28** emit at 543 nm which is likely due to aggregation and broadening of size distributions[131]. A quantum yield of 1% for **28** was markedly less than the parent QDs (38%). This poor QY is due to surface defects associated with the ligand exchange and also interaction with water molecules as detailed previously in section 4.1.2.

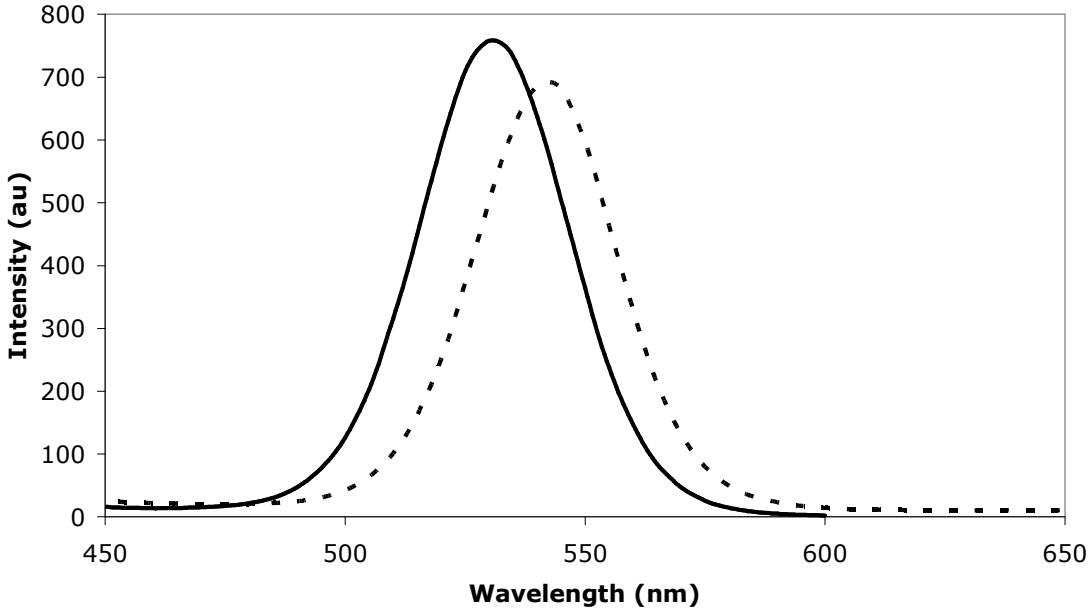

Figure 4.17 *Emission spectrum of parent CdSe/ZnS QDs (—) and* ***28*** *(---). Parent CdSe/ZnS QDs dispersed in $CHCl_3$ [2.0 x 10^{-7} M].* ***28*** *dispersed in H_2O [8.5 x 10^{-6} M].*

4.4.3 Selectivity studies of 28

The selectivity of **28** was tested against a number of nucleotides, namely ATP, ADP, AMP, GTP, GDP and GMP. The analyses were carried out in a 100% aqueous solution buffered with HEPES (0.1M) at pH 7.4. A plot of relative fluorescence intensity against concentration is shown in figure 4.18 for each of the nucleotides tested. The top plot (figure 4.18a) represents ATP, ADP and AMP and shows a significant reduction of the original fluorescence intensity for ATP with an approximate 80% quench observed at a concentration of 0.07 M ATP. In contrast, virtually no change was observed in the intensity of **28** upon addition of a similar quantity of ADP or AMP. The lower plot (figure 4.18b) shows the effect of adding GTP, GDP and GMP to a solution of **28**. Again, only minor changes were observed with GTP causing a 25% quench at a concentration of 0.07 M, while GDP and GMP caused virtually no effect. These results suggest that the greater charge on ATP relative to ADP or AMP and for GTP relative to GDP or GMP results in a greater attraction to the positively charged nanoparticle surface, where due to their oxidisability guanine and adenine can engage in electron transfer with the QD and quench its fluorescence,

(a)

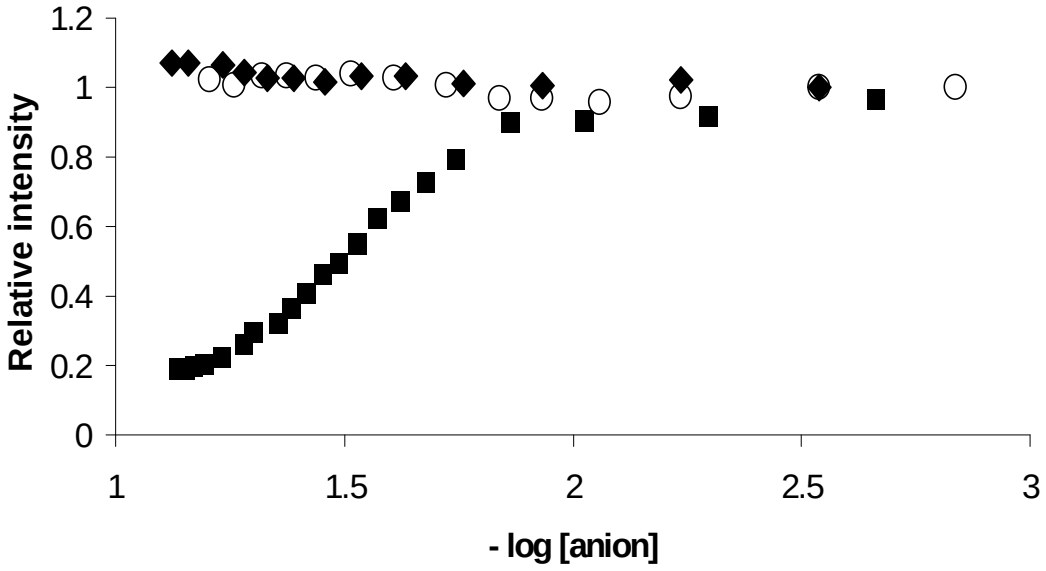

(b)

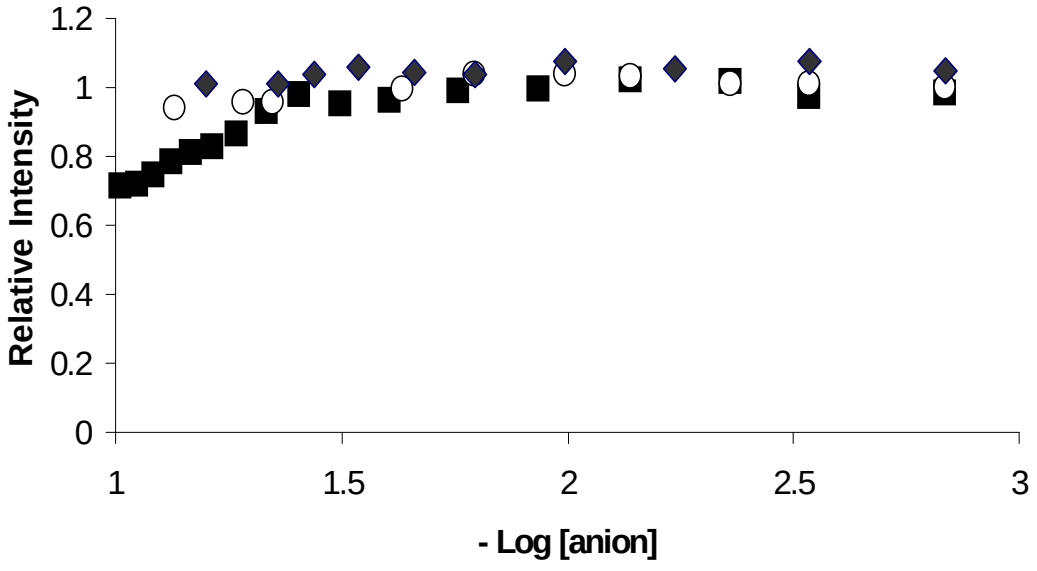

Figure 4.18 *Plot of relative fluorescence intensity against –log [anion] for (a)* ***27*** *titrated with AMP (o), ADP (♦) and ATP (■) and (b)* ***28*** *titrated with GMP (o), GDP (♦), GTP (■). [****28****] = 3.5 x 10^{-6} M, 0.1 M HEPES at pH 7.4, excitation wavelength = 370 nm.*

as shown schematically in figure 4.19. However, one would expect a greater quench for GTP compared to ATP due to the lower oxidation potential of guanine (1.29 V for guanine compared to 1.42 V for adenine vs NHE). The reason for this is unclear, however the results do show that **28** exhibits good selectivity for ATP when tested against other physiologically relevant nucleotides.

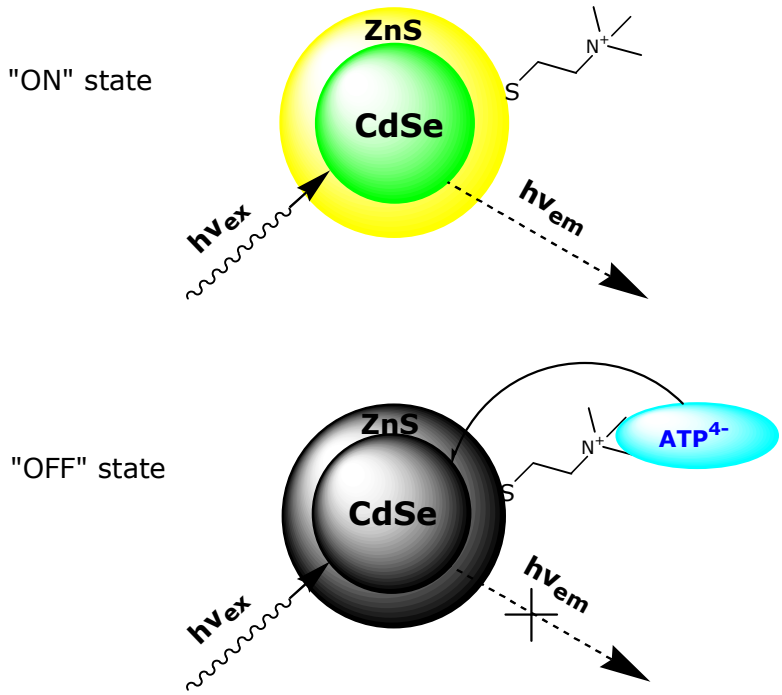

Figure 4.19 *Schematic diagram illustrating the quenching effect on addition of ATP to positively charged CdSe/ZnS QDs. The quaternary ammonium ligand attracts the tetravalent ATP to the surface of the QD and engages in electron transfer thus quenching the excited state energy.*

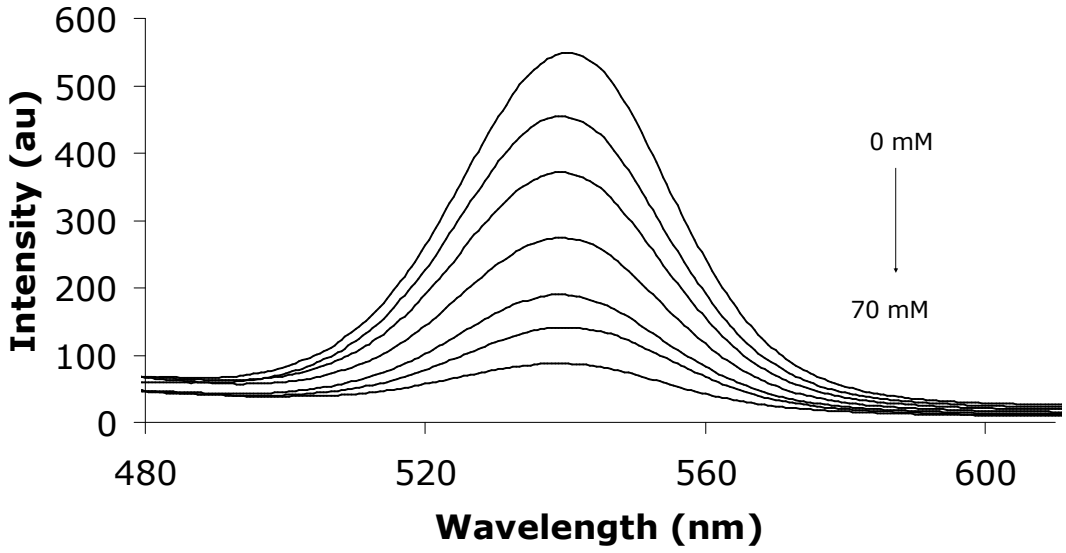

Figure 4.20 *Plot of fluorescence intensity against wavelength for* ***28*** *upon increasing addition of ATP. [****28****] = 3.5 x* 10^{-6} *M, excitation wavelength = 370 nm.*

Figure 4.20 shows a spectral plot of **28** upon titration with ATP in HEPES buffer (pH =7.4). An almost full quench (~80 %) was achieved after 70 mM addition of ATP with no shift in λ_{max} at 540 nm being observed. This is in contrast with the red-shift observed for the interaction of **21** or **22** with Cu^{2+} and would suggest that surface effects are not responsible for the quenching of QD fluorescence.

4.4.4 Effect of pH on the interaction of 28 with ATP

To determine the effect of pH on the interaction of ATP and **28** a pH titration was performed. By varying the extent of ionisation of the ATP it was thought it may affect its attraction to the QD surface. Figure 4.21 shows a plot of relative fluorescence intensity against pH for a solution of **28** (pink squares) and a solution of **28** in the presence of ATP (0.065 M) (blue diamonds). For **28** alone, as the pH is lowered from physiological range, the fluorescence is quenched. Lowering the pH causes thiol desorption from the surface of **28**[169] which reduces the passivation of the QD core and a reduction of luminescent intensity results. The pH titration of **28** in the presence of ATP shows that the fluorescence suppression is

unperturbed regardless of what the pH value is. It was thought that reducing the pH of this solution would cause more of the ATP's phosphate groups to become protonated thus reducing their attraction to **28** leading to recovery in the fluorescence intensity. However, this effect would also compete with the thiol desorption process meaning that even if the ATP becomes protonated, the competing thiol desorption process means the fluorescence intensity would remain low. Therefore, this demonstrates the importance for working in buffered media for **28** to be effective at measuring ATP concentrations.

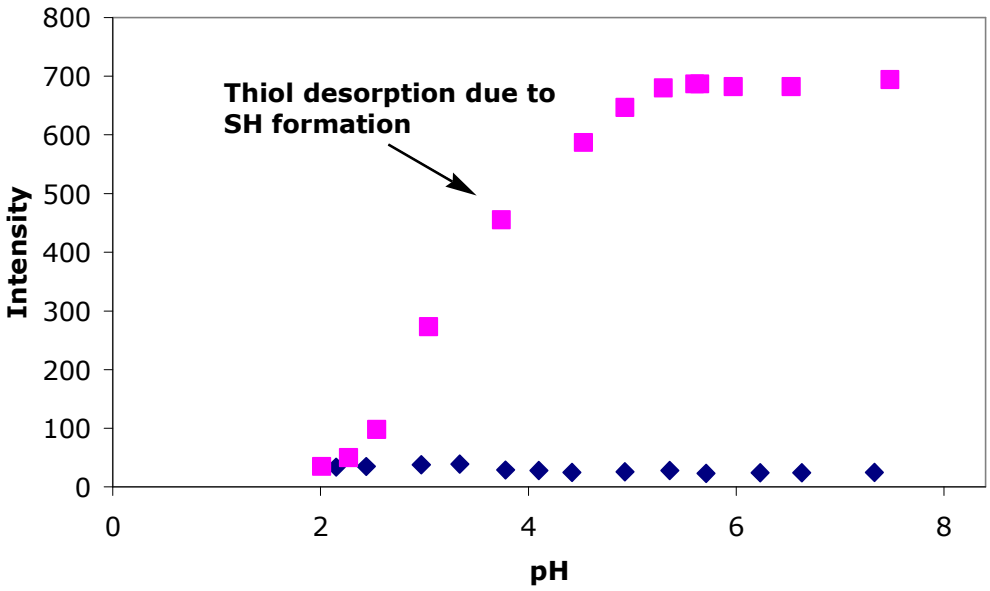

Figure 4.21 *Plot of fluorescence intensity against pH for* ***28*** *(shown by pink squares) and a plot of* ***28*** *in the presence of ATP against pH (shown by blue diamonds). [****28****] = 3.5 x* 10^{-6} *M, [ATP] = 0.065 M.*

4.5 Conclusions

CdSe/ZnS QDs purchased from Evident technologies were modified with ligand **27**. These water soluble QDs were luminescent albeit of much lesser magnitude than the parent QDs (Φ = 1%). Selectivity studies revealed an almost complete quench for ATP (80%) with a minor quench for GTP (25%). No quench was observed for the other nucleotides tested i.e. ADP, AMP, GDP or GMP. The quench for ATP was attributed to its

greater net negative charge resulting in a more significant attraction to the QD surface where it could engage in electron transfer with the QD resulting in a quench of the fluorescence emission.

CHAPTER FIVE

ANION SENSING WITH QDs

5.1 Background

As discussed in section 1.8.2, the photoinduced electron transfer (PET) mechanism has been central to the design of many organic dye based sensors and there are many examples of these within the literature[49, 51]. This mechanism has also been incorporated in the design of QD based probes, although examples are limited in comparison to their organic counterparts[8]. Most of the early examples of PET controlled QD sensors relied on redox active substrates being attracted to the QD surface and engaging in electron transfer with the excited QD to perturb the fluorescence output[91, 93, 94, 170-172]. In this chapter we will examine PET sensing with QDs where the receptor is designed to specifically undergo a change in its redox properties upon binding an analyte and this change is manifested by a modulation in the emission intensity of the QD.

5.2 Proof of principle for receptor mediated PET with QDs

The examples of Cu^{2+} and ATP sensing with surface charged QDs, discussed in sections 4.2 – 4.4 are examples of QD sensing by electron transfer. However, these were cases in which the analyte itself was responsible for the electron transfer process. To expand the power of this technique, it is desirable to design systems in which the electron transfer occurs from the receptor itself with the process being modulated by analyte binding. This means that non-redox active substrates can be targeted. As mentioned in section 4.4.1 CdSe QDs can be oxidized and reduced at relatively moderate potentials, similar in magnitude to organic dyes[166]. Therefore, in principle these QDs should engage in electron exchange reactions with PET active receptors. Although it is now commonly accepted that QDs engage in electron transfer with surface bound ligands, this was not the case at the outset of this project. To determine if receptor mediated analyte binding was sufficient to alter the redox properties of a receptor and register the binding event as a change in the QD fluorescence, the following experiment was performed. The PET active 4-aminothiophenol was chosen as a receptor due to its low oxidation potential (0.73 V)[173] and presence of a thiol group that should adhere to the surface of the QD. 4-Aminothiophenol was added to a solution of CdSe/ZnS QDs and it was observed that fluorescence was

quenched, most likely by electron transfer from the anilinic moiety to the QD (Figure 5.1). Addition of 4-acetamidothiophenol, however, resulted in no fluorescence quenching. This was attributed to delocalisation of the amine lone pair over the amide bond, leading to an increase in its oxidation potential and making electron transfer energetically unfavourable. This suggested that PET type sensing was possible with QDs as a simple modification in the chemistry of the receptor unit resulted in a significant change in its interaction with the excited QD. However, this particular case involves a non-reversible interaction and practical sensors require reversible interactions between receptor and substrate. Nonetheless, it demonstrated that PET active organic receptors that engage in electron transfer processes with organic dyes should also engage in similar processes with QDs.

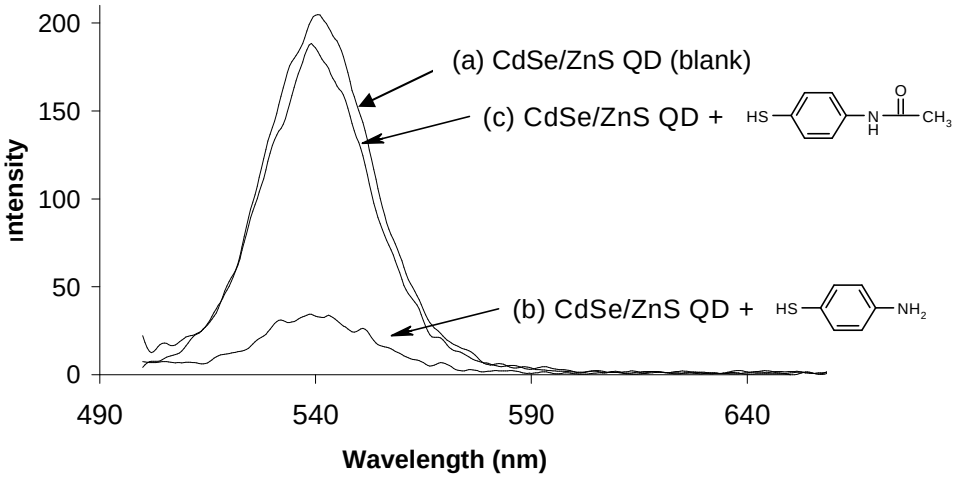

Figure 5.1 *(a) Emission spectrum of CdSe/ZnS QDs, (b) emission spectrum of CdSe/ZnS QDs after addition of 0.05 mM 4-aminothiophenol and (c) emission spectrum of CdSe/ZnS QDs after the addition of 0.05 mM 4-acetamidothiophenol. All spectra were recorded in toluene [sensor] = 2.1 x 10^{-8} M, λ_{ex} = 370 nm).*

5.3 Anion Sensing

The sensing and quantitative determination of inorganic anions such as fluoride, chloride and phosphate is of considerable current interest[62, 174, 175]. The agricultural and industrial sectors are producing vast quantities of materials containing these anions, whether it is fertilisers or raw materials

for the chemical industry and this has a knock-on effect for the environment. The physiological significance of anion sensing is well documented in the literature and the monitoring of these substrates can be of critical importance. In haemodialysis patients, high levels of arterial acetate can develop leading to cardiovascular instability and dialysis problems[176]. Therefore, acetate recognition is an area of particular interest. Other anions like fluoride is well known for its role in the prevention of dental caries[177] and as a treatment for osteoporosis[178]. As a result there is a need for the development of highly selective and sensitive sensors for anions. The attractiveness of anion sensing monitored by fluorescence spectroscopy lies in the fact that the method is highly sensitive, very adaptable and relatively inexpensive. There are many challenges associated with anion sensing that have hampered and discouraged its progress. The fact that anions are larger than isoelectronic cations and as a result have a lower charge-to-radius ratio means they form less effective electrostatic binding with receptors[179, 180]. Anions are also likely to be present in a delocalised form and pH can be an issue due to solvation, meaning detecting them in aqueous environments can be problematic. Competition with certain solvents (i.e. DMSO) can also contribute to recognition difficulties and cause irreproducibility of results.

A common approach in the fluorescent detection of anions is to employ charge neutral PET sensors with thiourea and urea functionality[62, 63, 108, 175, 181-183]. Recognition of anions is achieved through hydrogen bonding of the receptor with the substrate and this is communicated to the fluorophore by a change in the rate of PET between the two. Thioureas are stronger hydrogen bond donors with respect to ureas due to their more acidic nature (pKa = 21.0 and 26.9, respectively in DMSO)[184]. It is therefore expected that they will bind more strongly to anions and form complexes with greater stability. Substituents on the (thio)urea receptors can influence the acidity of the N-H bonds and in turn can tune the sensitivity of the sensor. For example, an electron withdrawing group such as CF_3 can increase the acidity of the thio(urea) protons and make them stronger hydrogen bond acceptors.

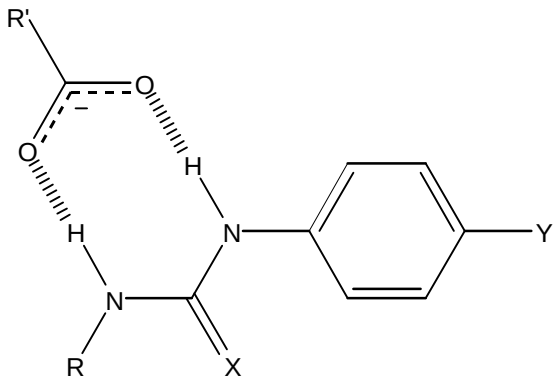

X = S or O
Y = CF_3 or H

Figure 5.2 *Hydrogen bonding of a receptor with anion substrate. When Y = CF_3, the acidity of the (thio)urea protons increases altering its selectivity and sensitivity.*

Gunnlaugsson *et al* have developed a number of anion sensors based on the thiourea motif[61-63, 108, 175]. In one report, with the aim of demonstrating PET sensing, several charge neutral aliphatic and aromatic thiourea receptors were prepared from isothiocyanates, with the organic dye anthracene used as the fluorescent signalling unit[108]. Quenching of these probes was observed with F^-, AcO^- and $H_2PO_4^-$ with Cl^- and Br^- showing no effect. A chiral PET sensor **31** was also synthesised that showed selectivity towards *N*-acetyl protected amino acids. No significant enantioselectivity was achieved but the potential of this type of detection was established from these studies thus meriting more attention.

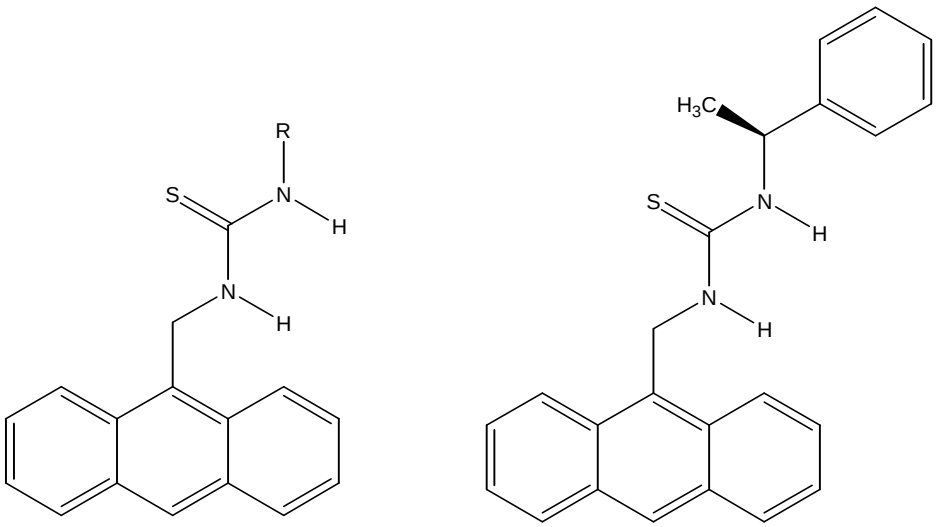

R = CH_3 or $PhCF_3$

(30) **(31)**

Figure 5.3 *Examples of thiourea based anion PET sensors. Sensor* ***31*** *is a chiral probe designed for the enantioselective detection of carboxylates such as N-acetyl protected amino acids*[108]*.*

In another report, naphthalimide replaced anthracene as the fluorophore due to its lower background autofluorescence and light scattering tendencies[185]. It also emits in the visible region at longer wavelengths (λ_{max} ~ 540-550 nm) and with higher quantum yields. A further improvement to the sensor saw a second aromatic unit integrated into the design which further tuned its anion recognition[185]. Similar selectivity was achieved for this probe with the added feature of colorimetric detection with the naked eye.

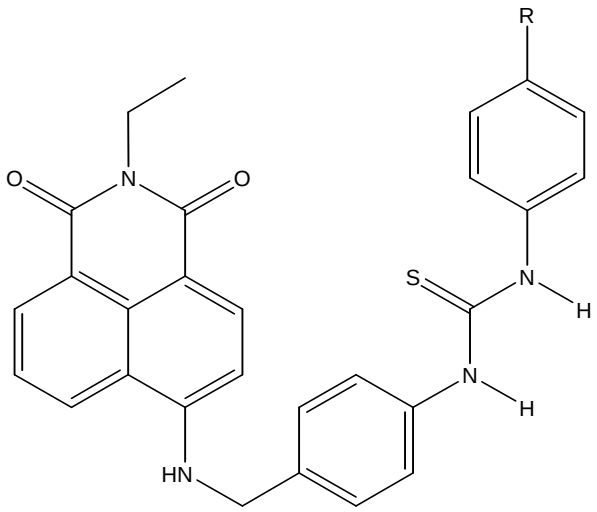

R = H or CF_3

(32)

Figure 5.4 *Anion PET sensor with naphthalimide fluorophore. A second aromatic ring is incorporated into the design further tuning selectivity*[185]*.*

Anion sensing with quantum dots is a relatively unexplored field and only a few examples exist[186-188]. Recently, Li *et al* reported iodide recognition using a thiourea receptor anchored to a CdSe QD via a 4-substituted pyridine type ligand (PyTU)[140]. The design of the sensor relies on a three pronged approach. Firstly, the thioureas can align parallel with each other and the 4 N-H protons can form a complex with the anion. Secondly, iodide being a large ion can be encapsulated within the flexible PyTU ligand. Thirdly, the pyridine end group allows the anchoring of the receptor onto the QD surface.

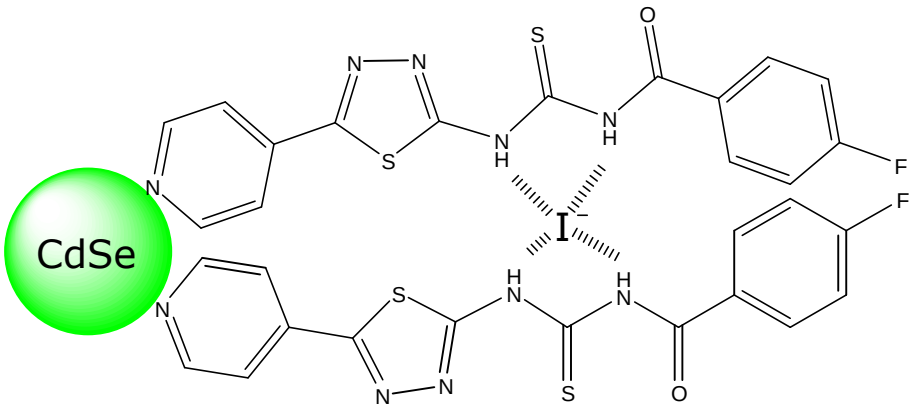

(33)

Figure 5.5 *QD probe selective for iodide ions. Encapsulation and complexing of the large iodide anion within the thiourea moiety and flexible ligands*[140]*.*

A number of mechanisms for the quenching of fluorescence were proposed by the authors. It is believed that the introduction of iodide may disrupt the hydrogen bonding that exists between the PyTU ligands and cause a destabilisation of the QDs that results in a modulation of the fluorescence. It was also suggested that due to the large surface-to-volume ratio of the QDs there may be some adherence of iodide to the surface of the nanoparticles as has been observed before with the negatively charged cyanide ion on films of CdSe QDs[189]. The preference for iodide was attributed to the size of the cavity formed between the H-bonds of the two PyTU ligands which is more complimentary to the size of the iodide ion.

Anion recognition by photo-activated CdSe QDs is described by Sanz-Medel and co-workers[190]. They report that when mercaptoethane sulfonate (MES) modified CdSe QDs were exposed to sunlight for 24 hrs, they were photoactivated and exhibited an order of magnitude increase in emission intensity with a slight blue shift in wavelength. This activation caused a change and reconstruction of the surface atoms on the QD and recognition studies with a number of common anions showed it to be very selective for cyanide.

As described in section 5.2, it was possible to alter QD emission by changing the chemistry of the receptor. As PET sensing is a modular concept defined by a fluorophore-spacer-receptor structural motif, the aim of this section was to determine if PET active receptors with proven selectivity could be anchored to a QD to produce a QD-spacer-receptor conjugate with a retention in selectivity. Thus, a modular approach will be adopted. Gunnlaugsson's thiourea anion receptor present in **34** (figure 5.6b) was adapted to permit anchorage to the QD surface, and the effect of anions on the emission intensity of the resulting conjugate were examined.

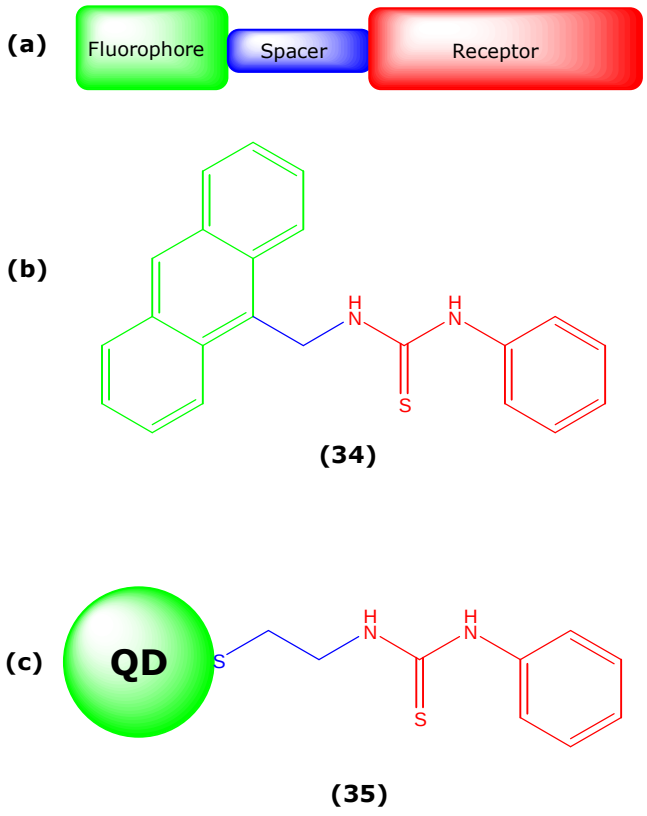

Figure 5.6 *(a) fluorophore-spacer-receptor format of a typical PET sensor. (b) PET anion sensor* ***34*** *designed by Gunnlaugsson et al, comprising a thiourea receptor. (c) Analogous QD based sensor* ***35****.*

5.4 Synthesis of receptor 38 and QD-conjugate 39

The receptor, 1-(2-mercapto-ethyl)-3-phenyl-thiourea **38** was synthesized in one step by reaction of phenylisothiocyanate and 2-aminoethanethiol in chloroform as described in section 2.2.1.4. Ligand exchange of the parent TOP/TOPO ligands with the synthesised thiourea receptor was achieved following a procedure outlined in section 2.2.4.1. Surface functionalisation was confirmed by ^{1}H NMR spectroscopy, figure 5.8 showing spectra of the free QD and the QD-receptor conjugate. As

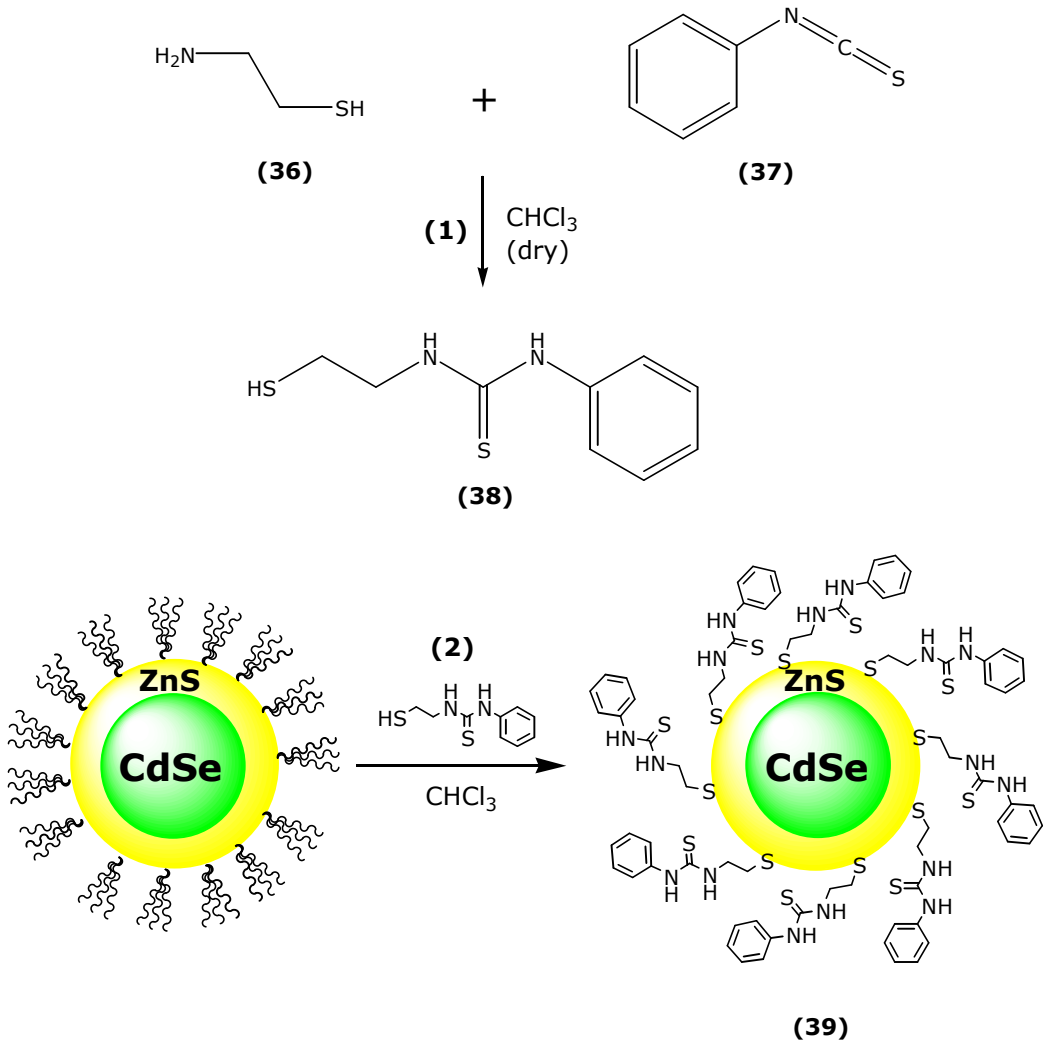

Scheme 5.1 *Synthesis of QD receptor conjugate. (1) chloroform (dry) room temperature, 18 hrs (2) ligand exchange of TOP/TOPO with receptor, chloroform, 24 hrs reflux (3) QD-receptor conjugate* ***39****.*

observed by Landi *et al*,[191] the addition of the receptor did not displace all the ligands on the surface of the QD with shifts at 0.8 and 1.2 ppm again representing the methyl and methylene protons respectively of trioctylphosphine oxide (TOPO)[82]. However, the magnitude of these resonances are significantly reduced in the spectrum of **39** compared to the parent QDs. Even when the loading ratio was increased (i.e. more ligand with respect to QD) a similar spectrum was obtained, suggesting complete exchange of the QD with receptor **38** was not possible. Clearly evident though are the thiourea protons, CH_2-N<u>H</u> and Ar-N<u>H</u> at 6.4 and 7.7 ppm respectively with the signals at 2.9 and 3.9 ppm representing the methylene protons for S-<u>CH_2</u> and N-<u>CH_2</u> respectively of the spacer. Again, there was no significant change in the position of these resonances when compared to the receptor alone. A similar effect was observed in section 4.4.2 for the ATP sensor **28**. This initially led to the belief that the receptor had not anchored to the QD surface. However, if this was the case then after the repeated precipitations and centrifugations conducted during the work-up all the free ligand should have been removed and therefore should not have shown up in the NMR spectrum of **38**. In addition, the precipitate isolated after the ligand exchange reaction was fluorescent when dissolved in $CHCl_3$ illustrating the precipitate contained the QD. The possibility of the receptor oxidising to the disulfide was also considered. However, even when receptor **38** was treated with $NaBH_4$, a similar NMR spectrum after exchange was observed. Furthermore, Raymo's group have shown that disulfides adsorb onto the surface of QDs[121]. They showed that dithiolane ligands (such as that shown in figure 5.7) exchange on to the surface of CdSe/ZnS QDs even without being reduced to their corresponding thiols. Therefore, it can be concluded that the methylene protons of cysteamine based ligands do not exhibit significant changes in terms of chemical shift when adsorbed onto a QD surface.

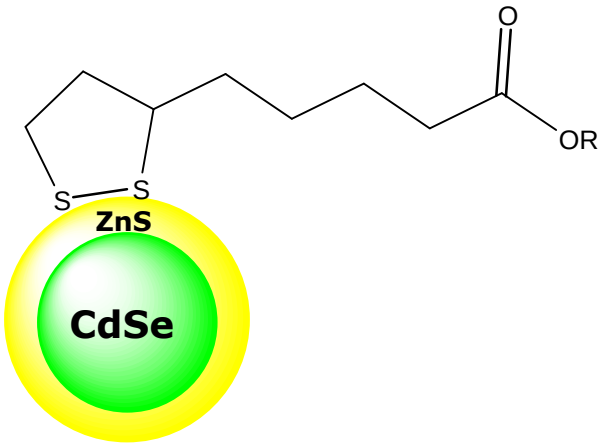

(40)

Figure 5.7 *Raymo's CdSe/ZnS QDs appended with a dithiolane anchor. (R = polymeric ligand with polyethylene glycol (PEG) backbone)*[121].

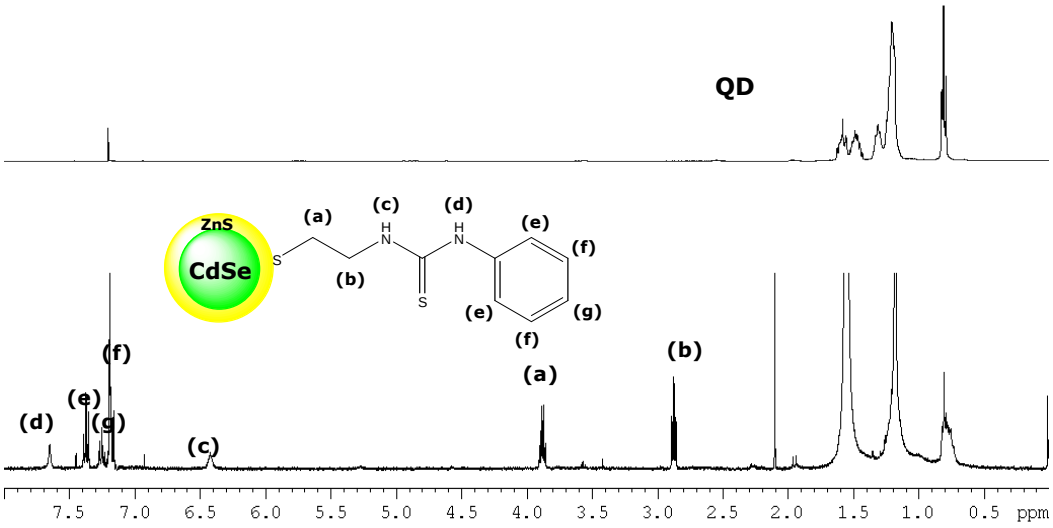

Figure 5.8 *Stacked ^{1}H NMR spectra of top: CdSe/ZnS QDs recorded in $CDCl_3$ and bottom:* ***39*** *recorded in $CDCl_3$.*

5.4.1 Photophysical properties of 39

UV-Vis absorption analysis before and after surface functionalization (Figure 5.8) showed no difference in the visible region, the position of the 1st exciton peak being unchanged at λ_{max} = 516 nm. When the optical density was fixed at 0.1 for both samples at this wavelength a difference was observed at ~ 300 nm with the absorbance of the QD-receptor

conjugate greater (2.9) than the QD alone (1.4). The increase in absorbance at this wavelength was due to absorbance by the phenyl chromophore (λ_{max} = 264) of the receptor component.

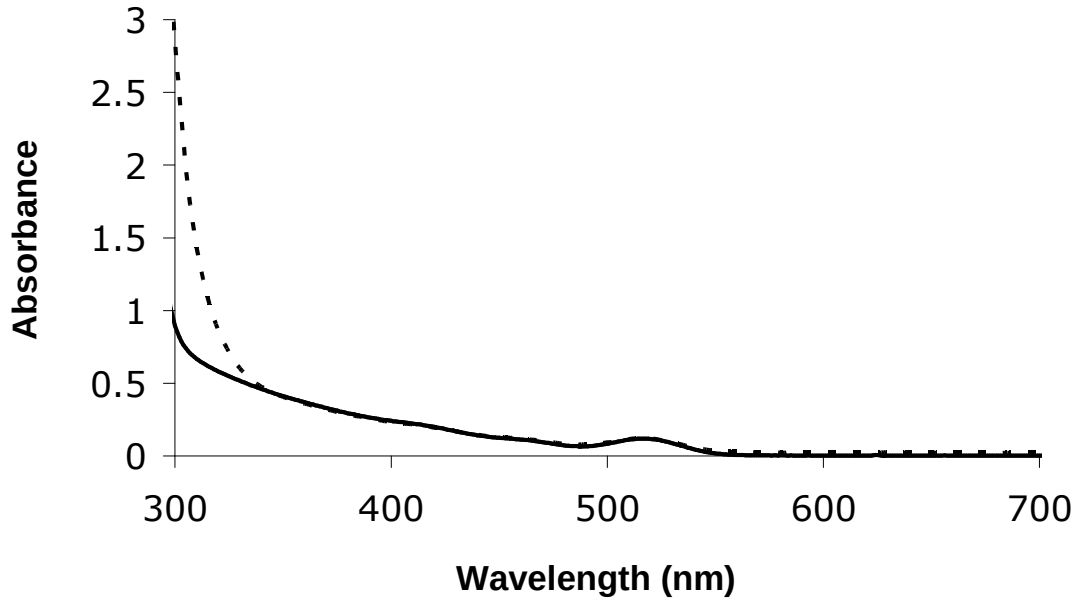

Figure 5.9 *UV trace of parent CdSe/ZnS QDs (—) and **39** (---). [**39**] and [QD-TOPO] = 1.8 x 10^{-6} M.*

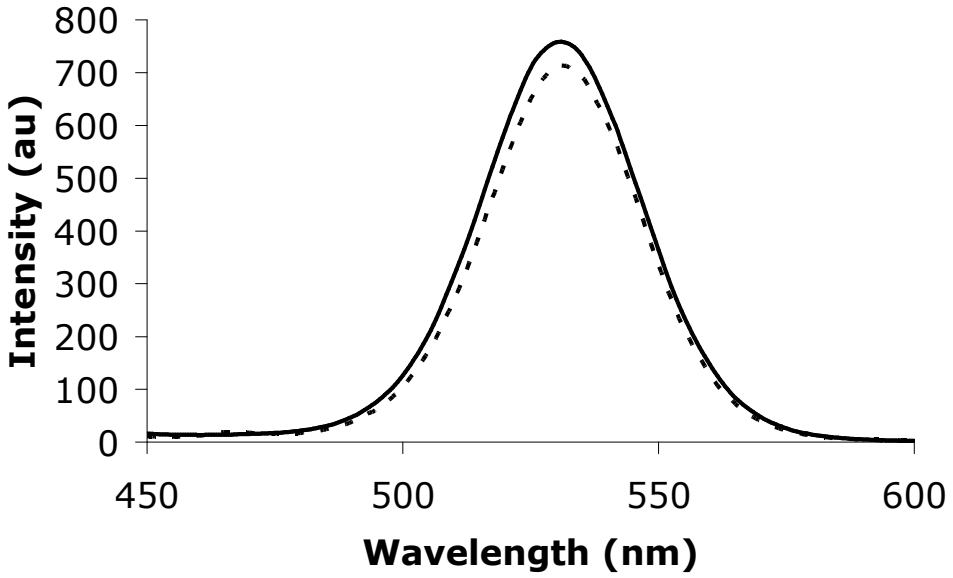

Figure 5.10 *Emission spectra of parent CdSe/ZnS QDs (—) and **39** (---). [Parent CdSe/ZnS QDs], [**39**] = 1.8 x 10^{-7} M. Solvent = $CHCl_3$.*

This is further evidence that the receptor was effectively exchanged onto the QD surface. However, an attempt to accurately determine the number of surface ligands attached per nanoparticle by UV proved unsuccessful. From the UV-vis spectrum a size of 2.54 nm was calculated for **39** using equation 3.1. As expected, the size didn't differ greatly from the parent QDs as this method for size determination only accounts for the core size.

Excitation of **39** at 370 nm resulted in emission at 540 nm, with little change in the profile compared to the parent QD (see Figure 5.10), although the quantum yield (Φ) did drop from 0.38 to 0.33. This suggests a small degree of PET quenching even in the absence of anions, as observed by Gunnlaugsson *et al* for the anthracene based sensor **34**. However, the position and profile of the emission peak was comparable to the parent QDs with a FWHM of 37 nm determined for **39**.

5.4.2 Selectivity of 39 for common monovalent anions

The probe was screened for selectivity against the tetrabutylammonium salts of AcO^-, F^-, Cl^-, Br^- and HSO_4^- in chloroform. The emission spectra for each of the anions tested are presented in figure 5.11. Significant quenches of the QD fluorescent intensity at 540 nm were observed upon addition of F^-, Cl^- and AcO^-, with only minor changes observed for $H_2SO_4^-$ and Br^-. In addition, there was no evidence of any significant change in the position of the emission maximum upon addition of Cl^- and AcO^-. However, at higher concentrations of F^- a distinct red-shift was observed. This suggests some interaction between F^- and the QD surface at higher concentrations. A plot of relative intensity against –log anion concentration was made for F^-, Cl^- and AcO^- and are shown in figure 5.12. Again, due to the inability to accurately determine the number of surface ligands present on the surface of each QD, the binding stoichiometry could not be accurately determined. However, the quenching profile observed for AcO^- and F^- occurred over approximately two log unit suggesting a 1:1 binding interaction between **39** and these analytes[108]. Using equation 4.1, a binding constant log β of 1.94 and 2.15 was determined for AcO^- and F^- respectively. In contrast, a more distinct quenching profile was observed for Cl^-, with quenching occurring over

about one log unit. The results observed here compare favourably with those observed by Gunnlaugsson *et al* for similar experiments conducted with **34**. They observed significant quenches with F^- and AcO^- but only minor quenches for Cl^-, Br^- and HSO_4^-. Similarly, the calculated binding constants were in a similar range with 2.90 observed for F^- and 2.15 observed for AcO^-. The slight reduction in sensitivity observed for **39** may be due to an extra methylene unit in the spacer (which was included for synthetic convenience) reducing the effectiveness of PET, as PET efficiency has previously been shown to be distance dependent[167].The only major discrepancy in the results observed between **34** and **39** is the selectivity observed for Cl^-. This effect is difficult to explain but may be due to a co-operative binding effect between adjacent receptors on the QD surface when binding Cl^-, which is not possible for free receptors in solution, i.e. **34**. Similar effects have been observed for a Schiff base functionalised QD discussed in chapter 6. In addition, polysiloxanes with appended thioureas have produced different binding profiles when compared to the monomer alone[192], suggesting co-operative binding may be occurring between adjacent thiourea residues. Due to the inorganic nature and size of the QD core, obtaining single crystals is obviously not possible.

The reason for the quenching of the QD fluorescence upon addition of F^-, Cl^- and AcO^- can be explained as follows: in aprotic solvent such as $CHCl_3$, these ions form strong H-bonds with the thiourea receptor resulting in an increase in its reduction potential and a concomitant increase in the rate of PET between receptor and excited QD[108, 193]. Therefore, the anion binding event is signaled by a decrease in emission intensity. A similar phenomenon has been reported by Gunnlaugsson for **34** and other similarly constructed sensors. The selectivity of the receptor for F^- and Cl^- over Br^- can be related the higher charge density of these ions enabling them to form stronger hydrogen bonds with the receptor, although steric reasons may also play a part. Steric factors may also explain the selectivity for acetate over hydrogen sulfate, with the former able to form stronger linear hydrogen bonds[108].

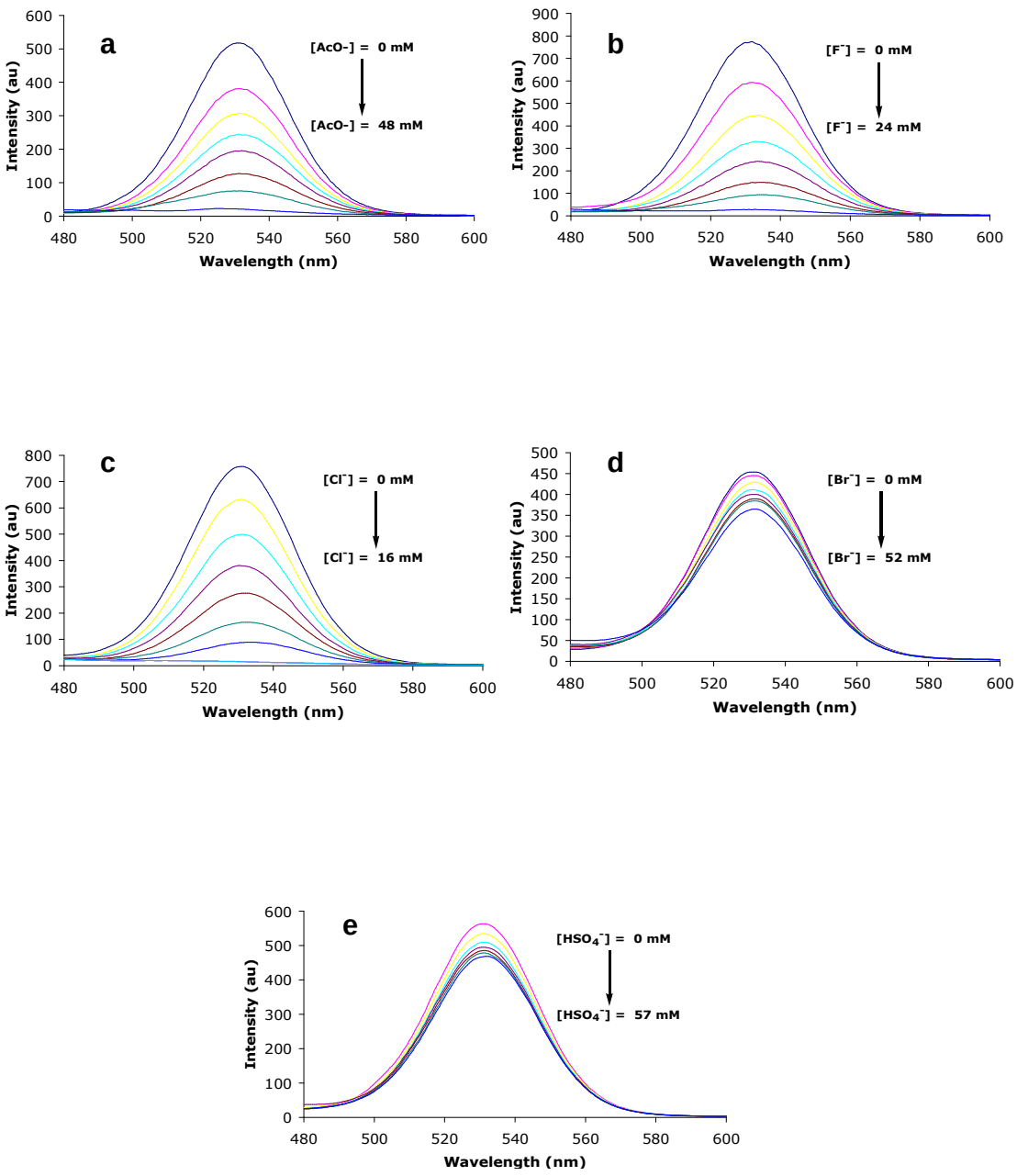

Figure 5.11 *Emission spectra for **39** titrated with monovalent anions. (a) acetate (b) fluoride (c) chloride (d) bromide (e) hydrogen sulfate. All titrations conducted in spectrograde chloroform. [**39**] = 7.96 x 10^{-9} M.*

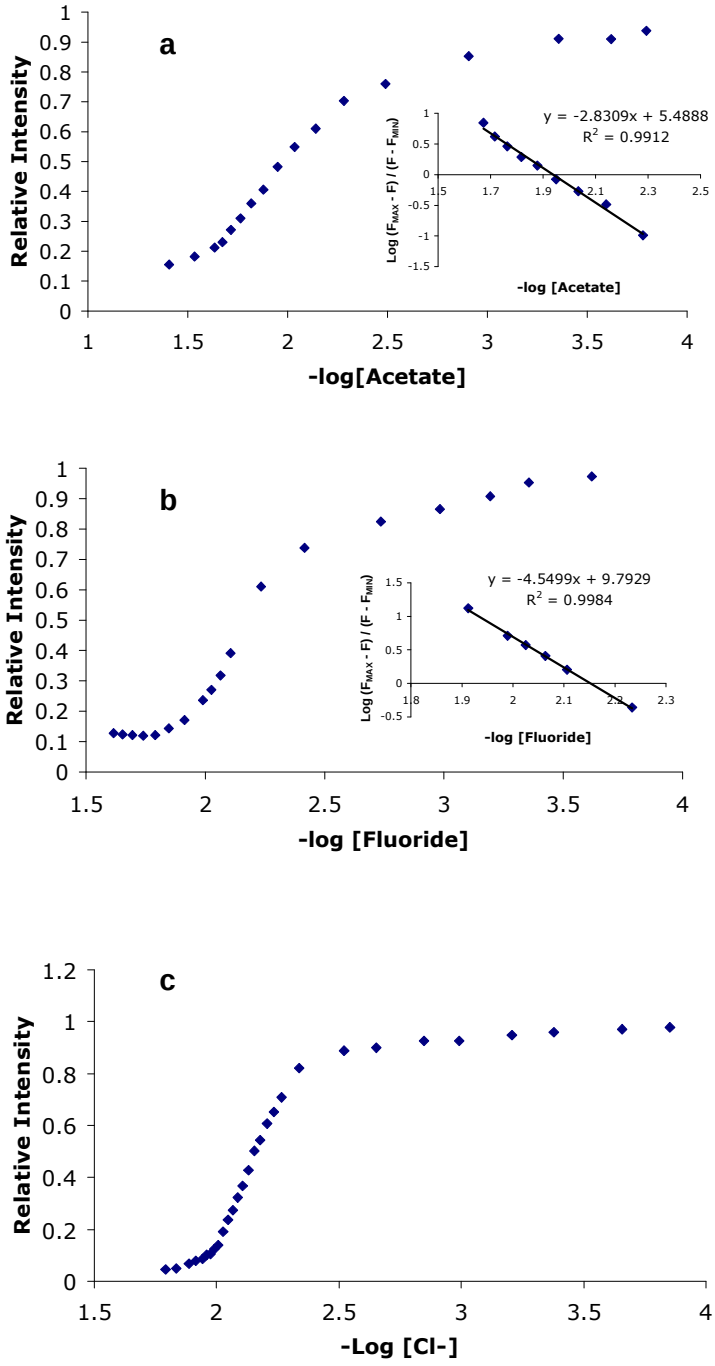

Figure 5.12 *Plot of relative fluorescence intensity versus –log [anion]. Inset: plot of* log $[F_{MAX} - F] / [F - F_{MIN}]$ *against –log [anion] for* ***39*** *with anions. Where (a) = acetate (b) = fluoride and (c) = chloride. All titrations conducted in spectrograde chloroform.*

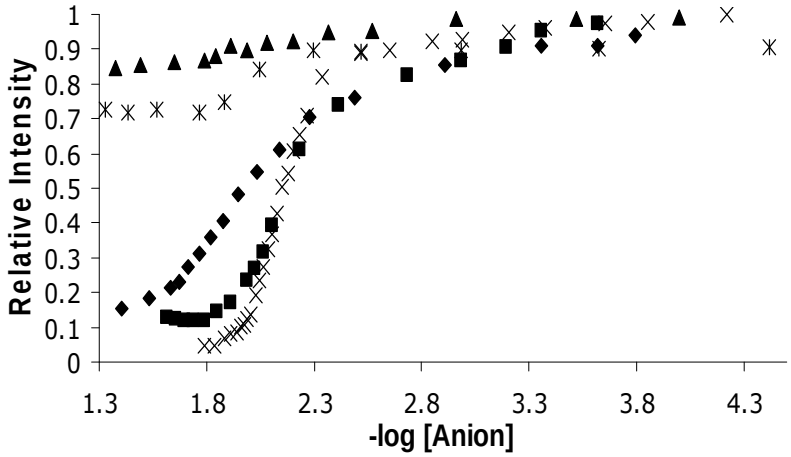

Figure 5.13 *Plot of relative intensity against –log [anion] for all ions, Br^- (▲), HSO_4^- (*), Cl^- (**X**), AcO^- (♦) and F^- (■). [**39**] = 7.96 x 10^{-9} M. All measurements conducted in $CHCl_3$.*

To confirm that an H-bonding interaction was occurring between the receptor component of **39** and F^-, Cl^- and AcO^- an NMR experiment was conducted in which a solution of tetrabutylammonium acetate in $CDCl_3$ was added to a solution of **38** in $CDCl_3$. The ^1H NMR spectrum was recorded before and after the anion addition. Anion-receptor binding was confirmed by changes in the chemical shift of the thiourea protons, with CH_2-N<u>H</u> moving downfield by 0.4 ppm to 6.8 ppm and Ar-N<u>H</u> by 0.5 to 8.1 ppm upon addition of 1 eq of AcO^- (figure 5.15). In addition, these resonances become significantly broader after anion addition while the aromatic protons and the methylene protons of the spacer (not shown) remain unaffected. This data suggests a hydrogen bonding interaction between the acetate anion and thiourea protons of the receptor as depicted in Figure 5.14. In terms of the model described by Gunnlaugsson for **34**, the quenching effect by Cl^-, F^-, and AcO^- is a result of this hydrogen bonding interaction and leads to an increase in the reduction potential of the receptor, enhancing the rate of PET from the HOMO of the receptor to the QD[63, 108, 194].

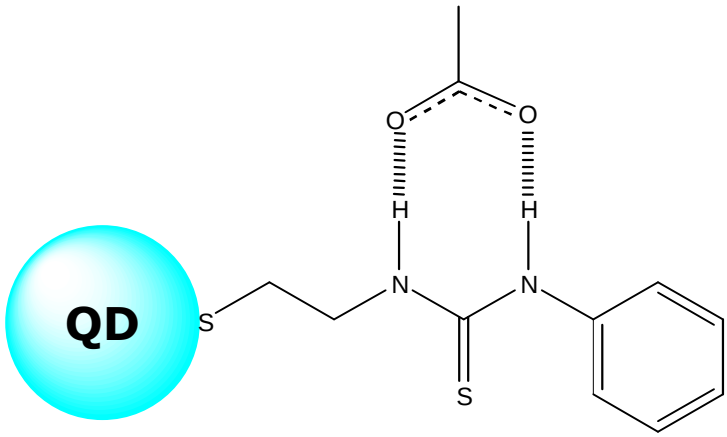

Figure 5.14 *Hydrogen bonding interaction of acetate with* ***39****.*

This is opposite to typical PET sensing behavior where the oxidation potential of the receptor is raised upon analyte recognition, thus removing the thermodynamic driving force for PET and fluorescence is "Switched On"[49153, 195-198].

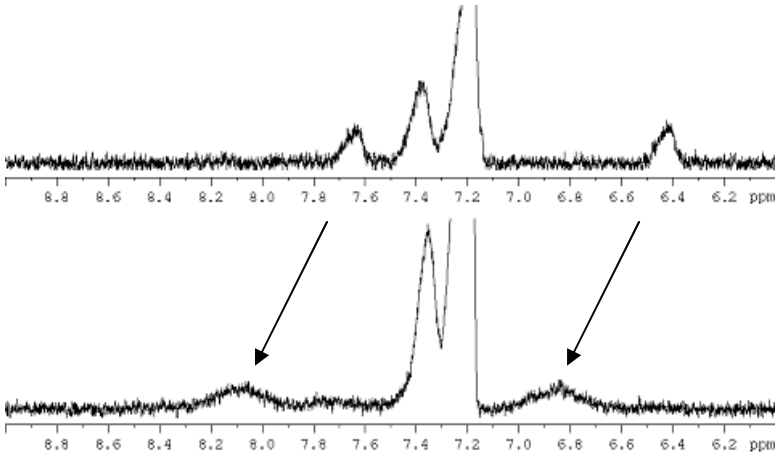

Figure 5.15 *Expansion of the receptor region showing free receptor* ***38*** *(top) and after the addition of 1 eq of* AcO^- *(bottom). Both spectra recorded in* $CDCl_3$ *at 400 MHz.*

To prove the requirement of the receptor for quenching upon addition of AcO^-, F^- and Cl^- a titration was performed in which AcO^- was

added to a solution of the parent QDs alone, i.e. no receptor attached. The results are shown in figure 5.17 where relative intensity is plotted against –log[anion] and is presented alongside the results of **39** with AcO^- for comparison. A minor reduction in relative intensity was observed for the parent QDs upon increasing AcO^- addition, attributed to a dilution effect but there was no evidence of a defined binding event. In contrast, the addition of AcO^- to **39** shows approximately 60% greater decrease in relative intensity over the same concentration range. This control experiment confirms the requirement of the urea receptor for efficient QD quenching.

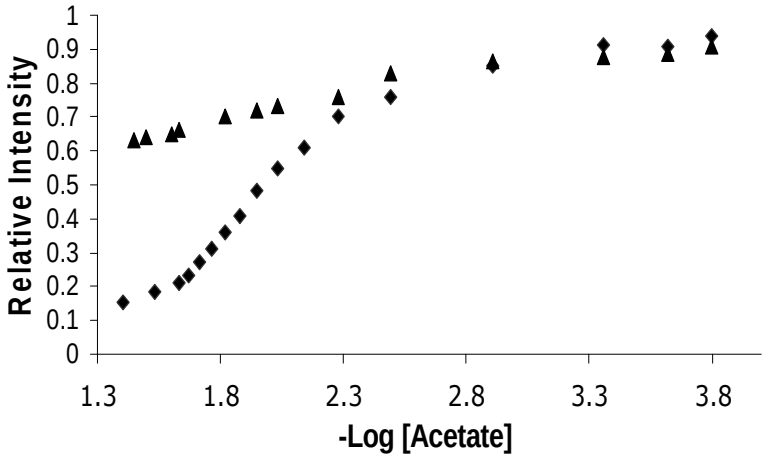

Figure 5.16 Plot of relative intensity against –log [acetate] for as received QDs (▲) and **39** (♦). [QD] = 5.45 x 10^{-9} M. [**39**] = 7.96 x 10^{-9} M.

Table 5.1 *Photophysical properties for* ***39*** *before and after the addition of anions. (a) Quantum yield calculated with reference to fluorescein. (b) % reduction in fluorescence spectral area. (c) Binding constant calculated from a plot of –log (F_{MAX}-F) / (F-F_{MIN}) against –log [anion].*

Sensor	Φ_F[a]	%F_{red}[b]	Log β[c]
39	0.334	-	-
F^-	0.042	87.3	2.15
Cl^-	0.015	95.4	-
Br^-	0.281	15.7	-
AcO^-	0.037	88.9	1.94
HSO_4^-	0.268	19.8	-

5.5 Conclusions

CdSe/ZnS QDs purchased from Evident technologies were modified with 1-(2-mercapto-ethyl)-3-phenyl-thiourea (**38**). The resulting QD probe (**39**) was very soluble in $CHCl_3$ and strongly luminescent with a quantum yield of 33%, marginally lower than the parent QDs. Characterisation of the probe was performed using ^{1}H NMR, UV-vis and fluorescence. The spectral characteristics were well defined, with a 1st exciton peak present at 516 nm and a narrow emission peak centred at 540 nm with FWHM of 37 nm.

The probe was screened against common monovalent anions and was shown by fluorescence to be selective for AcO^-, F^- and Cl^-. Binding of the anions by the thiourea protons through hydrogen bonding resulted in an increase in the reduction potential with a concomitant increase in the rate of PET between the receptor and the QD.

The combined results presented above illustrate that tried and tested organic receptors with proven selectivity may be adapted for anchorage to the surface of preformed QDs to produce conjugates with similar selectivity / sensitivity profiles to the all-organic probes. These new sensors may, however, benefit from the improved optical properties the QDs offer.

5.6 "Off – On" QD sensor for fluoride

The previous results illustrate that receptors with proven PET activity when part of all-organic systems are also effective in QD based systems. In section 5.4 an "on – off" sensor for anions was developed. This section details the design, synthesis and photophysical evaluation of a ferrocene based "off – on" QD sensor for fluoride.

The ability of ferrocene based compounds to quench the excited state of QDs has been demonstrated by Palaniappan *et al*.[199] They prepared CdS and CdSe QDs decorated with perthiolated cyclodextrin units (**43**) (see figure 5.17). They then added ferrocene methylamine to the solution containing the QDs and the QD fluorescence was quenched by 95%. Upon addition of adamantane carboxylic acid the original fluorescence intensity was recovered. The initial quenching of intensity upon addition of ferrocene was due to it being encapsulated in the cyclodextrin cavity, which brought it close enough to the QD surface to engage in electron transfer and quench QD fluorescence. The subsequent addition of adamantane, which being a better fit for the cyclodextrin cavity than ferrocene, ejected the ferrocene into the bulk solution meaning it was no longer close enough to the QD to engage in electron transfer. Therefore, the ability of QD fluorescence to be switched "off" by ferrocene and back "on" by its removal means incorporation of ferrocene into the design of analyte specific organic receptors may be an appropriate method to develop "off – on" fluorescent QD sensors.

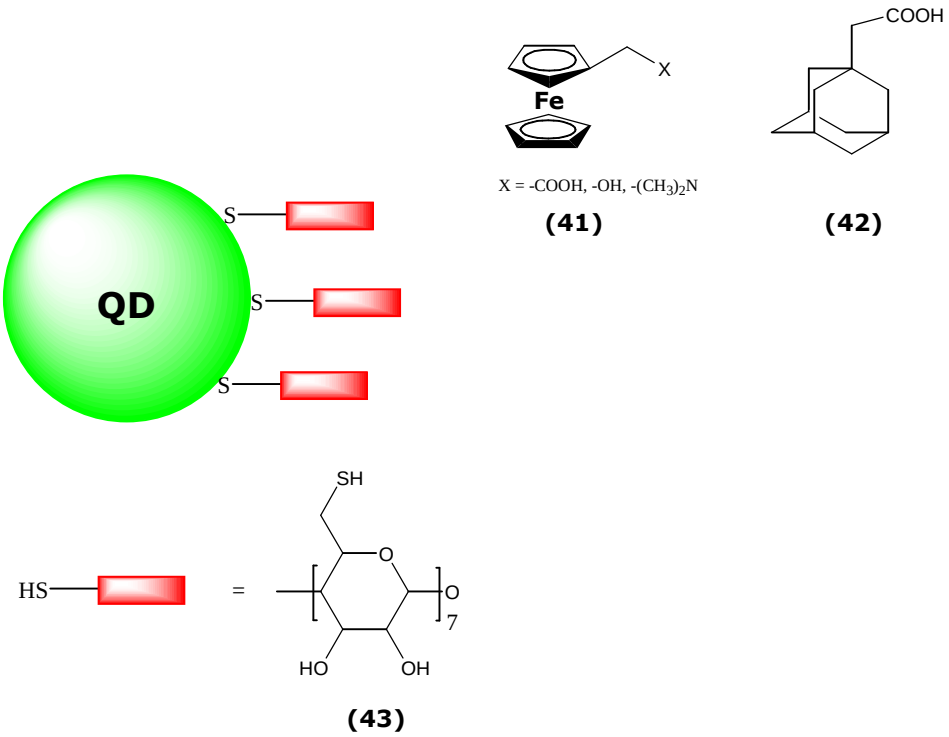

Figure 5.17 *Palaniappan's perthiolated β-cyclodextrin-modified QDs. Also shown are the competing species: substituted ferrocene compound (**41**) and adamantine carboxylic acid (**42**)*[199].

It has also been demonstrated by Beer and colleagues that amperometric anion sensing can be achieved through perturbation of the ferrocene/ferrocenium redox couple[200, 201]. They have demonstrated using a lower-rim ferrocenyl substituted calixarene that upon addition of $H_2PO_4^-$ a sizable cathodic shift of 160 mV was observed in the cyclic voltammogram. In another study using mono and bis-substituted ferrocene ureas they showed by electrochemical means selectivity for $H_2PO_4^-$, Cl^- and AcO^-.[202] In addition, ^1H NMR studies revealed significant downfield shifts of the N-H signals upon titration with both $H_2PO_4^-$ and Cl^- proving the interaction and binding of the anions with the urea protons. The majority of studies of anion sensing involving ferrocene based receptors utilise electrochemical detection. One notable example where both electrochemical and fluorescent detection are used within the same probe was developed by Molina and co-workers[201]. They appended a ferrocene with two urea groups both terminating at an aromatic group (e.g. naphthalene), functioning as the reporting fluorophore.

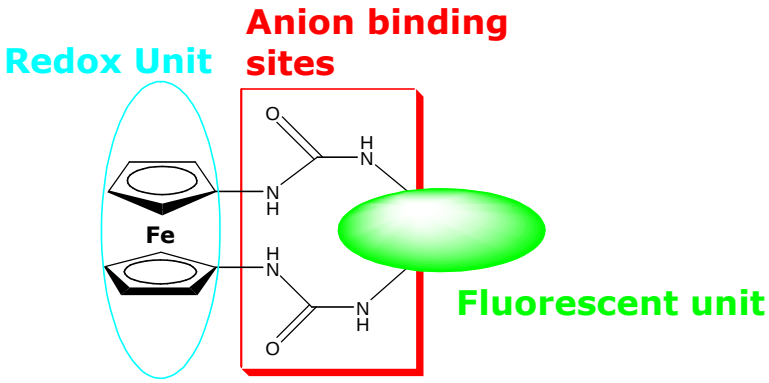

(44)

Figure 5.18 *Molina's ferrocene-based urea as a multi-signalling sensor for anions*[201].

As discussed in section 5.3, ureas are attractive for anion recognition due to the formation of strong hydrogen bonds and in the case of Molina's design, two ureas were employed resulting in the formation of an eight-membered chelate ring with the target analyte. They demonstrated that **44** displayed selectivity for F^- and also to a lesser extent for $H_2PO_4^-$. Both fluorescence and electrochemical detection were utilised with a large cathodic shift observed in the cyclic voltammogram and a substantial enhancement in the emission spectrum upon addition of F^-. Therefore, these results showed that the presence of ferrocene close to the naphthalene chromophore was sufficient to quench fluorescence, most likely by electron transfer. Addition of fluoride to the sensor resulted in an enhancement of fluorescence emission most likely due to a modulation of the electron transfer process. Unfortunately, the authors did not provide a reason for the fluorescence enhancement.

In this section ligand **51** was prepared containing a ferrocenyl urea unit similar to that developed by Pratt and Beer[202] but also containing a lipoic acid linker for anchorage to the QD surface. The resulting conjugate **53** was screened for selectivity against commonly occurring monovalent anions.

5.6.1 Synthesis of receptor 51 and QD-conjugate 53

The receptor, 1-ferrocenyl-3-[4-(1,2-dithiolan-3-yl)butyl]urea **51** was synthesised from the isocyanate **50** and ferrocenemethylamine **47**, as shown in scheme 5.2. Ferrocene carboxaldehyde **45** was first reacted with hydroxylamine to generate oxime **46** which was reduced using $LiAlH_4$ to produce ferrocenmethylamine **47**. The isocyanate was formed by first reacting lipoic acid **48** with diphenylphosphorylazide to produce azide **49** which was subjected to Curtius degradation in hot toluene to furnish the isocyanate **50**. This was then reacted with ferrocenemethyl amine to produce the urea **51** which was reduced using sodium borohydride to give the dihydrolipoic acid ferrocenyl urea **52**. This was then exchanged on to the surface of preformed CdSe/ZnS QDs (540 nm) as described in 2.2.4 to furnish the desired sensor **53**.

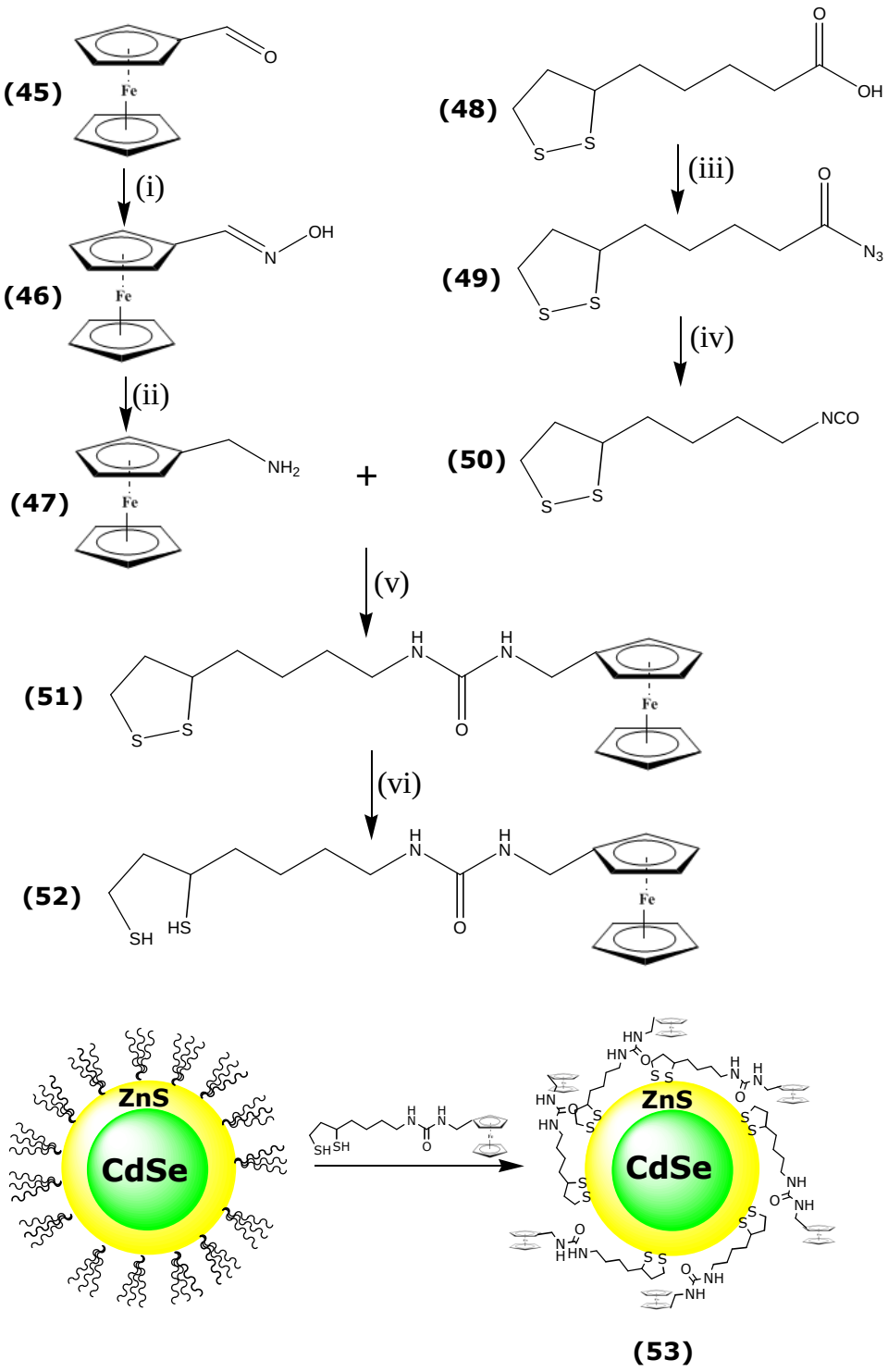

Scheme 5.2 *Synthesis of* ***53****. (i) sodium hydroxide, hydroxylamine hydrochloride, Δ, ethanol. (ii) $LiAlH_4$, Δ, anhydrous THF. (iii) triethylamine, diphenylphosphoryl azide, DMF. (iv) Δ, toluene. (v) ferrocenemethylamine, toluene (iv) sodium borohydride, THF. (v) CdSe/ZnS QDs, $CHCl_3$, tetrabutylammonium hydroxide (TBAOH).*

5.6.2 Characterisation of 53

Functionalisation of the QD surface with ligand **52** was confirmed by ^{1}H NMR spectroscopy with figure 5.19 showing the spectra of the QDs and the QD-conjugate **53**. As in the case of **39** (figure 5.8) again the methyl and methylene protons of the QD TOPO groups are evident by resonances centred at 0.8 and 1.2 ppm respectively. The appearance of the cyclopentadienyl protons at 4.15 ppm and the methylene protons adjacent to the cyclopentadienyl ring at 4.05 ppm in the spectrum of **53** confirms the attachment of ligand **52**. In addition, there was a significant reduction in the intensity of the TOP/TOPO protons after ligand exchange indicating a substantial exchange. The urea protons were not observed in the ^{1}H NMR spectrum of **53**, most likely due to the broadness of the peaks.

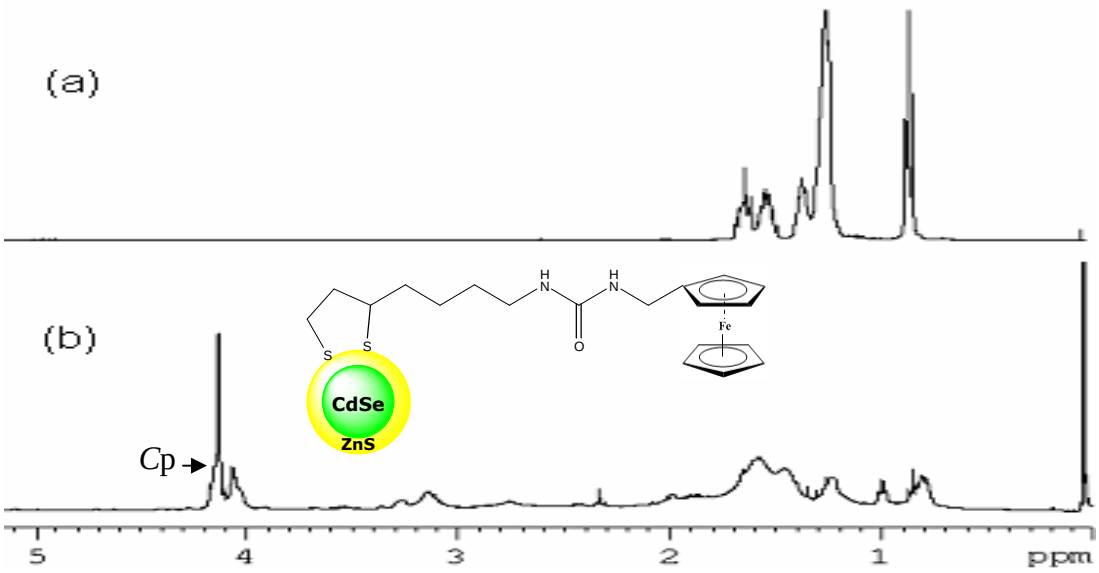

Figure 5.19 *^{1}H NMR spectra of (a) CdSe/ZnS QDs and (b) QD-ligand conjugate **53**. Both spectra recorded in $CDCl_3$. (Cp = cyclopentadienyl).*

It was initially thought that the use of tetrabutylammonium hydroxide (TBAOH) to generate the thiolate anion in the exchange reaction may cause deprotonation of the urea protons. However, both urea protons were also not apparent in the ^{1}H NMR spectrum of **52** even though the mass spectrum for this compounds confirmed its identity. Therefore, the absence of resonances for the urea protons in the spectrum of **52** and **53** may be due to the paramagnetic iron present in the ferrocene ring leading to a broadening of the peaks. In addition,

anchorage of the receptor onto the QD surface in the case of **53** may further broaden the peaks as observed in polymeric compounds where protons in or near the backbone suffer an ineffective averaging of their chemical shift anisotropies[203]. When the fluorescence spectrum of **53** was recorded after excitation at 370 nm, no QD emission was observed illustrating a complete quenching effect by the ferrocenyl ligand.

DLS spectra for QDs before and after ligand exchange are shown in figure 5.20. The average hydrodynamic diameter of **53** was found to be 8.70 nm, slightly larger than the parent QDs (8.54 nm) but significantly more mono-disperse. Again, this may be attributed to an extra precipitation step involved in the work up of **53**.

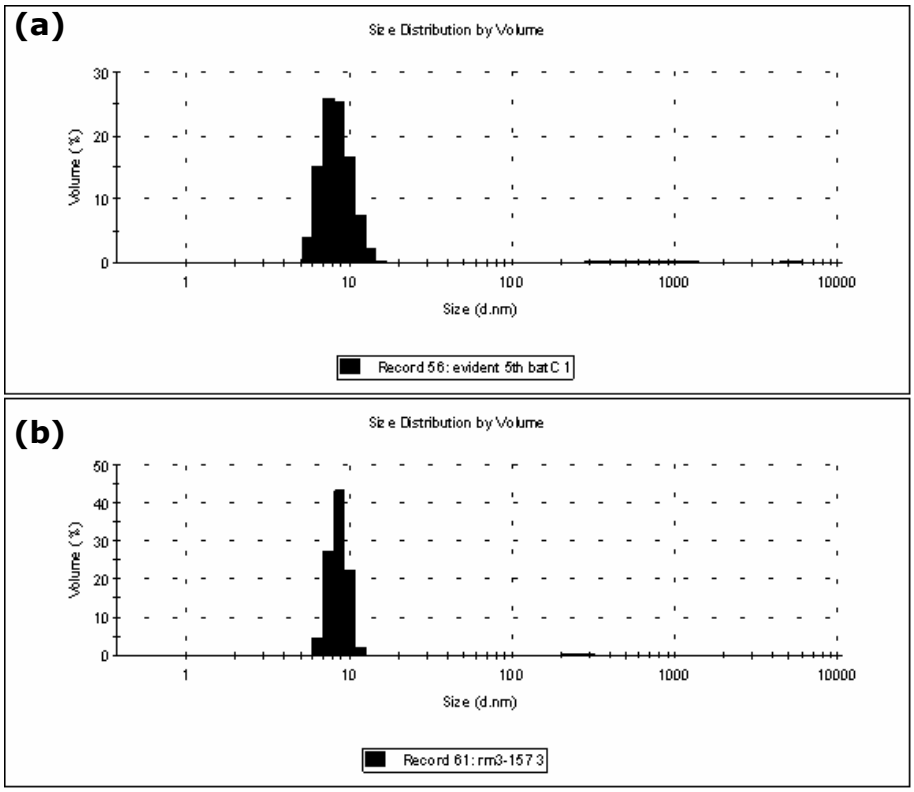

Figure 5.20 *Dynamic light scattering (DLS) histogram plot of (a) parent CdSe/ZnS QDs and (b)* ***53*** *dispersed in toluene.*

To confirm that the ferrocenyl moiety was responsible for the quenching process a control compound was prepared, similar in structure to **51** but lacking a ferrocene unit. Ligand **54** was prepared by the reaction of lipoic acid isocyanate **50** (prepared in a similar manner as in

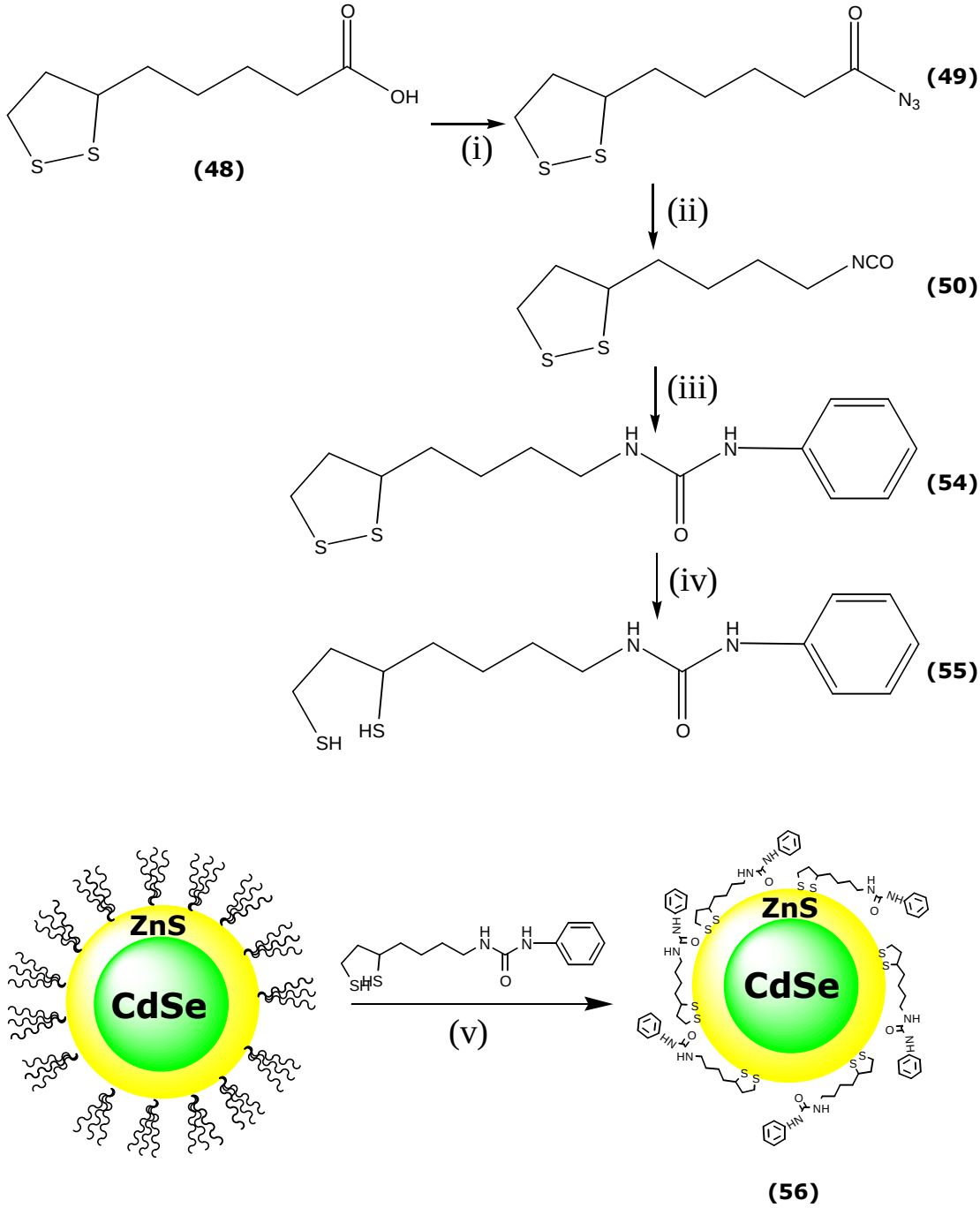

Scheme 5.3 *Synthesis of* ***56****. (i) triethylamine, diphenylphosphoryl azide, DMF. (ii) Δ, toluene. (iii) aniline, toluene (iv) sodium borohydride, THF. (v) CdSe/ZnS QDs, $CHCl_3$, tetrabutylammonium hydroxide.*

scheme 5.2) with aniline. The resulting urea was reduced with sodium borohydride and exchanged on to the QD surface as described in section

2.2.1.11. This control compound contains the same DHLA linker, a urea unit and aromatic ring and resembles ligand **51** with the exception of the ferrocene unit. Figure 5.21 shows the UV-vis and emission spectra for QD-conjugate **56** and in contrast to **53** exhibits a strong emission peak with λ_{max} at 545 nm. This suggests the lack of fluorescence observed for **53** is due to the presence of the ferrocene unit.

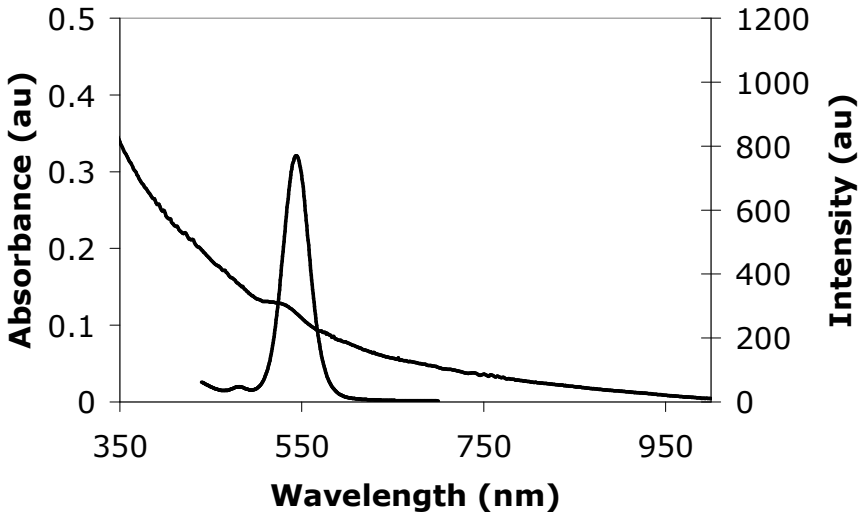

Figure 5.21 *Absorbance [1.5 x 10^{-6} M] and emission [7.6 x 10^{-9} M] profiles for* ***56****. QDs dispersed in $CHCl_3$ and excited at 420 nm.*

5.6.3 Selectivity and sensitivity of 53 against monovalent anions

The probe was screened against a number of monovalent anions to assess its selectivity. Titrations were carried out in chloroform with fluoride, acetate, hydrogen sulfate, dihydrogen phosphate, chloride, bromide and perchlorate added to solutions of **53** as their tetrabutylammonium salts (figure 5.22). Figure 5.23 shows the results of these titrations as a plot of fluorescence intensity against concentration. A substantial fluorescence enhancement (~25 fold) was observed upon addition of fluoride (0.2 M) which was significantly greater than for any of the other anions tested. Only acetate and dihydrogen phosphate produced fluorescence enhancements of any significance but of somewhat lesser magnitude (~5 fold) than for fluoride at the same concentration. However, virtually no enhancement in fluorescence was observed for hydrogen sulfate, chloride, bromide and perchlorate.

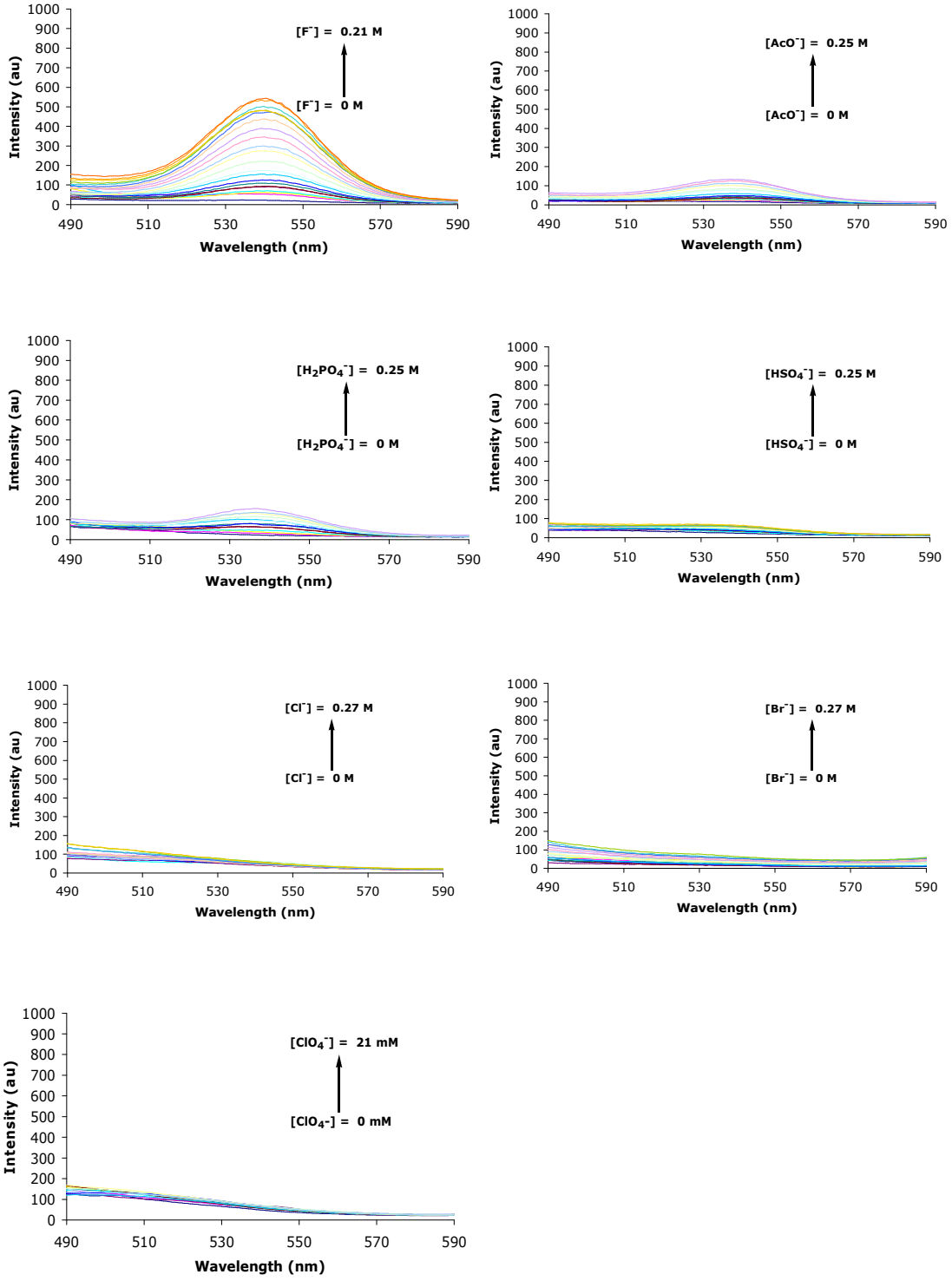

Figure 5.22 *Emission spectra of* ***53*** *titrated with various anions. [****53****] = 8 x* 10^{-9} *M. All measurements conducted in spectrograde* $CHCl_3$.

This highlights that **53** has good selectivity for fluoride over other commonly occurring monovalent anions. Again, it was not possible to determine the stoichiometry of the complex formed between **53** and fluoride and therefore a binding constant could not be determined. By plotting the relative intensity of **53** against concentration of F^-, good linearity was observed in the range 0.3 – 5.6 mM F^- (figure 5.25).

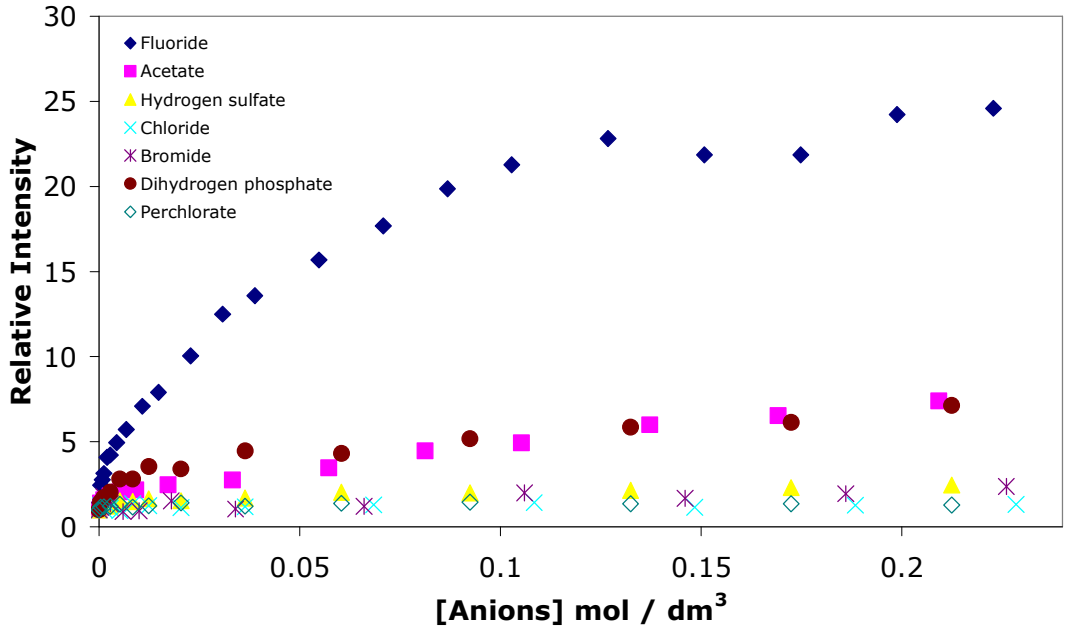

Figure 5.23 *Plot of relative intensity against [anion] for Br^- (*), HSO_4^- (▲), $H_2PO_4^-$ (●), Cl^- (X), AcO^- (■) and F^- (♦). [**53**] = 8 x 10^{-9} M. All measurements conducted in spectrograde $CHCl_3$.*

The fluorescence response upon the addition of fluoride to **53** was so significant that it could be detected with the naked eye. Figure 5.24 shows a photograph of **53** before and after the addition of fluoride and reveals a switching "on" of the green QD fluorescence upon F^- addition.

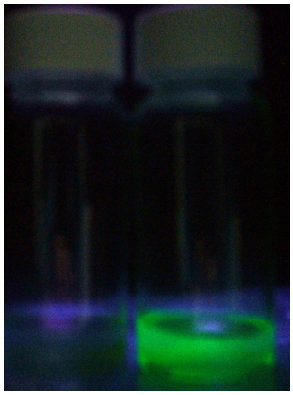

OFF ON

Figure 5.24 *Photograph of the QD probe in the "off" and "on" state. On the left is* ***53*** *dispersed in chloroform with no fluoride added. The vial on the right shows the dramatic effect on addition of fluoride with the probe emitting fluorescence demonstrating the "off" to "on" effect.*

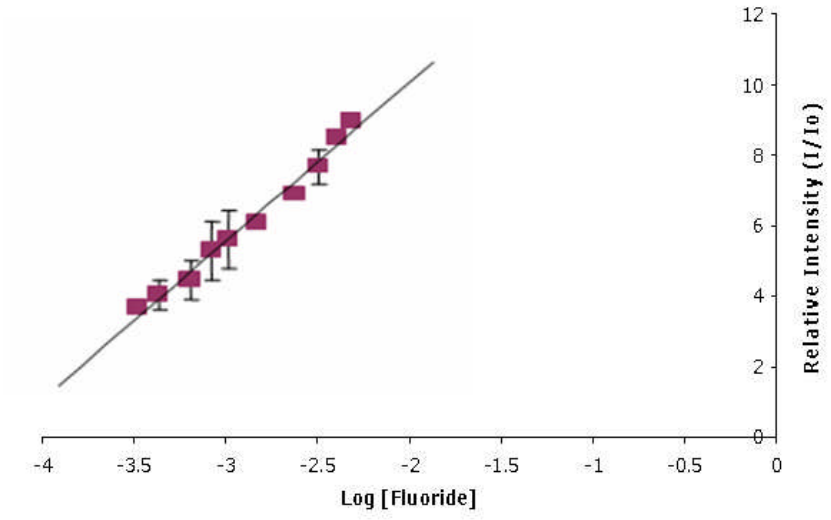

Figure 5.25 Plot of relative intensity (I/Io) of **53** against log [fluoride].

As mentioned previously, Pratt and Beer have shown using electrochemical means that H_2PO4^- , Cl^- and AcO^- bind to the urea of **57** resulting in a significant cathodic shift. The binding unit of this compound is identical to the binding unit present in **53**. The difference in selectivity for **53** which was selective for F^-, is attributed to a co-operative binding between adjacent urea receptors on the nanoparticle surface. Molina's **44**, which contained two urea receptors in close proximity within the same molecule also displayed selectivity for F^- by changes in the cyclic

voltammogram and emission spectra. To prove that fluoride was switching "on" the QD fluorescence of **53** by binding to the urea unit and not through QD surface binding a number of experiments were conducted.

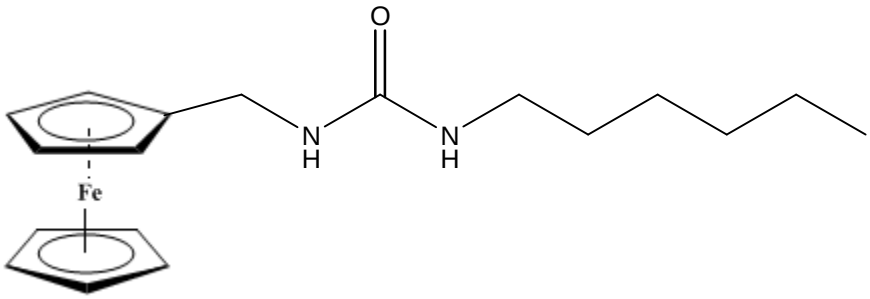

(57)

Figure 5.26 *Pratt and Beer's mono-urea substituted ferrocene receptor*[202]*.*

First, the ^{1}H NMR spectra of **51** in the presence and absence of F^- were recorded. As the urea protons were not apparent in the ^{1}H NMR spectrum of **52** or **53**, ligand **51** was chosen instead. As shown in figure 5.27 the urea proton, observed at 4.42 ppm shifted significantly downfield to 5.70 ppm upon addition of 0.01 M F^-. As explained in section 5.1.5 this downfield shift is indicative of H-bonding interaction between the urea protons and the fluoride[108].

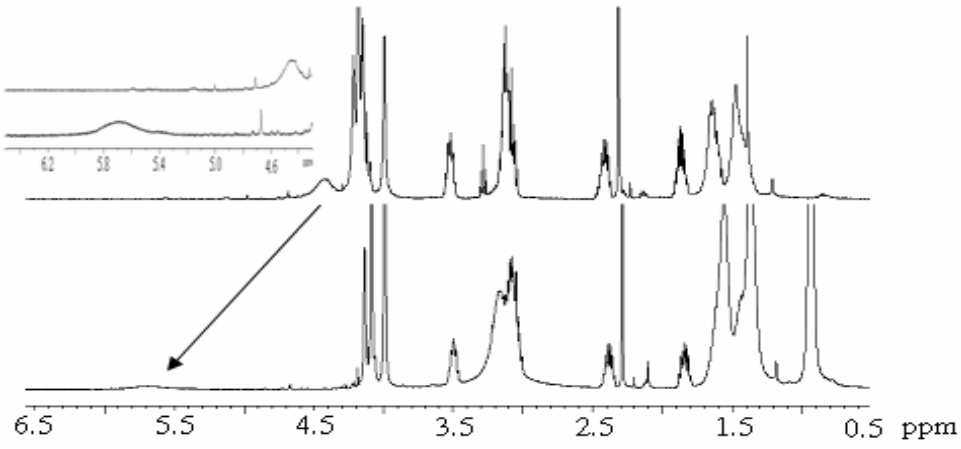

Figure 5.27 *^{1}H NMR spectra of **51** (top) and **51** in the presence of 0.01 M tetrabutylammonium fluoride (bottom). Inset shows the expanded region between 4.30 to 6.50 ppm. Solvent = $CDCl_3$.*

Secondly, methanol was added to a chloroform solution of **53** in the presence of F^- and a 90% reduction in emission intensity was observed, indicating the protic methanol solvent was competing with F^- for H-bonding sites of the urea (figure 5.28). Collectively, these experiments provide evidence that F^- switches the fluorescence of **53** "on" by binding to the urea component of the receptor and not by surface or other effects. This H-bonding interaction must modulate the electron transfer process between the ferrocene and the excited QD in a manner that reduces the PET rate. In normal "off-on" PET sensors binding of the analyte to the receptor increases the oxidation potential of the receptor reducing the rate of PET[68]. However, Beer and Molina both showed that anions bind to the ferrocenyl urea receptor and cause a cathodic shift which indicates an decrease in the oxidation potential. Therefore, further studies would be required to investigate the electrochemistry of **53** in the absence and presence of F^- to gain a fuller understanding of this mechanism.

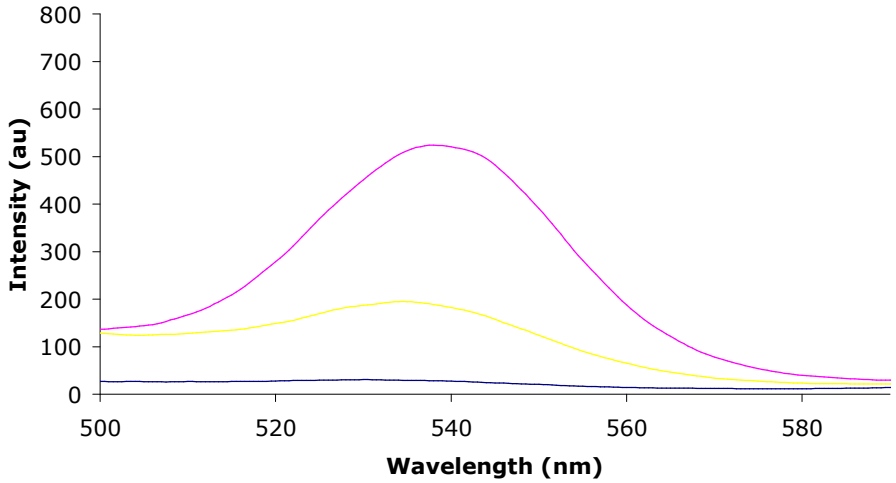

Figure 5.28 *Emission spectra for (a)* ***53*** *(blue spectrum), (b)* ***53*** *in the presence of 0.02 M F^- (pink spectrum) and (c)* ***53*** *in the presence of 0.02 M F^- to which MeOH was added.*

It has also been reported in some cases that ferrocene can quench fluorescence by energy transfer[204]. For effective energy transfer to occur, the absorption spectrum of the quencher should overlap well with the emission spectrum of the fluorophore. The absorption λ_{max} of the ferrocenyl receptor, at 442 nm overlaps poorly with the QD

fluorescence λ_{max} (540 nm) reducing the likelihood of FRET as a possible quenching mechanism (see Figure 5.29). In addition, there was no change in either the position or magnitude of the absorption λ_{max} after the addition of fluoride. This further confirms that energy transfer is not responsible for either the quenching or recovery of fluorescence emission observed for **53** in the absence and presence of fluoride.

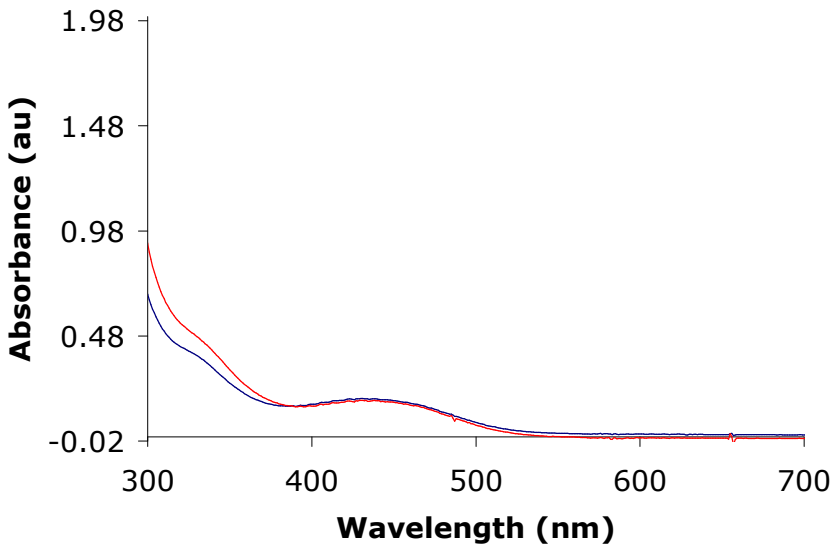

Figure 5.29 Absorption spectrum of **51** in the absence (blue line) and in the presence of fluoride (red line). [**51**] = 2.4 x 10^{-2} M, [F^-] = 1.9 x 10^{-1} M.

Furthermore, when fluoride was added to a solution of **53** already containing one of the other tested ions, the fluorescence was recovered showing that **53** could possibly operate in competitive media. Figure 5.30 shows the fluorescence spectrum of **53** in the presence of 0.1 M Br^- and for **53** in the presence of 0.1 M Br^- to which 0.1 M F^- has been added. For the former, the fluorescence remains quenched whereas in the latter solution, the QD fluorescence is switched "on". This indicates that F^- binds more strongly to the urea than bromide and this strong binding is the basis for the selectivity of **53** over the other tested monovalent anions.

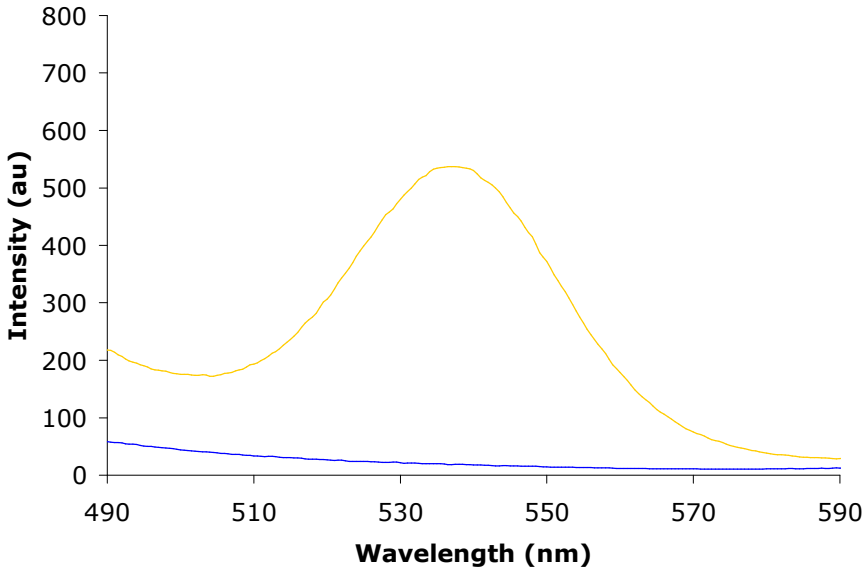

Figure 5.30 *Emission spectra of* ***53*** *in (a) the presence of 0.1 M [Br] (blue line) and (b) in the presence of 0.1 M [Br$^-$] to which was added 0.1 M [F$^-$](yellow line).*

5.7 Conclusions

The anchorage of a ferrocenyl receptor onto a CdSe/ZnS QD was shown to switch the QD fluorescence "off" by an electron transfer mediated process. The resulting probe was tested for selectivity against a range of monovalent anions, as their tetrabutylammonium salts and displayed good selectivity for F^- by a switching "on" fluorescence. This "off-on" process was attributed to a modulation in the rate of PET between the QD and ferrocenyl urea due to a strong hydrogen bonding interaction between the F^- and the urea.

Both **39** and **53** prove that it is possible to utilise QDs in a similar manner to organic dyes as the emissive component of fluorescent sensors and that the PET mechanism may be used as a mode of communication between the receptor and QD components. Thus, many different receptor types with proven selectivity may be adapted for use in QD sensors, to provide a range of probes which benefit from the optical properties QDs offer.

CHAPTER SIX

QDs AS FRAMEWORK FOR RECEPTOR ASSEMBLY

6.1 Introduction

6.1.1 Background

The previous chapters focussed on developing functional chemosensors for the single detection of biologically and environmentally important analytes. As an extension of this, designing probes capable of simultaneously detecting multiple analytes is more demanding. A number of examples exist in the literature of such probes and they tend to involve either the insertion of multi chromogenic units in one sensor[205], use multichannel detection methods (fluorescence, electrochemical and colorimetric)[206] or elaborate mathematical tools to process results[207]. Recently, a move away from selective detection (i.e. one analyte per sensor) and focusing more on a differential response (i.e. semi-selective sensors) has facilitated the simultaneous detection of two analytes by a single chromophore[208, 209]. Kaur *et al* developed the chromogenic chemosensor **58** for the simultaneous detection of Cu^{2+} and Ni^{2+}[208]. This differential complexation was achieved through two distinctly ionisable groups, i.e. phenol OH and secondary amine NH, with Cu^{2+} binding resulting in a change from ~490 nm to ~610 nm and Ni^{2+} binding from ~490 nm to ~700 nm.

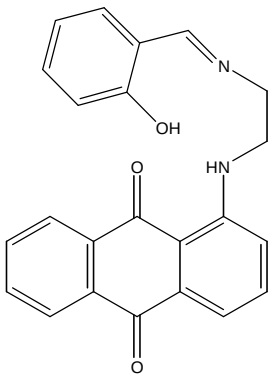

(58)

Suzuki's group has also synthesised a sensor that allows the intracellular detection of multiple analytes using a single probe[210]. Prior to

this, their attempts in simultaneous multiple analyte sensing involved loading a number of sensors into the cell and monitoring each individually. This proved unsuccessful due to the different metabolisms and photobleaching rates of each sensor. Also, a larger invasive effect and excessive cross talk meant this approach was unsuitable for quantitative analysis. Further research saw them develop the sensor KCM-1 **59**, a single probe for the simultaneous detection of intracellular Ca^{2+} and Mg^{2+}[210].

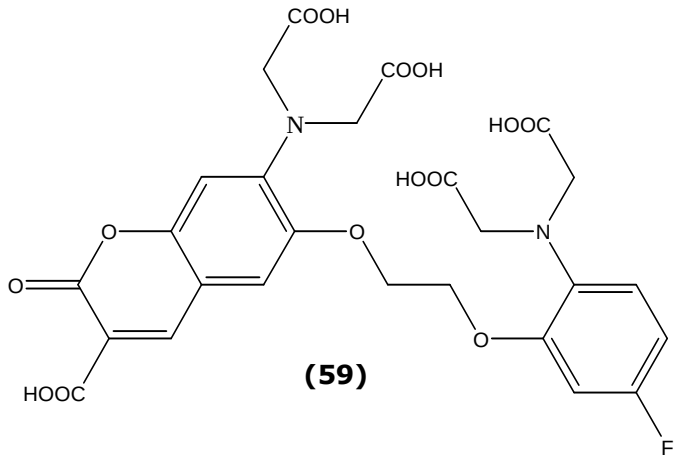

(59)

The molecule consists of a coumarin fluorophore with a fluorine substituted BAPTA (*O*,*O*'-bis(2-aminophenyl)ethyleneglycol-*N*,*N*,*N*',*N*'-tetraacetic acid) as the Ca^{2+} binding site on the electron-donor component of the chromophore. The Mg^{2+} binds to the charged *β*-diketone which is the electron accepting site. Upon Ca^{2+} recognition, the binding of the cation to the electron-donor site on the BAPTA chromophore produced a blue shift in the absorbance and fluorescence spectra of 45 nm and 5 nm respectively. With Mg^{2+} complexation, a red-shift was observed leading to a 21 nm offset in the absorbance spectrum and a 5nm shift in the fluorescence spectrum.

6.1.2 The Schiff base

The Schiff base is a condensation product of carbonyl compounds with primary amines. They were first discovered in 1864 by Hugo Schiff[211] and are noted by the common structural feature of RHC=N-R', where R and R' are aryl, alkyl, heterocyclic or cyclo alkyl groups. The presence of a lone pair of electrons on the sp^2 hybridised nitrogen atom makes them very useful and of considerable chemical and biological importance[212]. They are generally quite easy to prepare, requiring little or no purification steps and due to the properties of the imino group, they are excellent chelating agents[213, 214]. This is especially the case when there is an OH or SH group near the Schiff base. Due to this property, their use in sensors for biologically and environmentally relevant ions has increased and several reports have emerged of such probes. Gao and colleagues have exploited this field making use of the imino functionality in the sensor design of **60**[215]. They demonstrated that calix[4]arene probes with two spirobenzopyran groups attached to the lower rim can recognise lanthanide ions. No specificity was shown until a Schiff base was incorporated into the upper rim of the design. With this modification the dipodal probe displayed selectivity for both Dy^{3+} and Er^{3+} visible by a colorimetric change.

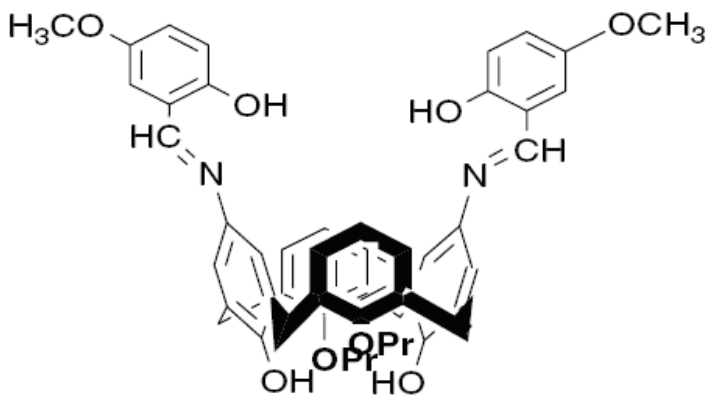

(60)

Figure 6.1 *Gao's dipodal Schiff base functionalised calix[4]arene probe for lanthanide detection*[215].

Bhardwaj *et al* described the synthesis of a series of tripodal receptors based on the mesitylene anchor **62** and has shown that when these receptors were incorporated into a tripodal arrangement, chromogenic selectivity for Ag^+ was observed[216]. When **61** was the receptor component of **62** (through a thioether linkage), its affinity for Ag^+ was evidenced by a marked enhancement in its fluorescence intensity.

R =

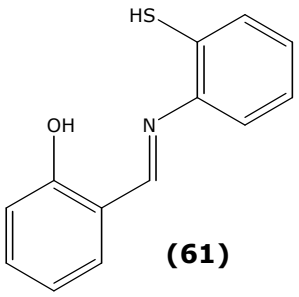

(61)

R' = Me / Et

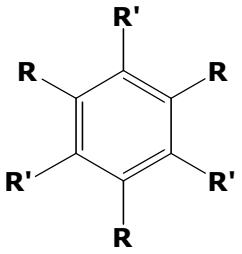

(62)

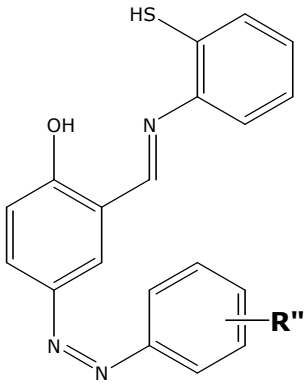

R" = NO_2 or Cl

(63)

The results presented in figure 6.2 show that a band centred at λ_{max}= 413 nm, assigned to intraligand (π-π^*) fluorescence from the excited enolic state, has low intensity due to PET from the N and O lone pairs, quenching the fluorescence. On addition of Ag^+, this band increases in intensity signalling the chelating of this metal with these lone pairs and cancelling the PET process. The probe was also tested against a number of other metal ions namely, Cu^{2+}, Ni^{2+}, Co^{2+}, Zn^{2+}, Hg^{2+} and showed no affinity for these metals under the same experimental conditions. A ^1H

NMR study revealed the nature of the binding between the receptor and Ag^+. A distinct gradual broadening and upfield shift from δ13.13 to δ12.79 of the OH signal pointed to an important role of the binding of Ag^+. Changes in the imino proton signal was small and no movement of the $-SCH_2$ protons was observed suggesting that the chelation of the cation was mainly through the O lone pairs.

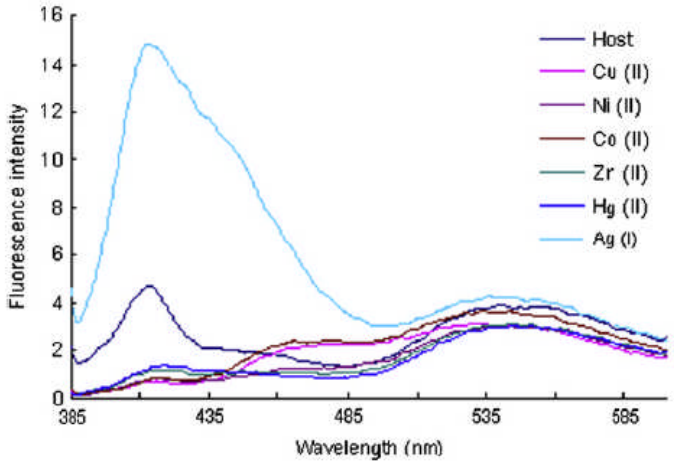

Figure 6.2 *Emission spectra of tripodal sensor incorporating receptor* ***61*** *illustrating its selectivity for* Ag^+ *over other metal ions*[217].

In subsequent work, when **63** was the component of **62** (again through a thioether linkage) it was shown to enable the optical detection of Ag^+ by a colour change from yellow to red upon complexation. Studies conducted in an almost fully aqueous system (dioxane:water ,1:9 v/v) revealed a distinct bathochromic shift in the UV-vis absorption spectrum on addition of Ag^+. A number of metal ions were screened for selectivity with **63** and the results are presented in figure 6.3. No significant changes were observed for Li^+, Na^+, K^+, Sr^{2+}, Ca^{2+}, Cd^{2+}, Zn^{2+}, Hg^{2+}, Pb^{2+}, Ni^{2+} and Cu^{2+}. However, upon addition of Ag^+ a new band emerged at 510 nm while the original band at 384 nm reduced in intensity. This bathochromic shift from 394nm to 510 nm was responsible for the colour change from yellow to red.

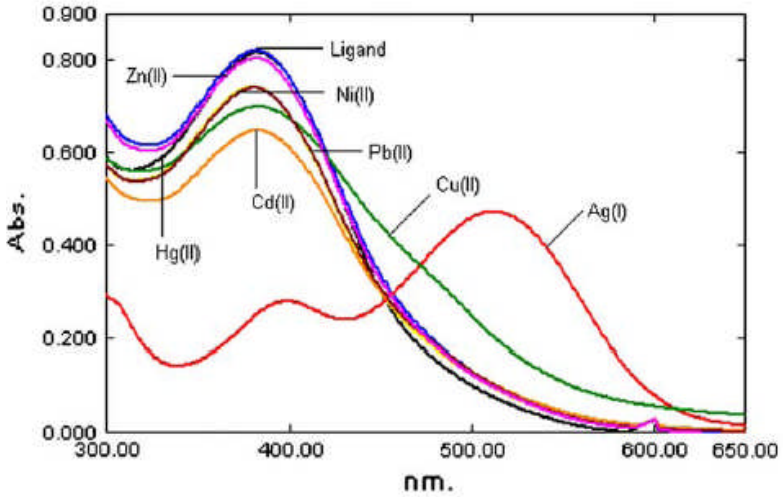

Figure 6.3 *Changes in λ_{max} on addition of various metal ions to* ***63*** *(dioxane:water, 1:9 (v/v))*[216].

From the studies with **61** and **63** the authors have postulated that the selectivity observed for a particular metal ion is due to the reduced binding affinity of these receptors when incorporated into a tripodal arrangement[217, 218].

6.2 Quantum Dot-Schiff base conjugate studies.

The incorporation of Schiff base receptors into tripodal arrangements has proved an effective strategy for increasing the selectivity of this class of receptor. This method of assembly and the subsequent selectivity these probes provide parallel the approach offered by self assembled monolayers (SAMs) on gold. [219]. The added feature of these SAMs is the ordered and oriented layers they create thus enabling control of the morphology and reactivity[220]. The three dimensional surface of a QD also offers the opportunity of organising receptor molecules in a manner that may improve their selectivity. The thiol functionality present on the Schiff base **61** means it is an ideal candidate for attachment to a QD surface.

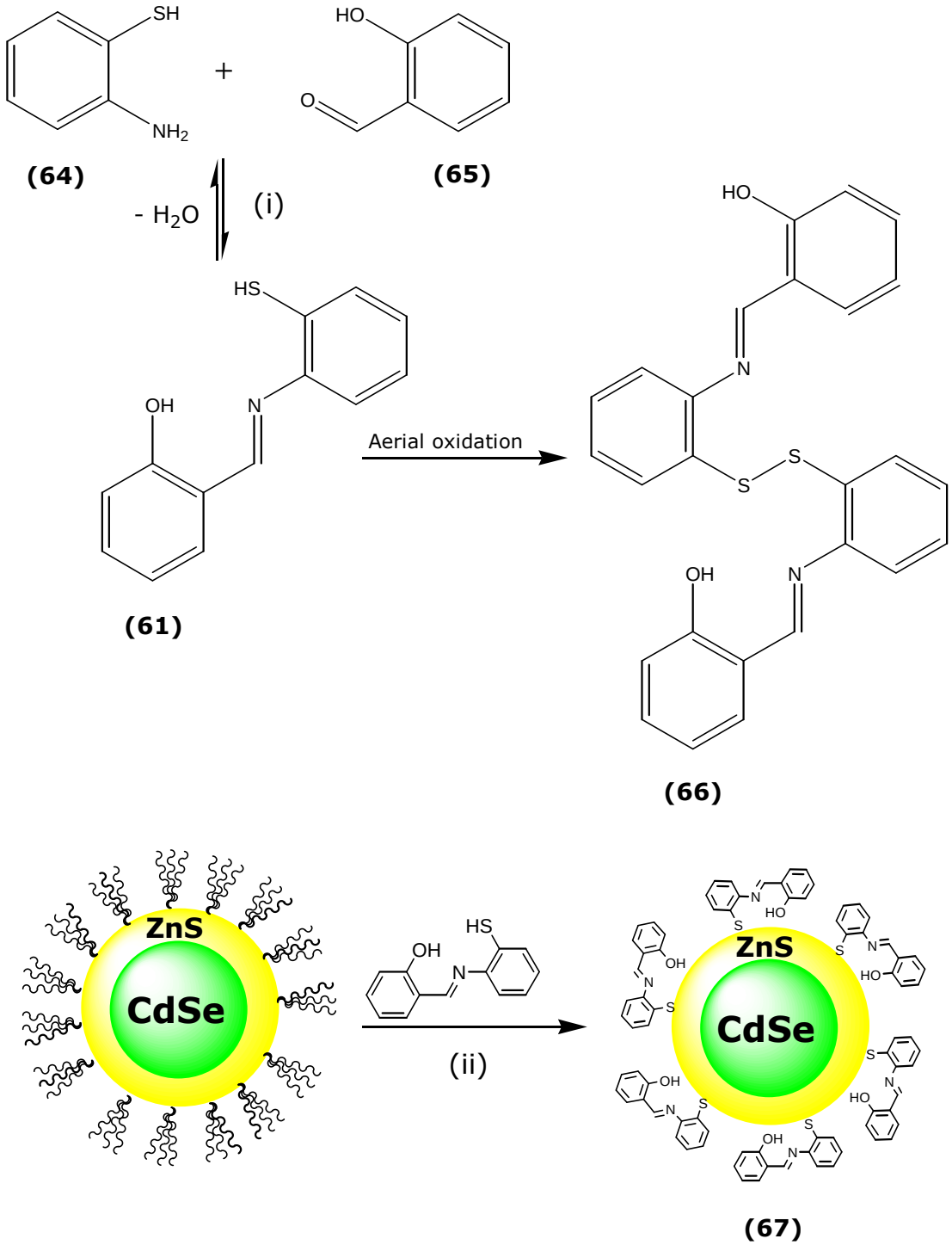

Scheme 6.1 *Synthesis of* ***67****. (i) ethanol, RT. (ii) CdSe/ZnS QDs, $CHCl_3$, tetrabutylammonium hydroxide.*

Furthermore, as it is electron rich it may interact with the excited QD and switch "off" fluorescence, enabling possibilities for sensing.

6.2.1 Synthesis of QD-receptor conjugate 67 and control compounds

Receptor **61** was synthesised in one step after reaction of salicylaldehyde and 2-mercaptoaniline following a literature procedure[112] (scheme 6.1). **61** was exchanged onto the surface of CdSe/ZnS QDs following a ligand exchange reaction as detailed in section 2.2.3. The disulfide **66** was prepared through aerial oxidation of receptor **61**.

6.3 Characterisation of 67

6.3.1 ^{1}H NMR characterisation

Surface functionalisation of **67** was confirmed by ^{1}H NMR spectroscopy, with figure 6.4 showing the stacked spectra of QD-conjugate (**67**), the receptor (**61**) and the parent QDs. This reveals an almost complete exchange of TOP/TOPO groups with the methyl and methylene protons of TOP/TOPO at 0.85 – 1.80 ppm respectively being significantly reduced in the spectrum of **67**. Also evident from figure 6.4 are the changes in the spectra of **61** before and after the exchange reaction. There was a notable downfield shift of the imino proton from 7.25 ppm in **61** to 8.70 ppm in **67**. There was also a slight downfield shift of the aromatic protons when anchored to the QD surface due to their new electronic environment. The thiol proton, present at 4.60 ppm in the spectrum of **61** was absent in the spectrum of **67**, also suggesting an effective exchange of the receptor onto the QD.

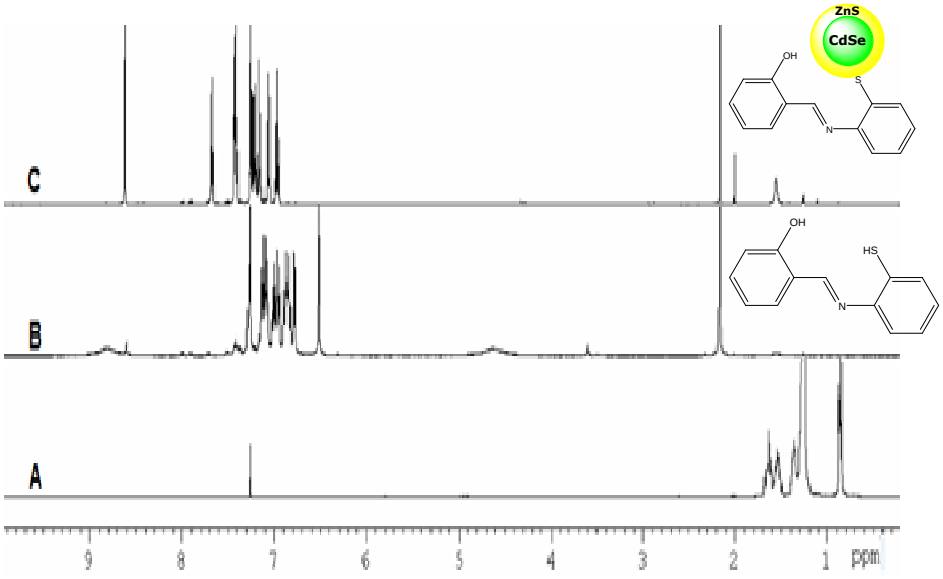

Figure 6.4 *Stacked ^{1}H NMR of (A) as received CdSe/ZnS QDs, (B) Receptor* ***61*** *and (C) QD-conjugate* ***67****. Spectra A, B and C recorded in* $CHCl_3$*.*

6.3.2 Photophysical properties of 67

The UV-vis absorption spectrum of **67** (figure 6.5) reveals peaks for both the bound receptor in the UV region and also the distinctive 1st exciton peak observable in the visible region with λ_{max} 510 nm. The low intensity of the 1st exciton peak relative to the receptor illustrates a high grafting efficiency of the receptor on the QD surface. At this wavelength and at an optical density of ~ 0.15 a.u., the core size was determined using equation 3.1 to be 2.45 nm, similar to the parent QDs. When excited at 370 nm there was no evidence of QD emission indicating a quenching process occurring upon excitation. As **61** is quite electron rich, this quenching most likely occurs due to electron transfer from the receptor to the nanoparticle as has been observed in section 5.6 with ligand **52** and for other electron rich analytes which were added to solutions of QDs.[101, 199]

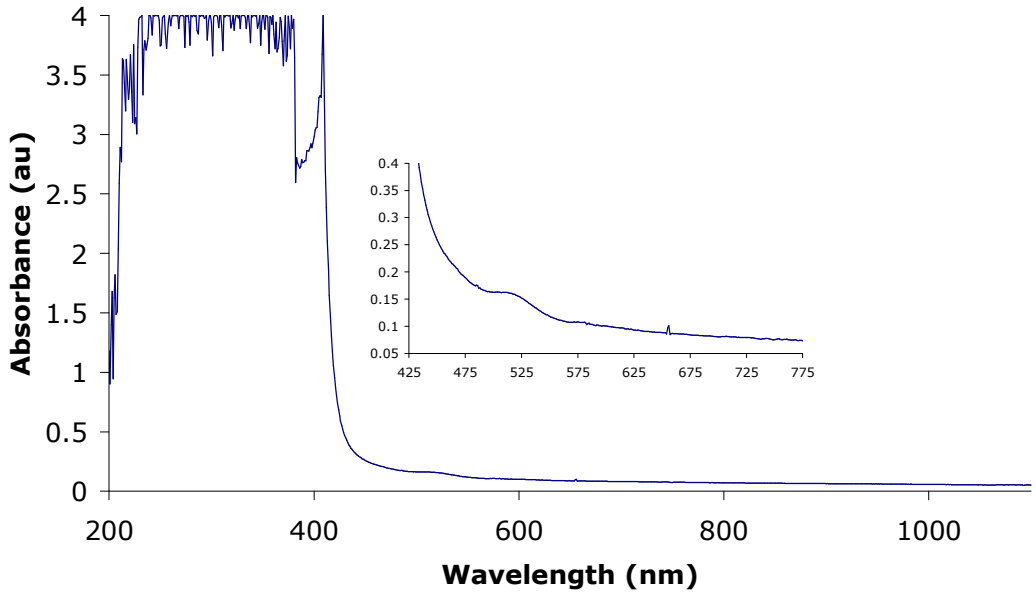

Figure 6.5 *Enhanced UV-vis absorption spectrum of* ***67*** *recorded in 100% THF to show the 1st exciton peak centred at 510 nm. [****67****] = 2.0 x 10-6. M.*

6.3.3 Size characterisation of 67

The QD-receptor conjugate **67** was further characterised by DLS (see figure 6.6). A small sample dispersed in THF was diluted to an optical density of ~ 0.1. The hydrodynamic diameter was determined to be 15 ± 2 nm, slightly larger than the parent QDs (12 ± 2 nm). This may be due to the presence of the rigid ligand **61** on the QD surface as compared to the more conformationally calamatic TOP/TOPO groups present on the native QDs. Again, a more monodisperse distribution observed for **67** due to the extra precipitation step involved in its preparation. The presence of nanoparticles was further confirmed by TEM (figure 6.7), from which a size of 3.70 nm was calculated which was slightly larger than 3.40 nm obtained for the parent CdSe/ZnS QDs.

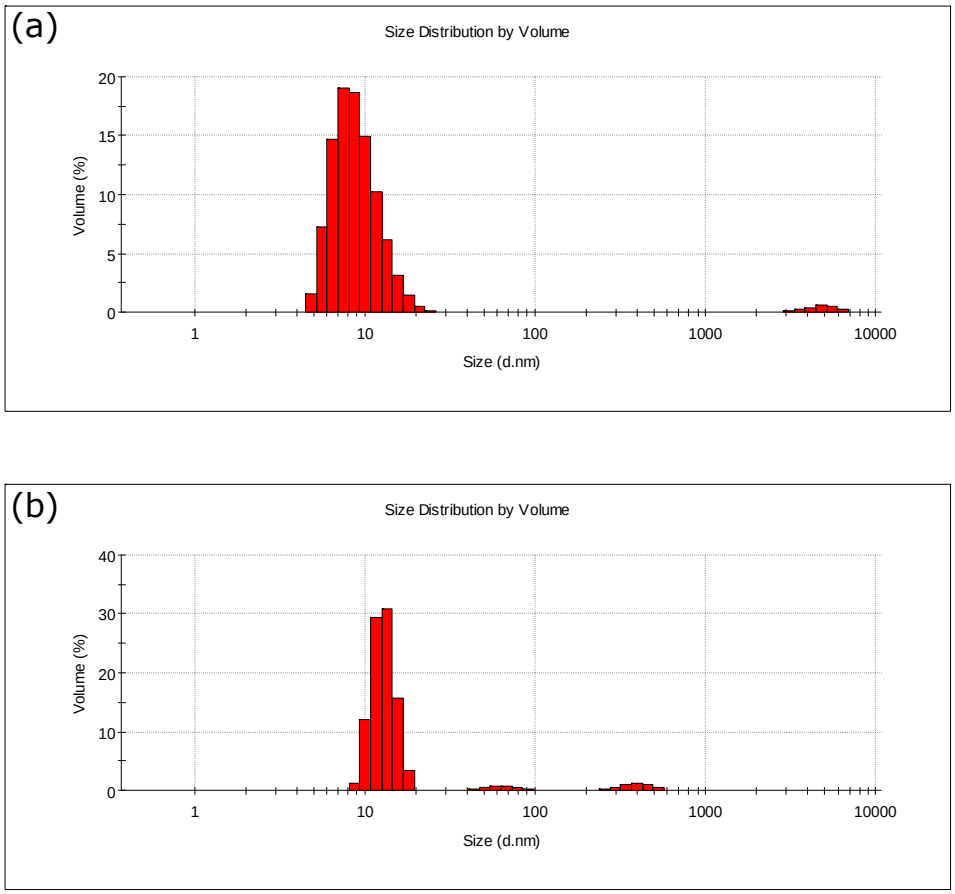

Figure 6.6 *DLS plots of (a) CdSe/ZnS-TOP/TOPO (size = 12 ± 2 nm) QDs and (b)* ***67*** *(size = 15 ± 2 nm).*

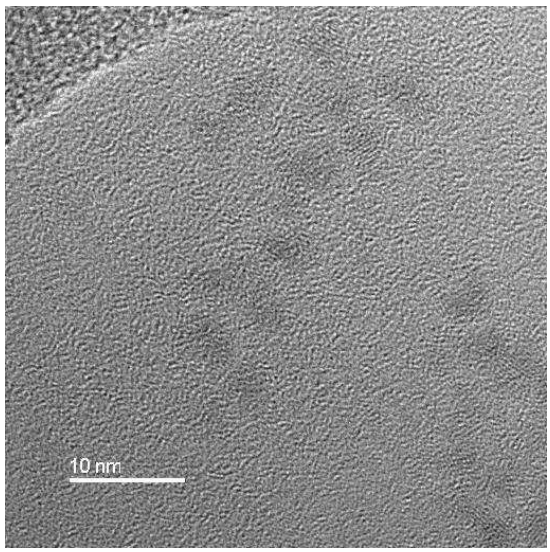

Figure 6.7 *TEM image of the* ***67****. Size determined to be 3.70 nm.*

6.4 Selectivity of receptors 61 and 66

6.4.1 UV-vis selectivity study of receptors 61 and 66 for various metal ions

The UV-vis plots in figure 6.8 illustrate the binding affinities of receptor **61** and its disulfide **66** for the various metal ions. In figure 6.8, there were bathochromic shifts observed for seven out of the twelve metal ions tested for **61** with minor intensity increases for the remaining ions. This demonstrates the non-selective nature of the receptor but also more importantly, the effective binding ability that it exhibits. The disulfide analogue **66** (figure 6.9) also displays poor selectivity for any particular metal ion with intensity increases for many of the ions tested and the appearance of new red-shifted absorbance bands for Cd^{2+}, Cu^{2+} and Ag^{+}.

(a)

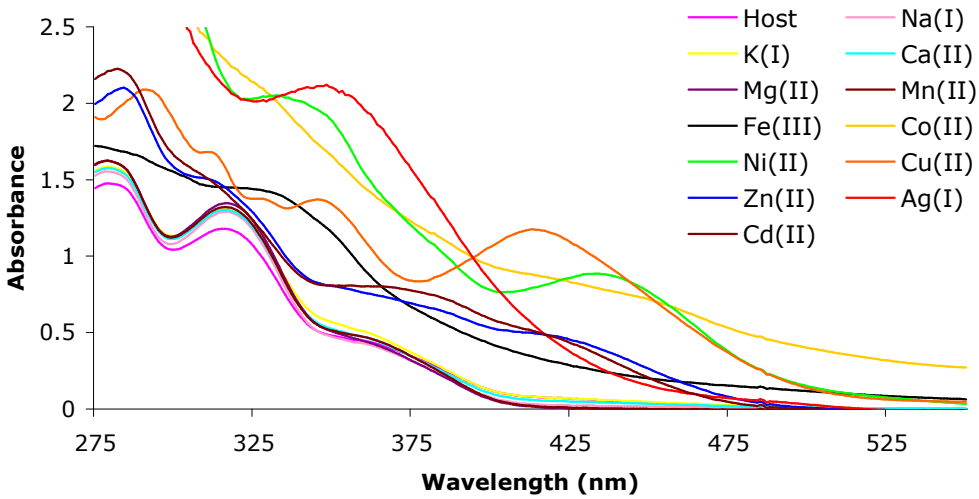

Figure 6.8 *UV-vis absorption spectra of **61** in the presence of various metal ions. [**61**] = 1 x 10^{-6} M; [ion] = 5 x 10^{-5} M; in a 80% THF / 20% 0.01 M HEPES buffer solution at pH = 7.0.*

(b)

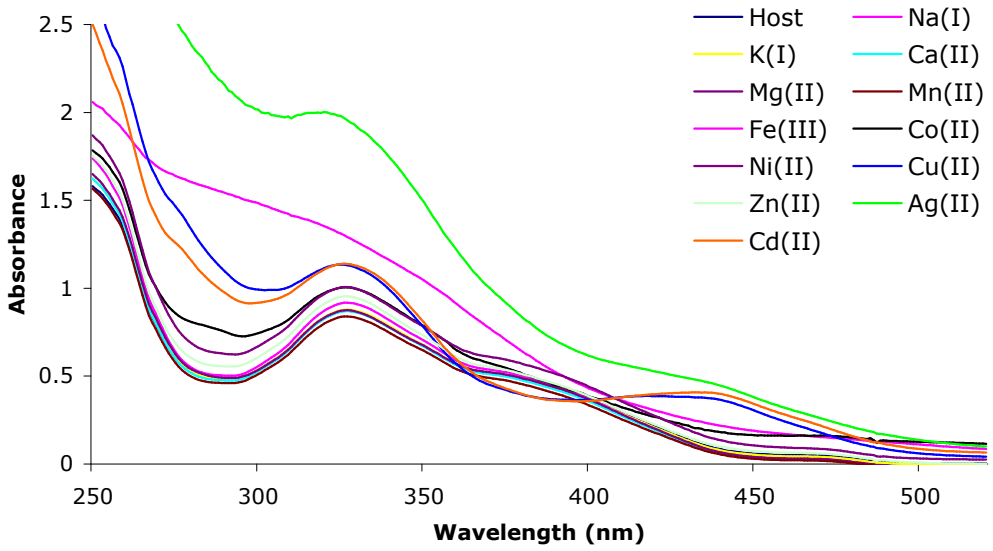

Figure 6.9 *UV-vis absorption spectra of **66** in the presence of various metal ions. [**66**] = 1 x 10^{-6} M; [ion] = 5 x 10^{-5} M; in a 80% THF / 20% 0.01 M HEPES buffer solution at pH = 7.0.*

6.5 Selectivity of probe 67

6.5.1 UV-vis investigations

As mentioned above, the QD emission was quenched upon exchange of **61** onto the QD surface. Thus, it was hoped that the addition of certain metal ions to a solution of **67** may result in a restoration of its emission signal. Therefore, the probe was screened against a number of physiologically and environmentally important cations (as their chloride salts) in a buffered THF-H_2O (80:20) solution at pH 7.0 but unfortunately no restoration of the emission was observed. However, it was noted that a distinct colour change had occurred in the QD solutions that contained Fe^{3+} and Cu^{2+}, from colourless to brown for Fe^{3+} and from colourless to green for Cu^{2+} (see figure 6.11). Two main bands were present in the UV-vis spectrum of **67**, one centred at 275 nm and the other at 355 nm (figure 6.10), the latter being attributed to an intraligand charge transfer transition of the imine chromophore[221]. As observed in figure 6.10, a substantial increase in intensity of both bands was observed upon addition of Fe^{3+} while with Cu^{2+} there was a distinct bathochromic shift of both

bands to 295 nm and 410 nm respectively. In contrast, the UV spectra of **61** and **66** show binding to many different ions illustrating that selectivity is improved when **61** is anchored to the QD surface.

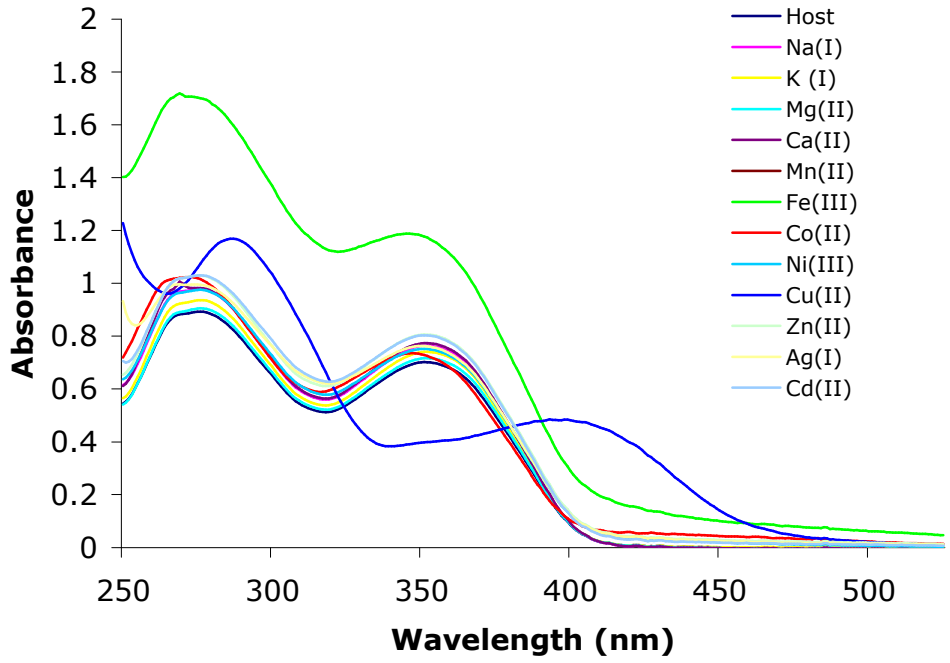

Figure 6.10 *UV-vis absorption spectra for* ***67*** *in the presence of various metal ions.*

Figure 6.11 *Photo illustrating the effect of Fe^{3+} and Cu^{2+} metal ions on* ***67*** *in THF-H_2O (80:20) pH 7.0.*

The bar chart in figure 6.12 shows the selectivity of **67** for the various metal ions tested when measured at 325 nm for Fe^{3+} and 410 nm for Cu^{2+}. These two wavelengths were selected because 325 nm represents an isosbestic point for all the ions except Fe^{3+} which reduces the possibility of interference while 410 nm was the λ_{max} for Cu^{2+} induced

changes. From the plot it is evident that only Fe^{3+} causes any interference with Cu^{2+} at 410 nm while at 325 nm there was no significant effect from any metal ion toward Fe^{3+}.

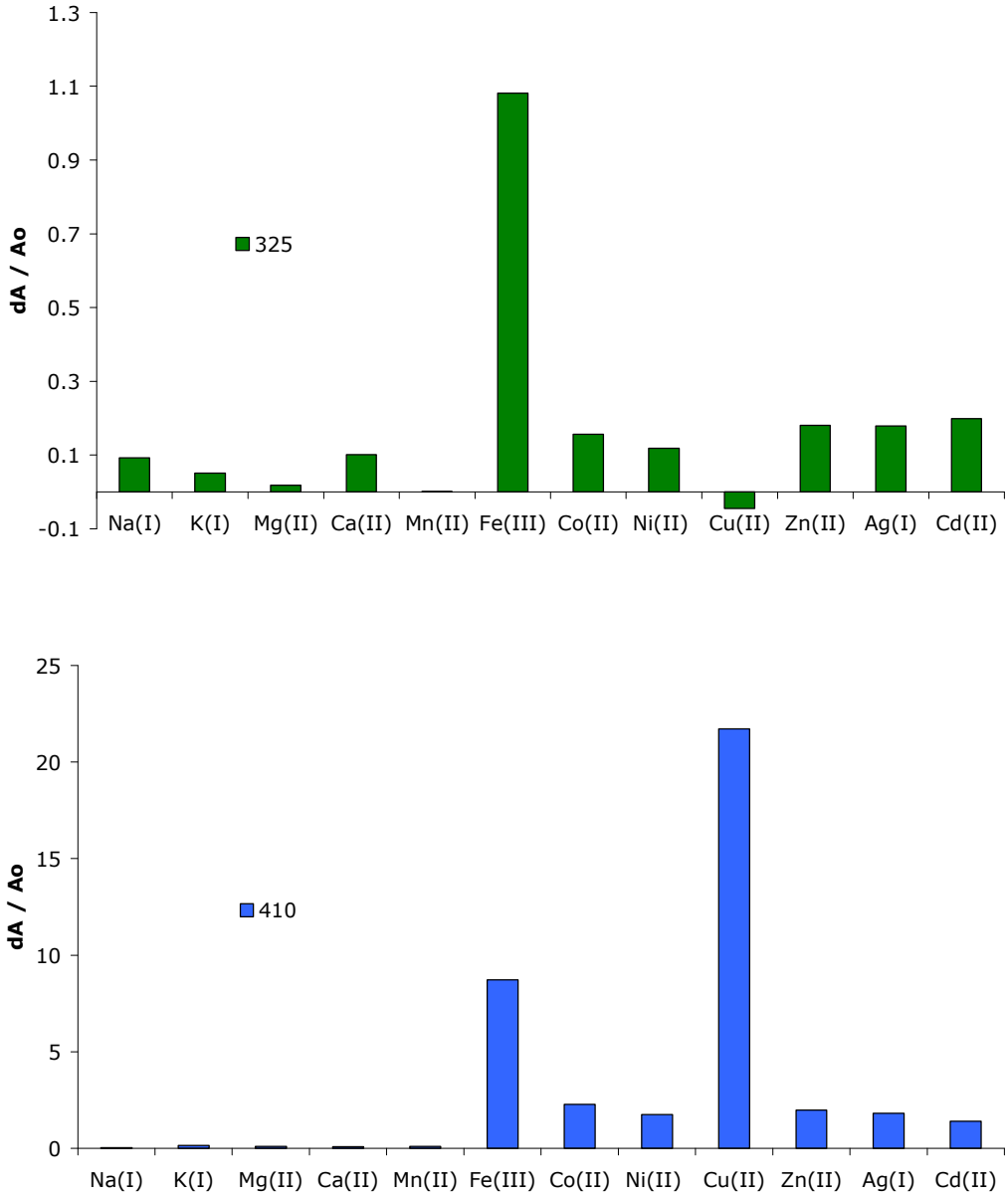

Figure 6.12 *Bar charts revealing the selectivity of* ***67*** *for metal ions when determined at 325 nm for Fe^{3+} (top) and 410 nm for Cu^{2+} (bottom). [**67**] = 4.0 x 10^{-8} M; [ion] = 50 μM.*

Table 6.1 *Illustrating the dA/A_o ratios for various metal ions at λ_{max} = 325 and 410 nm, where dA is the change in absorbance of the host on addition of ion and A_0 is the absorbance of the host without any ion added.*

Ion	dA/Ao 325 nm	dA/Ao 410 nm
Na^+	0.095	1.025
K^+	0.050	1.140
Mg^{2+}	0.029	1.099
Ca^{2+}	0.102	1.073
Mn^{2+}	0.084	1.092
Fe^{3+}	1.081	9.716
Co^{2+}	0.164	3.271
Ni^{2+}	0.130	2.748
Cu^{2+}	-0.049	22.717
Zn^{2+}	0.191	2.977
Ag^+	0.188	2.822
Cd^{2+}	0.213	2.410

6.5.2 Sensitivity of 67 to Fe^{3+} and Cu^{2+}.

Figure 6.13 shows the UV-vis absorption spectral plots for the titration of **67** in the presence of Cu^{2+} and Fe^{3+}. It can be observed in figure 6.13a that as the Cu^{2+} concentration increases two new bands gradually appear at 295 nm and 410 nm with a gradual decrease in the original bands centred at 275 nm and 355 nm. Also evident is the presence of two isosbestic points at 325 nm and 380 nm. Upon increasing Fe^{3+} concentration, a gradual increase in the original absorbance at 275 nm and 355 nm was observed.

(a)

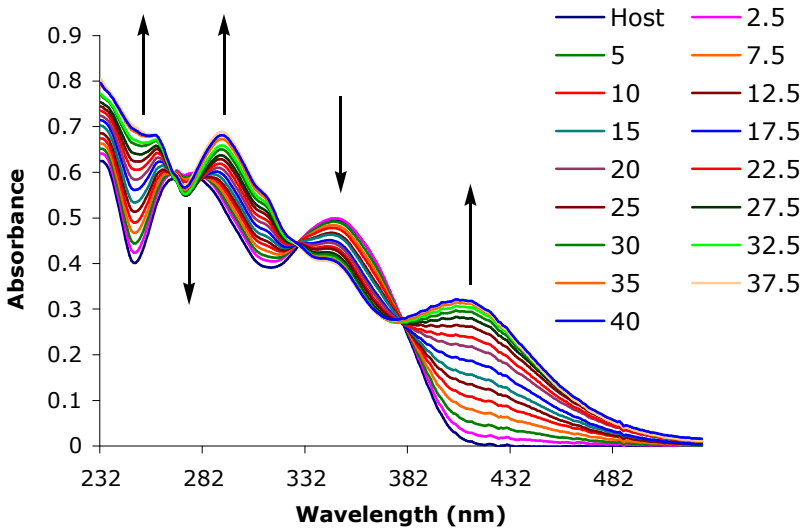

(b)

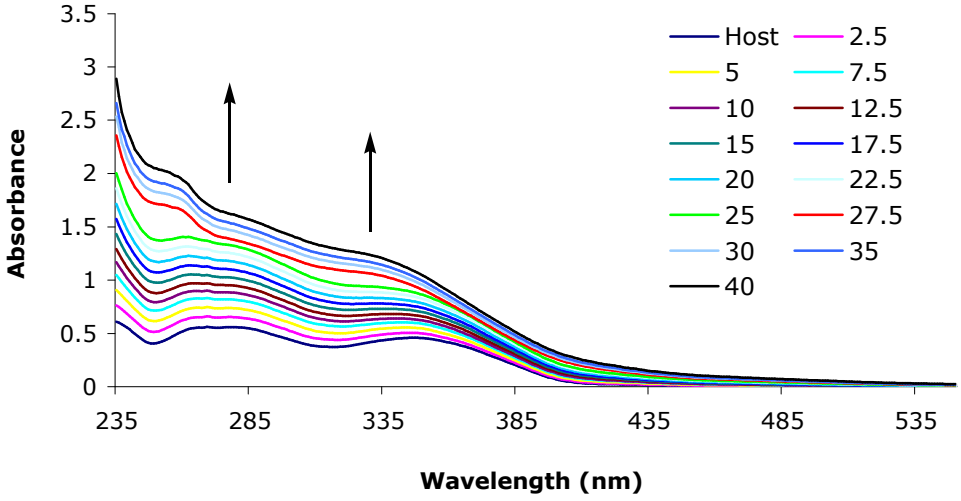

Figure 6.13 *UV spectra of* ***67*** *in the presence of (a) increasing* Cu^{2+} *concentration and (b) increasing* Fe^{3+} *concentration. Inset reflects concentration of ions used in* μM. [**67**] = 4 x 10^{-8} M.

From the spectra shown in figure 6.13 a plot of absorbance intensity against concentration was made for Cu^{2+} at 410 nm and Fe^{3+} at

325 nm and is presented in figure 6.14. Good linearity was observed for both ions up to a concentration of 25 μM.

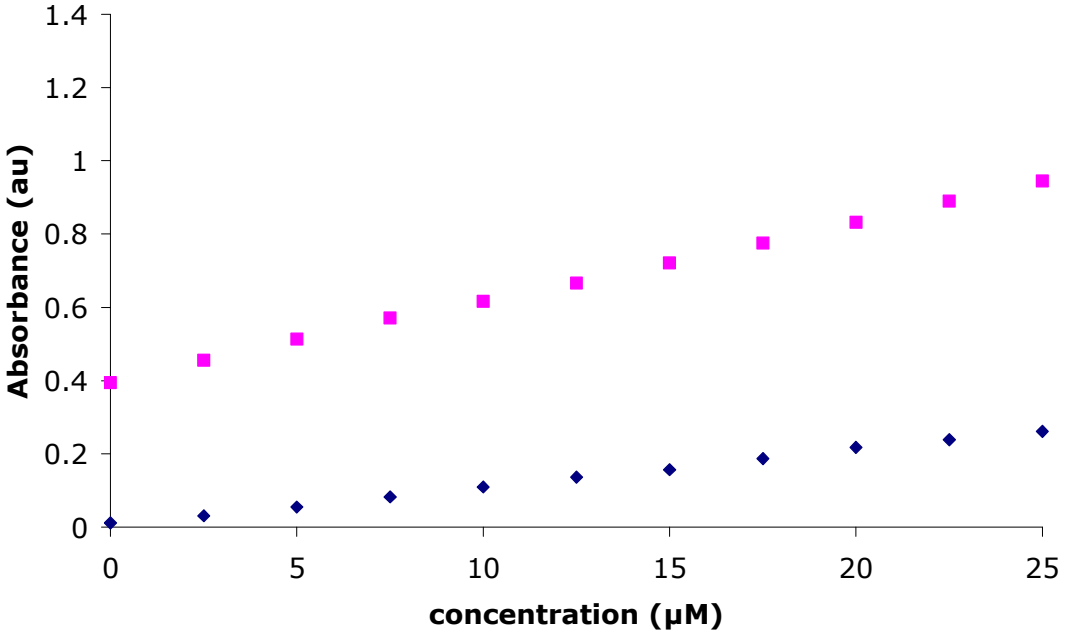

Figure 6.14 *Plot of concentration against absorbance for Cu^{2+} (blue diamonds) at 410 nm and also Fe^{3+} (pink squares) at 325 nm.*

6.5.3 Competitive titration of 67 with Cu^{2+} and Fe^{3+}.

Simultaneous detection of multiple targets is dependent on ensuring there is no competitive interference from other metal ions in solution. From the selectivity experiments it was determined that only Fe^{3+} and Cu^{2+} caused any change in the UV-vis spectrum, therefore any recognition studies conducted in the presence of both ions would confirm the viability of this probe.

Solutions were prepared containing **67** in the presence of various concentrations of Cu^{2+} and Fe^{3+}. To evaluate possible Cu^{2+} interference with Fe^{3+} measurements, solutions containing equimolar concentrations of Fe^{3+} and Cu^{2+} were prepared at 2.5, 5.0, 7.5, 10, 12.5, 15, 17.5 and 20 μM. These concentrations reflect the concentration of the Fe^{3+} ion present, with an equimolar amount of Cu^{2+} present. The UV spectrum of each solution was recorded and is shown in figure 6.15. To evaluate possible Fe^{3+} interference with Cu^{2+} measurements, solutions were prepared, again containing 2.5, 5.0, 7.5, 10, 12.5, 15, 17.5 and 20 μM of Cu^{2+} and Fe^{3+}. However, this time it was only possible to have 25% of Fe^{3+} present

relative to Cu^{2+}. For example, the 2.5 μM solutions contained 2.5 μM Cu^{2+} and 0.625 μM Fe^{3+}. The UV-vis spectrum of each solution was recorded and is shown in figure 6.16. The results from these titrations are shown graphically in figure 6.17, with Cu^{2+} monitored at 410 nm and Fe^{3+} monitored at 325 nm. Good linearity was observed for both sets of solutions up to a concentration of 20 μM with very little deviation from solutions containing only Cu^{2+} or Fe^{3+}. Therefore, **67** can measure Fe^{3+} concentration in the presence of equimolar Cu^{2+} and Cu^{2+} concentration in the presence of 0.25 equivalents of Fe^{3+}. Unfortunately, at higher equivalents of Fe^{3+} the match between Cu^{2+} only samples deviated significantly.

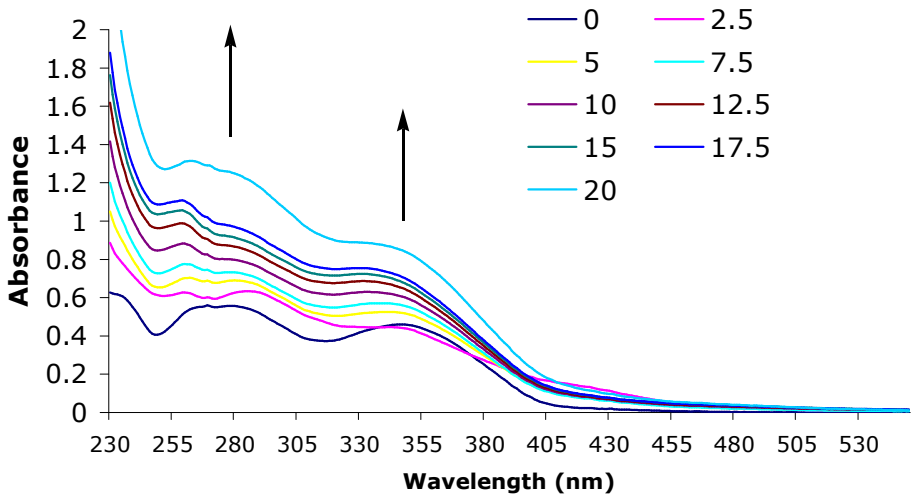

Figure 6.15 *UV-vis spectra of* ***67*** *in the presence of Fe^{3+} and Cu^{2+}. The values shown in the inset are the μM concentrations of Fe^{3+} with equimolar concentration of Cu^{2+}. Solutions prepared in a 80% THF / 20% 0.01 M HEPES buffer solution at pH = 7.0. [**67**] =4.0 x 10^{-8} M.*

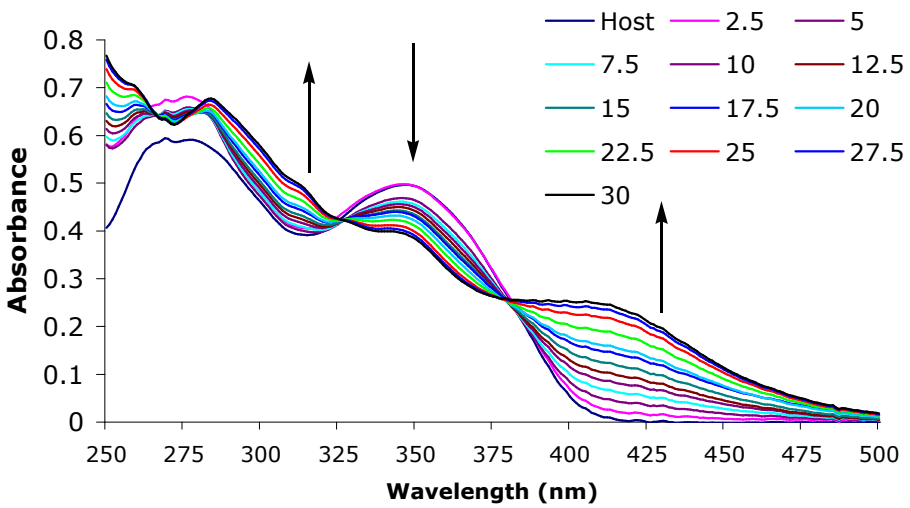

Figure 6.16 *UV-vis spectra of* ***67*** *in the presence of Cu^{2+} and Fe^{3+}. The values shown in the inset are the μM concentrations of $Cu^{2+}$with Fe^{3+} being present at 25% of this concentration. Solutions prepared in a 80% THF / 20% 0.01 M HEPES buffer solution at pH = 7.0. [****67****] =4.0 x 10^{-8} M.*

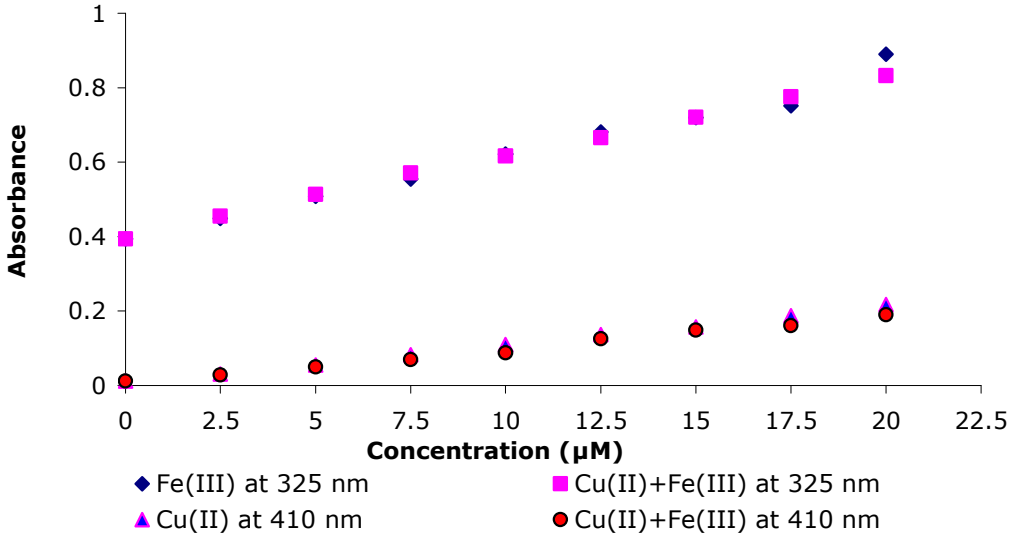

Figure 6.17 *Plot of absorbance intensity of* ***67*** *against metal ion concentration for Fe^{3+} (blue diamonds), for Fe^{3+} in the presence of equimolar Cu^{2+} (pink squares), for Cu^{2+} (pink/blue triangles) and Cu^{2+} in the presence of 0.25 molar equivalents of Fe^{3+} (blue/red circles). Fe^{3+} and Cu(II) measurements were recorded at 325 nm 410 nm respectively. [****67****] = 4.0 x 10^{-8} M.*

6.5.4 Effect of pH on probe

The UV-vis spectrum of **67** was found to be strongly influenced by solution pH. At a low pH (~3.5), a prominent band was observed which was centred at 325 nm. This band reduced in intensity upon increasing pH and a new red shifted band appeared with λ_{max} = 382 nm (figure 6.18) a result most likely of the deprotonation of the phenolic group on the receptor. The position and shape of this band was similar to the Cu^{2+} induced band at λ_{max} 410 nm (figure 6.3) suggesting a Cu^{2+} induced deprotonation of the phenolic group may occur upon Cu^{2+} binding. A plot of absorbance intensity at 382 nm against solution pH (see figure 6.19) shows a sigmoidal profile with an enhancement occurring over 2 log units. Assuming a 1:1 interaction between receptor and base the pK_a, calculated from equation 6.1 was found to be 8.92.

$$\log[(A_{max} - A)/(A - A_{min})] = pK_a - \log \beta \qquad \textit{equation 6.1}^{69}$$

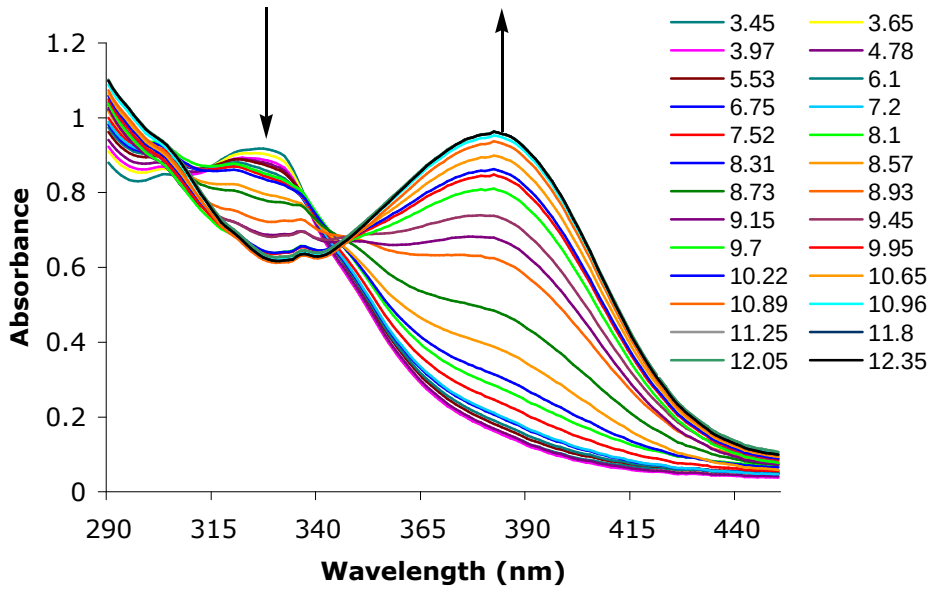

Figure 6.18 *UV-Vis pH titration of **67**. [**67**] = 4 x 10^{-8} M in an 80% THF / 20% H_2O solution. Inset lists the pH values tested.*

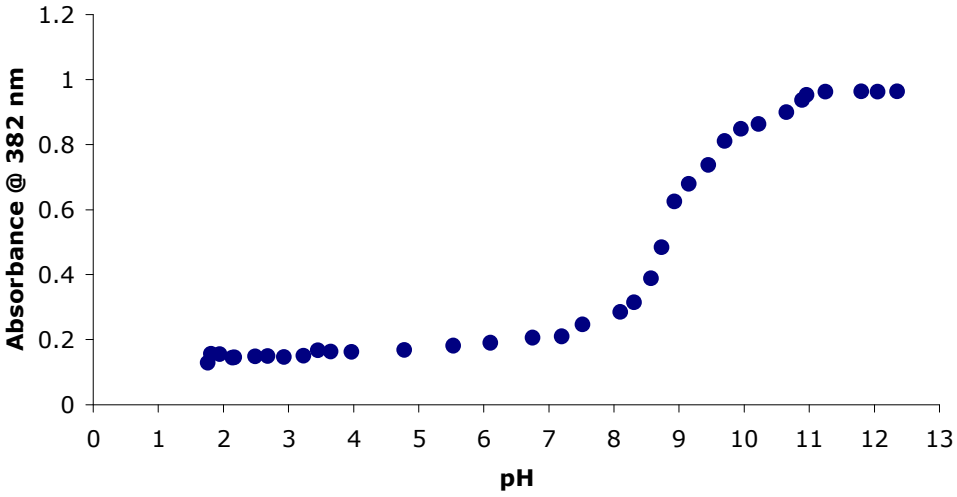

Figure 6.19 *Plot of absorbance intensity against pH for* ***67****. [****67****] = 4.0 x* 10^{-8} *M in an 80% THF / 20%* H_2O *solution.*

6.6 Conclusions

A chromogenic sensor for the simultaneous detection of multiple analytes was designed using a CdSe/ZnS QD as a nanoparticle scaffold. Although the Schiff base receptor itself displayed no selectivity for any of the metal ions that were tested, when assembled on the QD, semi-selective behaviour was observed for Cu^{2+} and Fe^{3+}. The recognition of these cations were noticeable by a colour change with Cu^{2+} also displaying a bathochromic shift in the absorption spectrum while Fe^{3+} displayed a significant intensity increase. However, no fluorescent emission was observed from this probe, most likely due to an electron transfer from the electron rich ligand to the QD.

Analyses conducted in THF:H_2O (80:20) solution buffered to pH 7.0 with HEPES revealed that the probe was capable of measuring both Cu^{2+} and Fe^{3+} in the presence of each other, however in the case of Cu^{2+} it was only possible to measure with 0.25 equivalents of Fe^{3+} present. Thus QDs provide an ideal framework for the organisation of receptors and can improve the selectivity of receptors which possess no prior selectivity. Thus many other receptors could be tested to determine if organisation on a QD surface increases their selectivity.

CHAPTER SEVEN

CONCLUSIONS AND FUTURE WORK

7.1 Conclusions

The primary aim of this work was to establish the photoinduced electron transfer (PET) mechanism with quantum dots (QDs). By anchoring tried and tested receptors for various ions and small molecules on to the surface of these QDs, their suitability as chemical and biological sensors could be assessed. At the outset of this project no examples of PET mediated fluorescent sensors using QDs as the emitting unit existed. This has since changed in the intervening years and is now quickly establishing itself [95,96,102,222,223].

The work presented in this thesis can be divided into a number of specific goals and objectives.

1. Synthesis of CdSe and CdSe/ZnS QDs.
2. Design of water soluble QDs with appended surface ligands providing dual functionality (i.e. water solubility and receptor modality).
3. Establishing the PET mechanism with QDs.
4. Anion sensing with QDs using urea and thiourea charge neutral receptors.
5. Using the QD surface as a framework for the assembly of Schiff base receptors.

In chapter 3 the synthesis and characterisation of CdSe and CdSe/ZnS QDs is described. CdSe QDs are the prototypical QD and most often used in chemical and biological applications. To demonstrate the versatility of these nanocrystals, three sizes of both core and core-shell QDs were prepared by simply varying the reaction time of the syntheses. Absorption and emission profiles for each size revealed broad absorption profiles and narrow emission spectra typical of CdSe QDs. The sizes were determined using three methods. These were TEM, DLS and a UV-vis method derived by Peng. Of these methods, DLS provided the most realistic measurement when considering biological applications.

The synthesised QDs were modified with mercaptosuccinic acid (MSA) rendering them water soluble. These functionalised QDs were screened against environmentally and biological relevant metal ions and

were found to be selective for Cu^{2+} and to a lesser extent Fe^{2+}. From these studies the quantum yields for these functionalised QDs were quite low and it was clear that any further work would need to be conducted with better quality nanocrystals. As a result, the remainder of the project was carried out using very high quality QDs purchased from Evident technologies.

Another set of water soluble QDs were also prepared, replacing the native TOP/TOPO groups with a quaternised amine providing a positive surface. These QDs were shown to be selective for ATP and to a lesser extent GTP over other the nucleotides tested. The selectivity toward ATP and GTP was attributed to a greater net negative charge of these nucleotides over the mono and diphosphates.

In chapter 5 it was shown that altering the receptor chemistry could influence the rate of PET between the receptor and the QD. This was observed quite effectively using an amine and an amide. In the presence of an amine, PET occurred from the nitrogen lone pair to the QD resulting in a complete quench of fluorescence. When the corresponding amide was added to a solution of QD, minimal quenching was observed. This experiment demonstrated that PET was possible with QDs in a similar fashion to organic based sensors.

Gunnlaugsson's strategy for anion recognition by employing charge neutral thioureas was embraced and incorporated into a QD based design. With proof of the PET principle with QDs in place it was envisaged that similar selectivity would be observed. This indeed was the case with acetate and fluoride being detected while chloride, not detected with the organic analogue was also bound by the thiourea receptor, most likely by co-operative binding with adjacent receptors. Hydrogen bonding of the anions with the thiourea receptor was believed to be responsible for the quench and was proven by a visible shift in the ^{1}H NMR spectrum of the thiourea protons.

Also in this chapter an "off-on" QD sensor was prepared providing selective detection for fluoride and to a lesser extent with acetate and dihydrogen phosphate. From the literature it was observed that when redox active ferrocene was brought close to the surface of QDs a complete quench in fluorescence was observed[199]. This phenomenon coupled with

work reported by Pratt and Beer[202] that demonstrated amperometric detection of acetate and dihydrogen phosphate by hydrogen bonding with a urea receptor led to a sensor design incorporating these two components. No fluorescence was observed from the QD conjugate attributed to the proximity of the ferrocene. This was reversed by the addition of fluoride and a substantial increase in the fluorescence resulted. A minor effect was observed with acetate and dihydrogen phosphate. As with the previous example with the thiourea receptor, hydrogen bonding of the anions with the urea receptor was proven by a visible shift in the ^{1}H NMR spectrum of the urea protons. A further experiment involving the addition of methanol, a competitive solvent for the hydrogen bonding sites, further proved the pivotal role of the urea.

In chapter 6 the use of QDs as a framework or scaffold for assembling receptors was examined and produced some interesting results. A Schiff base receptor showing no particular selectivity for a number of cations displayed semi-selective behaviour for Cu^{2+} and Fe^{3+} when assembled on CdSe/ZnS QDs. In addition, monitoring each cation in the presence of the other was also possible. To the best of our knowledge, this was the first reported example of simultaneous detection of two analytes with QDs.

7.2 Future work

The focus of this project over the last three years has been to synthesise a variety of ligands and investigate their response by spectroscopic means upon anchorage to QDs. Anion sensing was an attractive area to focus on due to its relatively unexplored background and this comprised a major part of the thesis. The probe **39** discussed in chapter 5 returned impressive results and this could be expanded by preparing other QD sensors containing a similar receptor with different substituents on the para position of the aromatic ring to tune the acidity of the urea group. This may affect the selectivity / sensitivity of the probes. Also in chapter 5 the mechanism of the quenching process involved between the ferrocene and the QD needs to be explored in more detail by electrochemical means and it is hoped Dr. J Tucker at the University of Birmingham may help with this. Another possible area of

future work would be to assess if probe **53** could detect anions by electrochemical means in addition to fluorescence, with perhaps different sensitivity/selectivity.

A further study that would have been interesting to perform with the Cu^{2+} probe in chapter 4 would have been to see how the thickness of the ZnS shell could affect the fluorescence quench. From the work presented it was noted that with the core shell QDs a more sensitive quench was observed compared to the bare core QDs. It is well known that the thickness of the shell can influence the electronic properties of the QD but it can also affect its quenching ability[224].

A number of other receptors were synthesised during the course of the project and after anchorage to the QD surface varying degrees of success resulted from selectivity studies. A notable example was a probe designed to measure zinc similar in design to Gunnlaugsson's probe[225] (see figure 7.1). It became clear however, that due to the composition of the QD, the addition of zinc was in fact passivating the surface of the QD and any fluorescence enhancement was likely due to this phenomenon.

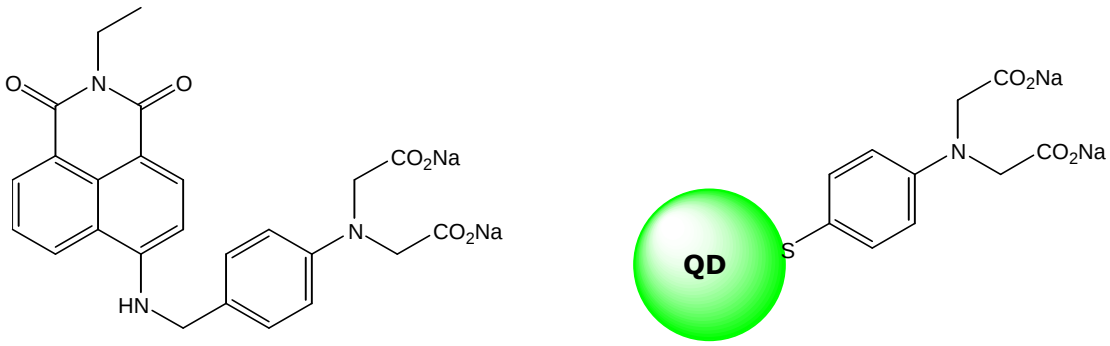

(a) (b)

Figure 7.1 *(a) Gunnlaugsson's PET chemosensor for Zn(II)[225]. (b) Analogous QD probe.*

Future work on the development of a QD probe incorporating this design will require the use of alternative materials in its composition.

References

(1) Rendell, D. In *Fluorescence and Phosphorescence;* Wiley-India: **2008**; pp 3.

(2) Efros, A. L. *Sov. Phys. Semicond.* **1982**, *16*, 722.

(3) Ekimov, A. I.; Onushchenko, A. A. *Sov. Phys. Semicond.* **1982**, *16*, 755.

(4) Brus, L. E. *J. Chem. Phys.* **1983**, *79*, 566.

(5) Ekimov, A. I.; Efros, A. L.; Onushchenko, A. A. *Solid State Commun.* **1985**, *56*, 921.

(6) Bailey, R. E.; Smith, A. M.; Nie, S. *Physica E* **2004**, *25*, 1-12.

(7) Somers, R. C.; Bawendi, M. G.; Nocera, D. G. *Chem. Soc. Rev.* **2007**, *36*, 579-591.

(8) Callan, J. F.; de Silva, A. P.; Mulrooney, R. C.; McCaughan, B. *J. Inclusion Phenom. Macrocyclic Chem.* **2007**, *58*, 527.

(9) Jaiswal, J. K.; Mattoussi, H.; Mauro, J. M.; Simon, S. M. *Nat. Biotechnol.* **2002**, *21*, 47-51.

(10) Bruchez Jr., M.; Moronne, M.; Gin, P.; Weiss, S.; Alivisatos, A. P. *Science* **1998**, *281*, 2013.

(11) Hanaki, K.; Momo, A.; Oku, T.; Komoto, A.; Maenosono, S.; Yamaguchi, Y.; Yamamoto, K. *Biochem. Biophys. Res. Commun.* **2003**, *302*, 496-501.

(12) Coe-Sullivan, S.; Woo, W.; Steckel, J. S.; Bawendi, M.; Bulovic, V. *Organic Electronics* **2003**, *4*, 123-130.

(13) Zhao, J. L.; Zhang, J. Y.; Jiang, C. Y.; Bohnenberger, J.; Basche, T.; Mews, A. *J. Appl. Phys.* **2004**, *96*, 3206-3210.

(14) Sun, Q.; Wang, Y. A.; Li, L. S.; Wang, D.; Zhu, T.; Xu, J.; Yang, C.; Li, Y. *Nat. Photonics* **2007**, *1*, 717-722.

(15) http://www.nightmarker.com/.

(16) Murray, C. B.; Norris, D. J.; Bawendi, M. G. *J. Am. Chem. Soc.* **1993**, *115*, 8706-8715.

(17) Peng, Z. A.; Peng, X. *J. Am. Chem. Soc.* **2001**, *123*, 183-184.

(18) Boatman, E. M.; Lisensky, G. C.; Nordell, K. J. *J. Chem. Educ.* **2005**, *82*, 1697-1699.

(19) Hines, M. A.; Scholes, G. D. *Adv. Mater.* **2003**, *15*, 1844-1849.

(20) Joo, J.; Na, H. B.; Yu, T.; Yu, J. H.; Kim, Y. W.; Wu, F.; Zhang, J. Z.; Hyeon, T. *J. Am. Chem. Soc.* **2003**, *125*, 11100-11105.
(21) Micic, O. I.; Ahrenkiel, S. P.; Bertram, D.; Nozik, A. J. *Appl. Phys. Lett.* **1999**, *75*, 478-480.
(22) Manz, A.; Birkner, A.; Kolbe, M.; Fischer, R. A. *Adv. Mater.* **2000**, *12*, 569-573.
(23) Guzelian, A. A.; Banin, U.; Kadavanich, A. V.; Peng, X.; Alivisatos, A. P. *Appl. Phys. Lett.* **1996**, *69*, 1432-1434.
(24) Cao; Banin, U. *J. Am. Chem. Soc.* **2000**, *122*, 9692-9702.
(25) Anderson, K. E.; Fong, C. Y.; Pickett, W. E. *J. Non-Cryst. Solids* **2002**, *299-302*, 1105.
(26) Wang, S. *Prentice-Hall: Englewood Cliffs, NJ.* **1989**, .
(27) Murphy, C. J. *Anal. Chem.* **2002**, 520A.
(28) http://www.evidenttech.com/.
(29) Alivisatos, A. P. *Science* **1996**, *217*, 933.
(30) Smith, A. M.; Nie, S. *Analyst* **2004**, *129*, 672-677.
(31) Tomasulo, M.; Yildiz, I.; Kaanumalle, S. L.; Raymo, F. M. *Langmuir* **2006**, *22*, 10284-10290.
(32) Qu, L.; Peng, X. *J. Am. Chem. Soc.* **2002**, *124*, 2049-2055.
(33) Vassiltsova, O. V.; Zhao, Z.; Petrukhina, M. A.; Carpenter, M. A. *Sensors Actuators B: Chem.* **2007**, *123*, 522-529.
(34) Rogach, A. L. *Semiconductor Nanocrystal Quantum Dots: Synthesis, Assembly, Spectroscopy and Applications*, **2008**, pg 11.
(35) Pradhan, N.; Reifsnyder, D.; Xie, R.; Aldana, J.; Peng, X. *J. Am. Chem. Soc.* **2007**, *129*, 9500-9509.
(36) Murphy, C. J.; Coffer, J. L. *Appl. Spectrosc.* **2002**, *56*, 16A-27A.
(37) Dabbousi, B. O.; Rodriguez-Viejo, J.; Mikulec, F. V.; Heine, J. R.; Mattoussi, H.; Ober, R.; Jensen, K. F.; Bawendi, M. G. *The Journal of Physical Chemistry B* **1997**, 101, 9463-9475.
(38) Wuister, S. F.; de, M. D.; Meijerink, A. *The Journal of Physical Chemistry B* **2004**, *108*, 17393-17397.
(39) Gaponik, N.; Talapin, D. V.; Rogach, A. L.; Hoppe, K.; Shevchenko, E. V.; Kornowski, A.; Eychmuller, A.; Weller, H. *The Journal of Physical Chemistry B* **2002**, *106*, 7177-7185.
(40) Yin, Y.; Alivisatos, A. P. *Nature* **2005**, *437*, 664-670.

(41) Talapin, D. V.; Rogach, A. L.; Shevchenko, E. V.; Kornowski, A.; Haase, M.; Weller, H. *J. Am. Chem. Soc.* **2002**, *124*, 5782-5790.
(42) Kudera, S.; Carbone, L.; Carlino, E.; Cingolani, R.; Cozzoli, P. D.; Manna, L. *Physica E: Low-dimensional Systems and Nanostructures* **2007**, *37*, 128-133.
(43) Yu, W. W.; Qu, L.; Guo, W.; Peng, X. *Chem. Mater.* **2003**, *15*, 2854-2860.
(44) Wehrenberg, B. L.; Wang, C.; Guyot-Sionnest, P. *The Journal of Physical Chemistry B* **2002**, *106*, 10634-10640.
(45) Chan, W. C. W.; Nie, S. *Science* **1998**, *281*, 2016.
(46) Gao, X.; Cui, Y.; Levenson, R. M.; Chung, L. W. K.; Nie, S. *Nat. Biotechnol.* **2004**, *22*, 969-976.
(47) Jaiswal, J. K.; Simon, S. M. *Trends Cell Biol.* **2004**, *14*, 497.
(48) Derfus, A. M.; Chan, W. C. W.; Bhatia, S. N. *Nano Lett.* **2004**, 4, 11-18.
(49) de Silva, A. P.; Gunaratne, H. Q. N.; Gunnlaugsson, T.; Huxley, A. J. M.; McCoy, C. P.; Rademacher, J. T.; Rice, T. E. *Chem. Rev.* **1997**, *97*, 1515-1566.
(50) Rurack, K. *Spectrochim. Acta, Part A* **2001**, *57*, 2161.
(51) Callan, J. F.; de Silva, A. P.; Magri, D. C. *Tetrahedron* **2005**, *61*, 8551-8588.
(52) Peters, K.; Avouris, P.; Rentzepis, P. M. *Biophys. J.* **1978**, *23*, 207-217.
(53) Wasielewski, M. R. *Chem. Rev.* **1992**, *92*, 435.
(54) Weller, A. *Pure Appl. Chem.* **1968**, *16*, 115-123.
(55) Bryan, A. J.; de Silva, A. P.; De Silva, S. A.; Rupasinghe, R. A. D. D.; Sandanayake, K. R. A. S. *Biosensors* **1989**, 4, 169-179.
(56) Bissell, R. A.; de Silva, A. P.; Gunaratne, H. Q. N.; Lynch, P. L. M.; Maguire, G. E. M.; Sandanayake, K. R. A. Samankumara *Chem. Soc. Rev.* **1992**, *21*, 187-195.
(57) Leray, I.; Lefevre, J.; Delouis, J.; Delaire, J.; Valeur, B. *Chem. Eur. J.* **2001**, 7, 4590.
(58) Grabchev, I.; Chovelon, J.; Qian, X. *New J. Chem.* **2003**, *27*, 337-340.

(59) Cooper, C. R.; James, T. D. *J. Chem. Soc. , Perkin Trans. 1* **2000**, , 963-969.

(60) Arimori, S.; Bell, M. L.; Oh, C. S.; Frimat, K. A.; James, T. D. *J. Chem. Soc., Perkin Trans. 1* **2002**, , 803-808.

(61) Gunnlaugsson, T.; Davis, A. P.; Glynn, M. *Chem. Commun.* **2001**, , 2556-2557.

(62) Gunnlaugsson, T.; Davis, A. P.; O'Brien, J. E.; Glynn, M. *Org. Lett.* **2002**, 4, 2449-2452.

(63) Gunnlaugsson, T.; Davis, A. P.; O'Brien, J. E.; Glynn, M. *Org. Biomol. Chem.* **2005**, 3, 48.

(64) Kavarnos, G. J.; Turro, N. J. *Chem. Rev.* **1986**, *8*6, 401.

(65) Fox, M. A.; Chanon, M. *Elsevier:Amsterdam* **1988**, Parts A-D.

(66) Kavarnos, G. J. In VCH, Weinheim, Eds.; New York, **1993**.

(67) www.fluorophores.org.

(68) de Silva, A. P.; Fox, D. B.; Huxley, A. J. M.; Moody, T. S. *Coord. Chem. Rev.* **2000**, *20*5, 41-57.

(69) Magri, D. C.; Callan, J. F.; de Silva, A. P.; Fox, A. P.; McClenaghan, N. D.; Sandanayake, K. R. A. S. *J. Fluoresc* **2005**, *1*5, 769.

(70) Kagan, C. R.; Murray, C. B.; Nirmal, M.; Bawendi, M. G. *Phys. Rev. Lett.* **1996**, *7*6, 1517-1520.

(71) Willard, D. M.; Carillo, L. L.; Jung, J.; Van Orden, A. *Nano Lett.* **2001**, 1, 469-474.

(72) Medintz, I. L.; Clapp, A. R.; Mattoussi, H.; Goldman, E. R.; Fisher, B.; Mauro, M. J. *Naturematerials* **2003**, 2, 630-638.

(73) Clapp, A. R.; Medintz, I. L.; Mauro, J. M.; Fisher, B. R.; Bawendi, M. G.; Mattoussi, H. *J. Am. Chem. Soc.* **2004**, *12*6, 301-310.

(74) Goldman, E. R.; Medintz, I. L.; Whitley, J. L.; Hayhurst, A.; Clapp, A. R.; Uyeda, H. T.; Deschamps, J. R.; Lassman, M. E.; Mattoussi, H. *J. Am. Chem. Soc.* **2005**, *127*, 6744-6751.

(75) Anni, M.; Manna, L.; Cingolani, R.; Valerini, D.; Creti, A.; Lomascolo, M. *Appl. Phys. Lett.* **2004**, *8*5, 4169.

(76) Mamedova, N. N.; Kotov, N. A.; Rogach, A. L.; Studer, J. *Nano Letters* **2001**, 1, 281-286.

(77) Clapp, A. R.; Medintz, I. L.; Fisher, B. R.; Anderson, G. P.; Mattoussi, H. *J. Am. Chem. Soc.* **2005**, *127*, 1242-1250.

(78) Medintz, I. L.; Mattoussi, H. *Phys. Chem. Chem. Phys.* **2009**, *1*1, 17-45.
(79) Stryer, L.; Haugland, R. P. *Proc. Nat. Acad. Sci. U. S. A.* **1967**, *5*8, 719-726.
(80) Zhou, D.; Piper, J. D.; Abell, C.; Klenerman, D.; Kang, D. J.; Ying, L. *Chem. Commun.* **2005**, 4807-4809.
(81) Mitchell, G. P.; Mirkin, C. A.; Letsinger, R. L. *J. Am. Chem. Soc.* **1999**, *12*1, 8122-8123.
(82) Chen, C.; Cheng, C.; Lai, C.; Wu, P.; Wu, K.; Chou, P.; Chou, Y.; Chiu, H. *Chem. Commun.* **2006**, 263-265.
(83) Kunz, W.; Henle, J.; Ninham, B. W. *Curr. Opin. Colloid Interface Sci.* **2004**, 9, 19-37.
(84) Tomasulo, M.; Yildiz, I.; Raymo, F. M. *J. Phys. Chem. B* **2006**, *11*0, 3853-3855.
(85) Alivisatos, A. P. *J. Phys. Chem.* **1996**, *10*0, 13226.
(86) Spanhel, L.; Weller, H.; Henglein, A. *J. Am. Chem. Soc.* **1987**, *10*9, 6632-6635.
(87) Sharma, S. N.; Pillai, Z. S.; Kamat, P. V. *The Journal of Physical Chemistry B* **2003**, *107*, 10088-10093.
(88) Chen, Y.; Rosenzweig, Z. *Anal. Chem.* **2002**, *7*4, 5132-5138.
(89) Isarov, A. V.; Chrysochoos, J. *Langmuir* **1997**, *1*3, 3142-3149.
(90) Chen, J.; Zhu, C. *Analytica Chimica Acta* **2005**, *54*6, 147-153.
(91) Gattas-Asfura, K. M.; Leblanc, R. M. *Chem. Commun.* **2003**, , 2684.
(92) Xie, H.; Liang, J.; Zhang, Z.; Liu, Y.; He, Z.; Pang, D. *Spectrochim. Acta, Part A* **2004**, *6*0, 2527-2530.
(93) Bo, C.; Ping, Z. *Anal. Bioanal. Chem.* **2005**, *38*1, 986.
(94) Lai, H.; Yu, Y.; Zhong, P.; Wu, J. *Anal. Lett.* **2006**, *3*9, 1201.
(95) Sandros, M. G.; Gao, D.; Benson, D. E. *J. Am. Chem. Soc.* **2005**, *127*, 12198-12199.
(96) Yildiz, I.; Tomasulo, M.; Raymo, F. M. *Proc. Nat. Acad. Sci. U. S. A.* **2006**, *103*, 11457.
(97) Burda, C.; Green, T. C.; Link, S.; El-Sayed, M. *The Journal of Physical Chemistry B* **1999**, *103*, 1783-1788.
(98) Yildiz, I.; Raymo, F. M. *J. Mater. Chem.* **2006**, *1*6, 1118-1120.

(99) Ong, W.; Gomez-Kaifer, M.; Kaifer, A. E. *Org. Lett.* **2002**, 4, 1791-1794.

(100) Ong, W.; Kaifer, A. E. *J. Org. Chem.* **2004**, *6*9, 1383-1385.

(101) Cordes, D. B.; Gamsey, S.; Singaram, B. *Angew. Chem. Int. Ed.* **2006**, *4*5, 3829-3832.

(102) Banerjee, S.; Kar, S.; Santra, S. *Chem. Commun.* **2008**, , 3037-3039.

(103) Bronson, R. T.; Michaelis, D. J.; Lamb, R. D.; Husseini, G. A.; Farnsworth, P. B.; Linford, M. R.; Izatt, R. M.; Bradshaw, J. S.; Savage, P. B. *Org. Lett.* **2005**, 7, 1105-1108.

(104) Prodi, L.; Montalti, M.; Zaccheroni, N.; Bradshaw, J. S.; Izatt, R. M.; Savage, P. B. *Tetrahedron Lett.* **2001**, *4*2, 2941-2944.

(105) Uyeda, H. T.; Medintz, I. L.; Jaiswal, J. K.; Simon, S. M.; Mattoussi, H. *J. Am. Chem. Soc.* **2005**, *127*, 3870-3878.

(106) Bernardes, G. J. L.; Chalker, J. M.; Errey, J. C.; Davis, B. G. *J. Am. Chem. Soc.* **2008**, *13*0, 5052-5053.

(107) Heinelt, U.; Schultheis, D.; Jäger, S.; Lindenmaier, M.; Pollex, A.; Beckmann, H. S. g. *Tetrahedron* **2004**, *6*0, 9883-9888.

(108) Gunnlaugsson, T.; Davis, A. P.; Hussey, G. M.; Tierney, J.; Glynn, M. *Org. Biomol. Chem.* **2004**, 2, 1856-1863.

(109) Baramee, A.; Coppin, A.; Mortuaire, M.; Pelinski, L.; Tomavo, S.; Brocard, J. *Bioorg. Med. Chem.* **2006**, *1*4, 1294-1302.

(110) Fidesser, E.; Haider, N.; Jbara, S. *Arkivoc* **2001**, *5*, 133-139.

(111) Chittiboyina, A. G.; Venkatraman, M. S.; Mizuno, C. S.; Desai, P. V.; Patny, A.; Benson, S. C.; Ho, C. I.; Kurtz, T. W.; Pershadsingh, H. A.; Avery, M. A. *J. Med. Chem.* **2006**, *49*, 4072-4084.

(112) Tisato, F.; Refosco, F.; Mazzi, U.; Bandoli, G.; Nicolini, M. *J. Chem. Soc. , Dalton Trans.* **1987**, , 1693.

(113) Wang, D.; Behrens, A.; Farahbakhsh, M.; Gätjens, J.; Rehder, D. *Chem. Eur. J.* **2003,** *9*, 1805-1813.

(114) Asokan, S.; Krueger, K. M.; Alkhawaldeh, A.; Carreon, A. R.; Mu, Z.; Colvin, V. L.; Mantzaris, N. V.; Wong, M. S. *Nanotechnology* **2005**, *16*, 2000-2011.

(115) Chen, Y.; Ji, T.; Rosenzweig, Z. *Nano Lett.* **2003**, *3*, 581-584.

(116) Williams, A. T. R.; Winfield, S. A.; Miller, J. N. *Analyst* **1983**, *108*, 1067-1071.
(117) Lee, C.; Liu, D. *Appl. Surf. Sci.* **1996**, *92*, 519-525.
(118) Dimitrijevic, N. M.; Kamat, P. V. *J. Phys. Chem.* **1987**, *91*, 2096.
(119) Peng, Z. A.; Peng, X. *J. Am. Chem. Soc.* **2002**, *124*, 3343-3353.
(120) Streetman, B. G.; Banerjee, S. *Solid State electronic Devices (5th edition ed.)* **2000**, , 524.
(121) Yildiz, I.; Ray, S.; Benelli, T.; Raymo, F. M. *J. Mater. Chem.* **2008**, *18*, 3940-3947.
(122) Derfus, A. M.; Chan, W. C. W.; Bhatia, S. N. *Nano Lett.* **2004**, *4*, 11.
(123) Xia, Y.; Zhu, C. *Mater Lett* **2008**, *62*, 2103-2105.
(124) McNeil-Watson, F.; Tscharnuter, W.; Miller, J. *Colloids Surf. Physicochem. Eng. Aspects* **1998**, *140*, 53-57.
(125) Pons, T.; Medintz, I. L.; Mattoussi, H. *Colloidal Quantum Dots for Biomedical Applications* **2006**, *6096*, 281-290.
(126) Zimmer, J. P.; Kim, S.; Ohnishi, S.; Tanaka, E.; Frangioni, J. V.; Bawendi, M. G. *J. Am. Chem. Soc.* **2006**, *128*, 2526-2527.
(127) Pons, T.; Uyeda, H. T.; Medintz, I. L.; Mattoussi, H. *The Journal of Physical Chemistry B* **2006**, *110*, 20308-20316.
(128) Peng, X.; Wickham, J.; Alivisatos, A. P. *J. Am. Chem. Soc.* **1998**, *120*, 5343-5344.
(129) Peng, Z. A.; Peng, X. *J. Am. Chem. Soc.* **2001**, *123*, 1389-1395.
(130) Huang, C.; Liu, H.; Tsao, C.; Yin, L.; Chiu, S.; Chen, T. *Sensors Actuators B: Chem.* **2005**, *108*, 713-720.
(131) Wuister, S. F.; Swart, I.; van Driel, F.; Hickey, S. G.; de, M. D. *Nano Letters* **2003**, *3*, 503-507.
(132) Mattoussi, H.; Mauro, J. M.; Goldman, E. R.; Anderson, G. P.; Sundar, V. C.; Mikulec, F. V.; Bawendi, M. G. *J. Am. Chem. Soc.* **2000**, *122*, 12142-12150.
(133) Ji, X.; Naistat, D.; Li, C.; Orbulescu, J.; Leblanc, R. M. *Colloids and Surfaces B: Biointerfaces* **2006**, *50*, 104-111.
(134) Dubbois, L. H.; Nuzzo, R. G. *Annu. Rev. Phys. Chem* **1992**, *43*, 437.

(135) Zanchet, D.; Tolentino, H.; Martins Alves, M. C.; Alves, O. L.; Ugarte, D. *Chemical Physics Letters* **2000**, *323*, 167-172.
(136) Tomasulo, M.; Yildiz, I.; Kaanumalle, S. L.; Raymo, F. M. *Langmuir* **2006**, *22*, 10284-10290.
(137) Susumu, K.; Uyeda, H. T.; Medintz, I. L.; Mattoussi, H. *J. Biomed. Biotechnol.* **2007**, *2007*.
(138) Yildiz, I.; McCaughan, B.; Cruickshank, S. F.; Callan, J. F.; Raymo, F. M. *Langmuir* , **2009***, 25, 7090-7096*.
(139) Rosenthal, S. J.; Tomlinson, I.; Adkins, E. M.; Schroeter, S.; Adams, S.; Swafford, L.; McBride, J.; Wang, Y.; DeFelice, L. J.; Blakely, R. D. *J. Am. Chem. Soc.* **2002**, *124*, 4586-4594.
(140) Li, H.; Han, C.; Liang, Z. *J. Mater. Chem.* **2008**, *18*, 4543-4548.
(141) Kalyuzhny, G.; Murray, R. W. *The Journal of Physical Chemistry B* **2005**, *109*, 7012-7021.
(142) Wang, S.; Jarrett, B. R.; Kauzlarich, S. M.; Louie, A. Y. *J. Am. Chem. Soc.* **2007**, *129*, 3848-3856.
(143) Yu, W. W.; Chang, E.; Drezek, R.; Colvin, V. L. *Biochem. Biophys. Res. Commun.* **2006**, *348*, 781-786.
(144) Gerion, D.; Pinaud, F.; Williams, S. C.; Parak, W. J.; Zanchet, D.; Weiss, S.; Alivisatos, A. P. *The Journal of Physical Chemistry B* **2001**, *105*, 8861-8871.
(145) Crichton, R. R.; Lallemand, F.; Psalti, I. S. M.; Ward, R. J. **2008**, .
(146) Mattoussi, H.; Mauro, J. M.; Goldman, E. R.; Anderson, G. P.; Sundar, V. C.; Mikulec, F. V.; Bawendi, M. G. *J. Am. Chem. Soc.* **2000**, *122*, 12142-12150.
(147) Hirota, S.; Okumura, H.; Arie, S.; Tanaka, K.; Shionoya, M.; Takabe, T.; Funasaki, N.; Watanabe, Y. *J. Inorg. Biochem.* **2004**, *98*, 849-855.
(148) Berdanier, C. D. **1998**, .
(149) Beeching, N.; Dassanayake, A. *Medicine* **2007**, *35*, 49-53.
(150) Fernandez-Arguelles, M. T.; Jun Jin, W.; Costa-Fernandez, J. M.; Pereiro, R.; Sanz-Medel, A. *Anal. Chim. Acta* **2005**, *549*, 20-25.
(151) Koneswaran, M.; Narayanaswamy, R. *Sensors Actuators B: Chem.* , *In Press, Corrected Proof*.
(152) Xia, Y.; Zhu, C. *Analyst* **2008**, *133*, 928-932.

(153) Fabbrizzi, L.; Poggi, A. *Chem. Soc. Rev.* **1995**, *24*, 197.
(154) Irving, H.; Williams, R. J. P. *J. Chem. Soc.* **1953**, , 3192-3210.
(155) Liang, J. G.; Ai, X. P.; He, Z. K.; Pang, D. W. *Analyst* **2004**, *129*, 619.
(156) Susha, A. S.; Munoz Javier, A.; Parak, W. J.; Rogach, A. L. *Colloids Surf. , A: Physiochem. Eng. Aspects* **2006**, *281*, 40-43.
(157) Bottechia, O. L. *J. Braz. Chem. Soc.* **1998**, *9*, 515.
(158) www.ktf-split.hr/periodni/en/abc/kpt.html.
(159) Connors, A. K. In *Chemical Kinetics;* VCH Publishers: New York, **1990**; pp 281-283.
(160) de Silva, A. P.; Gunaratne, H. Q. N. *J. Chem. Soc. , Chem. Commun.* **1990**, *18*6, 14.
(161) de Silva, A. P.; Gunaratne, H. Q. N.; Lynch, P. L. M. *J. Chem. Soc. , Perkin Trans. 2* **1995**, , 685.
(162) Murray, R. K.; Granner, D. K.; Harper, H. A.; Mayes, P. A.; Rodwell, V. W. In Harper's illustrated biochemistry; **2003**; pp 82-85.
(163) Wu, S. T.; Pieper, G. M.; Salhany, J. M.; Eliot, R. S. *Biochemistry (N. Y.)* **1981**, *2*0, 7399-7403.
(164) Kanekiyo, Y.; Naganawa, R.; Tao, H. *Chem. Commun.* **2004**, , 1006-1007.
(165) Burrows, C. J.; Muller, J. G. *Chem. Rev.* **1998**, *9*8, 1109-1152.
(166) Raymo, F. M.; Yildiz, I. *Phys. Chem. Chem. Phys.* **2007**, 9, 2036.
(167) Balzani, V.; Venturi, M.; Credi, A. *In Molecular Devices and Machines, Wiley-VCH, Weinheim, Germany* **2003**, .
(168) www.malvern.com.
(169) Liu, Y. S.; Sun, Y.; Vernier, P. T.; Liang, C. H.; Chong, S. Y.; Gundersen, M. A. *J. Phys. Chem. C. Nanomater Interfaces* **2007**, *11*1, 2872-2878.
(170) Cheng, Y.; Gattas-Asfura, K. M.; Konka, V.; Leblanc, R. M. *Chem. Commun.* **2002**, *235*0.
(171) Xie, H. Y.; Liang, J. G.; Zhang, Z. L.; Liu, Y.; He, Z. K.; Pan, D. W. *Spectrochim. Acta, Part A* **2004**, *6*0, 2527.
(172) Chen, Y.; Rosenzweig, Z. *Anal. Chem.* **2002**, *7*4, 5132.
(173) Hayes, W. A.; Kim, H.; Yue, X.; Perry, S. S.; Shannon, C. *Langmuir* **1997**, *1*3, 2511-2518.

(174) Mehata, M. S.; Tripathi, H. B. *Journal of Luminescence* **2002**, *9*9, 47-52.

(175) Duke, R. M.; Gunnlaugsson, T. *Tetrahedron Letters* **2007**, *4*8, 8043-8047.

(176) Jaraba, M.; Rodríguez-Benot, A.; Guerrero, R.; del Castillo, D.; Martín-Malo, A.; Rodríguez, M.; Aljama, P. *Kidney Int.* **1998**, *5*4, S86-S91.

(177) Kirk, K. L. In *Biochemistry of the Halogens and Inorganic Halides;* Plenum Press: New York, **1991**; pp 58.

(178) Kleerekoper, M. *Endocrinol. Metab. Clin. North Am* **1998**, *2*7, 441-452.

(179) Schmidtchen, F. P.; Berger, M. *Chem. Rev.* **1997**, *9*7, 1609-1646.

(180) Gadre, S. R.; Koelmel, C.; Shrivastava, I. H. *Inorg. Chem.* **1992**, *3*1, 2279-2281.

(181) Jose, D. A.; Kumar, D. K.; Ganguly, B.; Das, A. *Tetrahedron Letters* **2005**, *4*6, 5343-5346.

(182) Kim, Y.; Kwak, H.; Lee, S. J.; Lee, J. S.; Kwon, H. J.; Nam, S. H.; Lee, K.; Kim, C. *Tetrahedron* **2006**, *6*2, 9635-9640.

(183) Gunnlaugsson, T.; Glynn, M.; Tocci (née Hussey), G. M.; Kruger, P. E.; Pfeffer, F. M. *Coordination Chemistry Reviews* **2006**, *25*0, 3094-3117.

(184) Bordwell, F. G.; Algrim, D. J.; Harrelson, J. A. *J. Am. Chem. Soc.* **1988**, *11*0, 5903-5904.

(185) Gunnlaugsson, T.; Kruger, P. E.; Lee, T. C.; Parkesh, R.; Pfeffer, F. M.; Hussey, G. M. *Tetrahedron Letters* **2003**, *4*4, 6575-6578.

(186) Callan, J. F.; Mulrooney, R. C.; Kamila, S.; McCaughan, B. *J. Fluoresc* **2008**, *1*8, 527-532.

(187) Costa-Fernandez, J. M.; Pereiro, R.; Sanz-Medel, A. *Trends Anal. Chem.* **2006**, *2*5, 207-218.

(188) Jun Jin, W.; Costa-Fernandez, J. M.; Pereiro, R.; Sanz-Medel, A. *Anal. Chim. Acta* **2004**, *52*2, 1-8.

(189) Sarkar, S. K.; Chandrasekharan, N.; Gorer, S.; Hodes, G. *Appl. Phys. Lett.* **2002**, *8*1, 5045-5047.

(190) Jun Jin, W.; Fernandez-Arguelles, M. T.; Costa-Fernandez, J. M.; Pereiro, R.; Sanz-Medel, A. *Chem. Commun.* **2005**, , 883-885.

(191) Landi, B. J.; Evans, C. M.; Worman, J. J.; Castro, S. L.; Bailey, S. G.; Raffaelle, R. P. *Materials Letters* **2006**, *6*0, 3502-3506.
(192) Singh, N.; Kaur, N.; Dunn, J.; Behan, R.; Mulrooney, R. C.; Callan, J. F. *European Polymer Journal* **2009**, *4*5, 272-277.
(193) Gunnlaugsson, T.; Davis, A. P.; O'Brien, J. E.; Glynn, M. *Org. Lett.* **2002**, 4, 2449-2452.
(194) Martinez-Manez, R.; Sancenon, F. *Chem. Rev.* **2003**, *10*3, 4419.
(195) Tsein, R. Y. *Am. J. Physiol.* **1992**, *26*3, C723.
(196) Bissell, R. A.; de Silva, A. P.; Gunaratne, H. Q. N.; Lynch, P. L. M.; Maguire, G. E. M.; McCoy, C. P.; Sandanayake, K. R. A. S. *Top. Curr. Chem.* **1993**, *16*8, 223.
(197) Czarnik, A. W. *Adv. Supramol. Chem.* **1993**, 3, 131.
(198) Czarnik, A. W. *Acc. Chem. Res.* **1994**, *2*7, 302.
(199) Palaniappan, K.; Hackney, S. A.; Liu, J. *Chem. Commun.* **2004**, *2*3, 2704.
(200) Gale, P., A.; Chen, Z.; Drew, M. G. B.; Heath, J. A.; Beer, P. D. *Polyhedron* **1998**, *17*, 405-412.
(201) Oton, F.; Tarraga, A.; Espinosa, A.; Velasco, M. D.; Molina, P. *J. Org. Chem.* **2006**, *7*1, 4590-4598.
(202) Pratt, M. D.; Beer, P. D. *Polyhedron* **2003**, *2*2, 649-653.
(203) Singh, N.; Kaur, N.; Dunn, J.; Behan, R.; Mulrooney, R. C.; Callan, J. F. *European Polymer Journal* **2009**, *4*5, 272-277.
(204) Fery-Forgues, S.; Delavaux-Nicot, B. *J. Photochem. Photobiol. , A* **2000**, *13*2, 137-159.
(205) Komatsu, H.; Citterio, D.; Fujiwara, Y.; Minamihashi, K.; Araki, Y.; Hagiwara, M.; Suzuki, K. *Org. Lett.* **2005**, 7, 2857.
(206) Schmittel, M.; Lin, H. W. *Angew. Chem. Int. Ed.* **2007**, *4*6, 893.
(207) Mikami, D.; Ohki, T.; Yamaji, K.; Ishihara, s.; Citterio, D.; Hagiwara, M.; Suzuki, K. *Anal. Chem.* **2004**, *7*6, 5726.
(208) Kaur, N.; Kumar, S. *Chem. Commun.* **2007**, , 3069.
(209) Kaur, N.; Kumar, S. *Tetrahedron Lett.* **2008**, *4*9, 5067.
(210) Komatsu, H.; Miki, T.; Citterio, D.; Kubota, T.; Shindo, Y.; Yoshiichiro, K.; Oka, K.; Suzuki, K. *J. Am. Chem. Soc.* **2005**, *12*7, 10798.
(211) Schiff, H. *annls. Chem.* **1864**, *13*1, 118.

(212) Dey, K. *J. Sci. Ind. Res.* **1974**, *3*3, 76-94.

(213) Costes, J. P.; Dahan, F.; Donnadieu, B.; Fernandez-Garcia, M. I.; Rodriguez-Douton, M. J. *Dalton Trans.* **2003**, *19*, 3776-3779.

(214) Coles, S. J.; Hursthouse, M. B.; Kelly, D. G.; Toner, A. J.; Walker, N. M. *J. Chem. Soc. , Dalton Trans.* **1998**, *20*, 3489-3494.

(215) Liang, Z.; Zhilian, L.; Gao, Y. *Tetrahedron Lett.* **2007**, *48*, 3587-3590.

(216) Bhardwaj, V. K.; Singh, N.; Hundal, M. S.; Hundal, G. *Tetrahedron* **2006**, *62*, 7878-7886.

(217) Bhardwaj, V. K.; Pannu, A. P. S.; Singh, N.; Hundal, M. S.; Hundal, G. *Tetrahedron* **2008**, *64*, 5384-5391.

(218) Bhardwaj, V. K.; Singh, N.; Hundal, M. S.; Hundal, G. *Tetrahedron* **2006**, *62*, 7878-7886.

(219) Grygołowicz-Pawlak, E.; Palys, B.; Biesiada, K.; Olszyna, A. R.; Malinowska, E. *Analytica Chimica Acta* **2008**, *625*, 137-144.

(220) Thery-Merland, F.; Methivier, C.; Pasquinet, E.; Hairault, L.; Pradier, C. M. *Sens. Actuators, B* **2006**, *114*, 223-228.

(221) Singh, N.; Kumar, M.; Hundal, G. *Inorg. Chim. Acta* **2004**, *357*, 4286-4290.

(222) Yuan, J.; Guo, W.; Yang, X.; Wang, E. *Anal. Chem.* **2009**, *81*, 362-368.

(223) Hu, D.; Wu, H.; Liang, J.; Han, H. *Spectrochimica Acta Part A: Molecular and Biomolecular Spectroscopy* **2008**, *69*, 830-834.

(224) Zhang, Y.; Kong, X.; Qu, Y.; Jing, P.; Zeng, Q.; Sun, Y.; Wang, A. Y.; Zhao, J.; Zhang, H. *J Lumin* , *In Press, Corrected Proof*.

(225) Gunnlaugsson, T.; Lee, C. T.; Parkesh, R. *Org. Biomol. Chem.* **2003**, 1, 3265-3267.

CHAPTER NINE

PUBLICATIONS

The following journal articles were published as a result of the work presented in this thesis:

1. J.F.Callan, A.P. deSilva, R.C. Mulrooney and B. M^{c} Caughan: *J. Incl. Phenom*. *Macrocyclic. Chem.*, **58**, 527, (2007). "Luminescent Sensing with Quantum Dots".

2. J.F. Callan, R.C. Mulrooney, S. Kamila and B. McCaughan: *J. Fluoresc.* **18**, 527, (2008). "Anion Sensing with Luminescent Quantum Dots- A Modular Approach Based on the Photoinduced Electron Transfer (PET) Mechanism."

3. J.F. Callan, R.C. Mulrooney and S. Kamila: *J. Fluoresc.* **18**, 1157-1161, (2008). "Luminescent Identification of ATP in Aqueous Solution using positively charged CdSe/ZnS Quantum Dots."

4. N. Singh, R.C. Mulrooney, N. Kaur and J.F. Callan: *Chem. Commun.* 4900, (2008) "A Nanoparticle Based Chromogenic Chemosensor for the Simultaneous Detection of Multiple Analytes". *Hot Paper*.

   Highlights of this paper in other media:

   1. *Chemical Science,* October 2008, Volume 12, C67 (reported by Z. Whitelock) "Quantum Leap in Chemical Sensing".
   2. Chemistry World, Volume 5, Number 12, page 28. "Quantum Leap in Chemical Sensing". Dec 2008.

5. R.C. Mulrooney, N. Singh, N. Kaur and J.F. Callan: *Chem. Commun.* 686, (2009) "An Off-On Fluorescent Sensor for Fluoride using Functionalised CdSe/ZnS Quantum Dots". DOI: 10.1039/b817569a.

6. J.F. Callan and R.C. Mulrooney: *Phys. Status Solidi C* ***6****, No. 4, 920–923 (2009)* "Luminescent Detection of Cu(II) Ions in Aqueous Solution Using CdSe And CdSe-ZnS Quantum Dots functionalized with Mercaptosuccinic Acid**."** DOI 10.1002/pssc.200880571.

Journal of Inclusion Phenomena and Macrocyclic Chemistry (2007) 58:257–262
DOI 10.1007/s10847-006-9152-8

Luminescent Sensing with Quantum Dots

JOHN F. CALLAN[1,*], A. P. DE SILVA[2], R. C. MULROONEY[1] and B. MC CAUGHAN[2]
[1]*School of Pharmacy, The Robert Gordon University, Aberdeen, Scotland, AB10 1FR, UK;* [2]*School of Chemistry, Queen's University of Belfast, Belfast, Northern Ireland, BT9 5AG, UK*

(Received: 1 September 2006; in final form: 27 September 2006)

Key words: quantum dots, sensors, semiconductor, nanocrystal, luminescence

Summary

This review highlights recent advances in the use of quantum dots (QD's) as luminescent sensors. The bulk of the study concentrates on systems that possess organic ligands bound to the surface of QD's. These ligands vary from low molecular weight thiols to larger molecules such as maltose binding protein. All have one thing in common: when a target analyte binds to the ligand/receptor, a perturbation of the system occurs, that registers itself as a change in the luminescence intensity of the QD. Two main mechanisms are prevalent in controlling the luminescent intensity in such systems. The first is Photoinduced Electron Transfer (PET) and the second energy transfer. This review looks at current sensors that operate by using these mechanisms. Two component systems are also investigated where a quencher is first added to a solution of the QD, followed by addition of the target analyte that interacts with the quencher to influence the luminescence intensity.

Introduction

Semiconducting nanocrystals, otherwise known as Quantum Dots (QD's) were first discovered in the early 1980's [1]. Since then, interest in QD's as alternatives to traditional organic dyes has increased dramatically. Their use has mainly been restricted to fluorescent labelling in biological environments [2–4], but recently more and more examples of QD based sensor systems can be found in the literature. The superior optical properties of QD's compared to organic dyes is the main attraction to the user. These include broad absorption spectra, higher quantum yields, reduced photobleaching, and narrow emission spectra without red tailing [3]. But the most endearing feature must be the size dependent nature of the emission wavelength. By controlling the growth of the nanocrystal the emission wavelength can be tailored. This, in addition to their broad absorption spectra means QD's of different sizes can all be excited with a single wavelength. The possible applications for such systems are many.

This review will be restricted to those examples where QD's have been incorporated into sensor systems. Primarily, the focus will be on those QD's with bound organic ligands and the selectivity they display towards metal ions and small organic molecules. The application of QD's as biolabels, and those sensors using phosphorescent emission will not be studied here but are covered elsewhere [5].

* Author for correspondence. E-mail: j.callan@rgu.ac.uk

Synthesis of QD's

Core QD synthesis

Typically, QD's consist of a group IIB metal, usually cadmium, combined with a chalcogenic element e.g. CdS, CdSe or CdTe [6]. The synthetic preparation normally involves the high temperature addition of a Cd^{2+} source ($CdMe_2$ or CdO) to a chalcogenic element (S, Se or Te) in a strongly co-ordinating solvent such as trioctylphosphine (TOP) or trioctylphosphine oxide (TOPO) [4]. The reaction time, temperature and metal to chalcogenide ratio can be varied to control the size of the nanocrystal and hence its spectral properties.

The pioneering work of Peng [7] in using CdO as an alternative to the highly toxic and pyrophoric $CdMe_2$ has no doubt been responsible for the increased willingness of scientists to synthesise QD's. The quality of the nanocrystals produced from this much easier and safer synthetic approach are comparable to those obtained from $CdMe_2$. In fact, QD's of various size's can now be prepared in undergraduate laboratories with simple apparatus in less than 1 h [8].

Core-shell synthesis

Core QD's usually require surface capping to produce materials with high quantum efficiencies. The reasons for surface capping are mainly to prevent aggregation of the QD's caused by steric hindrance or charge and to

passivate dangling bonds at the surface. Surface passivation involves coating the core QD with a substance that has a larger band gap such as ZnS. Modified thiols can also be used to cap the core and also provide an opportunity for structural modifications [9].

Size selective precipitation

Core and core-shell QD's are purified/isolated by centrifugation. First, the addition of a non-solvent to a colloidal suspension of the QD is required to induce flocculation. The flocculated suspension is then centrifuged and the nanocrystal collected as the solid. This procedure is repeated if necessary.

Ligand exchange

In order to tailor the physical properties of QD's to their desired use i.e. as biolabels or sensors, the surface ligands (TOP/TOPO) must be exchanged with ligands of suitable functionality. Surface ligand displacement normally occurs by heating a solution of the desired ligand with the Core QD/Core-Shell QD. The ligand usually bears a pendant thiol group for surface attachment although amines and alcohols have also been used. For biolabelling purposes the new ligand will also contain functionality that permits attachment to the intended target and encourages water solubility [5, 10]. Where chemosensing is the aim, the design is even more crucial. The new ligand must not only provide a receptor for the target but it has to be designed in such a way that the binding event causes a perturbation of the QD fluorescence. To date, several systems have been designed that use PET, inner filtering (or competitive absorption) effects and Forster Resonance Energy Transfer (FRET) mechanisms to report the binding event.

QD sensing systems

Sensors based on energy transfer

Quantum dots have been utilised effectively as either donors or acceptors in Forster Resonance Energy Transfer (FRET) based luminescent sensors. Their broad absorption spectra make them ideal energy acceptors. Chen *et al.* [11] cleverly devised a CdSe/ZnS dual QD system to measure K^+ ion at the μM level in aqueous solution (**1**). Two different sized quantum dots were employed: a 3.2 nm (em = 545 nm) QD served as the energy donor and a 5.6 nm (em = 635 nm) particle as the energy acceptor. To each was bound a 15-crown-5 receptor using a lipoic acid linker. The crown ether showed selectivity for K^+ and formed a QD (545 nm):K^+:QD (635 nm) sandwich complex upon addition of the metal ion. Formation of the complex resulted in the different sized quantum dots coming close enough together to engage in energy transfer. A ratiometric response was therefore realised upon increasing levels of K^+, the emissions at 545 nm and 635 nm decreasing and increasing respectively. Of course QD (545 nm):K^+:QD (545 nm) and QD (635 nm):K^+:QD (635 nm) complexes are also possible but are statistically less probable (25% each) than the mixed size complex (50%).

The ability of the benzoxazine **2** to convert to the hemiaminal **3** on addition of hydroxide ion was used to develop a CdSe/ZnS QD sensor sensitive to pH [12]. The benzoxazine was again linked to the QD using lipoic acid. In acidic medium **2** shows an absorption band centred at 375 nm which is lost on addition of hydroxide ion and replaced by a band centred at 574 nm by its conversion to **3** (Figure 1). The absorbance maxima of **3** at 574 nm, overlaps well with the emission wavelength of the QD (555 nm). Therefore, the QD acts as an energy donor for **3** and an estimation of solution pH is determined by a reduction in the QD emission. The photoluminescence (PL) of the QD-2 conjugate can be recovered upon addition of trifluoroacetic acid, clearly demonstrating the reversibility of the system. However, the requirement of chloroform as the solvent leads to obvious restrictions.

The addition of Maltose Binding Protein (MBP) to CdSe/ZnS QD's has been used to sense for the disaccharide maltose [13] and the explosive TNT [14]. MBP was bound to a CdSe QD via an oligohistidine tag (**4**), and in the absence of maltose the fluorescence was quenched by addition of an energy accepting non-fluorescent dye bonded to *β*-cyclodextrin. The cyclodextrin sugar binds to the central binding pocket of MBP, and the QD emission quenched by FRET to the dye. Addition of maltose ejects the cyclodextrin–dye complex from the binding pocket by competitive displacement and the fluorescence is restored (**5**). A similar strategy was employed in the detection of TNT. Anti-TNT specific antibody fragments (scFvs) were again attached to the CdSe–ZnS QD's via an oligohistidine sequence. The dye-labelled TNT analogue **6**, binds to the scFv binding/recognition site and quenches QD fluorescence by FRET as before. Addition of TNT (**7**) displaces its dye-labelled analogue, the FRET channel is removed, and fluorescence is recovered.

Sensors based on photoinduced electron transfer (and other mechanisms)

The Photoinduced Electron Transfer (PET) mechanism is central to the design of many luminescent sensors with organic fluorophores [15, 16]. PET has also been used to influence the fluorescence emission of quantum dots. Addition of *p*-phenylenediamine (PPD) to a colloidal solution of CdSe quantum dots resulted in quenching of the fluorescence emission [17]. Upon excitation, PPD (E_{ox} 0.26 eV) reduces a hole in the valence band of the CdSe QD, (band gap 1.2 eV) thus disrupting the radiative recombination process of the electron-hole pair. Addition of *n*-butylamine (E_{ox} > 1.9 eV) was shown to enhance the fluorescence emission by passivation of

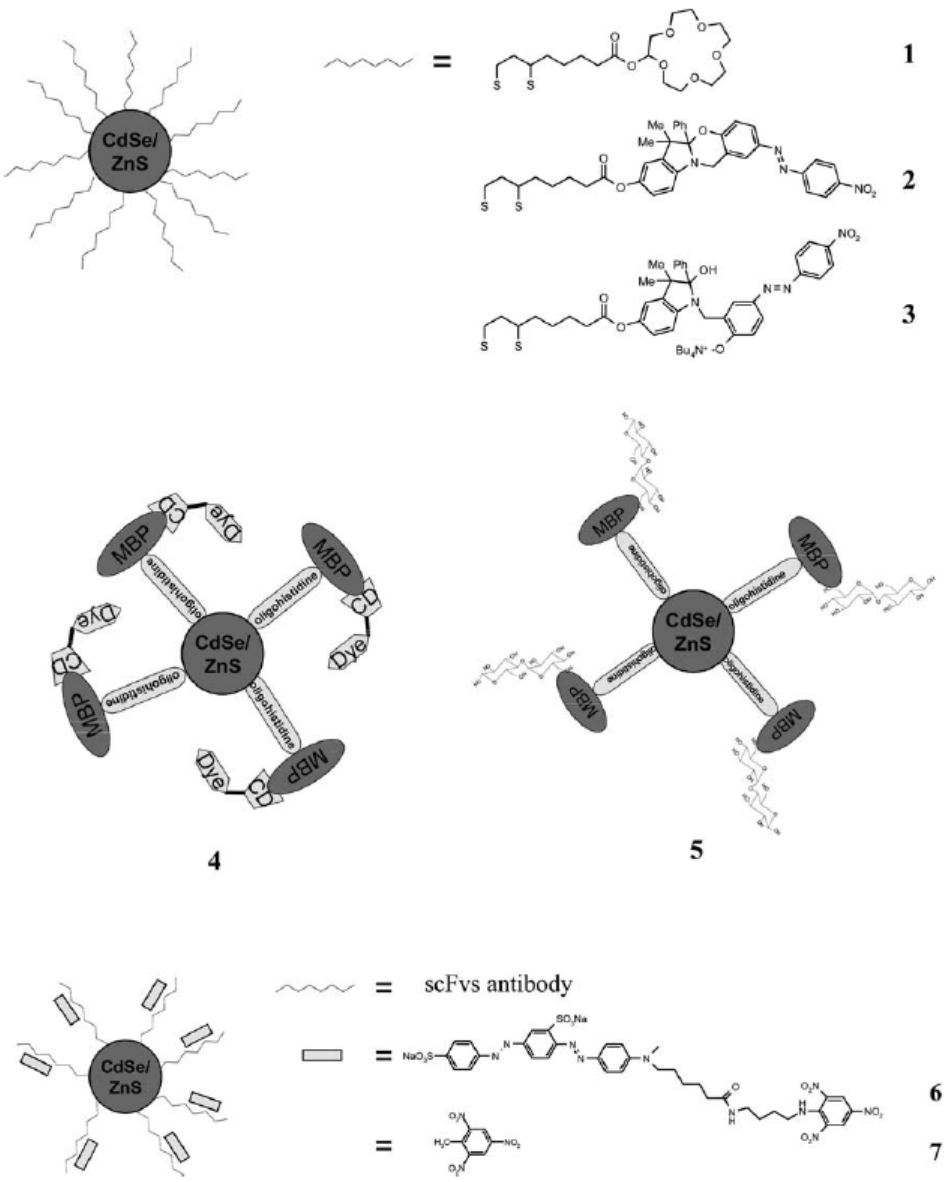

surface trap sites. However, other studies have shown the same reagent to quench fluorescence by acting as a hole acceptor [18, 19].

A quenching effect was also observed when the neurotransmitter serotonin was bound to CdSe QD's (**8**) via its phenolic group [20]. Distancing the neurotransmitter from the QD shell by the addition of a spacer restored the fluorescent emission.

CdS QD's, with perthiolated β-cyclodextrin ligands (**9**) attached to the surface were used by Palaniappan *et al*. [21] to demonstrate a redox controlled "On-Off-On" switching behaviour in aqueous solution. In the absence of analyte, the natural fluorescence of the CdS QD is observed. Addition of the redox active ferrocene quenches the fluorescence most likely by PET to the QD. Fluorescence emission is restored on addition of adamantane carboxylic acid, which, being a better fit for the hydrophobic cyclodextrin cavity ejects the offending ferrocene. The CdS QD used displayed a low luminescence efficiency which was improved upon in a subsequent study by utilising CdSe–CdS core-shell QD's [22]. Calixarenes have also been bound to CdSe–ZnS QD's, however no selectivity for any particular analyte was observed [23].

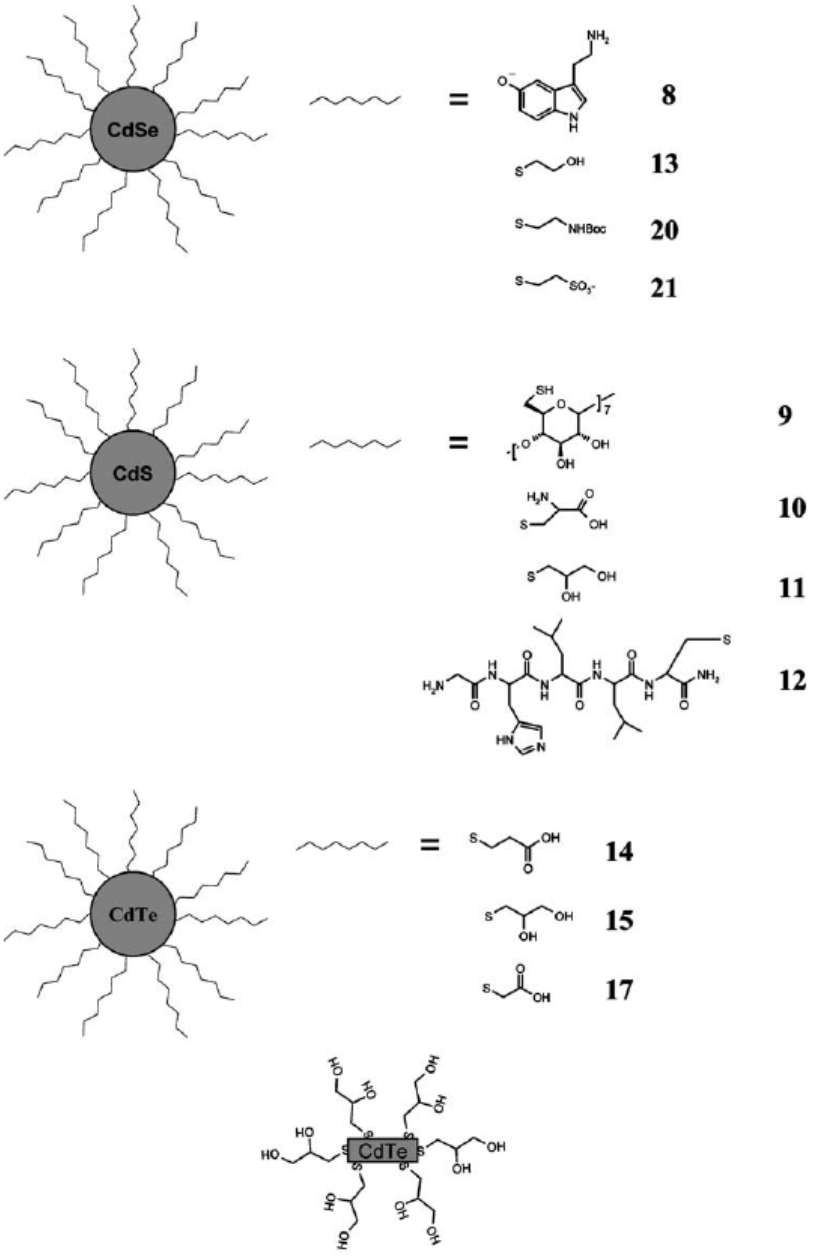

16

The amino acid L-cysteine has been bound to CdS QD's in more than one study (**10**). Chen and Rosenzweig [24], who were first to demonstrate that QD-organic ligand conjugates could be used as quantitative reporters of ion concentration, found that addition of Zn^{2+} ion increased the fluorescence intensity of the CdS-cysteine QD's. Chen and Zhu [25] found the same system to demonstrate selectivity for Ag^{+}, this ion not being tested in the former study. Both systems "switched on" fluorescence on addition of analyte. Chen and Rosenzweig also used thioglycerol as a ligand (**11**) which demonstrated selectivity for Cu^{2+}. Binding Cu^{2+}

resulted in a quenching and a red shift of luminescence emission, attributed to effective electron transfer from the thioglycerol to the Cu^{2+}.

Gattas-Asfura and Leblanc [26] showed that the addition of short peptides to the CdS QD surface resulted in fluorescence being "switched off" in the presence of Ag^{+} and Cu^{2+}. The peptide sequence Gly-His-Leu-Leu-Cys showed the best selectivity of those tested (**12**). The Leu-Leu unit was incorporated to provide a hydrophobic sheath to prevent both the metal ions and the basic histidine residue from interfering with the surface of the QD. The Gly-His dipeptide was selected as it previously demonstrated selectivity for Cu^{2+} [27]. Again electron transfer is the likely culprit for the fluorescent quenching, although the visible spectrum of Cu^{2+} means energy transfer is also possible.

The protein Bovine Serum Albumin (BSA) has been bound to CdSe–ZnS QD's and was shown to display selectivity for Cu^{2+} [28]. The CdSe–ZnS BSA conjugate's luminescence was quenched on addition of Cu^{2+} and Fe^{3+} ions in aqueous solution. The quenching of the latter was attributed to an inner filter effect and was cancelled by addition of fluoride ions to form the colourless FeF_6^{3-} complex. The quenching effect of Cu^{2+} was attributed to a surface displacement of Cd^{2+} ions from the surface of the QD by Cu^{2+} ions. The driving force behind this exchange was the increased solubility of CdSe compared to CuSe in the aqueous solvent. CdSe/CdS QD's coated with mercaptoethanol ligands (**13**) [29] and CdTe QD's with mercaptopropionic acid ligands (**14**) [30] also displayed similar quenching effects with Cu^{2+} (Figure 2).

A striking difference in sensitivity was observed between thioglycerol capped CdTe quantum dots and nanorods [31]. Although the same core shell – ligand system was used, the QD's (**15**) demonstrated only a 4% increase in luminescence on addition of Zn^{2+}, compared to a 68% increase for the nanorods (**16**). The selectivity of these particular compounds were poor however, with calcium ion also increasing luminescence, while the addition of manganese, nickel and cobalt ions resulted in luminescence quenching.

CdTe QD's, capped with thioglycolic acid have been prepared by Susha *et al.* [32] and tested for selectivity against a range of metal ions in aqueous solution. No great selectivity was observed but the results were interesting nonetheless. Small amounts (2×10^{-6} to 5×10^{-5} M) of Mg^{2+} and Ca^{2+} led to a 20–40% enhancement of luminescence which was quenched three fold by an increase in the concentration range of between 5×10^{-5} and 5×10^{-4} M. Further increases in concentration had no effect on the luminescence intensity. Both Ag^{+} and Fe^{2+} proved to be very efficient quenchers of the QD fluorescence, the mechanism again most likely being electron transfer from the QD reducing Fe^{2+} to Fe^{+} and Ag^{+} to Ag^{0}. This same study also investigated the effect of pH on the fluorescent emission of the CdTe QD's. No effect on the luminescence intensity was observed on addition of base from pH 12 to pH 6, after which a linear decrease was observed from pH 6 to pH 4, resulting in a 90% quenching of fluorescence.

As mentioned previously, Maltose Binding Protein (MBP) was used in the construction of the FRET sensor **4** for the detection of maltose. The improved maltose sensor prepared by Sandros *et al.* [33, 34] is based on a PET mechanism. A metallothionein protein-MBP conjugate (MT-MBP) was orthogonally bonded to both a CdSe–ZnS QD and a Ru(II) complex. The geometry is such that in the absence of maltose, the Ru(II) complex is close enough to the QD to participate in PET and quench luminescence by reduction of a hole in valence band. On addition of maltose, a lever-action conformational change increases the "through space" distance between the Ru(II) complex and the QD, resulting in a cancellation of the PET process and concomitant increase in luminescence intensity is observed. This same study investigated the effect of the ZnS shell on the efficiency of the PET process but found only a slight increase in luminescence intensity on addition of maltose to the CdSe QD's compared to the CdSe–ZnS system. This system has an advantage over **4** as it is a reagentless system, in so far as it does not require the addition of a cyclodextrin–dye complex to achieve luminescence quenching.

Another example of a two component system similar to **4** was employed by Cordes *et al.* for the detection of glucose [35]. Here, a boronic acid substituted viologen (**18**) acts as a quencher/receptor. When added to an aqueous solution of CdSe/ZnS QD's coated with surface amine groups, it quenches luminescence due to PET from the excited QD to the substituted viologen. This type of quenching behaviour has been demonstrated before with methyl viologen [36], but the boronic acid substituted version showed a significant fluorescence re-enhancement upon the addition of D-Glucose, due to the formation of the boronate (**19**) (Figure 3). No selectivity data was provided against other physiological relevant monosaccharides, and the fluorescent enhancement was modest in the physiological range, but again this illustrates that receptors used in traditional organic based sensors can prove effective with QD's also.

Sensing for the toxic and environmentally important cyanide ion has been achieved by Jin *et al.* [37, 38] using

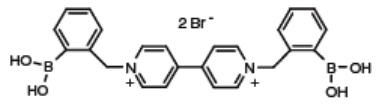

18

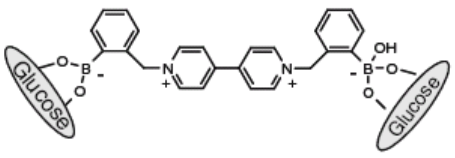

19

CdSe QD's. Their initial attempt using N-Boc cysteamine as the ligand (**20**), although successful in quantitatively determining cyanide ion concentration at μM levels, required methanol as the solvent. This was subsequently improved upon using the water soluble 2-mercaptosulfonate ligand (**21**). Both demonstrated a quenching of fluorescence on addition of CN^-.

Conclusion

This review highlighted some of the recent examples of QD-sensor systems based primarily on electron and energy transfer mechanisms. Still in its infancy in terms of sensor research, QD's could some day be as common as, or even supersede organic dyes as the prevalent signalling unit in luminescent sensing systems. The synthesis and chemical adaptability of QD's is becoming more straightforward and offers increasing variability to the chemist. However, it still remains a challenge to produce cheap, robust well functioning QD sensor that are suitable for *in vivo* applications. Nonetheless, if progress continues to be as rapid as it has been in the last 5 years, then the future looks very promising indeed.

References

1. A.I. Ekimov, A.L. Efros, and A.A. Onushchenko: *Solid State Commun.* **56**, 921 (1985); L.E. Brus: *J. Chem. Phys.* **79**, 566, (1983); A.L. Efros: *Sov. Phys. Semicond.* **16**, 722 (1982); A.I. Ekimov and A.A. Onushchenko: *Sov. Phys. Semicond.* **16**, 755 (1982).
2. W.J. Parak, T. Pellegrino, and C. Plank: *Nanotechnology* **16**, R9 (2005); X. Michalet, F.F. Pinaud, L.A. Bentolila, J.M. Tsay, S. Doose, J.J. Li, A.M. Wu, S.S. Gambir, and S. Weiss: *Science* **307**, 538 (2005); B.N.G. Giepmans, S.R. Adams, M.H. Ellisman, and R.Y Tsein: *Science* **312**, 217 (2006).
3. J.K. Jaiswal and S.M Simon: *Trends Cell Biol.* **14**, 497 (2004).
4. M. Green: *Curr. Op. Solid State Mater. Sci.* **6**, 355 (2002).
5. J.M. Costa-Fernadez, R. Pereiro, and Sanz-Medel: *Trends Anal. Chem.* **25**, 207 (2006).
6. The reader should be aware that other, lower temperature methods have also been used to prepare both CdS and CdTe QD's. For examples of thiol capped CdS QD's see refs 18 and 19 and for thiol capped CdTe QD's see: N. Gaponik *et al.*: *J. Phys. Chem. B* **106**, 7177 (2002).
7. Z.A. Peng and X.G. Peng: *J. Am. Chem. Soc.* **123**, 183 (2001).
8. E.M. Boatman and G.C. Lisensky: *J. Chem. Edu.* **82**, 1697 (2005).
9. A.L. Rogash, A. Kornowski, M. Gao, A. Eychmuller, and Weller: *J. Phys. Chem. B.* **103**, 3065 (1999).
10. W.C.W. Chan and S. Nie: *Science* **281**, 2016 (1998).
11. C.Y. Chen, C.T. Cheng, C.W. Lai, P.W. Wu, K.C. Wu, P.T. Chou, Y.H. Chou, and H.T. Chiu: *Chem. Commun.* **263** (2006).
12. M. Tomasulo, I. Yildiz, and F.M. Raymo: *J. Phys. Chem. B.* **110**, 3853 (2006).
13. I.L. Medintz, A.R. Clapp, H. Mattoussi, E.R. Goldman, B. Fisher, and J.M. Mauro: *Nat. Mater.* **2**, 630 (2003).
14. E.R. Goldman, I.L. Medintz, J.L. Whitely, A. Hayhurst, A.R. Clapp, H. Tetsuo Uyeda, J.R. Deschamps, M.E. Lassman, and H. Mattoussi: *J. Am. Chem. Soc.* **127**, 6744 (2005).
15. A.P. de Silva, H.Q.N Gunaratne, T. Gunnlaugsson, A.J.M. Huxley, C.P. Mc Coy, J.T. Rademacher, and T.E. Rice: *Chem. Rev.* **97**, 1515 (1997).
16. J.F. Callan, A.P. de Silva, and D.C. Magri: *Tetrahedron* **61**, 8551 (2005).
17. S.N. Sharma, Z.S. Pillai, and P.V. Kamat: *J. Phys. Chem. B* **107**, 10088 (2003).
18. C. Landes, C. Burda, M. Braun, and M.A. El-Sayed: *J. Phys. Chem. B* **105**, 2981 (2001).
19. C.J. Murphy and J.L. Coffer: *Appl. Spectrosc.* **56**, 16A (2002).
20. S.J. Rosenthal, I. Tomlinson, E.M. Adkins, S. Schroeter, S. Adams, L. Swafford, J. McBride, Y. Wang, L.J. DeFelice, and R.D. Blakely: *J. Am. Chem. Soc.* **124**, 4586 (2002).
21. K. Palaniappan, S.A. Hackney, and J. Liu: *Chem. Commun.* 2704 (2004).
22. K. Palaniappan, C. Xue, G. Arumugam, S.A. Hackney, and J. Liu: *Chem. Mater.* **18**, 1275 (2006).
23. T. Jin, F. Fujii, H. Sakata, M. Tamura, and M. Kinjo: *Chem. Commun.* 2829 (2005).
24. Y. Chen and Z. Rosenzweig: *Anal. Chem.* **74**, 5132 (2002).
25. J.L. Chen and C.Q. Zhu: *Anal. Chim. Acta.* **546**, 147 (2005).
26. K.M. Gattas-Asfura and R.M. Leblanc: *Chem. Commun.* **2684** (2003).
27. Y. Cheng, K.M. Gattas-Asfura, V. Konka, and R.M. Leblanc: *Chem. Commun.* **2350** (2002).
28. H.Y. Xie, J.G. Liang, Z.L. Zhang, Y. Liu, Z.K. He, and D.W. Pan: *Spectrochim. Acta A* **60**, 2527 (2004).
29. H. Lai, Y. Yu, P. Zhong, and J. Wu: *Anal. Lett.* **39**, 1201 (2006).
30. C. Bo and Z. Ping: *Anal. Bioanal. Chem.* **381**, 986 (2005).
31. J. Li, D. Bao, X. Hong, D. Li, J. Li, Y. Bai, and T. Li: *Colloids Surf. A* **257–258**, 267 (2005).
32. A.S. Susha, A.M. Javier, W.J. Parak, and A.L. Rogash: *Colloids Surf. A* **281**, 40 (2006).
33. M.G. Sandros, V. Shete, and D.E. Benson: *Analyst* **131**, 229–235 (2006).
34. M.G. Sandros, D. Gao, and D.E. Benson: *J. Am.Chem. Soc.* **127**, 12198 (2005).
35. D.B. Cordes, S. Gamsey, and B. Singaram: *Angew Chem. Int. Ed.* **45**, 3829 (2006).
36. S. Logunov, T. Green, S. Marguet, and M.A. El-Sayed: *J. Phys. Chem. A* **102**, 5652, (1998); Y. Nosaka, H. Miyama, M. Terauchi, and T. Kobayashi: *J. Phys. Chem.* **92**, 255 (1988); D. Duonghong, E. Borgarello, and M. Gratzel: *J. Am. Chem. Soc.* **103**, 4685 (1981); D. Ishii, K. Kinbara, Y, Ishida, M. Okochi, M. Yohda, and T. Aida: *Nature* **423**, 628, (2003).
37. W.J. Jin, J.M. Costa-Fernandez, R. Pereiro, and A. Sanz-Medel: *Anal. Chim. Acta.* **522**, 1 (2004).
38. W.J. Jin, M.T. Fernandez-Arguelles, J.M. Costa-Fernandez, R. Pereiro, and A. Sanz-Medel: *Chem. Commun.* 883 (2005).

J Fluoresc (2008) 18:527–532
DOI 10.1007/s10895-007-0295-9

ORIGINAL PAPER

Anion Sensing with Luminescent Quantum Dots – A Modular Approach Based on the Photoinduced Electron Transfer (PET) Mechanism

John F. Callan · Ray C. Mulrooney · Sukanta Kamila · Bridgeen McCaughan

Received: 23 October 2007 / Accepted: 19 November 2007 / Published online: 20 December 2007

Abstract A CdSe–ZnS quantum dot (QD) has been surface functionalised with 1-(2-mercapto-ethyl)-3-phenyl-thiourea in the fluorophore–spacer–receptor format typical of Photoinduced Electron Transfer (PET) based organic dye sensors. The resulting QD conjugate was tested for selectivity toward the tetrabutylammonium salts of fluoride, chloride, bromide, hydrogen sulfate and acetate. Addition of fluoride, chloride and acetate ions resulted in an approximate 90% quenching of the original fluorescence intensity, while bromide and hydrogen sulfate had almost no effect. The observed quench was attributed to an increase in the reduction potential of the receptor upon anion binding resulting in an increase in PET from the excited QD to the receptor and a concomitant reduction in fluorescence intensity. The selectivity and sensitivity were comparable to an analagous organic dye based sensor where a similar receptor was bound to an anthracene fluorophore. Thus a modular approach is evident where a receptor used in an organic dye based sensor can be adapted and successfully used with QD's.

Keywords Quantum dots · Photoinduced electron transfer · Thiourea · Anions · Luminescent · Sensor

Introduction

Since their discovery in the early 1980s, luminescent Quantum Dots (QDs) have rapidly emerged as viable alternatives to organic dyes for use in bio-labelling applications [1–3]. Their high quantum yields, reduced susceptibility to photobleaching, broad absorption spectra and size-dependent emission spectra make them ideal for use in this type of environment. However, their development as the signalling unit in luminescent sensors has not been as rapid. Among the current approaches to sensing with QDs, Forster Resonance Energy Transfer (FRET) based systems have found greatest success [4–7]. Although examples do exist of QD sensors that operate using an electron transfer mechanism, these are primarily for re-dox active transition metals [8–13], involve elaborate conformational manipulations in their design [14, 15] or are two component systems where a quencher is first added to a solution of the QD followed by the addition of an analyte [16]. Quite recently though, Raymo and co-workers have demonstrated a pH dependent "Off – On" switching QD – oxazine conjugate, where modulation of the oxidation potential of the oxazine was shown to be responsible for the luminescent switching behaviour of the QD [17]. Inspired by this we have designed a QD based sensor for anions according to the Photoinduced Electron Transfer (PET) design principle. PET based sensing is well established with organic dyes and proves popular as its modular nature offers a degree of simplicity and predictability [18–26]. The application of this design principle to QDs would provide the opportunity for many more QD based probes, thereby taking advantage of their superior optical properties. We have adopted the Fluorophore-Spacer-Receptor format of PET systems to generate the first reported example of a PET operated QD probe for anions (Fig. 1). Gunnlaugsson *et al* have previously shown that charge neutral thiourea's were useful receptors for anions when bound to an anthracene fluorophore in a PET format [27]. Therefore we selected 1-(2-mercapto-ethyl)-3-phenyl-thiourea as receptor and bound it to the surface of a

J. F. Callan (✉) · R. C. Mulrooney · S. Kamila · B. McCaughan
School of Pharmacy, The Robert Gordon University,
Aberdeen, Scotland AB10 1FR, UK
e-mail: j.callan@rgu.ac.uk

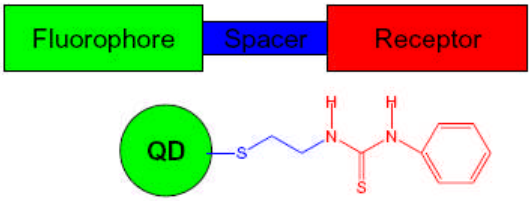

Fig. 1 Schematic representation of the fluorophore – spacer – receptor format of PET systems (*top*) and the analogous QD – spacer – thiourea receptor conjugate used in the present study

green emitting CdSe–ZnS QD. The resulting QD-spacer-receptor conjugate was tested against the tetrabutylammonium salts of fluoride, chloride, bromide, hydrogen sulfate and acetate and the selectivity and sensitivity compared against its organic counterpart.

Experimental

Reagents and materials

All reagents were purchased from Aldrich at the highest quality available. CdSe–ZnS QDs were purchased from Evident technologies, New York (Product No. ED-C10-TOL-0545).

UV and fluorescence spectroscopy

Absorbance measurements were recorded on an Agilent UV–Vis Spectrometer using 10 mm quartz cuvettes. Fluorescence measurements were recorded on a Perkin Elmer LS55 Luminescence Spectrometer using 10 mm quartz cuvettes. Excitation wavelength unless otherwise stated was set at 370 nm. Excitation slit size was 10.0 nm and emission slit size was 10.0 nm. Scan speed was set at 500.

^{1}H and ^{13}C-NMR spectroscopy

All spectra were recorded on a Bruker Ultrasheild 400 MHz. ^{1}H NMR samples were prepared by dissolving 5 mg of sample in 1.0 mL of $CDCl_3$. ^{13}C NMR samples were prepared by dissolving 50 mg of the sample in 1 mL of $CDCl_3$. Chemical shifts are reported in parts per million (δ) downfield of TMS.

Synthesis of 1-(2-mercapto-ethyl)-3-phenyl-thiourea

To a solution of 2-aminoethanethiol (2.0 g, 26 mmol, 1 eq) in anhydrous chloroform (25 mL) was added phenyl isothiocyanate (3.13 mL, 26.3 mmol, 1.eq). The contents were stirred at room temperature for 18 h. The solvent was evaporated under reduced pressure yielding a white solid. This was triturated with diethyl ether (20 mL) and ethanol (50 mL) was added to the precipitate and the contents stirred for 30 min. The product was filtered under reduced pressure and washed with ethanol (50 mL) and dried in vacuo. The crude product was purified by dissolving in a hot solution of methanol/ethyl acetate and precipitating with cold hexane. Yield=2.49 g, 45.2%. ^{1}H NMR ($CDCl_3$) δ=7.66 (br.s, 1H, PhN*H*), 7.43 (dd, *J*=7.8 Hz, 4 Hz, 2H, aryl), 7.33 (dd, *J*=7.8 Hz, 4 Hz, 1H, aryl), 7.31 – 7.00 (m, 2H, aryl), 6.49 (br.s, 1H, $-CH_2NH$), 3.96 (q, *J*=4.0 Hz, 2H, $-SCH_2-$), 2.95 (t, *J*=6.0 Hz, 2H, $HNCH_2$). ^{13}C NMR ($CDCl_3$) δ, 180.91 (C, –C=S), 135.85 (CH), 130.28 (CH), 127.61 (C), 125.41 (CH), 43.85 (CH_2), 37.14 (CH_2). ESMS Expected: m/z 213 (M^+ + H), 445 (Disulfide + Na^+); Found: 445 (100%), 213 (10%), 211 (70%). Melting point=150 °C.

Ligand exchange reaction

The procedure developed by Tomasulo et al. was followed for ligand exchange [17]. A solution of CdSe/ZnS core

Scheme 1 Synthesis of QD-spacer receptor conjugate

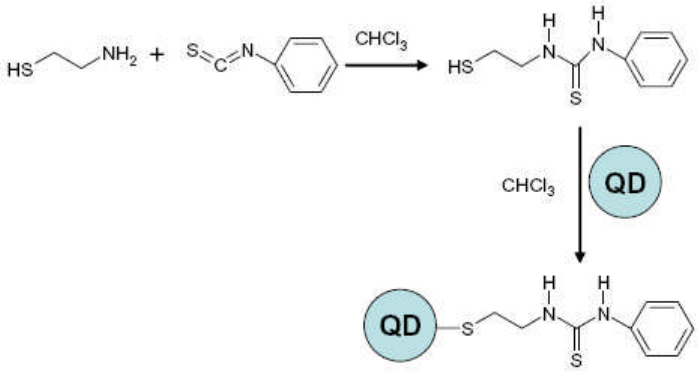

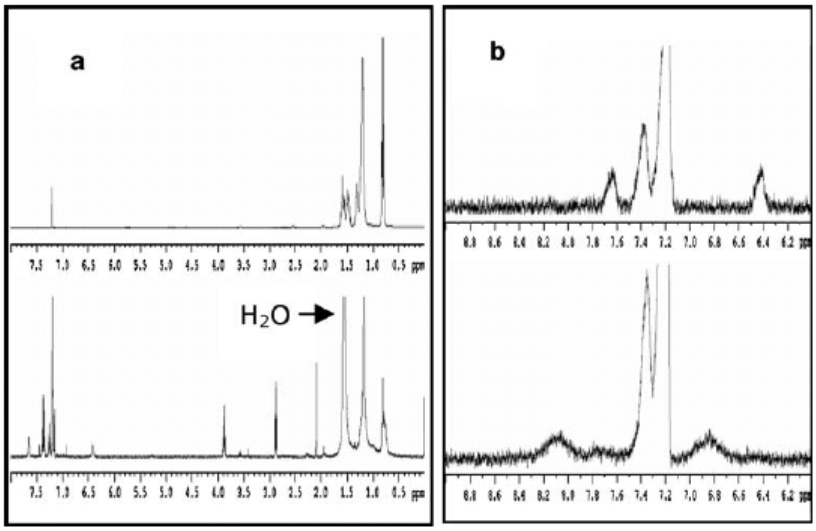

Fig. 2 a showing ^{1}H nmr spectra of the free QD (*top*), and the QD-ligand conjugate (*bottom*). b expansion of the receptor region showing free receptor (*top*) and after the addition of 1 eq of AcO^- (*bottom*). Both spectra recorded in $CDCl_3$ at 400 MHZ

shell QDs (0.5 mL, 0.027 mol) and 1-(2-mercapto-ethyl)-3-phenyl-thiourea (0.03 g, 150 mol) in chloroform (20 mL) was heated under reflux for 24 h. After cooling to ambient temperature, the solvent was removed under reduced pressure. The residue was suspended in acetonitrile (8 mL) and centrifuged at 12,500 rpm for 5 min. The centrifugation step was repeated three more times to afford the modified CdSe/ZnS core shell QDs as a yellow powder (0.015 g).

Results and discussion

The receptor, 1-(2-mercapto-ethyl)-3-phenyl-thiourea was synthesized in one step by reaction of phenylisothiocyanate and 2-aminoethanethiol (Scheme 1). The thiol terminated ethyl spacer permits anchorage to the nanoparticle fluorophore after refluxing in chloroform for 24 h. The nanoparticle chosen was a 2.4 nm CdSe/ZnS QD purchased from Evident Technologies [28]. The resulting QD-Spacer-Receptor conjugate was isolated by precipitation with acetonitrile [17].

Surface functionalisation was confirmed by ^{1}H nmr spectroscopy, Fig. 2a showing spectra of the free QD and the QD-Receptor conjugate. As observed in a previous study, the addition of the receptor does not displace all the ligands on the surface of the QD with shifts at 0.8 and 1.2 ppm representing the methyl and methylene protons respectively of trioctylphosphine (TOP), a strongly coordinating surfactant used in the synthesis of the core QD [4]. Clearly evident though are the urea protons, CH_2-N*H* and Ar-N*H* at 6.4 and 7.7 ppm, respectively, with the signals at 2.9 and 3.9 ppm representing the methylene protons for N-CH_2 and S-CH_2 respectively of the spacer. UV–Vis analysis before and after surface functionalization (Fig. 3) shows no difference in the visible region, the position of the

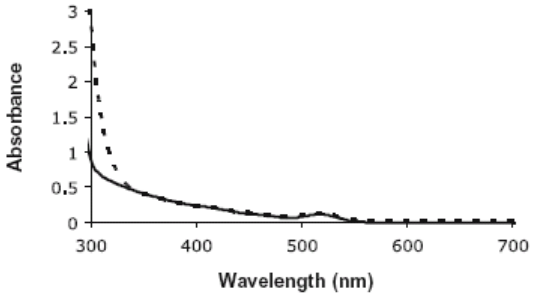

Fig. 3 UV trace of QD before (*solid line*) and after (*dashed line*) surface functionalisation with thiourea recorded in $CHCl_3$. Concentration = 1.81×10^{-6} M

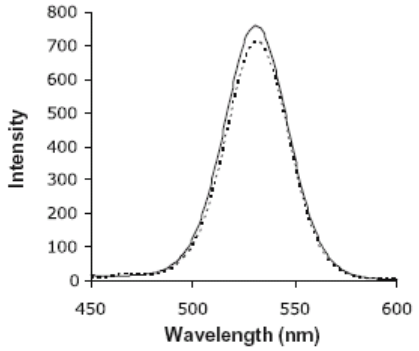

Fig. 4 Fluorescence Spectra of QD before (*dashed line*) and after (*solid line*) ligand exchange with 1-(2-mercapto-ethyl)-3-phenyl-thiourea

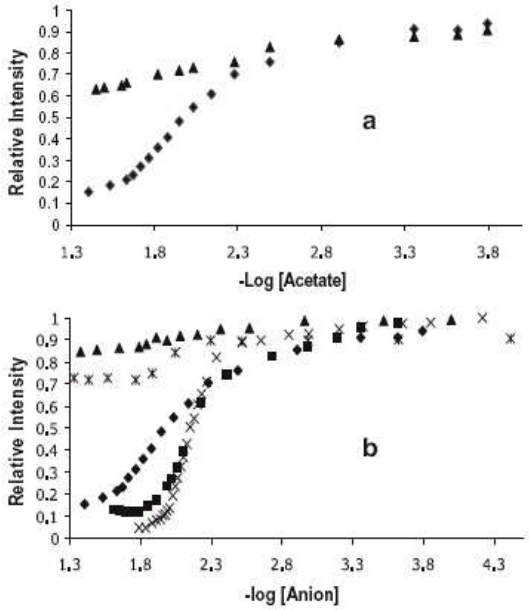

Fig. 5 a Plot of relative intensity against – log [acetate] for as received QDs (*filled triangle*) and the QD-receptor conjugate (*filled diamond*). [QD]=5.45×10^{-9}, [QD-Receptor]=7.96×10^{-9}; b plot of relative intensity against −log [anion] for Br^- (*filled triangle*), HSO_4^- (*), Cl^- (X), AcO^- (*filled diamond*) and F^- (*filled square*). [QD–Receptor]=7.96×10^{-9} M. All measurements conducted in $CHCl_3$

first exciton peak being unchanged at 516 nm. When the optical density was fixed at 0.1 for both samples at this wavelength a difference was observed at ~300 nm with the absorbance of the QD-receptor conjugate greater (2.9) than the QD alone (1.1). The increase in absorbance at this wavelength is due to absorbance by the phenyl choromophore (λ_{max}=264) of the receptor component.

Excitation of the QD-spacer–receptor conjugate at 370 nm resulted in emission at 540 nm, with little change in the profile compared to the parent QD (see Fig. 4), although the quantum yield (Φ) did drop from 0.38 to 0.33. This suggests a small degree of PET quenching even in the absence of anions [27, 29].

Table 1 Photophysical properties for sensor before and after the addition of anions

Sensor	Φ_F^a	$\%F_{red}^b$	Log β^c
Free sensor	0.334	–	–
F^-	0.042	87.3	2.15
Cl^-	0.015	95.4	2.15
Br^-	0.281	15.7	–
AcO^-	0.037	88.9	1.94
HSO_4^-	0.268	19.8	2.12

[a] Quantum yield calculated with reference to fluorescein
[b] % reduction in fluorescence spectral area
[c] Binding constant calculated from a plot of $-\log (F_{MAX}-F)/(F_{MIN}-F)$ against −log [onion]

The probe was then screened for selectivity against the tetrabutylammonium salts of AcO^-, F^-, Cl^-, Br^- and HSO_4^- in chloroform. A plot of relative intensity against −log [anion] is shown in Fig. 5b and reveals significant quenches for Cl^-, F^- and AcO^- with only minor changes observed for Br^- and HSO_4^-. In contrast, addition of these anions to a solution of the "as purchased" QDs (i.e. with no thiourea receptor attached) produced only minimal quenching (shown for AcO^- in Fig. 5a). This suggests anion binding to the thiourea receptor must be responsible for the modulation of the fluorescence output. To investigate this further we recorded the ^1H NMR spectrum of the QD – receptor upon addition of 1 equivalence of AcO^-. Anion-receptor binding was confirmed by changes in the chemical shift of the urea protons, with CH_2-N*H* moving downfield by 0.4 ppm to 6.8 ppm and Ar-N*H* by 0.5 to 8.1 ppm upon addition of 1 eq of AcO^- (Fig. 1b). In addition, these resonances become significantly broader after anion addition while the aromatic protons and the methylene protons of the spacer (not shown) remain unaffected. This data suggests a hydrogen bonding interaction between the acetate anion and thiourea protons of the receptor as depicted in Fig. 6a. In terms of a previously described model, the quenching effect by Cl^-, F^-, and AcO^- is a result of this hydrogen bonding interaction and leads to an increase in the reduction potential of the receptor, enhancing the rate of PET from the HOMO of the receptor to the QD [27, 30, 31]. This is

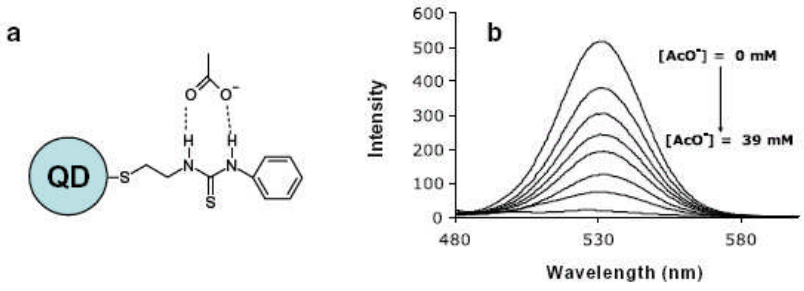

Fig. 6 a Schematic representation of QD-spacer-receptor on addition of acetate ion and b fluorescence spectra of QD-conjugate upon addition of increasing amounts of Acetate ion

opposite to typical PET sensing behavior where the oxidation potential of the receptor is raised upon analyte recognition, thus removing the thermodynamic driving force for PET and fluorescence is "Switched On" [17].

From Fig. 5b it can also be observed that acetate anions quench fluorescence less efficiently than fluoride or chloride over about 2 log units signifying a 1:1 binding [27]. The selectivity of the receptor for F^- and Cl^- over Br^- can be related the higher charge density of these ions enabling them to form strong hydrogen bonds with the receptor, although steric reasons may also play a part. Steric factors may also explain the selectivity for acetate over hydrogen sulfate, with the former able to form stronger linear hydrogen bonds [27].

The binding constants, Log β were calculated from equation 1 [32, 33] and the values are presented in Table 1.

$$-\log\left(F_{MAX}-F\right)/\left(F-F_{MIN}\right)=\mathrm{Log}[\mathrm{Anion}]+\mathrm{Log}\,\beta \quad (1)$$

where F_{MAX} is the maximum fluorescence intensity, F_{MIN} is the minimum fluorescence intensity and F the observed fluorescence intensity. The values compare favorably with those observed by Gunnlaugsson *et al* in their study into the ability of this ligand to sense anions when connected in a PET format to anthracene [27]. For example we find log β for AcO^- and F^- to be 1.94 and 2.15, respectively, compared to 2.15 and 2.90, respectively, found by them. The slight reduction in sensitivity observed by us may be due to an extra methylene unit in the spacer (which was included for synthetic convenience) reducing the effectiveness of PET, as PET efficiency has previously been shown to be distance dependent [34].

Conclusion

We have demonstrated for the first time that a receptor component from a PET based organic dye sensor can be adapted and used effectively with Quantum Dots. Thus, a modular approach is evident in which a tried and tested receptor from the literature can be modified slightly and used to produce a functioning QD sensor. Moreover, this approach should ensure that the selectivity and sensitivity of the receptor is retained but the enhanced optical properties offered by the QDs are utilized. We believe this approach could lead to a new generation of luminescent sensors.

Acknowledgement The authors would like to acknowledge financial assistance from RGU and the Leverhulme Trust UK.

References

1. Parak WJ, Pellegrino T, Plank C (2005) Labeling of cells with quantum dots. Nanotechnology 16:R9
2. Michalet X, Pinaud FF, Bentolila LA, Tsay JM, Doose S, Li JJ, Wu AM, Gambir SS, Weiss S (2005) Quantum dots for live cells, in vivo imaging, and diagnostics. Science 307:538
3. Giepmans BNG, Adams SR, Ellisman MH, Tsein RY (2006) The fluorescent toolbox for assessing protein location and function. Science 312:217
4. Chen CY, Cheng CT, Lai CW, Wu PW, Wu KC, Chou PT, Chou YH, Chiu HT (2006) Potassium ion recognition by 15-crown-5 functionalized CdSe/ZnS quantum dots in H_2O. Chem Commun 263–265
5. Tomasulo M, Yildiz I, Raymo FM (2006) pH-sensitive quantum dots. J Phys Chem, B 110:3853
6. Medintz IL, Clapp AR, Mattoussi H, Goldman ER, Fisher B, Mauro JM (2003) Self-assembled nanoscale biosensors based on quantum dot FRET donors. Nat Matters 2:630
7. Goldman ER, Medintz IL, Whitely JL, Hayhurst A, Clapp AR, Uyeda HT, Deschamps JR, Lassman ME, Mattoussi H (2005) A hybrid quantum dot-antibody fragment fluorescence resonance energy transfer-based TNT sensor. J Am Chem Soc 127:6744
8. Gattas-Asfura KM, Leblanc RM (2003) Peptide-coated CdS quantum dots for the optical detection of copper(II) and silver(I). Chem Commun 21:2684–2685
9. Cheng Y, Gattas-Asfura K, Konka V, Leblanc RM (2002) A dansylated peptide for the selective detection of copper ions. Chem Commun 20:2350–2351
10. Xie HY, Liang JG, Zhang ZL, Liu Y, He ZK, Pan DW (2004) Luminescent CdSe–ZnS quantum dots as selective Cu^{2+} probe. Spectrochim Acta, A 60:2527
11. Lai H, Yu Y, Zhong P, Wu J (2006) Development of novel quantum dots as fluorescent sensors for application in highly sensitive spectrofluorimetric determination of Cu^{2+}. Anal Lett 39:1201
12. Bo C, Ping Z (2005) A new determining method of copper(III) ions at ng per ml levels based on quenching of the water-soluble nanocrystals fluorescence. Anal Bioanal Chem 381:986
13. Chen Y, Rosenzweig Z (2002) Luminescent CdS quantum dots as selective ion probes. Anal Chem 74:5132
14. Sandros MG, Shete V, Benson DE (2006) Selective, reversible, reagentless maltose biosensing with core-shell semiconducting nanoparticles. Analyst 131:229
15. Sandros MG, Gao D, Benson DE (2005) A modular nanoparticle-based system for reagentless small molecule biosensing. J Am Chem Soc 127:12198
16. Cordes DB, Gamsey S, Singaram B (2006) Fluorescent quantum dots with boronic acid substituted viologens to sense glucose in aqueous solution. Angew Chem, Int Ed 45:3829
17. Tomasulo M, Yildiz I, Kaanumalle SL, Raymo FM (2006) pH-sensitive ligand for luminescent quantum dots. Langmuir 22:10284
18. Tsien RY (1992) Intracellular signal transduction in 4 dimensions – from molecular design to physiology. Am J Physiol 263:C723
19. Bissell RA, de Silva AP, Gunaratne HQN, Lynch PLM, Maguire GEM, McCoy CP, Sandanayake KRAS (1993) Fluorescent PET (phoroinduced electron transfer) sensors. Top Curr Chem 168:223
20. Czarnik AW (1994) Chemical communication in water using fluorescent chemosensors. Acc Chem Res 27:302
21. Fabbrizzi L, Poggi A (1995) Sensors and switches from supramolecular chemistry. Chem Soc Rev 24:197
22. de Silva AP, Gunaratne HQN, Gunnlaugsson T, Huxley AJM, McCoy CP, Rademacher JTR, Rice TE (1997) Signaling recognition events with fluorescent sensors and switches. Chem Rev 97:1515
23. Fabbrizzi L, Licchelli M, Pallavicini P (1999) Transition metals as switches. Acc Chem Res 32:846
24. Fabbrizzi L (2000) The design of luminescent sensors for anions and ionisable analytes. Coord Chem Rev 205:1
25. de Silva AP, McClean GD, Moody TS, Weir SM (2003) Handbook of photochemistry and photobiology. American Scientific, Stevenson Ranch, CA, pp 217

26. Callan JF, de Silva AP, Magri DC (2005) Luminescent sensors and switches in the early 21st century. Tetrahedron 61:8551
27. Gunnlaugsson T, Davis AP, Hussey GM, Tierney J, Glynn M (2004) Design, synthesis and photophysical studies of simple fluorescent anion sensors using charge neutral thiourea receptors. Org Biomol Chem 2:1856
28. See http://www.evidenttech.com/nanomaterials/evidots/quantum-dot-research-materials.php
29. Magri DC, Callan JF, de Silva AP, Fox DB, McClenaghan ND, Sandanayake KRAS (2005) The anthracen-9-ylmethoxy unit: an underperforming motif within the fluorescent PET (Photoinduced Electron Transfer) sensing framework). J Fluoresc 15:769
30. Gunnlaugsson T, Davis AP, O'Brien JE, Glynn M (2005) Synthesis and photophysical evaluation of charge neutral thiourea or urea based PET sensors for bis-carboxylates and pyrophosphate. Org Biomol Chem 3:48
31. Martinez-Manez R, Sancenon F (2003) Fluorogenic and chromogenic chemosensors and reagents for anions. Chem Rev 103:4419
32. de Silva AP, Gunaratne HQN (1990) Fluorescent PET (Photoinduced Electron Transfer) sensors selective for submicromolar calcium with quantitatively predictable spectral and ion-binding properties. J Chem Soc, Chem Commun 186:14
33. de Silva AP, Gunaratne HQN, Lynch PLM (1995) Luminescence and charge transfer.4. On-Off fluorescent PET (Photoinduced Electron Transfer) sensors with pyridine receptors-1,3-Diaryl-5-pyridyl-4,5-dihyropyrazoles. J Chem Soc Perkin Trans 2:685
34. Balzani V, Venturi M, Credi A (2003) Molecular devices and machines. Wiley-VCH, Weinheim, Germany

J Fluoresc (2008) 18:1157–1161
DOI 10.1007/s10895-008-0367-5

ORIGINAL PAPER

Luminescent Detection of ATP in Aqueous Solution Using Positively Charged CdSe–ZnS Quantum Dots

John F. Callan · Ray C. Mulrooney · Sukanta Kamila

Received: 16 January 2008 / Accepted: 14 March 2008 /Published online: 25 April 2008

Abstract Commercially available CdSe–ZnS Quantum Dots (QDs) have been modified by exchanging the hydrophobic surface ligands with (2-mercaptoethyl)-trimethylammonium chloride. The resulting water soluble conjugate was titrated with solutions of adenosine triphosphate (ATP), adenosine diphosphate, adenosine monophosphate, guanosine triphosphate (GTP), guanosine diphosphate and guanosine monophosphate in 0.01 M 4-(2-hydroxyethyl)-1-piperazineethanesulfonic acid buffer (pH 7.4). A strong fluorescence quench of about 80% was observed for ATP, a quench of 25% was observed for GTP while the others had virtually no effect. The quenching effect of ATP and GTP was attributed to the high negative charge density associated with these substrate's resulting in a strong attraction to the QD surface enabling them to engage in electron transfer with the excited QD. The lack of fluorescence quenching associated with the other nucleotides was most likely due to their reduced charge density resulting in a lower affinity for the QD surface.

Keywords Quantum dots · Fluorescence · ATP · Nucleotides

Introduction

Semiconducting nanocrystals, also known as Quantum Dots (QDs), have recently emerged as a new class of luminophore and offer many advantages over traditional organic dyes, such as broader absorption spectra, narrow size dependent emission spectra and a reduced susceptibility to photobleach [1–4]. Although commercially sold as fluorescent tags for biomolecules, QDs have struggled to compete with their organic counterparts in a sensing arena. Our research is focussed on utilising QDs as the signalling unit in fluorescent sensors. Previously, we have demonstrated that a CdSe/ZnS QD, surface functionalised with a thiourea receptor, was effective at measuring anion concentration, such as acetate, by a quenching of fluorescent intensity [5]. Thioureas are charge neutral entities that bind anions through strong hydrogen bonds but tend to perform poorly in aqueous solution. Other common organic dye based anion receptors include positively charged species such as guanidinium groups or polyamine-Zn^{2+} complexes that tend to be more effective in aqueous solution [6]. Here, we design a simple, water soluble sensor based on a QD fluorophore for the detection of adenosine triphosphate (ATP). A charged quaternary ammonium group was used not only as a receptor but also to ensure aqueous solubility and was coordinated to the surface of a CdSe/ZnS QD via a thiol group. The oxidisability of guanine and adenine is well known as they have the lowest oxidation potentials among the nucleic acid bases [7]. CdSe QDs can be oxidised and reduced at relatively moderate potentials and can thus participate in electron transfer processes in a similar manner to organic dyes [8]. Therefore, our present design attempts to discriminate between nucleotides based on differences in their surface charge, which in turn modulates their attraction to the surface of the QD. Electron transfer efficiency is known to be distance dependant [9] and so only those nucleotides that are attracted close to the surface of the QD can participate in effective electron transfer.

The fluorescent discrimination of nucleotides by targeting differences in their charge is one approach that has been investigated [10–12]. For example, Kanekiyo et al. developed a "two component" approach which required the initial addition of a polycation to the nucleotide solution to enable the attraction of ATP to the polymer surface. A boronic acid functionalised pyrene sensor was then added

J. F. Callan (✉) · R. C. Mulrooney · S. Kamila
School of Pharmacy, The Robert Gordon University,
Aberdeen, Scotland AB10 1FR, UK
e-mail: j.callan@rgu.ac.uk

and formed a boronate ester with ATP at the polymer surface. This facilitated the self assembly of the pyrene units leading to a change from monomer to excimer emission upon binding. Addition of adenosine diphosphate (ADP) and adenosine monophosphate (AMP) resulted in reduced excimer formation as they did not bind as strongly to the polycationic surface. Progressing from this, we have designed a one component system where the cationic surface is inherent within the sensor design. This is the first reported example of a QD based fluorescent sensor for ATP and offers potential benefits over organic dye based ATP sensors due to the superior optical properties QDs offer.

Experimental

Reagents and chemicals

All reagents were purchased from Aldrich at the highest quality available. CdSe-ZnS QDs were purchased from Evident technologies, New York (Product No. ED-C10-TOL-0545).

Synthesis of (2-mercaptoethyl)-trimethylammonium iodide

To a solution of 2-dimethylamino-ethanethiol (1 g, 9.52 mmol, 1 eq) in anhydrous acetonitrile (10 mL) was added iodomethane (5.4 g, 38 mmol, 4 eq). The reaction was allowed to stir at room temperature for 18 h after which time the product precipitated from solution. The product was collected by filtration, washed with cold acetonitrile and dried in vacuo at 50 °C. Yield=2.3 g, 49.7%. ^{1}H nuclear magnetic resonance (NMR; D_2O) δ ppm=3.62 (m, 2H, NCH_2), 3.08 (s, 9H, 3 x CH_3), 3.06 (m, 2H, HSCH_2). ^{13}C NMR (D_2O) δ ppm=66.2 (HSCH_2), 53.0 (CH_3), 29.7 (CH_2N).

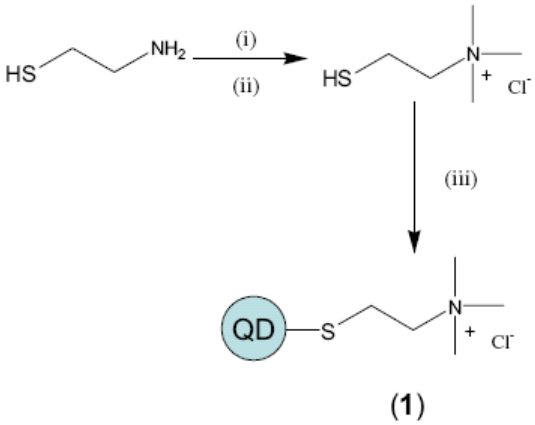

Scheme 1 Synthesis of QD-Receptor *1* (*i*) methyl iodide, dry DCM, 18 h, 25 °C. (*ii*) amberlite ion exchange resin. (*iii*) CdSe/ZnS QDs, MeOH, pH 10.0, 6 h

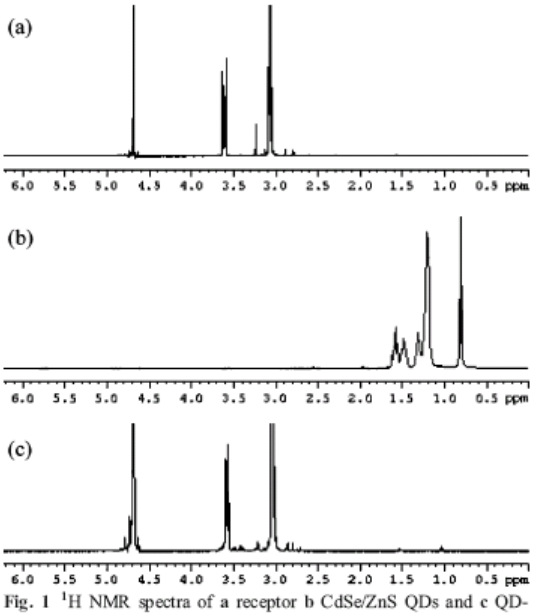

Fig. 1 ^{1}H NMR spectra of a receptor b CdSe/ZnS QDs and c QD-receptor conjugate. Spectra a and c were recorded in D_2O and spectrum b in $CHCl_3$, 400 MHz

Ion exchange

(2-Mercaptoethyl)-trimethylammonium iodide (1 g, 4.0 mmol) was dissolved in deionised water (100 mL). Amberlite resin (30 g) was paced into a separating funnel and washed with 2 M HCl (~200 mL). When all the HCl had drained from the resin, deionised water was flushed through until the pH had neutralised. The (2-mercaptoethyl)-trimethylammonium iodide iodide solution was washed through the resin a total of three times. The collected solution was concentrated to about one-half its original volume on a rotary evaporator. The product was then obtained by freeze drying. Yield=0.49 g, 77.7%.

Synthesis of *1*

To a solution of (2-mercaptoethyl)-trimethylammonium chloride (0.06 g, 386 μmol), dissolved in anhydrous methanol (45 mL) was added CdSe/ZnS QDs (2 mL, 108 nmol). The pH was adjusted to 10.5 with the aid of tetrabutylammonium hydroxide and the reaction heated under reflux for 5 h. After cooling, the solution was concentrated to about one third of its original volume and treated with diethyl ether (100 mL) to precipitate the product. The supernatant was carefully decanted off and the remaining solution centrifuged for 5 min at 13,500 rpm.

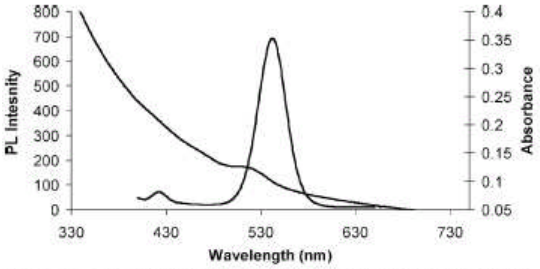

Fig. 2 Absorbance and fluorescence spectra of *1*. Fluorescence spectra recorded after excitation at 370 nm. [*1*]=1.0×10^{-5} M for absorbance measurements and 3.5×10^{-6} M for fluorescence measurements

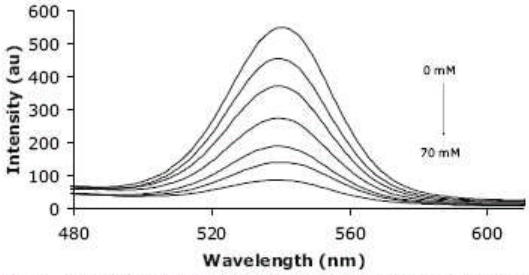

Fig. 4 Plot of fluorescence intensity against wavelength for *1* upon increasing addition of ATP. [1]=3.5×10^{-6} M, excitation wavelength= 370 nm

The pellet was redissolved in methanol, precipitated from ether and centrifuged a further two times. The resulting product was dried in vacuo for 18 h.

UV-vis and fluorescence analysis

Absorbance measurements were recorded on an Agilent UV-Vis Spectrometer using 10 mm quartz cuvettes. Fluorescence measurements were recorded on a Perkin Elmer LS55 Luminescence Spectrometer using 10 mm quartz cuvettes. Excitation wavelength unless otherwise stated was set at 370 nm. Excitation slit size was 10 nm and emission slit size was 10 nm. Scan speed was set at 500.

^{1}H NMR analysis

^{1}H and ^{13}C NMR spectra were recorded on a Bruker 400 MHz spectrometer. Chemical shifts are reported downfield of trimethylsilane.

Zeta potential determination

Zeta potential measurements were recorded in aqueous solution at 25 °C on a Malvern NanoZS zetasizer calibrated against polystyrene latex.

Results and discussion

Synthesis of receptor ligand and incorporation onto CdSe–ZnS surface

The synthetic scheme adopted for the synthesis of the charged receptor ligand and its attachment to the surface of the QD is shown in Scheme 1. The receptor was synthesized in one step by the direct *N*-alkylation of 2-dimethylamino-ethanethiol with iodomethane. An aqueous solution of the receptor was then passed through an ion exchange resin to exchange the iodide for chloride to prevent potential quenching by the heavy atom effect. Surface attachment of the ligand to the QD surface was performed at pH 10 to ensure generation of the thiolate. The ^{1}H NMR spectra of the free ligand, the free QD and the QD-ligand conjugate (*1*) are shown in Fig. 1. The S-CH_2-protons of the receptor were observed at 3.08 ppm while the $-CH_2$–N– and N–$(CH_3)_3$ protons were observed together at 3.60 ppm (Fig. 1a). The spectrum of the free QD shows the methyl and methylene protons of trioctyl-phosphine oxide (TOPO), the strongly coordinating surfactant used in the synthesis of the core QD, at 0.8 and 1.2 ppm respectively (Fig. 1b). After the ligand exchange reaction, these signals disappear almost completely as

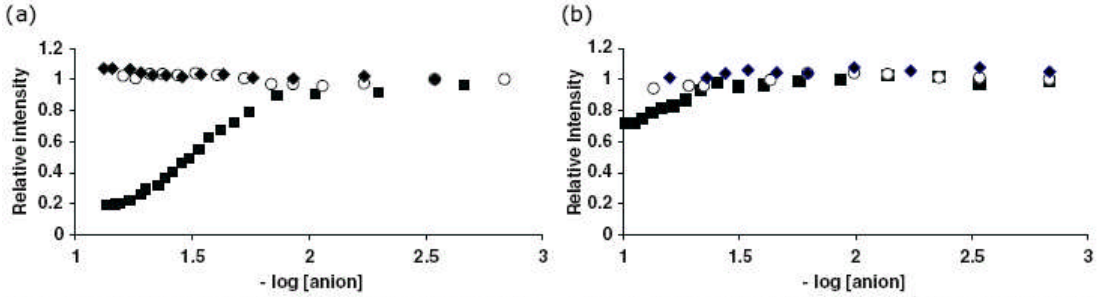

Fig. 3 Plot of relative fluorescence intensity against −log [anion] for a *1* titrated with AMP (*empty circle*), ADP (*filled diamond*) and ATP (*filled square*) and b *1* titrated with GMP (*empty circle*), GDP (*filled diamond*), GTP (*filled square*). [*1*]=3.5×10^{-6}, 0.1 M HEPES at pH 7.4, excitation wavelength=370 nm

shown in the spectrum of *1* (Fig. 1c). As expected however, the signals from the receptor remain and are relatively unaffected in terms of chemical shift. This confirms an almost complete exchange of the TOPO ligands for (2-mercaptoethyl)-trimethylammonium chloride. The zeta potential of an aqueous solution of the QD-receptor conjugate was +56 mV/mol, which was similar in magnitude but opposite in sign to a solution of QDs whose surface TOPO groups were exchanged for dihydrolipoic acid (zeta potential −61 mV/mol; Callan JF et al., unpublished work).

Photophysical properties of the QD-ligand conjugate

The UV-Vis and fluorescent spectra for *1* are shown in Fig. 2. The position of the first exciton peak, centred at 519 nm, enables calculation of the particle diameter which was found to be 2.55 nm [13]. When excited at 370 nm, *1* displayed an emission maxima centred at 542 nm, highlighting the large Stokes shifts possible with these nanoparticles.

Figure 3a shows a plot of relative fluorescence intensity against –log[anion] for ATP, ADP and AMP recorded in 0.1 M 4-(2-hydroxyethyl)-1-piperazineethanesulfonic acid solution at pH 7.4. Addition of ATP causes a 80% reduction of the original fluorescence intensity over about one log unit, while ADP and AMP has virtually no effect. The binding constant Log β for ATP, calculated from Eq. 1 was found to be 1.87 [14, 15].

$$-\log\ (F_{\mathrm{MAX}} - F)/F - F_{\mathrm{MIN}} = \log[\mathrm{Anion}] + \log\ \beta \qquad (1)$$

where F_{MAX} is the maximum fluorescence intensity, F_{MIN} is the minimum fluorescence intensity and F the observed fluorescence intensity.

Figure 3b shows a similar plot for guanosine triphosphate (GTP), guanosine diphosphate (GDP) and guanosine monophosphate (GMP). Again the mono- and di-phosphates produce virtually no quenching of the original fluorescence intensity. Surprisingly, addition of GTP resulted in only a 25% quench over the same concentration range as ATP. This quenching of fluorescence is most likely due to an electron transfer from the nucleotides to the excited QD, as has been observed before when other QD-ligand conjugates were exposed to electron rich analytes [16]. The reason for the enhanced quenching efficiency of ATP with respect to GTP is unclear and was not expected, as guanine has a lower oxidation potential than adenine (1.29 and 1.42 V vs normal hydrogen electrode respectively) [7]. The overall trend of increasing fluorescence intensity with decreased analyte charge suggests the extent of attraction between nanoparticle surface and analyte is responsible for modulation of the fluorescence output within each series of nucleotide.

A plot of fluorescence intensity of *1* against increasing concentrations of ATP is shown in Fig. 4. No change in the fluorescence λ_{MAX} was observed upon the addition of ATP, indicating that the substrate is neither affecting the nanoparticle surface nor causing sample aggregation.

Conclusions

We have produced the first reported example of a water soluble QD based fluorescent probe for ATP. By targeting differences in substrate charge the sensor was able to identify ATP among other nucleotides with good selectivity. The attractive interaction between the negatively charged ATP and the positively charged QD was sufficient to bring the two close enough so that an electron transfer mediated quench of fluorescence was observed. The reduced negative charge associated with ADP and AMP resulted in reduced attraction with the nanoparticle surface and a reduced quenching of the QD fluorescence. Similarly GTP displayed greater quenching than GDP or GMP but markedly less than ATP. More work is ongoing in this laboratory to gain a fuller understanding of this interaction.

Acknowledgements The authors acknowledge financial support from the Robert Gordon University and the Leverhulme Trust UK.

References

1. Parak WJ, Pellegrino T, Plank C (2005) Labeling of cells with quantum dots. Nanotechnology 16:R9
2. Michalet X, Pinaud FF, Bentolila LA, Tsay JM, Doose S, Li JJ, Wu AM, Gambir SS, Weiss S (2005) Quantum dots for live cells, in vivo imaging, and diagnostics. Sci 307:538
3. Giepmans BNG, Adams SR, Ellisman MH, Tsein RY (2006) The fluorescent toolbox for assessing protein location and function. Science 312:217
4. Callan JF, de Silva AP, Mulrooney RC, McCaughan B (2007) Luminescent sensing with quantum dots. J Incl Phenom Macrocyclic Chem 58:527
5. Callan JF, Mulrooney RC, Kamila S, McCaughan B (2008) Anion sensing with luminescent quantum dots—a modular approach based on the photoinduced electron transfer (PET) mechanism. J Fluoresc 18:527–532 DOI 10.1007/s10895-007-0295-9
6. Martinez-Manez R, Sancenon F (2003) Fluorogenic and chromogenic chemosensors and reagents for anions. Chem Rev 103:4419
7. Burrows CJ, Muller JG (1998) Oxidative nucleobase modifications leading to strand scission. Chem Rev 98:1109
8. Raymo FM, Yilidiz I (2007) Luminescent chemosensors based on semiconductor quantum dots. Phys Chem Chem Phys 9:2036
9. Balzani V, Venturi M, Credi A (2003) Molecular devices and machines. Wiley-VCH, Weinheim
10. Kanekiyo Y, Naganawa R, Yao H (2004) Fluorescence detection of ATP based on the ATP-mediated aggregation of pyrene-appended boronic acid on a polycation. Chem Commun 2004: 1006

11. Schneider SE, O'Neil SN, Anslyn EV (2000) Coupling rational design with libraries leads to the production of an ATP selective chemosensor. J Am Chem Soc 122:542
12. Ojida A, Park S, Mito-oka Y, Hamachi I (2002) Efficient fluorescent ATP-sensing based on coordination chemistry under aqueous neutral conditions. Tetrahedron Lett 43:6193
13. Yu WW, Qu L, Guo W, Peng X (2003) Experimental determination of the extinction coefficient of CdTe, CdSe and CdS nanocrystals. Chem Mater 15:2854
14. de Silva AP, Gunaratne HQN (1990) Fluorescent PET (photoinduced electron transfer) sensors selective for submicromolar calcium with quantitatively predictable spectral and ion-binding properties. J Chem Soc Chem Commun 186:14
15. de Silva AP, Gunaratne HQN, Lynch PLM (1995) Luminescence and charge transfer.4. On–off fluorescent PET (photoinduced electron transfer) sensors with pyridine receptors-1, 3-diaryl- 5-pyridyl-4,5-dihyropyrazoles. J Chem Soc Perkin Trans 2:685
16. Palaniappan K, Hackney SA, Liu J (2004) Supramolecular control of complexation-induced fluorescence change of water-soluble, beta-cyclodextrin-modified CdS quantum dots. Chem Commun 2004:2704

A nanoparticle based chromogenic chemosensor for the simultaneous detection of multiple analytes†

Narinder Singh, Ray C. Mulrooney, Navneet Kaur and John F. Callan*

Received (in Cambridge, UK) 4th August 2008, Accepted 3rd September 2008
First published as an Advance Article on the web 15th September 2008
DOI: 10.1039/b813423e

Quantum Dot–Schiff base conjugate 2 displays selectivity for Cu^{2+} and Fe^{3+} enabling the simultaneous detection of these ions in semi-aqueous solution; in contrast, the Schiff base itself displayed no selectivity.

Designing functional chemosensors for the identification and quantification of important physiological and environmental analytes is of considerable importance.[1] High sensitivity and selectivity of these chemosensors are pre-requisites for their effective operational usage.[2] Within this context, the development of sensors for multianalyte detection in real time is a challenge. Some examples of such sensors have been reported and tend to use either: the insertion of multichromogenic units combined in a single receptor,[3] a variety of detection methods (*i.e.* fluorescence and electrochemical)[4] or require detailed mathematical tools to help process the data.[5] But these methods can be tedious either from a receptor synthesis or operational viewpoint. More recently, a move from selective to differential receptors has enabled the detection of two analytes simultaneously by a single chromophore.[6]

In this study, we adopt an alternative strategy to enable differential receptor behaviour. The incorporation of an organic receptor onto the surface of a preformed CdSe/ZnS Quantum Dot (QD) results in a nanocrystal hybrid (**2**) with selectivity for both Cu(II) and Fe(III) ions. Thus, the nanoparticle surface appears to provide a framework for the self-organization of the receptors. The rationale behind the present design is based upon the fact that both **1** and its disulfide analogue **3** have effective binding affinity toward many transition metal ions (Fig. S1 and S2†). But when the same receptor pod is inserted into a framework of tripodal receptors, the final sensors (**4**, **5**) display selectivity for a particular metal ion, meaning receptor binding ability is reduced.[7] Thus, the platform (either aliphatic or aromatic) of these tripodal receptors provides a framework with divergent pods. The cation binding sites present on different pods are not easily accessible simultaneously to make an effective complex with various types of metal ions and hence selectivity is improved. For differential sensing the receptor should be semi-selective. The present design may provide some steric organization to pods and thus will not allow interaction with every metal ion. Nevertheless, the system should have enough binding sites from adjacent pods to complete the coordination sphere of some metal ions. As **1** has a thiol group present in its structure, it is an ideal candidate for attachment to a QD. To the best of our knowledge, this is the first reported example of a nanocrystal chemosensor for the simultaneous estimation of two metal ions.

Receptor **1**, 2-[(2-mercaptophenylimino)methyl]phenol, was synthesized in one step from 2-mercaptoaniline and salicylaldehyde following a literature procedure.[8] CdSe/ZnS QDs were then surface functionalized with **1** after refluxing in chloroform for 18 h. Following removal of the solvent by rotary evaporation the product was precipitated from acetonitrile and centrifuged to yield **2** as a yellow solid.

^{1}H NMR spectroscopy (Fig. 1) confirmed an almost complete ligand exchange with signals at 0.85–1.80 ppm, present in the parent QD and reflecting the methyl and methylene protons of the native trioctylphosphine oxide (TOPO) groups, being absent in the spectrum of **2**. In addition, there were significant changes in the spectra of the free receptor before

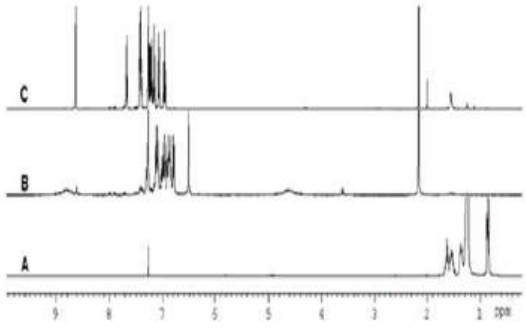

Fig. 1 Stacked ^{1}H NMR spectra of CdSe/ZnS QDs (A), **1** (B) and **2** (C). All spectra recorded in $CDCl_3$ at ambient temperature.

School of Pharmacy, The Robert Gordon University, Aberdeen, Scotland, UK AB10 1FR. E-mail: j.callan@rgu.ac.uk; Fax: +44 1224 262555; Tel: +44 1224 262555
† Electronic supplementary information (ESI) available: Experimental details and relevant spectra. See DOI: 10.1039/b813423e

and after conjugation to the QD surface. Most notable was the large downfield shift for the imine proton from 7.25 ppm in the free receptor to 8.70 ppm in **2**. The UV spectrum of **2** showed peaks in both the UV and visible regions, the former originating from the bound receptor and the latter due to the first exciton peak of the QD (Fig. S4†). The mean particle size of **2**, measured by dynamic light scattering (Fig. S5†), was found to be 15 ± 2 nm, slightly larger than the parent QD (12 ± 2 nm), most likely due to the presence of the more rigid **1** on the surface of the QD compared to flexible TOPO groups. However, when **2** was excited at 370 nm there was no evidence of QD emission. This suggests that the electron rich receptor quenches QD fluorescence, most likely by electron transfer, as has been observed when other electron rich entities have been added to solutions of QDs.[9]

Nonetheless, **2** shows remarkable chromogenic selectivity for Cu(II) and Fe(III) ions when tested against a range of other physiologically and environmentally important cations in a buffered THF–H_2O (80 : 20) solvent system. As shown in Fig. 2a, **2** is characterized by two UV bands, one centered at 275 nm and the other at 355 nm. Addition of Fe(III) resulted in a substantial increase in absorbance of these bands while the addition of Cu(II) caused a substantial bathochromic shift of both bands to 295 and 410 nm respectively. In fact these changes were so significant they could be detected by the naked eye (Fig. 3) with Fe(III) causing a change from colourless to orange and Cu(II) from colourless to green. In contrast, the addition of the other ions had a negligible effect on the UV profile of **2**. Fig. 2b shows the selectivity of **2** for various metal ions when measured at 325 and 410 nm. These particular wavelengths were chosen as 325 nm represents an isosbestic point for all ions except Fe(III) while 410 nm was the λ_{max} for Cu(II) induced changes. As is evident from Fig. 2b, only Fe(III) causes significant inference with Cu(II) at 410 nm while no

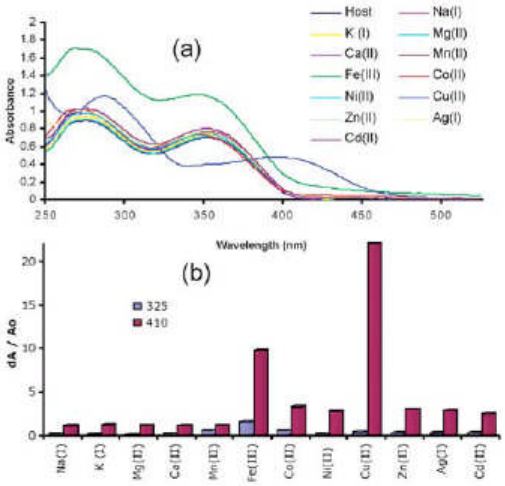

Fig. 2 (a) UV spectra for **2** in the presence of various metal ions and (b) bar chart revealing the selectivity of **2** for metal ions when determined at 325 nm (purple) and 410 nm (blue). [**2**] = 4.0×10^{-8} M; [ion] = 50 μM.

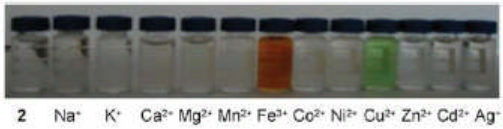

Fig. 3 Photograph illustrating the naked eye identification by **2** of Cu(II) and Fe(III). [**2**] = 4.0×10^{-8} M; [ion] = 100 μM; in an 80% THF–20% 0.01 M HEPES buffer solution at pH = 7.0.

metals produced any significant interference for Fe(III) at 325 nm.

The UV profile of **2** was also observed to be strongly dependent on solution pH (Fig. S7†). At low pH (~3.5) **2** displayed a prominent UV band with λ_{max} 325 nm. Upon increasing the pH, this absorbance gradually decreased while a new red shifted band appeared with λ_{max} 382 nm. This band most likely reflects the deprotonation of the phenolic group of the receptor and from a plot of absorbance against pH the pK_a was calculated as 8.92.[10] Thus, operating at pH 7.0 enables the clear observation of Cu(II) induced changes at 410 nm.

The titration of **2** with Cu(II) and Fe(III) is shown in Fig. 4. Both ions displayed good linearity up to a concentration of 40 μM with their binding constants (log β) being determined as 4.86 and 4.69 respectively.[11] Importantly, Fig. 4c shows that **2** is also capable of measuring Cu(II) in the presence of Fe(III) and of measuring Fe(III) in the presence of Cu(II) up to a concentration of 20 μM. Although it was possible to monitor Fe(III) concentrations in the presence of equimolar Cu(II) it was only possible to monitor Cu(II) in 0.25 molar equivalents of Fe(III). To the best of our knowledge this is the first reported

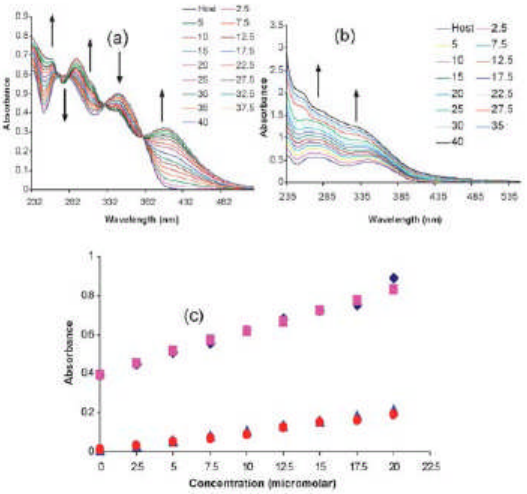

Fig. 4 UV spectra of **2** in the presence of (a) increasing Cu(II) concentration and (b) increasing Fe(III) concentration. (c) Plot of absorbance intensity of **2** against metal ion concentration for Fe(III) (blue diamonds), for Fe(II) in the presence of equimolar Cu(II) (purple squares), for Cu(II) (blue triangles) and Cu(II) in the presence of 0.25 molar equivalents of Fe(III) (red circles). Fe(III) and Cu(II) measurements were recorded at 325 and 410 nm respectively. [**2**] = 4.0×10^{-8} M.

example of a single sensor capable of measuring both Cu(II) and Fe(III) simultaneously.

We have demonstrated for the first time that the selectivity of a receptor can be altered by its incorporation onto the surface of a QD. The organization offered to the receptors by the three-dimensional surface of the nanoparticle was sufficient to enable the determination of Cu(II) and Fe(III) simultaneously, in buffered solution at physiological pH. This offers the ability to screen for these ions in competitive media by UV or the naked eye. The principle may also be extended to other receptors to help improve their selectivity and could potentially lead to a new generation of optical sensors.

The authors would like to acknowledge financial assistance from the EPSRC and RGU. They also thank the EPSRC national mass spectrometry and TEM services.

Notes and references

1 (*a*) R. Martínez-Máñez and F. Sancenón, *Chem. Rev.*, 2003, **103**, 4419; (*b*) J. F. Callan, A. P. de Silva and D. C. Magri, *Tetrahedron*, 2005, **61**, 8551; (*c*) A. P. de Silva, H. Q. N. Gunaratne, T. Gunnlaugsson, A. J. M. Huxley, C. P. McCoy, J. T. R. Rademacher and T. E. Rice, *Chem. Rev.*, 1997, **97**, 1515.
2 H. He, M. A. Mortellaro, M. J. P. Leiner, R. J. Fraatz and J. K. Tusa, *J. Am. Chem. Soc.*, 2003, **125**, 1468.
3 H. Komatsu, D. Citterio, Y. Fujiwara, K. Minamihashi, Y. Araki, M. Hagiwara and K. Suziki, *Org. Lett.*, 2005, **7**, 2857.
4 (*a*) M. Schmittel and H. W. Lin, *Angew. Chem., Int. Ed.*, 2007, **46**, 893; (*b*) D. Jiménez, R. Martínez-Máñez, F. Sancenón and J. Soto, *Tetrahedron Lett.*, 2004, **45**, 1257.
5 (*a*) D. Mikami, T. Ohki, K. Yamaji, S. Ishihara, D. Citterio, M. Hagiwara and K. Suzuki, *Anal. Chem.*, 2004, **76**, 5726; (*b*) T. A. Lee, L. M. Headley and J. K. Hardy, *Anal. Chem.*, 1991, **63**, 357.
6 (*a*) N. Kaur and S. Kumar, *Tetrahedron Lett.*, 2008, **49**, 5067; (*b*) N. Kaur and S. Kumar, *Chem. Commun.*, 2007, 3069; (*c*) H. Komatsu, T. Miki, D. Citterio, T. Kubota, Y. Shindo, K. Yoshiichiro, K. Oka and K. Suzuki, *J. Am. Chem. Soc.*, 2005, **127**, 10798.
7 (*a*) V. K. Bhardwaj, A. P. S. Pannu, N. Singh, M. S. Hundal and G. Hundal, *Tetrahedron*, 2008, **64**, 5384; (*b*) V. K. Bhardwaj, N. Singh, M. S. Hundal and G. Hundal, *Tetrahedron*, 2006, **62**, 7878; (*c*) N. Singh and G. Hundal, *J. Inclusion Phenom. Macrocyclic Chem.*, 2005, **52**, 253.
8 F. Tisato, F. Refosco, U. Mazzi, G. Bandoli and M. Nicolini, *J. Chem. Soc., Dalton Trans.*, 1987, 1693.
9 (*a*) I. Yilidiz, M. Tomasulo and F. M. Raymo, *Proc. Natl. Acad. Sci. U. S. A.*, 2006, **103**, 11457; (*b*) K. S. A. Palaniappan, S. A. Hackney and J. Liu, *Chem. Commun.*, 2004, 2704.
10 (*a*) A. P. de Silva and H. Q. N. Gunaratne, *J. Chem. Soc., Chem. Commun.*, 1990, 186; (*b*) A. P. de Silva, H. Q. N. Gunaratne and P. L. M. Lynch, *J. Chem. Soc., Perkin Trans. 2*, 1995, 685.
11 D. C. Magri, J. F. Callan, A. P. de Silva, D. B. Fox, N. D. McClenaghan and K. R. A. S. Sandanayake, *J. Fluoresc.*, 2005, **15**, 769.

An "off–on" sensor for fluoride using luminescent CdSe/ZnS quantum dots†

Ray C. Mulrooney, Narinder Singh, Navneet Kaur and John F. Callan*

Received (in Cambridge, UK) 6th October 2008, Accepted 17th November 2008
First published as an Advance Article on the web 12th December 2008
DOI: 10.1039/b817569a

The fluorescence emission of CdSe/ZnS QDs was switched "off" when the native trioctylphosphine oxide ligands were exchanged for 1-(bis(η^5-cyclopentadienyl)iron)-methyl-3-(5,7-dimercapto-heptyl)-urea (4); importantly, the emission of the resulting conjugate 5 was switched "on" upon addition of fluoride ions.

Quantum dots (QDs) are semiconducting nanocrystals with all three dimensions in the 2–10 nm range. Due to their small size and a phenomenon known as quantum confinement they are luminescent.[1] Indeed, the photophysical properties offered by QDs have significant benefits when compared to traditional organic dyes.[2] For example, they have broad absorption spectra that extend from the deep ultraviolet to the visible region of the electromagnetic spectrum while their emission properties can be tailored by altering their size and composition. In addition, they have a high resistance to photobleaching and possess longer fluorescent lifetimes than organic dyes meaning cellular autofluorescence may be reduced in time gated experiments. Although QDs are now commercially sold as biomolecule tags,[3] their use as the signalling component in fluorescent sensors is limited in comparison with their organic counterparts. The majority of reported examples where QDs form part of luminescent sensing assemblies utilise the Forster resonance energy transfer (FRET) mechanism in their operation.[4] The photoinduced electron transfer (PET) mechanism has also been used to control the excited state properties of QDs, although the number of sensors designed by this approach is significantly fewer than for FRET.[5] Our design is based upon the knowledge that ferrocene methyl amine has been shown to quench the fluorescence of CdS and CdSe/ZnS QDs when added to a solution containing the QDs functionalised with β-cyclodextrin units.[6] The ferrocene unit was brought close enough to the surface of the QD upon encapsulation by the appended cyclodextrin and quenched its fluorescence by PET. In addition, it has been shown by Otón and co-workers that ferrocenyl ureas bonded directly to a naphthalene fluorophore showed large enhancements in fluorescence upon the addition of fluoride ions.[7] Thus, the binding of the anion guest to the ferrocene urea appears to modulate the rate of PET between the ferrocene and QD such that a fluorescence enhancement (FE) results. The ability to accurately monitor anions is of considerable importance due to their biological and environmental significance. Fluoride is of particular interest owing to its role in preventing dental caries[8a] and its use as a treatment for osteoporosis.[8b]

Here, we attach a ferrocenyl urea receptor to the surface of a pre-formed CdSe/ZnS QD and investigate the photophysical properties in the presence and absence of anions. Specifically, we investigate if the fluorescence emission of QDs can be modulated by the attachment of receptor 4 and if the addition of anions to the resulting QD–receptor conjugate 5 has any effect on its fluorescence signature (Scheme 1).

The receptor 4 was formed from lipoic acid by first reacting it with diphenylphosphoryl azide, followed by the Curtius degradation of the azide with ferrocene methyl amine[9] to form the urea 3. The dithiolane ring of 3 was reduced with $NaBH_4$ to give 4 in 62.5% overall yield. 4 was then adsorbed onto the surface of pre-formed CdSe/ZnS core–shell QDs[10] after stirring for 18 h in a chloroform solution. The QD–receptor conjugate 5 was isolated by evaporation of the chloroform solvent, reconstituted in acetonitrile, and centrifuged to yield the product as an orange solid. Attachment of 4 to the surface of the QD was confirmed by ^{1}H NMR spectroscopy with Fig. 1 showing the stacked spectra of the native QDs and 5.

The native QDs were characterised by a resonance centred at 0.85 ppm and a group of resonances between 1.20 to 1.70 ppm, representing the methyl and methylene protons

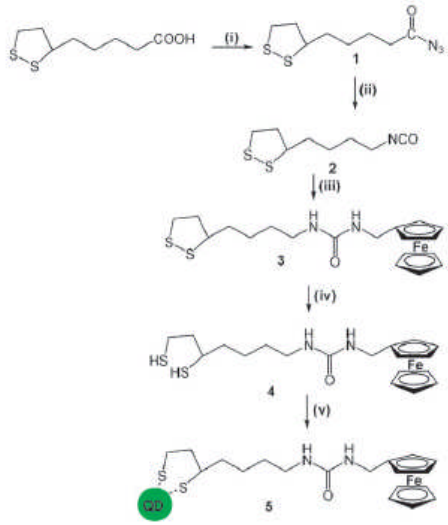

Scheme 1 Synthesis of QD–receptor conjugate 5: (i) triethylamine, diphenylphosphoryl azide, DMF; (ii) Δ, toluene; (iii) ferrocene methyl amine, toluene; (iv) $NaBH_4$, THF; (v) CdSe/ZnS QDs, $CHCl_3$.

School of Pharmacy and Life Sciences, The Robert Gordon University Aberdeen, Scotland, UK AB10 1FR. E-mail: j.callan@rgu.ac.uk; Fax: +44 (0)1224 262555; Tel: +44 (0)1224 262555
† Electronic supplementary information (ESI) available: Experimental details and relevant spectra. See DOI: 10.1039/b817569a/

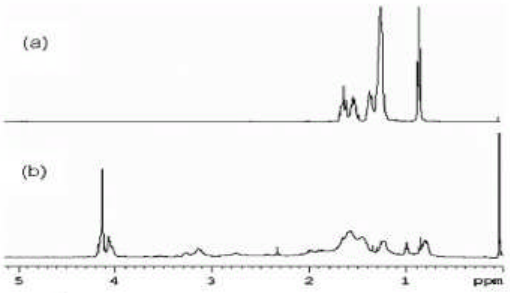

Fig. 1 ^{1}H NMR spectra of (a) CdSe/ZnS QDs and (b) QD–ligand conjugate **5**. Solvent = $CDCl_3$.

respectively of trioctylphosphine oxide (TOPO), a strongly co-ordinating, high boiling point ligand used to passivate the surface of the QD during synthesis. Upon exchange, the magnitude of these peaks was drastically reduced with the appearance of new peaks corresponding to the presence of the ferrocenyl urea ligand appearing in the spectrum of **5**. In particular, the ferrocene protons were housed on a resonance centred at 4.15 ppm, with the methylene protons adjacent to the ferrocene observed at 4.05 ppm. This indicates a good exchange of the TOPO groups for **5**. However, there was no evidence of the urea protons in the spectrum of **5**, most likely due to the broadness of the peaks. The hydrodynamic diameter of **5**, determined by dynamic light scattering was 8.7 ± 1.0 nm, slightly larger than the parent QDs (7.1 ± 1.1 nm) (see Fig. S1, ESI†).

The photophysical properties of **5** were investigated in $CHCl_3$ solution. When excited at 370 nm the QD fluorescence emission at λ_{max} 540 nm, evident in the parent QDs, was absent in the spectrum of **5** illustrating an almost complete quench. We then tested the effect of anions on the fluorescence profile of **5** by the addition of fluoride, chloride, bromide, acetate, hydrogen sulfate, perchlorate and dihydrogen phosphate as their tetrabutylammonium salts (Fig. 2d). A substantial FE (~25 fold) was observed for fluoride which was significantly greater than for any of the other anions tested. In fact, Fig. 2c shows that the FE upon addition of fluoride to **5** is sufficiently great to enable detection by the naked eye. Only acetate and dihydrogen phosphate also produced FEs but of a much lesser magnitude (~5 fold) than for fluoride, highlighting that **5** has good selectivity over other commonly occurring monovalent anions. The selectivity demonstrated by **5** is strikingly similar to that observed by Otón *et al.*,[7] where a ferrocenyl urea bonded to a naphthalene fluorophore displayed a significant FE upon addition of fluoride, a reduced FE for dihydrogenphosphate but negligible FEs for the other tested anions. Therefore, this particular receptor appears to be modular, in that it can be transferred from an organic dye sensor to a QD-based sensor with a retention of selectivity.

We also examined the ability of **5** to operate in competitive environments by adding 0.1 M fluoride to solutions of **5** in the presence of 0.1 M of the other anions tested. In each case, the fluorescence intensity was observed to increase to the same level as for that of **5** and 0.1 M fluoride alone, indicating that fluoride binds strongly to **5** even in the presence of other

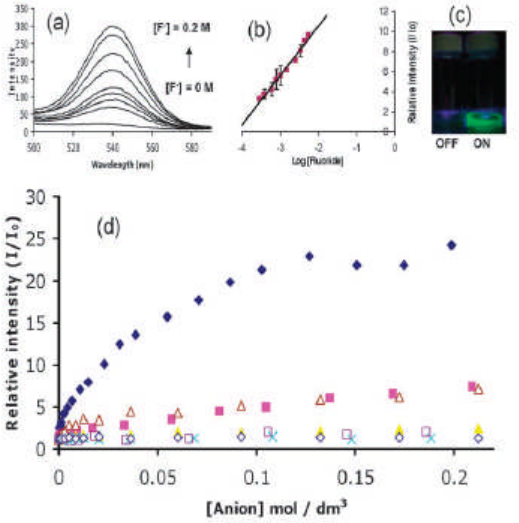

Fig. 2 (a) Fluorescence spectra of **5** upon addition of 0, 0.025, 0.050, 0.075, 0.10, 0.125, 0.150 and 0.20 M fluoride; (b) plot of relative intensity of **5** against −Log [fluoride]; (c) photograph of **5** in the off and on states and (d) plot of relative intensity against concentration for **5** titrated against F^- (◆), Cl^- (×), Br^- (□), AcO^- (■), HSO_4^- (▲), ClO_4^- (○) and $H_2PO_4^-$ (△). Solvent = $CHCl_3$, [**5**] = 1×10^{-7} M for (a), (b) and (d). [**5**] for (c) = 2×10^{-6} M, [F^-] = 3.8×10^{-2} M.

anions. By plotting relative intensity against fluoride concentration (Fig. 2b) we established linearity for fluoride in the range 0.3–5.6 mM with a minimum detection limit of 74.0 ± 0.11 μM. Unfortunately, due to the inability to determine the stoichiometry of the complex formed between **5** and fluoride, a binding constant could not be determined. To confirm the requirement of the ferrocenyl urea unit for QD quenching we subjected the parent QDs (*i.e.* with no ferrocene ligand attached) to the same procedure as that used for the preparation of **5**. The fluorescence of these parent QDs was not quenched (see Fig. S2, ESI†) highlighting the necessity of ferrocene in the quenching of fluorescence intensity.

The most likely reason for the quenching of QD fluorescence upon surface attachment of **4** is an electron transfer process occurring between the ferrocene and the excited QD. Fluorescence quenching of QDs has been observed before when ferrocene and other electron rich analytes were added to solutions of QDs.[11] It has also been shown by Pratt and Beer that ferrocenyl urea receptors like **4** displayed large cathodic shifts in the cyclic voltammogram upon addition of certain anions.[12] Therefore, it is clear that the redox potential of this type of receptor is considerably changed upon anion recognition. This change in redox potential could be sufficient to modulate the electron transfer process responsible for quenching and switch "on" fluorescence. In addition, it has been shown in organic dye-based PET sensors that cations placed in the path of PET can change its rate.[13] Therefore, it is also possible that the placement of a fluoride ion in the path of PET results in a similar effect.

To demonstrate that fluoride binds to the urea component of the receptor we examined the ^{1}H NMR spectra of the

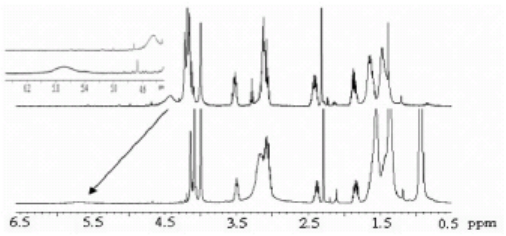

Fig. 3 ^{1}H NMR spectra of **3** (top) and **3** in the presence of 0.01 M tetrabutylammonium fluoride (bottom). Inset shows the expanded region between 4.30 to 6.50 ppm. Solvent = $CDCl_3$.

receptor in the absence and presence of fluoride. As the urea protons were not visibly apparent in the spectra of **5**, we examined the spectrum of **3** instead (Fig. 3). The broad resonance centred at 4.35 ppm in the spectrum of **3** was assigned to one of the urea protons and it was observed to move significantly downfield to 5.70 ppm upon addition of fluoride, while the remaining peaks remained relatively unchanged. This is consistent with a hydrogen bonding interaction between the acidic urea protons and fluoride ion.[12] This hydrogen bonding interaction between fluoride and the urea protons was further confirmed by the addition of methanol to a solution of **5** and fluoride, which quenched fluorescence to ~10% of its original intensity. In this more polar solvent system the ability of fluoride to bind with receptor **5** was significantly reduced, illustrating that the polar solvent competes with fluoride for hydrogen bonding sites. We believe it is this hydrogen bonding interaction between the urea protons and the fluoride ion that alters the rate of PET, resulting in the observed FE upon fluoride addition.

It has also been reported in some cases that ferrocene can quench fluorescence by energy transfer.[14] For effective energy transfer to occur, the absorption spectrum of the quencher should overlap well with the emission spectrum of the fluorophore. The absorption λ_{max} of the ferrocenyl receptor, at 442 nm overlaps poorly with the QD fluorescence λ_{max} (540 nm) reducing the likelihood of FRET as a possible quenching mechanism (see Fig. S3, ESI†). In addition, there was no change in either the position or magnitude of the absorption λ_{max} after the addition of fluoride. This further confirms that energy transfer is not responsible for either the quenching or recovery of fluorescence emission observed for **5** in the absence and presence of fluoride.

In summary, we have shown that a ferrocenyl urea receptor, attached to the surface of a pre-formed CdSe/ZnS QD *via* a dihydrolipoic acid linker, quenches QD fluorescence, most likely by an electron transfer mechanism. Interestingly, the addition of fluoride to the resulting QD-conjugate switched fluorescence back "on", by modulating the rate of PET between the ferrocene units and the QD. The observed selectivity was good for fluoride over other tested monovalent anions. To the best of our knowledge, this is the first "off–on" sensor for anions incorporating QDs as the signalling unit.

The authors would like to acknowledge financial assistance from the EPSRC and RGU. They also thank the EPSRC national mass spectrometry service.

Notes and references

1 K. E. Anderson, C. Y. Fong and W. E. Pickett, *J. Non-Cryst. Solids*, 2002, **299–302**, 1105–1110.
2 (*a*) W. J. Parak, T. Pellegrino and C. Plank, *Nanotechnology*, 2005, **16**, R9–R25; (*b*) X. Michalet, F. F. Pinaud, L. A. Bentolila, J. M. Tsay, S. Doose, J. J. Li, A. M. Wu, S. S. Gambir and S. Weiss, *Science*, 2005, **307**, 538–544; (*c*) B. N. G. Giepmans, S. R. Adams, M. H. Ellisman and R. Y. Tsein, *Science*, 2006, **312**, 217–224.
3 See www.invitrogen.com.
4 Examples of QD FRET sensors include: (*a*) C. Y. Chen, C. T. Cheng, C. W. Lai, P. W. Wu, K. C. Wu, P. T. Chou, Y. H. Chou and H. T. Chiu, *Chem. Commun.*, 2006, 263–265; (*b*) M. Tomasulo, I. Yildiz and F. M. Raymo, *J. Phys. Chem. B*, 2006, **110**, 3853–3855; (*c*) I. L. Medintz, A. R. Clapp, H. Mattoussi, E. R. Goldman, B. Fisher and J. M. Mauro, *Nat. Mater.*, 2003, **2**, 630–638; (*d*) E. R. Goldman, I. L. Medintz, J. L. Whitely, A. Hayhurst, A. R. Clapp, H. T. Uyeda, J. R. Deschamps, M. E. Lassman and H. Mattoussi, *J. Am. Chem. Soc.*, 2005, **127**, 6744–6751.
5 Examples of QD PET sensors include: (*a*) K. M. Gattas-Asfura and R. M. Leblanc, *Chem. Commun.*, 2003, 2684–2685; (*b*) Y. Cheng, K. M. Gattas-Asfura, V. Konka and R. M. Leblanc, *Chem. Commun.*, 2002, 2350–2351; (*c*) M. G. Sandros, V. Shete and D. E. Benson, *Analyst*, 2006, **131**, 229–235; (*d*) M. G. Sandros, D. Gao and D. E. Benson, *J. Am. Chem. Soc.*, 2005, **127**, 12198–12199; (*e*) S. Banerjee, S. Kar and S. Santra, *Chem. Commun.*, 2008, 3037–3039; (*f*) J. F. Callan, R. C. Mulrooney, S. Kamila and B. McCaughan, *J. Fluoresc.*, 2008, **18**, 527–532; (*g*) Y. Chen and Z. Rosenzweig, *Anal. Chem.*, 2002, **74**, 5132–5138.
6 (*a*) K. Palaniappan, S. A. Hackney and J. Liu, *Chem. Commun.*, 2004, 2704–2705; (*b*) K. Palaniappan, C. Xue, G. Arumugam, S. A. Hackney and J. Liu, *Chem. Mater.*, 2006, **18**, 1275–1280.
7 F. Otón, A. Tárraga, M. D. Velasco, A. Espinosa and P. Molina, *Chem. Commun.*, 2004, 1658–1659.
8 (*a*) K. L. Kirk, *Biochemistry of the Halogens and Inorganic Halides*, Plenum Press, New York, 1991, p. 58; (*b*) M. Kleerekoper, *Endocrinol. Metab. Clin. North Am.*, 1998, **27**, 441–452.
9 Ferrocene methyl amine was synthesised using a literature procedure—see ESI†.
10 Green emitting (λ_{max} 540 nm) CdSe/ZnS core–shell QDs were purchased from Evident Technologies, New York.
11 (*a*) I. Yilidiz, M. Tomasulo and F. M. Raymo, *Proc. Natl. Acad. Sci., U. S. A.*, 2006, **103**, 11457–11460.
12 M. D. Pratt and P. D. Beer, *Polyhedron*, 2003, **22**, 649–653.
13 A. P. de Silva, H. Q. N. Gunaratne, T. Gunnlaugsson, A. J. M. Huxley, C. P. McCoy, J. T. Rademacher and T. E. Rice, *Chem. Rev.*, 1997, **97**, 1515–1566.
14 S. Fery-Forgues and B. Delavaux-Nicot, *J. Photochem. Photobiol. A*, 2000, **132**, 137–159.

Phys. Status Solidi C 6, No. 4, 920–923 (2009) / DOI 10.1002/pssc.200880571

physica status solidi c
www.pss-c.com
current topics in solid state physics

Luminescent detection of Cu(II) ions in aqueous solution using CdSe and CdSe-ZnS quantum dots functionalised with mercaptosuccinic acid

John F. Callan* **and Ray C. Mulrooney**

School of Pharmacy, The Robert Gordon University, Aberdeen, Scotland, AB10 1FR, UK

Received 4 April 2008, revised 30 September 2008, accepted 28 October 2008
Published online 16 December 2008

PACS 78.55.Et, 78.67.Hc, 78.68.+m

* Corresponding author: e-mail j.callan@rgu.ac.uk, Phone: +44 (0)1224 262546, Fax: +44 (0)1224 262546

CdSe (core) and CdSe-ZnS (core-shell) Quantum Dots (QD's) surface functionalised with mercaptosuccinic acid ligands were prepared. The conjugates were screened against a variety of common metal ions in aqueous solution and selectivity was established for Cu(II) ions based on an "On-Off" change in fluorescence intensity. The presence of the ZnS shell was found to have a significant effect on both the sensitivity and the range of Cu^{2+} induced quenching.

1 Introduction

Luminescent Quantum Dots (QD's) are rapidly emerging as alternatives to organic dyes for bio-labelling applications [1]. Their high quantum yields, increased stability, broad absorbance spectra and size dependent emission spectra offer enhanced flexibility to the user [2]. Somewhat slower has been the progress in utilising QD's as the signalling unit in fluorescent sensors. Of all the common mechanisms involved in luminescent sensing namely Photoinduced Electron Transfer (PET), Internal Charge Transfer (ICT), Excimer/Exciplex formation and Forster Resonance Energy Transfer (FRET), the latter has unquestionably made the smoothest transition to QD sensor design [3]. However, it has been encouraging to see recent examples of QD sensors based on the PET mechanism, most notably for pH [4], anions [5], the biologically relevant glucose [6] and the environmentally important cyanide ion [7].

The desire to accurately measure Cu(II) concentrations at the sub μM level is inspired by the ions biological and environmental importance. Cu(II) is involved in critical catalytic, biosynthetic and transport processes within the cell and can also contribute to algae growth in seawater [8]. QD based probes may serve as alternatives to conventional organic dye based sensors in the pursuit to accurately measure Cu(II) concentrations in these types of environments. In particular, their long fluorescence lifetimes means problems encountered by autofluorescence can be overcome in time gated experiments. Here, we have prepared simple QD sensors and investigated their ability to selectively recognise Cu(II) by changes in fluorescence signature. CdSe and CdSe-ZnS QD's were synthesised and the organic ligands replaced with the hydrophilic mercaptosuccinic acid (MSA) to render them water soluble. At physiological pH the negatively charged MSA not only ensures aqueous solubility but also serves to electrostatically attract positively charged substrates close to the QD surface. It is known that Cu(II) can quench the excited state energy of fluorophores by electron/energy transfer [8]. In addition, our design strategy is helped by the position of Cu(II) in the Irving-William series, meaning it is expected to bind more strongly than any other divalent 1st row transition metal ion to ligands, irrespective of the nature or number of ligands involved [9]. In this capacity the MSA will serve as a receptor and thus a QD-receptor conjugate with an "On-Off" response is realised. We also investigate the effect the ZnS shell has on the quenching efficiency of Cu(II) by performing titrations of CdSe and CdSe-ZnS QD's with $CuCl_2$.

2 Experimental

2.1 Materials and reagents

All reagents were purchased from Aldrich at the highest quality available. CdSe-ZnS QD's were purchased from Evident technologies, New York (Product No. ED-C10-TOL-0545).

2.2 Synthesis of CdSe QD's

CdSe QDs were prepared modifying slightly a procedure developed by Peng et al. [10]. Briefly, a stock selenium solution was prepared by dissolving selenium powder (100 mg, 1.3 mmol, 1 eq.) and tributylphosphine (TBP), (333 μL, 1.3 mmol, 1 eq.) in octadecene (8.3 mL). The solution was heated to 150 °C and maintained at this temperature for 10 mins. Preparation of the cadmium solution involved dissolving cadmium oxide (65 mg, 0.5 mmol, 1 eq) and oleic acid (1.5 mL, 4.6 mmol, 9 eq) in octadecene (25 mL). This solution was heated to 250 °C and a 5 mL portion of the Se-TBP solution was added. The temperature was maintained for 40 seconds and the reaction quenched by pouring onto crushed ice (100 mL). After the ice melted, the QD's were separated from the aqueous solution as the upper intensely coloured layer.

2.3 Ligand exchange

In order to determine the stoichiometric amount of MSA required, the concentration of the QD solution was calculated by a reported procedure [11]. In a typical ligand exchange reaction, CdSe QD's in octadecene (12 mL, 8.72 x 10^{-7} moles) was charged to a solution of mercaptosuccinic acid (156 mg, 1.04 mmol) in anhydrous methanol (120 mL). The mixture was pH adjusted to 10 with the aid of tetrabutylammonium hydroxide and refluxed for 5 hrs. It was then concentrated to about one third of its original volume under reduced pressure and treated with diethyl ether (100 mL) to precipitate the QDs. The supernatant was carefully decanted off and the remaining solution was centrifuged for 5 mins at 13,500 rpm. The resulting pellet was vacuum dried overnight. The procedure was repeated for CdSe-ZnS QD's using the same concentrations of reactants.

2.4 NMR, UV and fluorescence spectroscopy

All spectra were recorded on a Bruker Ultrasheild 400 MHz. ^{1}H NMR samples were prepared by dissolving 5 mg of sample in 1.0 mL of $CDCl_3$. Chemical shifts are reported in parts per million (δ) downfield of TMS. Absorbance measurements were recorded on an Agilent UV-Vis Spectrometer using 10 mm quartz cuvettes. Fluorescence measurements were recorded on a Perkin Elmer LS55 Luminescence Spectrometer using 10 mm quartz cuvettes. Excitation wavelength unless otherwise stated was set at 370 nm. Excitation slit size was 2.5 nm and emission slit size was 5.0 nm. Scan speed was set at 500.

3 Results and discussion

Figure 1 shows the stacked ^{1}H NMR spectra for MSA, CdSe-ZnS QD's and the QD-MSA conjugate. The MSA is characterised by two distinct resonances, one for the methine proton centred at 3.60 ppm and one for the methylene protons centred at 2.85 ppm. The acidic carboxyl protons are observed at about 12 ppm and are not shown in the expanded Fig. 1. CdSe/ZnS QD's are coated with the organic surfactant tri-octylphosphine oxide (TOPO) which is used as a capping agent during synthesis and helps prevent aggregation. The resonances centred at 5.75 and 4.85 ppm represent the olefinic protons of octadecene, a non-coordinating solvent used in the synthesis of the QD, while the resonance at 1.95 ppm represents the methylene protons adjacent to the olefinic group. The remaining methylene protons of octadecene are represented by the large resonance centred at 1.20 ppm while the methyl protons are observed at 0.80 ppm. The methyl protons from TOPO overlap with those of octadecene. However, the methylene protons adjacent to the P = O bond are observed as small broad resonances at 1.50 and 1.25 ppm, the latter appearing as a shoulder on the main methylene peak observed for octadecene.

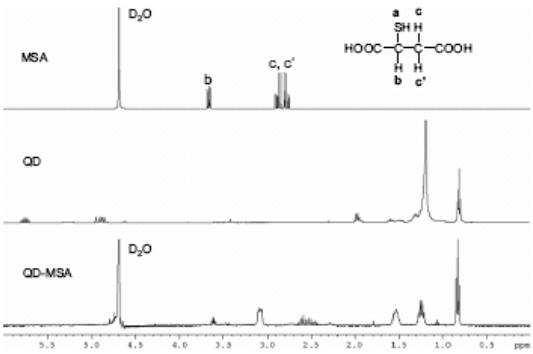

Figure 1 Stacked ^{1}H NMR spectra of top: mercaptosuccininc acid (MSA) recorded in D_2O, middle: CdSe –ZnS QD's recorded in $CDCl_3$ and bottom: QD-MSA conjugate recorded in D_2O.

The spectrum for the QD-MSA conjugate reveals that the ligand exchange and subsequent work-up results in the complete removal of the octadecene from the solution. In contrast, some TOPO groups remain with the resonances at 1.50 and 1.25 now more evident than in the spectrum of the QD alone.. Successful exchange was confirmed by the upfield shift of the methine proton b, from 3.60 ppm in free MSA to 3.05 ppm in the QD-MSA conjugate. The smaller upfield shift observed for methylene protons c and c' to 2.55 ppm is most likely due to these being further from the sulfur atom and consequently are less influenced by the QD surface.

The absorption spectra for CdSe QD's before and after ligand exchange with MSA are shown in Fig. 2a. No significant change in the wavelength of the first exciton peak (~ 515 nm) was observed after ligand exchange, from which the particle diameter was calculated as 2.4 nm [10]. Similarly, the absorption spectra for CdSe-ZnS QD's be-

fore and after ligand exchange are presented in Fig. 2c and are also relatively unchanged. Again the diameter of the nanocrystals obtained from the first exciton peak was 2.4 nm [10]. The similarity in size between the CdSe and CdSe-ZnS QD's means that their emission wavelengths are similar with CdSe QD's emitting at 525 nm and CdSe-ZnS nm and CdSe-ZnS at 535 nm (Figs. 2b and d). The more narrow emission peak for CdSe-ZnS QD's relative to CdSe is due to better passivation of the core with the higher band gap ZnS.

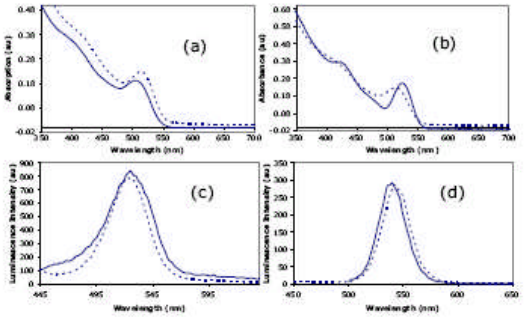

Figure 2 (a) Absorbance and (b) emission spectra for CdSe QD's before (–) and after (--) surface exchange with MSA. (c) and (d) Similar plots for CdSe-ZnS QD's. Before spectra recorded in toluene and after in 100% aqueous solution.

The selectivity of the core and core-shell QD's were tested against a range of common metal ions, the results shown in Fig. 3. For the CdSe QD's it is clear that Fe(II) and Cu(II) both result in significant quenching, with Cu(II) producing the greatest effect of 89.5 %.

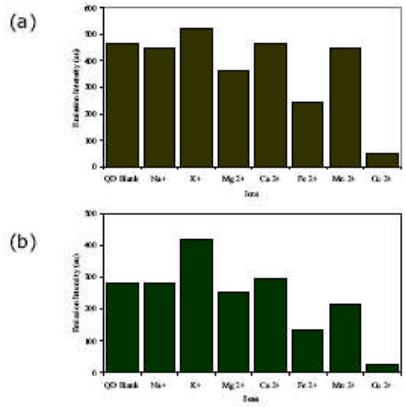

Figure 3 Selectivity data for (a) CdSe and (b) CdSe-ZnS QD's surface functionalised QD's. Ion concentration was 1 x 10^{-5} M, λ_{ex} = 370 nm.

The quenching effect caused by Fe(II) is most likely due to an inner filter (competitive absorption) effect and can be cancelled by the addition of fluoride ion to produce the colorless FeF_6^{3-} [12]. The large quenching effect by Cu(II) is most likely due to its position in the Irving Williams series, meaning it binds strongly to the MSA ligands leading to an annihilation of the excited state energy by electron/energy transfer. This type of quenching involving Cu(II) has also been observed in other QD-hydrophilic ligand systems [10]. For the CdSe-ZnS QD's, again Fe(II) and Cu(II) were the main quenchers but surprisingly, a significant enhancement was observed for K^+, the reason for which is unclear.

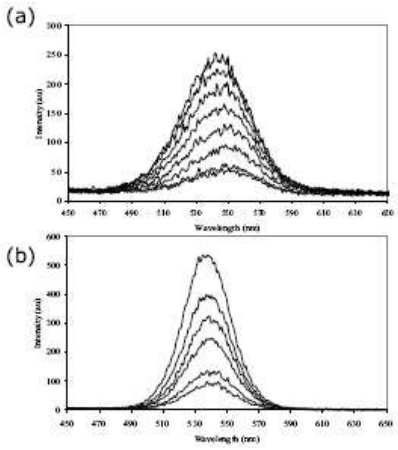

Figure 4 Emission spectra for (a) CdSe and (b) CdSe-ZnS QD's functionalised with MSA. Concentrations of Cu(II) shown in the emission plots for CdSe were 0, 0.019, 0.13, 0.59, 1.10, 1.78, 3.31 and 3.99 μm and for CdSe-ZnS were 0, 6.00, 14.00, 24.00, 64.00 and 104 nM with decreasing fluorescence intensity.

The emission spectra for CdSe and CdSe-ZnS QD's in the presence of increasing amounts of Cu(II) are shown in Fig. 4. For CdSe there is a distinct red shift in the emission wavelength (~ 10 nm) after the addition of 3.99 μM of Cu(II) which may be attributed to the formation of small amounts of CuSe at the surface of the QD. This type of exchange has been seen in other systems (the formation of Ag_2Se upon addition of Ag(I) ions to CdSe QD's [13] and the formation of HgTe on addition of Hg(I) ions to CdTe QD's [14]) and in the present case is explained by the much lower solubility product constant of CuSe (-log K_{SP} = 60) [15] compared to CdSe (-log K_{SP} = 35) [16]. A much smaller red shift (~4 nm) was observed for the CdSe-ZnS QD's after addition of 104 nM Cu(II). It is unlikely that this is due to the formation of CuSe due to the presence of the ZnS shell but could be due to the formation of small amounts of CuS or Cu_2S [15]. Again this is supported by the lower solubility product of CuS (-log K_{SP} = 35) [com-

pared to ZnS (-log K_{SP} = 20)] [17]. This indicates that at higher concentrations of Cu(II), the formation of CuSe and CuS/Cu_2S may contribute to the fluorescence quenching of CdSe-MSA QD's and CdSe-ZnS-MSA respectively.

To determine the sensitivity of the two QD-receptor conjugates toward Cu(II), and to investigate the effect the ZnS shell may have on the quenching efficiency, we have plotted relative fluorescence intensity against –log [Cu(II)] as shown in Fig. 5.

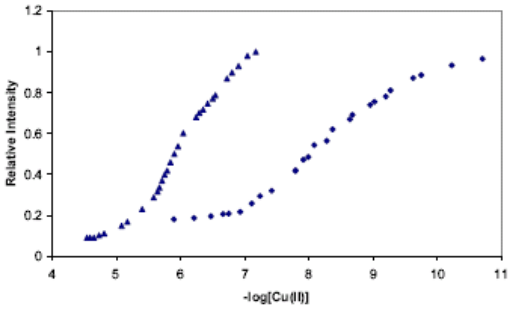

Figure 5 Plot of relative intensity against –log [Cu(II)] for MSA functionalised CdSe (▲) and CdSe-ZnS (■) QD's.

The MSA functionalised CdSe QD's fluorescence 'switched off' over *ca.* two log units suggesting a 1:1 binding between Cu(II) and the QD conjugate [18]. In contrast, the CdSe-ZnS-MSA conjugate's fluorescence 'switched off' over *ca.* four log units, this greater range of quenching most likely resulting from an increased insulation of the core by the ZnS shell thus requiring more Cu(II) to bind before effective quenching can occur [19]. It can also be observed from Fig. 5 that a more complete quench is observed for the CdSe probe with a residual fluorescence of 10% remaining after Cu(II) addition compared to 20% for the CdSe-ZnS, a feature again most likely due the insulating effect by the ZnS shell. The binding constants -Logβ, obtained by a plot of -log$[F_{MAX} - F]/[F - F_{MIN}]$ against -log [Cu(II)] [20], gave values of 5.89 for CdSe-MSA and 8.31 for CdSe-ZnS-MSA clearly illustrating a vast difference in sensitivity for the two probes.

In summary, easily prepared QD-MSA probes have been synthesized and shown to be effective at measuring Cu(II) ion concentration in aqueous solution based on an "On-Off" response. The presence of the ZnS shell has shown have a significant effect on the both the binding constant and the range over which quenching occurs. A slight red shift in the emission spectra of the CdSe and CdSe-ZnS signify after the addition of Cu(II) indicate the formation of small amounts of CuSe and CuS respectively at the QD surface. Our interests hope to expand on the progress already made in QD based sensing and deliver functioning probes for other important analytes preferably based on reversible binding and a fluorescence enhancement.

Acknowledgements The authors would like to thank RGU for financial support.

References

[1] W. J. Parak, T. Pellegrino, and C. Plank, Nanotechnology **16**, R9 (2005).
X. Michalet, F. F. Pinaud, L.A. Bentolila, J. M. Tsay, S. Doose, J. J. Li, A. M. Wu, S. S. Gambir, and S. Weiss, Science **307**, 538 (2005).
B. N. G. Giepmans, S. R. Adams, M. H. Ellisman, and R. Y Tsein, Science **312**, 217 (2006).
[2] J. K. Jaiswal and S. M. Simon, Trends Cell Biol. **14**, 497 (2004).
[3] C. Y. Chen, C. T. Cheng, C. W. Lai, P. W. Wu, K. C. Wu, P. T. Chou, Y. H. Chou, and H. T. Chiu, Chem. Commun. **263**, (2006).
M. Tomasulo, I. Yildiz, and F. M. Raymo: J. Phys. Chem. B **110**, 3853 (2006).
I. L. Medintz, A. R. Clapp, H. Mattoussi, E. R. Goldman, B. Fisher, and J. M. Mauro, Nature Mater. **2**, 630 (2003).
E. R. Goldman, I. L. Medintz, J. L. Whitely, A. Hayhurst, A. R. Clapp, H. T. Uyeda, J. R. Deschamps, M. E. Lassman, and H. Mattoussi, J. Am. Chem. Soc. **127**, 6744 (2005).
[4] M. Tomasulo, I. Yildiz, S. L. Kaanumalle, and F. M. Raymo, Langmuir **22**, 10284 (2006).
[5] J. F. Callan, R. C. Mulrooney, S. Kamila, and B. McCaughan, J. Fluoresc. **18**, 257 (2008); J. F. Callan, R. C. Mulrooney, and S. Kamila, J. Fluoresc. (2008), available online: DOI: 10.1007/s10895-008-0367-5.
[6] D. B. Cordes, S. Gamsey, and B. Singaram, Angew. Chem. Int. Ed. **45**, 3829 (2006).
[7] W. J. Jin, M. T. Fernandez-Arguelles, J. M. Costa-Fernandez, R. Pereiro, and A. Sanz-Medel, Chem. Commun. **883** (2005).
[8] L. Fabbrizzi and A. Poggi, Chem. Soc. Rev. **24**, 197 (1995).
[9] K. Rurack, Spectrochim. Acta A **57**, 2161 (2001).
[10] Z. A. Peng and X. G. Peng, J. Am. Chem. Soc. **123**, 183 (2001).
[11] W. W. Yu, L. Qu, W. Guo, and X. Peng, Chem. Mater. **15**, 2854 (2003).
[12] H. Y. Xie, J. G. Liang, Z. L. Zhang, Y. Liu, Z. K. He, D. W. Pan, Spectrochim. Acta A **60**, 2527 (2004).
[13] J. G. Liang, X. P. Ai, Z. K. He, and D. W. Pang, Analyst **129**, 619 (2004).
[14] A. S. Susha, A. M. Javier, W. J. Parak, and A. L. Rogash, Colloids Surf. A **281**, 40 (2006).
[15] O. L. Bottecchia and J. Braz, Chem. Soc. **9**, 515 (1998).
S. G. Dixit, A. R. Mahadeshwar, and S. K. Haram, Colloids Surf. A **133**, 69 (1998).
[16] Y. Chen and Z. Rosenzweig, Anal. Chem. **74**, 5132 (2004).
[17] See: http://www.ktf-split.hr/periodni/en/abc/kpt.html.
[18] T. Gunnlaugsson, A. P. Davis, G. M. Hussey, J. Tierney, and M. Glynn, Org. Biomol. Chem. **2**, 1856 (2004).
[19] We assume that the number of MSA ligands attached to the surface of the QD is the same in each of the probes as the loading ratio during the ligand exchange reaction was identical. Due to the absence of a chromophore in MSA it is difficult to accurately quantify this number.
[20] A. P de Silva and H. Q. N. Gunaratne, J. Chem. Soc., Chem. Commun. **186**, 14 (1990).
A. P de Silva, H. Q. N Gunaratne and P. L. M. Lynch, J. Chem. Soc. Perkin Trans. **2**, 685 (1995).